Quantitative Electroanalysis of Host-Guest Binding at Organized Supramolecular Interfaces

by

Lin Qi

M.Sc., Xi'an Jiaotong University, 2013

B.Sc., Xi'an Jiaotong University, 2011

Thesis Submitted in Partial Fulfillment of the

Requirements for the Degree of

Doctor of Philosophy

in the

Department of Chemistry

Faculty of Science

SIMON FRASER UNIVERSITY

Fall 2020

Approval

Name:	**Lin Qi**
Degree:	**Doctor of Philosophy**
Title:	**Quantitative Electroanalysis of Host-Guest Binding at Organized Supramolecular Interfaces**
Examining Committee:	**Chair:** Krzysztof Starosta Associate Professor
	Hua-Zhong Yu Senior Supervisor Professor
	Dipankar Sen Supervisor Professor
	Zuo-Guang Ye Supervisor Professor
	Loren Kaake Internal Examiner Associate Professor
	Gang-Yu Liu External Examiner Professor Chemistry University of California, Davis
Date Defended/Approved:	October 7, 2020

Abstract

As a young and important class of supramolecular host-guest chemistry, the macrocyclic cucurbit[n]uril (CB[n]) hosts consisting of one hydrophobic inner cavity and multiple carbonyl portals have shown dramatically increased research interests since 1980s, with tens of thousand publications focusing on their synthesis, distinct structural features, exceptional physical and chemical properties. More importantly, their excellent host-guest recognition behavior leads to their great application potentials in many fields, such as nanofabrication, biomedical/pharmaceutical science, analytical chemistry, catalytic chemistry, and adaptive chemistry, which have been explored extensively in the past two decades.

Particularly, CB[7], an attractive member of CB[n] family, shows ultra-strong host-guest binding ability towards small aromatic or ring-structured organic compounds, which is mainly attributed to its proper-sized inner cavity. As a representative, the host-guest complexes formed between CB[7] and various redox-active ferrocene (Fc) derivatives have extremely high binding affinities (10^9 to 10^{12} M^{-1}), which have been employed as an alternative of natural binding pairs (e.g., antigen-antibody, biotin-avidin) for fabricating versatile functional molecular and biomolecular interfaces.

In order to gain further understanding of this particular host-guest binding pair formed at molecular interfaces, in this thesis, based on both conventional cyclic voltammetry and advanced structural characterizations, the binding thermodynamics and kinetics were investigated on mixed ferrocenylundecanethiolate/octanethiolate self-assembled monolayers on gold as a highly-organized model system. The results show that the inclusion binding behavior of this host-guest pair, while significantly affected by the surface, still has satisfactory stability for practical application. In addition, the broad potential of this new interfacial Fc@CB[7] host-guest binding system is manifested as nanoscale probes for the distribution of Fc terminal groups on SAMs (as an indicative of their structural heterogeneity), as an environmental regulator of long-range electron transfer process, and as an electrochemical sensor for pharmaceutical drugs via competitive host-guest assay strategy. It is expected that this new interfacial host-guest binding system can be further explored for fabricating well-controlled, ratiometric electrochemical biosensors.

Keywords: cucurbit[7]uril; ferrocene; self-assembled monolayer; cyclic voltammetry

Acknowledgements

I would like to first show my sincerest gratitude to my senior supervisor, Dr. Hua-Zhong Yu, for providing me with the opportunity to study as a Ph.D. student at the Department of Chemistry of SFU, to attend academic conferences, and for his kind helps and guidance on my study and research, presentation skills, and scientific writing abilities during six past years.

I would also like to thank my other two supervisors, Dr. Dipankar Sen and Dr. Zuo-Guang Ye, for their valuable comments, questions and suggestions at my supervisory committee meetings, which helped me to have better and in-depth understandings about my experimental results, and promoted me to do more thinking and reading related to my research contents.

Deep thanks as well to following people: Yue Ma, an M.Sc. student graduated from the Department of Statistics and Actuarial Science of SFU, who helped me a lot with the fitting analysis based on Marcus-Hush-Chidsey model; Dr. Ruibing Wang, the associate professor at the Institute of Chinese Medical Sciences of University of Macau, who introduced us his brilliant researches on the application of cucurbit[n]uril in pharmaceutical science when visiting our lab in summer 2018, and collaborated with us on the research project of developing electrochemical assay for durg-cucurbit[7]uril complexations; all the current and past members in Dr. Yu's lab I have been worked with, especially Dr. Huihui Tian, a visiting student from 2012 to 2014, who helped me initiate my research and taught me many electrochemical knowledges and experimental skills.

Finally, I would like to thank my wife, Siqi Huo, and my parents for their love, care and help all the time in my life.

Table of Contents

List of Tables

List of Figures

List of Acronyms

SAM	Self-assembled monolayer
CV	Cyclic voltammetry
NMR	Nuclear magnetic resonance
FTIR	Fourier Transform Infrared Spectroscopy
MCT (detector)	Mercury cadmium telluride (detector)
ESI	Electrospray ionization
TGA	Thermalgravimetric analysis
MD	Molecular dynamics
DFT	Density functional theory
XRD	X-ray diffraction
ITC	Isothermal calorimetry
AFM	Atomic force microscopy
STM	Scanning tunneling microscopy
ET	Electron transfer
XPS	X-ray photoelectron spectroscopy
RAIRS	Reflection Adsorption Infrared Spectroscopy
SERS	Surface-enhanced Raman spectroscopy
SPR	Surface plasma resonance
SECM	Scanning electrochemical microscopy
SICM	Scanning ion-conductance microscopy
LOD	Limit of detection
MHC (model)	Marcus-Hush-Chidsey (model)
CuAAC	Cu(I)-catalyzed azide–alkyne cycloaddition
*μ*CP	Microcontact printing
EIS	Electrochemical Impedance Spectroscopy
DB	Denatonium benzoate
MCH	6-mercapto-1-hexanol

TCEP	Tris (2-carboxyethyl) phosphine hydrochloride
ALA	Alagebeium
AdOH	1-Adamantanol

Chapter 1.

General Introduction

1.1. Fascinating supramolecular host-guest chemistry

1.1.1. Supramolecular chemistry: definition, classification, and application

Supramolecular chemistry, although is still a young scientific field, has been rapidly developed and attracted tremendous interests since this concept was first proposed by Jean-Marie Lehn in 1987.[1] According to Lehn, supramolecular chemistry can be defined as "the chemistry beyond the molecule"; more specifically, it means the organized complexes formed by the association of two or more chemical species (as building blocks) via the combination of various noncovalent interactions (e.g., hydrogen bonding between properly oriented functional groups, hydrophobic interactions among nonpolar compounds, electrostatic interactions between charged species, coordinate bonding between metal ions and electron rich atoms, π–π stacking among aromatic rings, and van der Waals forces among instantaneous/transient dipoles). As a result, the supramolecular complexes usually keep a better and adjustable balance between their chemical stability and reversibility under moderately varied conditions with respect to traditional covalently conjugated molecular complexes; thus they are more adaptable in terms of practical use. More interestingly, the supramolecular complexes usually have significantly different physical and chemical properties compared to their constituent species, thus may possess distinct and exceptional functions.[1,2]

Based on the number of constituent molecules, the supramolecular chemistry can be classified into two major categories. One is the simplest and highly specific molecular recognition chemistry occurred between two or few molecules (e.g., biotin-streptavidin, antigen-antibody, and complementary DNA binding pairs), which serves as the fundamental process of supramolecular chemistry. The other is molecular assembly chemistry that is usually participated by many or even countless numbers of chemical molecules/species (e.g. amphiphilic complexes). As driven by their intra- and intermolecular noncovalent interactions, those chemical species can form large scale

compounds or polymers (hundreds of nanometer in size) with specific structural/morphological features via spontaneous self-assembly and self-organization process. A typical building block material of supramolecular assembly is amphiphilic molecules (i.e., molecules containing both hydrophobic and hydrophilic parts), which can form micelles, liposomes, and bilayer lipids in aqueous environments.[3]

Over the past three decades, supramolecular chemistry has been exhibiting great application potentials in multiple fields.[2,4] In nanotechnology, based on supramolecular assembly, many types of nanomaterials and nanodevices have been developed with exceptional properties and functions. For example, the supramolecular complexes consisting of conductive or insulating polymers can be used for fabricating molecular electronic devices;[5] the supramolecular complexes with distinctive light emission or adsorption properties are desired materials for developing molecular optical/imaging devices;[6] and the highly reversible and flexible supramolecular materials enable the construction of stimuli responsive molecular switches or machines.[7] Moreover, by combining supramolecular systems (same type of signal output) in response to different stimuli, it is possible to design molecular logic gates and computing devices.[2, 8] In analytical chemistry, the strong and specific molecular recognition chemistry serves as the basis for creating highly selective and sensitive biosensors; particularly, its regulation effect on the fluorescent emission/quenching efficiency have promoted the design of simple and sensitive optical biosensors.[10] In addition, it can help to extract or separate analytes from a complex matrix (e.g., heavy metal extraction from various chemical wastes);[9] Recently, there has been increasing interests in the application of supramolecular chemistry in pharmaceutical and biomedical science; for example, extensive efforts have been made on using supramolecular approaches to develop well controlled drug delivery systems, more efficient diagnostic tools and better therapeutic strategies.[2,11] Another major application of supramolecular chemistry is to regulate the activity of electron transfer (ET) based catalytic reactions, since the reorganization energies of ET could be modulated by the microenvironments created by different types of noncovalent interactions.[2,12] As in the proof-of-concept stage, the noncovalent supramolecular assemblies with high reversibility have been considered as the ideal material with constitutional dynamic characters for achieving adaptive or evolutionary chemistry.[13,14] One ultimate goal of supramolecular chemistry is to understand, control, and build the artificial mimics of biological compounds (e.g., nucleic acids, proteins, and membranes) with high complexity and functionality (e.g., energy conversion, selective ions channel, signal transduction, and enzymatic catalysis).[2]

1.1.2. Macrocyclic host-guest recognition systems

Before the field of supramolecular chemistry was initiated,[1] research on molecular recognition chemistry or the so called host-guest chemistry had proceeded for decades, and has been considered as the origin and fundation of supramolecular chemistry.[2] The main feature of molecular recognitions that distinguishes them from general molecular interactions is that they occur in much more specific and organized manner between selected host and guest pair, as expressed by equation 1.1:

$$\text{Guest} + \text{Host} \rightleftharpoons \text{Guest@Host complex} \qquad (1.1)$$

Since the pioneer studies in 19th century on exploring the strong and highly specific enzyme-substrate recognition occurred in biological systems, the important role of geometric or structural matches in the host-guest recognitions (i.e., the famous “lock-key” principle proposed by Fischer et al.[15,16]) has been gradually revealed, which determines how stable and how specific is the arrangement of noncovalent intermolecular interactions between them.

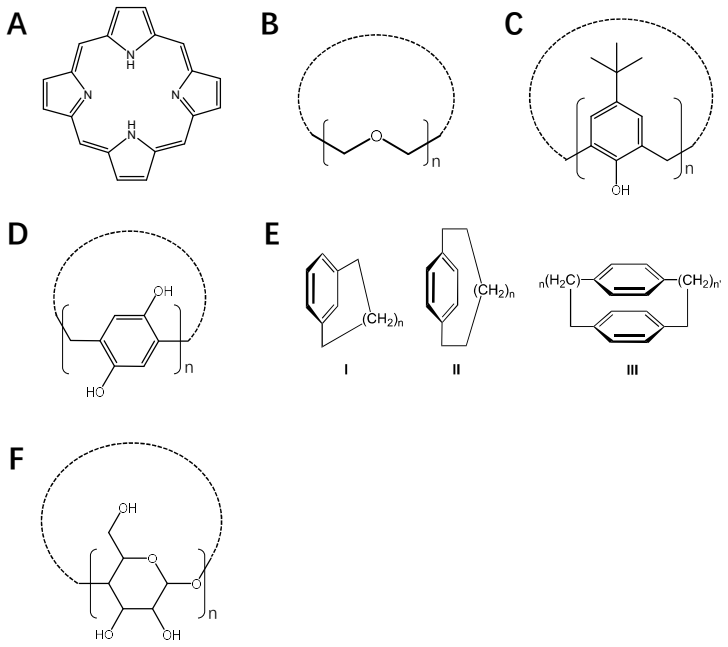

Figure 1.1. Representative macrocyclic compounds: (A) porphyrins; (B) crown-n-ethers; (C) calix[n]arenes; (D) pillar[n]arenes; (E) I: [n]metacyclophanes, II: [n]paracyclophanes, III: [n.n']cyclophanes; (F) cyclodextrins.

As an important branch of supramolecular chemistry, the “ring-structured” macrocyclic compounds are highly efficient “hosts” in molecular recognitions. Porphyrins (Figure 1.1A) are one of the earliest discovered macrocyclic compounds that can be formed naturally (through geological process or *in vivo* biosynthesis) or via laboratory synthesis; they consist of four pyrrole units interconnected via methine bridges, and are excellent hosts of divalent or trivalent metal ions by providing four equivalent coordination binding sites (i.e., total four lone pairs of electrons on the four nitrogen).

In 1967, a new type of macrocyclic host, the cyclic hexaether, was accidentally obtained by Pedersen as a byproduct during his synthesis of bisphenol.[17] It was found that the solubility of this cyclic ether compound can be improved in the presence of cations (e.g., Na^+ and K^+), which can be attributed to the complex structure formed between them;. i.e., the metal ions are trapped inside the cavity (via ion-dipole interactions) formed by the electronegative oxygens of ether subunits.[18] As this cyclic ether looks like a “crown” with a cation as the guest in the center, it was named as “crown ether”.[17] Besides the cyclic hexaether, other crown ethers with various numbers (n) of ether subunits (Figure 1.1B) were subsequently obtained by adjusting the synthetic conditions; these crown ethers also have different degrees of structural flexibility and cation binding affinity.[18,19]

The replacement of oxygen atoms in crown ethers with nitrogen atoms leads to another class of hosts, i.e., the macrocyclic polyamines. Although macrocyclic polyamines are analogous to crown ethers, the strongly basic nature of amine groups results in their unique guest recognition properties. For example, the protonated amines make this type of host capable of binding anions;[20] moreover, the softer nitrogen atom (i.e., more delocalized charges) of macrocyclic polyamines lead to their preferential accommodation towards soft transition metal ions.[21]

After the discovery of crown ethers and their analogues, the successful synthesis of other types of artificial macrocyclic hosts with distinctive structural property and guest recognition behavior have been reported, such as calix[n]arene (Figure 1.1C), pillar[n]arene (Figure 1.1D), and cyclophane hosts (Figure 1.1E).[2] As a common feature, all these macrocyclic host compounds consists of aromatic moieties as the repeating subunits, which endow them with more rigid cyclic structures and the ability to accommodate large guest species other than metal ions.[2,22]

As another type of natural macrocyclic host, the cyclodextrins (CDs) were discovered in the 1950s, which were obtained from starch via a certain enzymic process.[23] CDs are cyclic oligosaccharides (Figure 1.1F) consisting of six (*α*-CD), seven (*γ*-CD) or eight (*β*-CD) glycopyranoside subunits, which form a "conical frustum" shaped hydrophobic inner cavity with two asymmetric hydroxyl portals. With proper-sized inner cavities, CDs can accommodate guest species ranging from ions and gas molecules to small organic compounds.[23]

From thermodynamic view, the spontaneous formation of a host-guest binding pair benefits from the decrease in the Gibbs free energy.

$$\Delta \mathrm{G} = \Delta \mathrm{H} - \mathrm{T}\Delta S \qquad (1.2)$$

$$\Delta \mathrm{G} = -\mathrm{RT}\ln K \qquad (1.3)$$

As shown in equation 1.2, the change of Gibbs free energy (ΔG) involves the changes on enthalpy (ΔH) and entropy (ΔS). For host-guest complexes, their intermolecular noncovalent interactions result in decreased enthalpy (i.e., negative ΔH), which contributes largely to their overall reduced free energy. The contribution from entropy is complicated, as the binding between host and guest compounds (entropy loss) and their desolvation processes (entropy gain) have opposite effects on the total free energy of the entire system. Accompanied with the discovery of various macrocyclic host compounds, there are many studies regarding the thermodynamic stabilities of their host-guest complexations, i.e., important thermodynamic parameters (ΔG/dissociation constant, ΔH and ΔS) have been determined by calorimetric and various spectroscopic techniques.[2,24] These studies have revealed that the enthalpy and entropy contributions toward the overall free energy change/binding affinity of host-guest molecular recognitions depend on not only the chemical nature of host and guest compounds, but also the geometric size of hosts.[25,24]

1.1.3. Cucurbit[n]uril (CB[n]) hosts: new commers in supramolecular chemistry

Synthesis, structure, and properties. As the latest generation of macrocyclic host compound, the cucurbit[n]uril (CB[n]) family has drawn much attention and interests over other macrocyclic hosts owing to their unique structural features, exceptional physical/chemical properties, and distinctive host-guest recognition behavior. The

earliest recorded discovery of CB[n] can be dated back to 1905, when Behrend et al. condensed glycoluril and formaldehyde in concentrated HCl solution. In this process, an unknown insoluble, white amorphous compound with good yields (40%~70%) were obtained by recrystallizing the product from concentrated H_2SO_4 at high temperature (> 110 °C), which exhibited a good ability to form complexes with small molecules.[26] However, due to the lack of modern characterization techniques, the composition and structure of these synthetic compounds remained mysterious until 1981.[27] Based on NMR and X-ray crystallographic studies, Mock et al. revealed the chemical composition and molecular structure of the most dominant macrocyclic compound in the mixture of the products: It consists of six glycoluril subunits bridged by twelve methylene groups, which are cyclized to form a symmetrical cavity with two identical carbonyl openings/portals (each portal contains six carbonyl groups). Because its structure resembles a "pumpkin", Mock et al. named it "cucurbituril", which belongs to the botanical family, Cucurbitaceae.[27] The composition and structure of this initially discovered cucurbit[6]uril (CB[6]) macrocyclic host are displayed in Figure 1.2.

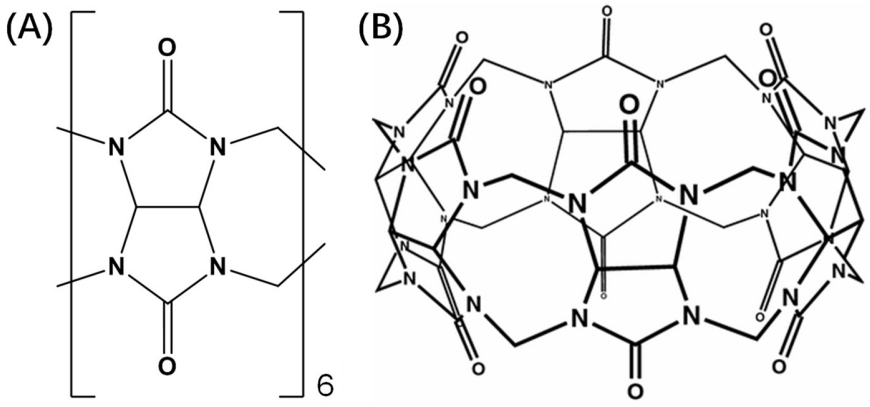

Figure 1.2. The (A) chemical composition and (B) structure of cucurbit[6]uril.
Note: (B) is reprinted with permission from Journal of Inclusion Phenomena and Macrocyclic Chemistry, 61(3-4), 343-346. Copyright (2008), *Springer Nature*.

Unfortunately, interests in such artificial macrocyclic compound were not popularized due to several limiting factors (e.g., poor solubility in common solvents, difficult functionalization/derivatization). Until early 1990, it started to attract considerable attention when Kim and co-workers successfully synthesized and isolated other cucurbit

homologues of different molecular sizes and with enhanced functionality.[28] As shown in Figure 1.3 (A), the key to obtain other cucurbit homologues is to condensate glycoluril and formaldehyde in concentrated acid (9 M H_2SO_4) at lower temperature (75 to 90 ℃), which would lead to the formation of mixed homologues of cucurbit[n]uril (n = 5 to 11) with different constituent fractions (10%~15% CB[5], 50%~60% CB[6], 20%~25% CB[7], 10%-15% CB[8], and trace amounts of CB[9]~CB[11]) as identified by NMR and ESI mass spectroscopy.[28] The mixture of cucurbit[n]uril homologues can be separated by multiple cycles of dissolution (in water, methanol, and diluted acid solutions) and fractional recrystallization.[28] Although the formation mechanism of CB[n] macrocycles is not clearly understood, it was believed that the acid condensation between glycoluril and formaldehyde would first result in the formation of linear oligomeric products, which are then cyclized to produce the macrocyclic structure.[29] Moreover, it was found that the alkali metal ions play important roles in the distribution of CB[n] homologues in the final products.[30] Based on spectroscopic and X-ray crystallographic characterizations, the molecular size and structure of CB[n] homologues have been fully discovered,[28] which are summarized in Figure 1.3 (B).

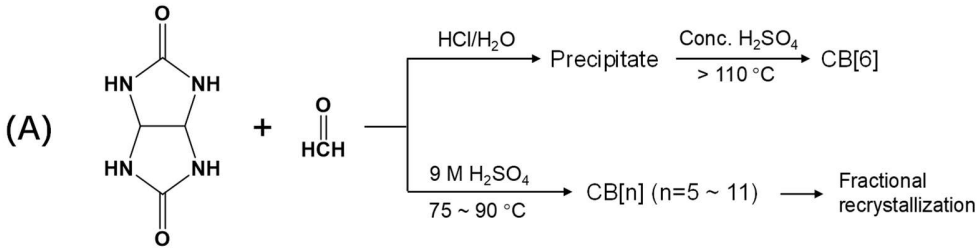

(B)

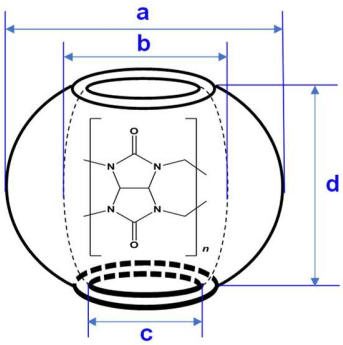

	CB[5]	CB[6]	CB[7]	CB[8]
a (outer diameter/Å)	13.1	14.4	16.0	17.5
b (cavity diameter/Å)	4.4	5.8	7.3	8.8
c (portal diameter/Å)	2.4	3.9	5.4	6.9
d (height/Å)	9.1	9.1	9.1	9.1
cavity volume/Å^3	82	164	279	479

Figure 1.3. (A) The synthetic routes and (B) structural parameters of CB[n] homologes.

The varied sizes of CB[n] homologues also bring significant differences in their physical and chemical properties: For example, the TGA analysis revealed that CB[7] and CB[5] have lower thermodynamic stability (< 370 °C) than CB[6] and CB[8] (> 420 °C);[28,31,32] the microscopic studies also showed that CB[7] and CB[5] powders become amorphous after thermo treatment, while CB[6] and CB[8] solids were still crystalline;[32] in addition, CB[7] and CB[5] have much higher water solubility (20 ~30 mM) than CB[6] and CB[8] (< 0.01 mM).[32] These could be attributed to an interesting "odd-even'' effect in CB[n] crystallinity, i.e., the CB[n]s consisting of odd numbers of glycoluril units have less "self-association" tendency than even numbered CB[n]s, which usually form large scale one, two, or even three dimensional network structures (possibly via CH---carbonyl interactions).[32] The carbonyl portals of CB[n]s (as weak Lewis base) can be protonated under acidic conditions, and the pK_a values of the "conjugated acid" of CB[n]s are different (e.g., pK_a of CB[6] is 3.02;[33] pK_a of CB[7] is 2.2[34]). The size of CB[n] also determines the number of "high-energy" water molecules that are trapped inside the inner cavities of CB[n]s (2 ~ 22 water molecules as calculated from their inner cavity volume, simulated by molecular dynamics, or determined by X-ray diffraction techniques[35,36]), which plays an important role in the thermodynamic stabilities of their host-guest complexations. In spite of the sizes, a general feature shared by all CB[n]s is that their inner cavities are poorly polarizable (e.g., the dielectric constant of CB[7] inner cavity was determined less than 10); [37] this is attributed to the nonpolar, hydrophobic nature of the cyclized glycolurils with symmetrically arranged polar bonds and no accessible electron pairs inside the inner cavity of CB[n]s (as shown in Figure 1.2 and Figure 1.3).[37,38] In addition, all CB[n]s have poor solubility in common organic solvents.[31]

To effectively modulate their physical and chemical properties, as well as reactivities, functionalization/derivatization of CB[n]s (either on CB[n]s or from aldehyde/glycoluril precursors) has been developed since early 1990s.[39-41] A commonly used strategy starts from the hydroxylation of CB[n]s (by using strong oxidant $K_2S_2O_8$ or UV photolysis of H_2O_2) so that other functional groups can be introduced to CB[n]s via the reaction with the active hydroxyl group.[40] However, the low yields of monohydroxylated CB[n] (5~30%) still remains a challenge for their practical applications.[40]

Distinctive host-guest recognition properties. The host-guest recognition properties of CB[n]s are strongly correlated to their structural features (i.e., a hydrophobic inner cavity along with two symmetric carbonyl-aligned portals). Theoretical calculations

and experimental measurements on the electrostatic potential map of CB[n]s have indicated that the regions around their carbonyl portals are negative,[31] which allow them to bind with cations through ion-dipole interactions. Moreover, the lone electron pairs at carbonyl oxygens of CB[n]s are capable of coordinating to cations, whose binding affinity and stoichiometry strongly depend on the solution conditions (e.g., type of solvent, ionic strength),[42] and the type of cations.[43] In contrast to the electronegative carbonyl portals, the inner cavities of CB[n]s are remarkably hydrophobic, which results in the preference of accommodating nonpolar organic guest compounds via strong hydrophobic effects.[31,44,45] As a result, the combination of ion-dipole interactions and hydrophobic effects leads to the emergence of ultrastable host-guest complexes formed between CB[n]s and cationic organic compounds, and their binding affinities could even surpass nanomolar level.[46]

In addition to the above described noncovalent interactions, which reduce the enthalpy of the system, the release of “high-energy” water molecules trapped inside the cavity of CB[n]s to the bulk solution contributes to the overall thermodynamic driving force of their host-guest recognitions. The reason for this is that those trapped water molecules have much more organized network structure than the water molecules in bulk aqueous solution; thus, the desolvation process associated with the CB[n]-guest binding result in large entropy gain.[47,48] In contrast, without such “high energy” water molecules trapping inside the inner cavities, the thermodynamic driving force of other macrocyclic host-guest recognitions is more dictated by the “enthalpy-entropy compensation” effect (the entropy loss caused by the formation of host-guest complex can be largely offset by their de-solvation process).[48]

Besides above described general features, the host-guest recognition behavior of CB[n]s are strongly dependent on the geometric factors of their inner cavities, which determine how well a guest compound can physically fit inside.[27,31,45] While CB[5] is only capable of accommodating gas molecules and small ions,[49] the doubled volume size of CB[6] (Figure 1.3B) can incorporate a variety of simple organic compounds, such as alcohols, amines, and alkyl-ammonium compounds.[50] With further enlarged inner cavity, CB[7] is able to bind with relatively large and more complicate organic compounds with aromatic or ring structures.[46] As for CB[8], its inner cavity becomes 10 times bigger than that of CB[5], ensuring its unique ability to accommodate two small organic guests simultaneously.[51,52] The even larger CB[n]s (n =10, 14, which are difficult to be synthesized) start to undergo certain degree of structural distortions (e.g., CB[14] has a twisted inner

cavity[53]); and their inner cavities are even large enough to include other small macrocyclic hosts, which enable the assembly of more sophisticated supramolecular complexes.[53,54]

Up to now, kinetic aspects of CB[n] host-guest complexations is much less studied than their thermodynamics, and, most of the studies are limited to CB[6] as its host-guest binding process is relatively slow. Nevertheless, it has been found that the inner cavity size plays a significant role in the kinetic behavior of CB[n] host-guest complexation, which accounts for the major activation barrier for their binding and dissociation processes. Generally, a kinetically stable host-guest complexation has a faster association but a slower dissociation process.[55] Addtionally, the kinetic mechanism of CB[n]s host-guest complexation is strongly correlated with the charged state of guest species. For neutral and nonpolar guest species, their association with CB[n]s is usually treated as an elementary process (i.e., a second-order reaction).[56] It is rather a complex process for guest molecules with cationic or electronegative functional groups because the binding activity may require a two-step process to complete: the ion-dipole interactions occurred at the carbonyl portals of CB[n]s results in the formation of an intermediate compound with the guest moiety still dangling outside; the subsequent incorporation of the guest moiety into the inner cavity via a “flip-flop” mechanism finalizes the complexation. Therefore, more considerations must be included when studying the kinetics of these types.[55,56] Also, the binding/dissociation kinetics of cationic guest compounds is sensitive to solution conditions (e.g., pH, type and concentration of ions) since the ion-dipole interactions can be influenced by the charge state, ionic strength, and degree of protonation in their surrounding microenvrioment.[56,57]

Application potentials of CB[n] family. Because of their intriguing chemical/physical properties and the excellent host-guest recognition behavior, CB[n]s based supramolecular chemistry has been blossoming at a remarkable rate in comparison to other macrocyclic hosts, with tremendous efforts and studies reported focusing on their broad applications.[44,58] Based on the strong and highly reversible host-guest binding between CB[n]s and organic species, it has been demonstrated that they are excellent building blocks for developing well-organized and highly-efficient self-assembly systems,[59-61] stimuli (e.g., temperature,[62] pH,[63-66] voltage,[67-70] and enzyme[71]) responsive molecular switches/devices, and different types of functional materials (e.g., polymers,[72,73] dendrimers,[74-76] nanoparticles,[77,78] nanosheets,[79] thin films,[80-82] and hydrogels[34,83]). Providing the distinctive host-guest inclusion, the microenvironment surrounding the guest

species can be modulated by CB[n]s, which results in their changed chemical properties (e.g., pKa,[84-86] electron transfer rates,[87,88] optical properties,[38,89,90] and solubility[91-93]). Furthermore, such a particular inner cavity enables CB[n] macrocycles to be used as efficient inhibitor or catalyst for many chemical reactions (e.g., cycloaddition reactions,[94] oxidation reactions,[95] hydrolysis reactions,[96] photocyclization and dimerization[97,98]). Not limited to the above functions, CB[n]s expand their application into the field of biosensors, in which CB[n]s are used to capture/extract analyte of interest from a sample matrix, or to specifically immobilize signal probes on solid substrates via host-guest binding.[100,101] In particular, the emission properties (e.g., peak wavelength, extinction coefficient) of some fluorescent dyes change remarkably upon their binding to CB[n]s or being replaced by other guest (analyte), which can be used for designing simple optical biosensors.[10] In pharmaceutical and biomedical science, efforts have been made to explore the application of CB[n]s as an excellent excipient to improve the in vivo drug delivery efficiency[102] and therapeutic activity.[58,103] Additionally, the use of CB[n]s as a new class of stationary phase for chromatographic separation/purification has been also explored.[104,105]

1.1.4. Host-guest complexation between CB[7] and ferrocene (Fc)

As an important member of CB[n]s family, CB[7] has drawn much interest due to its unique geometric feature (inner cavity volume = 242 $Å^3$), distinct chemical properties, and ultra-strong host-guest binding. Specifically, unlike other CB[n] homologues, which consist of "even" number of glycoluril units (solubility less than 10^{-5} M), CB[7] is moderately soluble in water due to its less crystallinity (20 to 30 mM).[28,32] Besides, by using fluorescent dye as a environemental probe, the result shows that the inner cavity of CB[7] has an extremely low polarity and polarizability.[37,38] More importantly, CB[7] exhibits ultra-strong host-guest binding towards a variety of small organic compounds, such as ferrocene, cobalotocene, adamantane, diamantane, and bicyclooctane. Their binding affinities (10^9–10^{15} M^{-1}) are even comparable with the naturally occurring strongest biotin-avidin binding pair.[46,106] Though *β*-CD shares a similar inner cavity size with CB[7], it only shows moderate binding affinities (K_f = 10^3–10^4 M^{-1}) towards the same type guest compounds.[23]

Besides the significant enthalpic contribution (the strong hydrophobic and ion-dipole interactions), CB[7] host-guest binding (~ 55% packing efficiency[35]) is rarely influenced by the common "enthalpy-entropy compensation effect" since there are 7–8 "highly ordered" water molecules (theoretically predicted based on molecular dynamics (MD) and density

functional theory (DFT)) residing in the inner cavity od CB[7], which results in a large amount of entropy gain upon releasing them to the bulk solution.[47,48] In comparison, CB[6] with a smaller inner cavity can only accommodate 3–4 "high energy" water molecules. Although CB[8] with an enlarged inner cavity can accommodate 13–14 water molecules, it cannot form highly ordered network structure (similar to the arrangement of water molecules in bulk solution) and thus have lower energies.[47,107,108]

Ultra-strong host-guest recognition between CB[7] and Fc. As one of the earliest synthesized organometallic compounds,[109] the bis(cyclopentadienyl) iron (II), also known as ferrocene (Fc), has demonstrated a unique structure and impressive properties: First, it has an 18-electron configuration including 12 π-electrons from the two cyclopentadienyl (cp) rings and 6 d-electrons from the Fe^{2+}, making it thermally stable below 400 °C; second, it is exceptionally electroactive that undergo fast and highly reversible redox process at a readily accessible potential range; third, the hydrogens of the cp rings can be easily derivatized/functionalized.[110] These properties strongly promote the wide application of Fc as a robust and versatile electrochemical probe in materials and analytical chemistry.[111,112] In 2003, Kaifer and co-workers first reported that both Fc and its oxidized form (ferrocenium, Fc^+) can be encapsulated by CB[7] to form stable host-guest complexes (Fc@CB[7]) from their UV/Vis spectrometry titration and electrochemical studies.[113] Later, X-ray diffraction (XRD) characterization revealed two co-existed crystal structures of this inclusion complex in which the angle formed between the main axes of Fc and CB[7] is either 22° or 79° (thermodynamically favored) [114] as displayed in Figure 1.4.

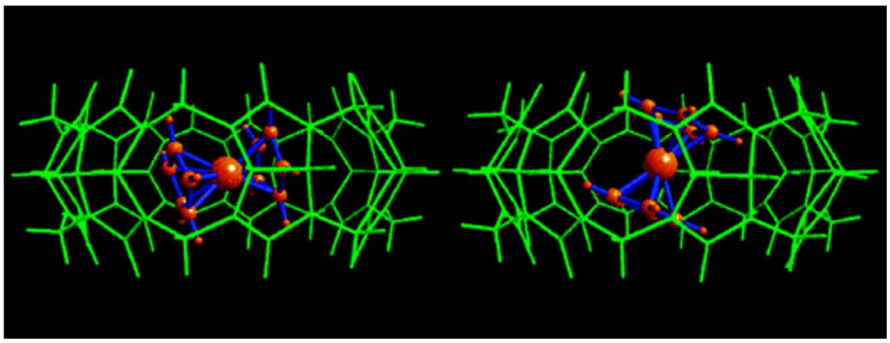

Figure 1.4. X-ray crystal structures of the Fc@CB[7] host-guest complex.
Note: Reprinted with permission from Ref. 115. Copyright (2005), *American Chemical Society*.

In order to overcome the problem of poor solubility of Fc in water when studying its host-guest binding behavior with CB[7], the collaboration conducted by Kaifer and Kim focused on using representative Fc derivatives with neutral, cationic or anionic substituents on their cp ring(s) that are more soluble in water.[114,115] With the improvement of solubility, the binding affinities between Fc derivatives and CB[7] were systematically studied using isothermal calorimetry (ITC) or NMR, and the results are summarized in Figure 1.5. Based on the competitive titration studies with each technique, it was found that both cationic (K_f = 10^{12}–10^{15} M^{-1}) and neutral Fc derivatives (K_f = 10^{7}–10^{10} M^{-1}) can form ultra-stable host-guest complexes with CB[7]. In contrast, nearly no binding is observed for anionic Fc derivative (i.e., ferrocene-carboxylic acid, K_f < 10^{2} M^{-1}), which could be due to the electrostatic repulsive force arising between the carbonyl portals of CB[7] and negatively charged substituents.[114]

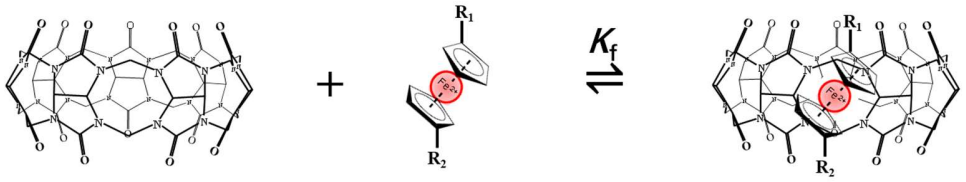

	R_1	R_2
A1	CH_2OH	H
A2	$CH_2NH^+(CH_3)_2$	H
A3	$CH_2N^+(CH_3)_3$	H
A4	$CH_2N^+(CH_3)_3$	$CH_2N^+(CH_3)_3$
A5	CH_2OH	CH_2OH
A6	$CH_2O(CH_2)_2O(CH_2)_2OCH_3$	H

	ΔH (kcal/mol)	TΔS (kcal/mol)	K_f (M^{-1})
A1	-21.5±0.5	-8.6±0.5	(3.2±0.5)×10^9
A2	-21.0±0.5	-4.1±0.5	(2.4±0.8)×10^{12}
A3	-21.0±0.5	-4.3±0.4	(4.1±1.0)×10^{12}
A4	-21.5±0.2	-0.5±0.5	(3.0±1.0)×10^{15}
A5	——	——	> 10^7
A6	——	——	> 10^7

Figure 1.5. Formation constants (K_f) of host-guest complexes formed between CB[7] and different Fc derivatives.
Note: A1-A4 values are from Ref. 114; A5-A6 values are from Ref. 115.

The influence of CB[7] on the redox behavior of Fc upon their complexation is an interesting topic that has been widely investigated using cyclic voltammetry technique.[113-

[116] It was found that the diffusion-controlled redox peak currents of Fc reduce significantly upon incubation with CB[7], which can be viewed as a strong indicator for the formation of Fc@CB[7] complex (smaller diffusion coefficient than free Fc compounds). Besides, the formal potentials of Fc derivatives shift positively (to different extents) upon binding with CB[7] (less than 30 mV for neutral Fc derivatives, but more than 80 mV for cationic Fc derivatives), indicating that the influence of CB[7] binding on the redox equilibrium of Fc guests are strongly charge-state dependent.[114-116] Although the reason behind this phenomenon has not been clearly understood, it was proposed that the cationic functional groups may prevent the ferrocenium from reaching the most favorable orientation inside the CB[7] due to the "locking" effect caused by their electrostatic repulsion force. This restriction of motion, especially rotation, and the imperfect position reduce the thermodynamic stability of Fc^+ upon oxidation.[115] In contrast, since the neutral substituents/functional groups demonstrate no "locking" effect, both the reduced and oxidized forms of Fc derivatives can adapt to their most favorable orientations inside CB[7]; thus, changes in redox thermodynamics would be negligible.[115] The comparison of experimentally determined ET rate constants (k_{et}) of various Fc derivatives indicate that their redox kinetics become sluggish upon encapsulation by CB[7], which might be owning to both the increased ET distance[115] and modulated environment.[68] Compared with the traditional non-electroactive natural binding pairs, the redox-active Fc guest and its changed redox properties upon CB[7] binding provide this exceptional supramolecular host-guest binding pair with additional "signaling" functions.

Formation of Fc@CB[7] host-guest binding pair at interfaces. As one of its broad applications, the Fc@CB[7] host-guest binding pair has been used as an alternative to conventional natural binding pairs for biological sample extraction/enrichment[121] and fabricating versatile bio-functional interfaces,[46] which also provide additional redox signaling function. These have been typically achieved by either immobilizing functionalized CB[7] chemically or depositing CB[7] physically on solid substrates as illustrated in Figure 1.6:

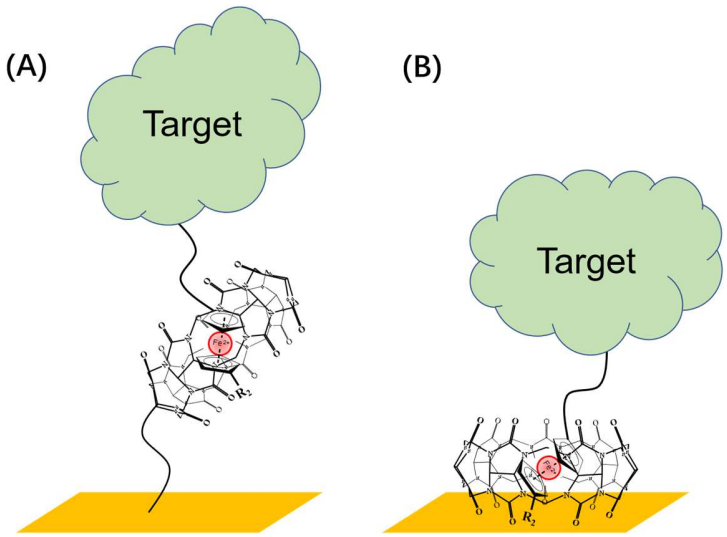

Figure 1.6. Surface immobilization of biomolecule via interfacial Fc@CB[7] host-guest binding: (A) covalently modified CB[7] on solid substrate. (B) directly deposited CB[7] on solid substrate.

For the former (Figure 1.6A), with CB[7] covalently bonded to the surfaces, Fc-labelled target species, like proteins and enzymes, can be introduced onto solid substrates via Fc@CB[7] host-guest binding following the traditional incubation/washing procedures. However, functionalization/derivatization of CB[n] is rather challenging and the search for a simple, cost-effective, and highly efficient method is still a long way to go.[117-119] Moreover, the chemical modifications on CB[7] may affect the host-guest binding stability.[119]

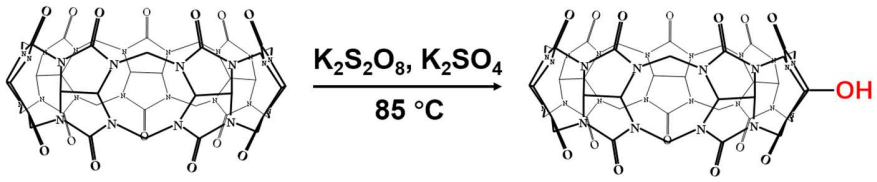

Figure 1.7. Monohydroxylation of CB[7] by $K_2S_2O_8$ and K_2SO_4.
Note: refer to Ref.105.

As shown in Figure 1.7, the current functionalization/derivatization of CB[7] is typically started with the oxidization of "equatorial" hydrogens using strong oxidants (e.g., $K_2S_2O_8$) as proposed by Kim and co-workers to generate "reactive" hydroxyl groups on CB[7].[118]

During the synthesis, they found that the number of substituent hydroxyl groups on CB[7] can be controlled by tuning the amount of K_2SO_4 added to regulate the extent of oxidation from fully substituted CB[7](OH)$_{14}$ to monohydroxylated CB[7]OH; the latter has a yield of 27%).[120] Besides using strong oxidizer, Ouari and Bardelang also reported an alternative method for CB[7] monohydroxylation (with a yield of 5–30%) based on UV photolysis (λ = 254 nm) of hydrogen peroxide as a source of hydroxyl radicals.[117] The hydroxylated CB[7] can then be covalently attached to solid substrates with N-hydroxysuccinimide (NHS) protected carboxy groups.[121] Further more, other functional groups (e.g., thiol, azide) can be introduced to the hydroxylated CB[7] to realize its covalent immobilization on surface or coupling with other molecules.[122,119]

To avoid the challenging and time-consuming functionalization of CB[7], An et al. proposed a strategy of directly depositing CB[7] on gold surfaces (Figure 1.6B) . The interactions between the carbonyl portals and gold allows CB[7]s to form a monolayer on the surface for subsequent immobilization of Fc-labeled analytes.[80,123-126] Similar strategies were also applied to their immobilization on gold nanoparticles[127] and graphene nanosheets.[128] However, the characterization based on CV studies of the immobilized Fc[123,126] and atomic force microscopy (AFM)[129] imaging of the surface have revealed that such directly deposited CB[7] monolayers have complicate orientations, multiple-layer defects, and only 40%-50% Fc packing efficiency,[123-126] which could significantly complicate their binding ability with guest species on surfaces. Another concern is the stability of directly deposited CB[7] monolayers merely via noncovalent interactions/physisorptions, which could be easily affected by other nonspecific adsorptions on surface, varied environmental conditions, and stronger CB[7]-guest interactions in solution.

Though the Fc@CB[7] host-guest binding pair is being studied on surfaces, a barrier to its wide adaptation is the lack of fundamental understanding of its stability when formed at interfaces with intrinsic spatial and orientational limitations. As one of the very few thermodynamic studies at the interface, Brinkmann et al. determined the formation constant (K_f = 3.4±0.5 × 10^3 M^{-1}) of Fc@CB[7] complex formed on directly deposited CB[7] monolayer on gold.[131] The dramatic decrease in the binding affinity for more than 6 orders of magnitude with respect to those determined in solution may not be viewed as a good example to reflect the general circumstances on surface, since the “imperfect” CB[7] monolayer and the large peptide coupled to Fc may bring more interfering factors to the

interfacial host-guest binding stability.[32] Recently, You et al. investigated the K_f of Fc@CB[7] host-guest complex (Fc is covalently coupled to DNA) formed at a protein/lipid nanopore interface, from which they also obtained a much lower binding affinity (K_f = 2.4 × 10^5 M^{-1}).[133] For better understanding the interfacial host-guest binding behavior between CB[7] and Fc, and further promoting its application, it is essential to perform fundamental studies and to explore the application of this particular host-guest binding pair formed at more ideal molecular interfaces; form example, the molecular interfaces should be easily accessible, highly-organized, and have the host-guest binding condition close to the assumption of Langmuir adsorption isotherm (i.e., independent, equivalent, and noninteracting binding sites).

1.2. Self-assembled monolayers (SAMs) for constructing organized molecular interfaces

Self-assembled monolayers (SAMs) are the single layer assemblies of organic molecules/compounds (a typical thickness of 1~3 nm) formed by their spontaneous adsorption (from solution or gas phase) and organization (into regular or semi-regular arrays) process on solid substrates. The constituent organic molecule has a “head group” with strong affinity to the substrate surface and is able to replace other nonspecifically adsorbed organic compounds, which serves as the basis for the high stability of SAMs. Moreover, the intermolecular interactions among constituent organic molecules contribute to the structural organization of SAMs, which play an important role in their re-organization process.[134,135]

As a special type of two-dimensional nanomaterials (so called ultrathin organic films), SAMs are suitable for the studies in nanoscience and nanotechnology. They can be easily prepared on either macroscopic or nanometer-scale substrates to modulate the physical and/or chemical properties of the original material (e.g., electric conductivity,[136] optical medium,[134] surface wettability,[137] corrosion resistance,[138] adhesion,[139] and friction[139-140]). More importantly, the terminal groups of SAMs with specific properties and functions[140] enable the development of versatile molecular devices, such as biosensors[141] and nano-electronic devices.[142] Another advantage of SAMs is that they can be patterned on solid substrate with micrometer or nanometer scale features by using microscopic techniques,[143] microcontact printings (μCPs),[144] photolithography,[145] or electron beam lithography.[146]

1.2.1. Alkanethiolate SAMs on gold

Thermodynamic stability and structural features. The adsorption of alkanethiol molecules on gold creates the most popular type of SAMs, which have been intensively studied for the past few decades since they were first reported in 1983.[147] Alkanethiolate SAMs on gold have a high degree of thermal stability (> 400 K);[135] their structural organization on the substrate surface is illustrated in Figure 1.8:

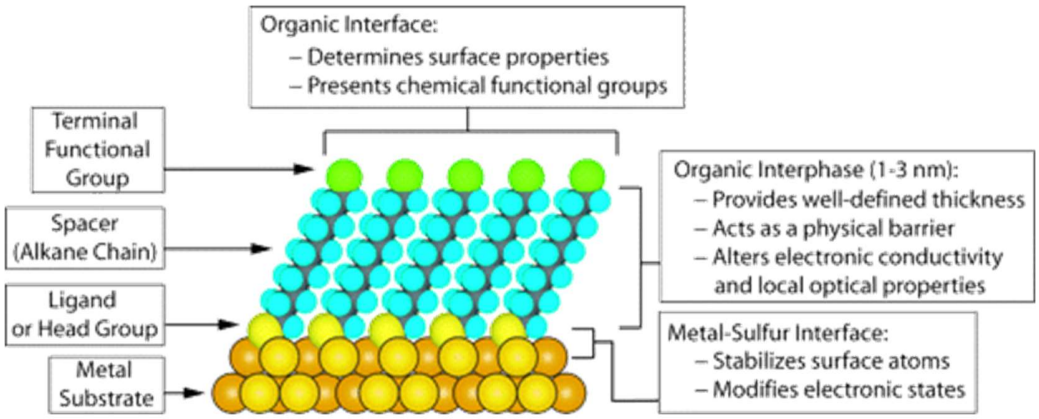

Figure 1.8. Schematic view of an "ideal" n-alkanethiolate SAM (n is the number of methylene units) on gold (111) surface.
Note: Reprinted with permission from Ref. 134. Copyright (2005), *American Chemical Society.*

As illustrated in Figure 1.8, the individual alkanethiol molecule consists of three parts: the sulfur head group (yellow circles), methylene chain (blue circles and dark sticks), and the terminal group (green circles). The strong interaction between gold and sulfur is the dominant contributor to the ultrahigh stability of alkanethiolate SAMs. Previous studies based on X-ray photoelectron spectroscopy (XPS), kinetic measurement of their thermal desorption process, and theoretical calculations have revealed that the binding energy is 100 ~ 200 kJ/mol for such gold-sulfur interaction,[148,134] which is comparable with covalent bonds (150 ~ 400 kJ/mol).[149] The molecular (microscopic) nature of gold-sulfur interaction still remains debatable as none of the proposed bonding models[150] and reaction mechanisms (e.g., adsorption of thiyl radical RS·, coordination bonds, oxidative addition) can explain all the fundamental questions (e.g., where does the mercaptan hydrogen go? what is the oxidation state of Au? why there are reconstructions on gold surface?) as well

as various characterization and simulation results. [135,150,151] The scenario becomes even more controversial for densely-packed alkanethiolate SAMs (less accessible to imaging/diffraction techniques due to the crowded surface) or on the surface with more complicate morphology (e.g., gold nanoparticles).[150] In addition to gold-sulfur interaction, the van der Waal forces among hydrocarbon chains also contribute to the high thermal stability of alkanethiolate SAMs (~ 7 kJ/mol per methylene group);[152] more importantly, they account for the spontaneous re-organization process of alkanethiols on gold.

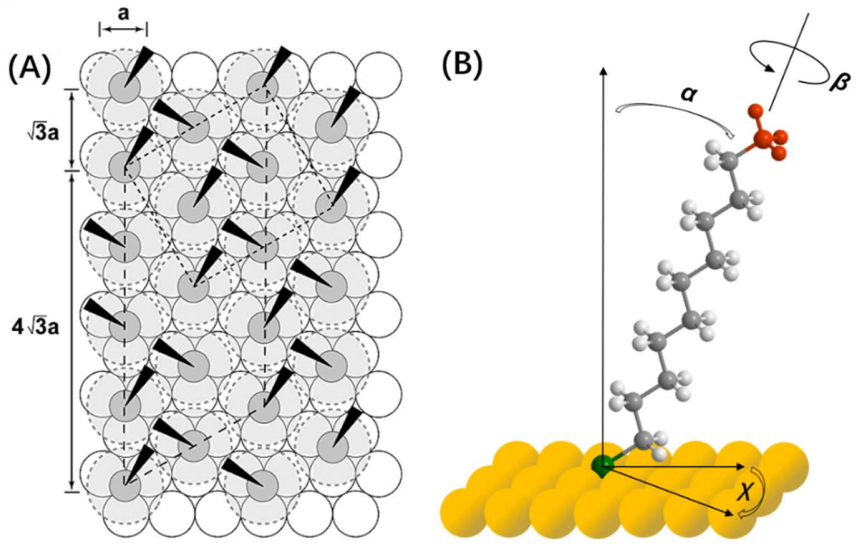

Figure 1.9. Schematic view of (A) the $\sqrt{3} \times \sqrt{3}\, R30°$ lattice arrangement of n-alkanethiols on Au (111). The white and gray circles represent the gold and sulfur atom, respectively; the light gray circles with dashed lines indicate the approximate projected area occupied by each alkanethiol chain; and the dark wedges indicate the projection of CCC plane of alkane chain on surface; a is the diameter of gold atom (2.88 Å). (B) The model of a single, long-chain alkanethiol adsorbed on gold surface, whose dynamic orientation is defined by molecular tilt angle (*α*), rotation angle (*β*) and projection angle (*χ*).

Note: (A) is reprinted with permission from Ref. 134. Copyright (2005), *American Chemical Society*.

Based on the results obtained by various microscopic characterization (AFM, STM), and diffraction techniques (X-ray, electron, atom), as well as theoretical calculations (DFT, MD), the lattice arrangement of fully packed long-chain alkanethiols on hexagonally-arranged Au (111) surface has been revealed. As shown in Figure 1.9 (A), the $\sqrt{3} \times \sqrt{3}\, R30°$ and its secondary $c(4 \times 2)$ superlattice arrangements are two generally

accepted models for densely packed long-chain alkanethiols.[156,157,158,159] Their coexistence was observed by STM, where the fraction of $\sqrt{3} \times \sqrt{3}\, R30°$ domain increases for alkanethiolate SAM of longer chains.[135,153] Nowadays, questions still remain regarding these proposed lattice structures; these include the exact position of sulfur on gold (111) surface (related to the chemical nature of gold-sulfur interaction), their lower calculated surface energy compared to the experimental values, as well as the conflicts in the characterization results derived from microscopic and diffraction techniques.[135,154,155,160] Further understanding on the true arrangement of alkanethiols on gold surface is still a long-term and important scientific topic for both fundamental study and practical applications.

The orientation/conformation of long-chain alkanethiols in a fully packed SAM on gold should allow strong van der Waals interactions among neighboring molecules (minimize the overall free energy), an their experimentally observed orientation/conformation can be described by a single-chain model with three parameters: the molecular tilt angle α, the molecular rotation angle β (around the alkyl chain axis), and the molecular projection angle on surface χ, as shown in Figure 1.9 (B). Based on ellipsometry and reflection adsorption infrared spectroscopy (RAIRS) studies,[175] the α, β, and χ of long-chain alkanethiols on gold (111) surface were determined to be ~30°, ~55°, and ~14°, respectively, confirming their well-oriented, standing up conformations.

Why gold is so popular. Although the metal-sulfur interaction were also reported for silver, copper, mercury and palladium, their affinity with alkanethiols are not as strong as gold; there are even more controversies regarding the structure and lattice arrangement of alkanethiolate SAMs formed on these metals.[135,160] Besides the strong interaction with sulfur, the choice of gold as a standard substrate material for preparing SAMs is also attributed to its chemical inertness (does not react with most chemicals under ambient conditions)[161] and other intriguing advantages. First, there are many types of commercially available gold substrates, particularly the fabrication of gold thin films on low-cost materials (e.g., mica, silicon, glass) is easy via physical (sputtering, evaporation)/chemical vapor depositions, flame annealing, or electrochemical deposition. Second, SAMs on gold surfaces can be conveniently patterned by using lithography, chemical etchants, microcontact printing (μCP), or other microscopic techniques.[145,162,163] Third, the desirable electrical[164] and optical properties[165] of gold enable it to be used as a robust supporting material for various characterization and analytical techniques (e.g., as

electrode for electrochemical study, as efficient quencher for fluorescent study, as reflective substrate for Raman and IR spectroscopy). Moreover, gold has adequate biocompatibility for biomedical / pharmaceutical applications (e.g., living cells can adhere to gold surfaces without losing their biological functionality).[166]

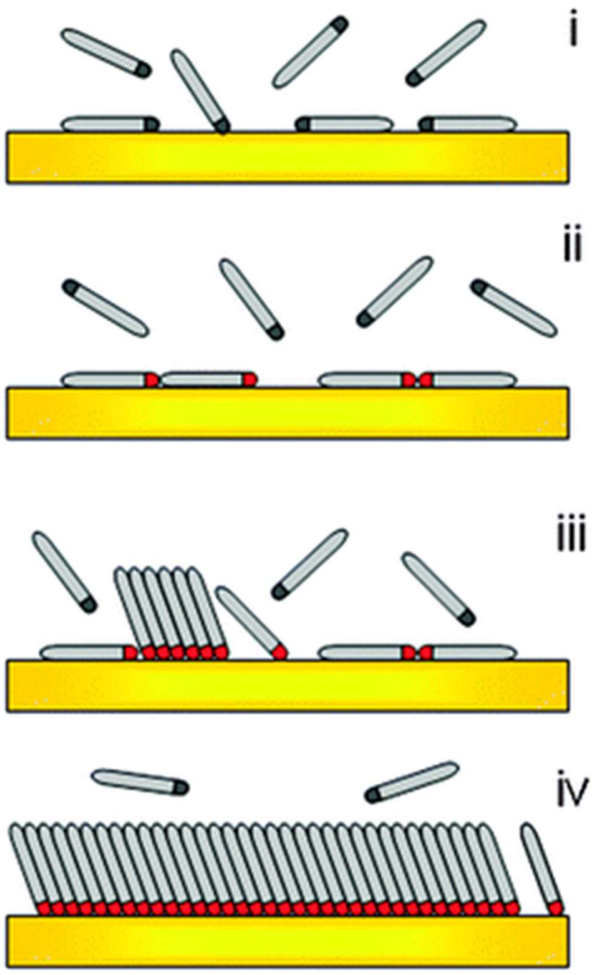

Figure 1.10. Schematic view of the step-by-step formation process of alkanethiolate SAMs on gold: (i) physisorption, (ii) lying down phase formation, (iii) nucleation of the standing up phase, (iv) completion of the standing up phase.

Note: Reprinted with permission from Ref. 155. Copyright (2010), *Royal Society of Chemistry*.

Formation kinetics of alkanethiolate SAMs on gold. As illustrated in Figure 1.10, the spontaneous formation process of alkanethiolate SAMs on gold involves several steps. The initial step starts with a combination of fast physisorption and chemisorption process

(i and ii in Figure 1.10) occurred in just a few minutes, resulting in the formation of low-density SAMs with mostly flat/lying down alkanethiols on gold (the so-called striped phase) as revealed by elliposometry, IR, and STM characterizations.[153-155] The STM characterizations also confirmed that at such a low-density phase there is large fraction of $m \times \sqrt{3}$ (m = 4, 22, 23, 11.5, etc.) lattice arrangement alkanethiols on gold (111) surface with "RS-Au(I)-SR" type of bonding existed (i.e., two alkanethiols are bridged by an Au adatom of +1 oxidation state).[150,151,155] The initial step is followed by a much slower (hours to days) transition process (iii and iv in Figure 1.10) from low-density to high-density phase with standing up alkanethiols on gold; and this process is mainly governed by the competition between the "alkane chain-gold surface" interactions and the "alkane chain-alkane chain" interactions.[155] It is believed that the formation of alkanethiolate SAMs on gold from gas or liquid phase follows the similar manner; however, the stripped phase is difficult to identify when in the liquid phase.[134]

Factors affecting the SAM quality. It should be noted that both the kinetic process and the final structure of alkanethiolate SAMs on gold can be affected by both intrinsic and extrinsic factors. The extrinsic factors such as the length[167-169] and concentration[170] of alkanethiol, cleanliness of gold substrate,[177] as well as the type of solvent,[171,172] temperature[173] and incubation time[174] used in the assembly process are usually controllable. Previous studies have confirmed that high-quality SAMs on gold (high surface density with standing up orientation and crystalline structure) can be reproducibly prepared by immersing a thoroughly cleaned gold substrate (e.g., by using hot piranha solution — a mixture of 96% H_2SO_4 and 30% H_2O_2 with a v/v ratio of 3:1)[160,177] in millimolar concentrations of alkanethiols in deoxygenated ethanol solution ($\geq$ 95%) for 12-18 hours at room temperature.[174-175] In comparison, the inappropriate assembly conditions (e.g., uncleaned gold substrate with physiosorbed organic contaminations, low concentration of alkanethiols, high concentration of impurities, too short or too long assembly time, non-deoxygenated solution) would lead to SAMs with low surface density and large fraction of defects (e.g., pinholes, collapsed or stripped domains).[134] Compared with short alkanethiols, longer alkanethiols with stronger intermolecular van der Waal forces usually have a slower assembly process (characterized by XPS)[168] but a more ordered crystalline structure at the equilibrium state (characterized by IR, ellipsometry, and ET kinetic study).[147,148,167] More interestingly, the orientation of longer alkanethiolate SAMs on gold also shows an obvious "odd-even" effect (e.g., larger tilt angle and less hydrophobic surface observed for alkanethiolate SAMs with odd number of methylene groups).[134, 228]

Besides using alkanethiols (R-SH), alkanethiolate SAMs on gold can be also prepared with alkylsulfides (R-S-R) or alkyldisulfides (R-S-S-R), but they usually lead to poor SAM quality which is possibly due to their lower solubility and inefficient adsorption on gold.[134]

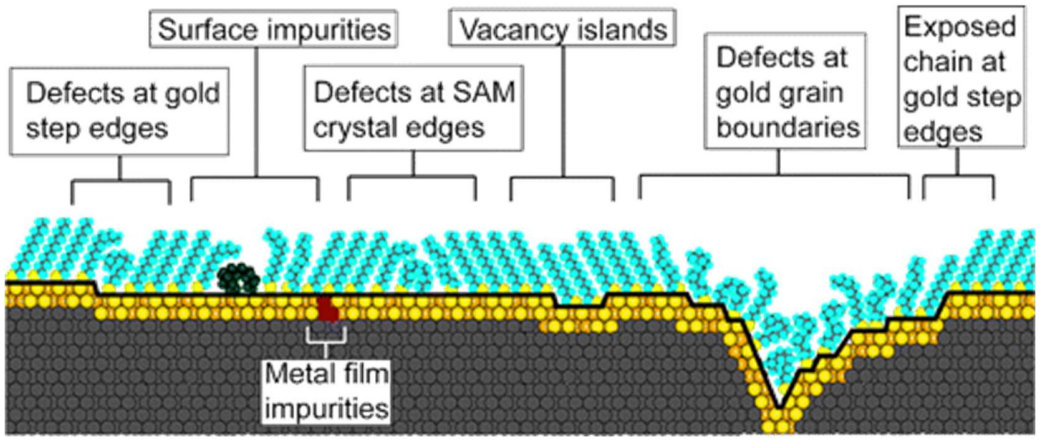

Figure 1.11 Schematic illustration of representative intrinsic and extrinsic defects found in SAMs formed on polycrystalline gold substrate.
Note: Reprinted with permission from Ref. 134. Copyright (2005), *American Chemical Society*.

As of many existing intrinsic factors, the real structure of alkanethiolate SAMs is more complex than the ideal case illustrated in Figure 1.8. The most common intrinsic factor is the polycrystalline gold substrates which have dense arrangement of low-index crystallographic facets (e.g., 110, 100), irregular textures (e.g., grain boundaries, step edges, atomic vacancies), and heterogeneous degree of surface roughness. These in turn bring in defects and heterogeneous structural domains to the ideal crystalline structure of alkanethiolate SAMs on gold,[176-180] as displayed in Figure 1.11.[134]

"Mixed" SAMs. Many applications of alkanethiolate SAMs require well dispersed functional terminal groups on surface in order to achieve the Langmuir-type interfaces. A simple and efficient way to approach this while maintaining the high density and crystalline structural features is to prepare mixed SAMs, where the functionalized alkanethiol (R'-SH) is diluted by another alkanethiol (R-SH) on gold surface.[181,182] Currently there are three different ways to prepare mixed SAMs: the first one is by co-adsorption from mixed assembly solution containing both functional and diluent alkanethiols (R'-SH and R-

SH);[183,184] the second one is based on the adsorption of asymmetric disulfides (R-S-S-R') or dialkysulfides (R-S-R');[185,186] the last one is by using the post-assembly exchange method (i.e., immersing the pre-assembled single-component alkanethiolate SAMs on gold in another alkanethiol solution, where the exchange process takes place at the defect sites of the original SAM).[187] However, it was found that different methods may result in distinct distributions of functional terminal groups on mixed SAMs;[188] the structure and composition of mixed SAMs also strongly depend on the molar ratio between the two alkanethiols in the mixed co-assembly solution,[182,183,188] the time of exchange process,[187] the polarity of the terminal groups,[183] and chain lengths,[175] which determine whether the self-assembly process is more thermodynamically or kinetically controlled. Additionally, the mixed alkanethiolate SAMs allow for easy patterning of gold surface through selective desorption of shorter alkanethiols at certain electrode potential.[134]

The observation of segregated domains in mixed SAMs, the thiol exchange process, as well as the above-mentioned transition process (from striped phase to high density phase) during the formation of single alkanethiol SAMs on gold are all strong experimental evidences indicating the dynamic nature/mobility of gold-sulfur interaction, which makes it distinctive from traditional covalent-type bonding.

1.2.2. Redox-active alkanethiolate SAMs on gold

The considerably evolved knowledge and understanding of alkanethiolate SAMs on gold are owing to the adaptation of various surface characterization techniques.[189] Specifically, convenient wetting studies based on water contact angle measurements help evaluate the surface energy of alkanethiolate SAMs on gold, which provide general information about their packing density, chemical composition, and degree of structural organization.[175,190] The microscopic techniques, mainly STM and AFM, are widely used characterization tools for exploring the atomic level structure of alkanethiolate SAMs on gold;[154,176,178,179] however, the interpretation of microscopic results is intrinsically limited by surface roughness and heterogeneity across large length scales. In addition to microscopic techniques, the characterizations of alkanethiolate SAMs were also widely conducted with various electronic (e.g., XPS)[168-170,183] and vibrational spectroscopies (e.g., FTIR, Raman spectroscopy),[169,174,184] and various reflection/diffraction techniques based on X-ray, atomic beam, or electron beam.[191-193] These techniques provide multiple information on the overall packing density, composition, stability, thickness, type and

degree of crystalline arrangement of alkanethiolate SAMs on gold. Other frequently used characterization methods include ellipsometry (evaluating the thickness of organic thin film by measuring the change on the polarization of light),[170,194] optical deflection cantilever (measuring surface stress),[154] as well as theoretical simulations based on DFT[195,196] and MD.[197,198]

Besides above mentioned methods, electrochemical techniques are also powerful tools for characterizing alkanethiolate SAMs on gold owing to their intrinsic advantages of simplicity (less sophisticated instrument), sensitivity, rapidity, and low cost.[204] Furthermore, in terms of electrochemical analysis the gold substrate is an excellent working electrode because of its good conductivity and chemical inertness within the usually adopted potential range in electrochemical studies. The earlier electrochemical characterizations of alkanethiolate SAMs on gold were carried out with redox species in solution phase.[167, 200-202] From their CV redox peak currents and potentials,[200, 202] their ET rate constants,[167] and the non-Faradic charging current responses, the structure of alkanethiolate SAMs (e.g., packing density, degree of defects, and orientation) can be conveniently evaluated.[203, 204]

In order to avoid the influence of mass transport process in solution (mainly diffusion process) on electrochemical analysis,[204] the electroactive alkanethiolate SAMs with redox-active terminal groups have been fabricated and widely studied in past two decades.[203] Benefiting from the redox responses of adsorbed redox couples, more quantitative information can be obtained for characterizing alkanethiolate SAMs since the surface redox response (especially the CV response) can be readily analyzed with various electrochemical theories and models (see chapter 2 for details), by which many parameters related to the physical and chemical properties of alkanethiolate SAMs can be determined. Besides electrochemical characterization, an important application of electroactive alkanethiolate SAMs is the study of long-range ET kinetics, where many important kinetic parameters can be determined, such as ET rate constant, tunneling constant, and electronic coupling coefficient for SAMs.[208,209] In addition, redox-active alkanethiolate SAMs also promote the design and fabrication of electronic devices, such as biosensors;[134,141] whose redox responses can be amplified by adding solution-diffused redox species through the recitification effect (irreversible mediated ET process).[295]

1.2.3. Ferrocene (Fc)-terminated alkanethiolate SAMs on gold

Ideally, redox couples used in electrochemical studies should fulfill the following requirements: (1) highly reversible redox behavior with small inner-sphere reorganization energy (no chemical bond formed/broken); (2) high solubility and stability in the electrolyte solution of choice; (3) easy accessibility; (4) the reduction potential lies within the potential range of -0.5 to 0.5 V where redox processes associated with the electrolyte solution (e.g., oxidation and reduction of water), atmospheric species (e.g., reduction of O_2), and the electrode material (oxidation of gold) are negligible. Based on above requirements several coordinative transition metal complexes (e.g., $K_3Fe(CN)_6$, $Ru(NH_3)_6Cl_3$) and organic compounds (e.g., methylene blue, MB) are popularly applied redox-active species. Fc as a nonpolar organometallic compound also fulfills most of the above requirements.[205] Although Fc is poorly soluble in aqueous solution, there has been many commercially available Fc derivatives with much improved water solubility (e.g., Fc-$(CH)_2$-OH, Fc-COOH, Fc-NH_2). Moreover, Fc is also the most widely used redox molecule as the terminal group of electroactive alkanethiolate SAMs since the thiolated Fc derivatives are easily accessible via the common Friedel-Crafts synthetic approach.[206,207] Another particular property of Fc is its different charge in reduction (neutral Fc) and oxidation state (positively charged ferrocenium cation, Fc^+). As a result the redox thermodynamics and kinetics of Fc^+/Fc couples are very sensitive to the local environmental factors (e.g., dielectric properties of solvent medium, ionic strength, and type of supporting electrolyte).

By using ferrocenylalkanethiolate SAMs on gold as trial system, we and others have performed intensive electrochemical characterizations on electroactive SAMs, not only to complement other surface characterization techniques, but also provide additional information regarding the structure and property of alkanethiolate SAMs. As mentioned in section 1.2.1, the polycrystalline arrangements and different degree of roughness of gold surfaces are intrinsic limiting factors that lead to “nonideal”, heterogeneously structured alkanethiolate SAMs. This has been clearly demonstrated by the significantly varied CVs of ferrocenyl-1-undecanethiolate (FcC11S-) SAMs formed on different types of gold substrates (polished gold disk, annealed gold bead, and evaporated gold film),[239, 296] as shown in Figure 1.12.

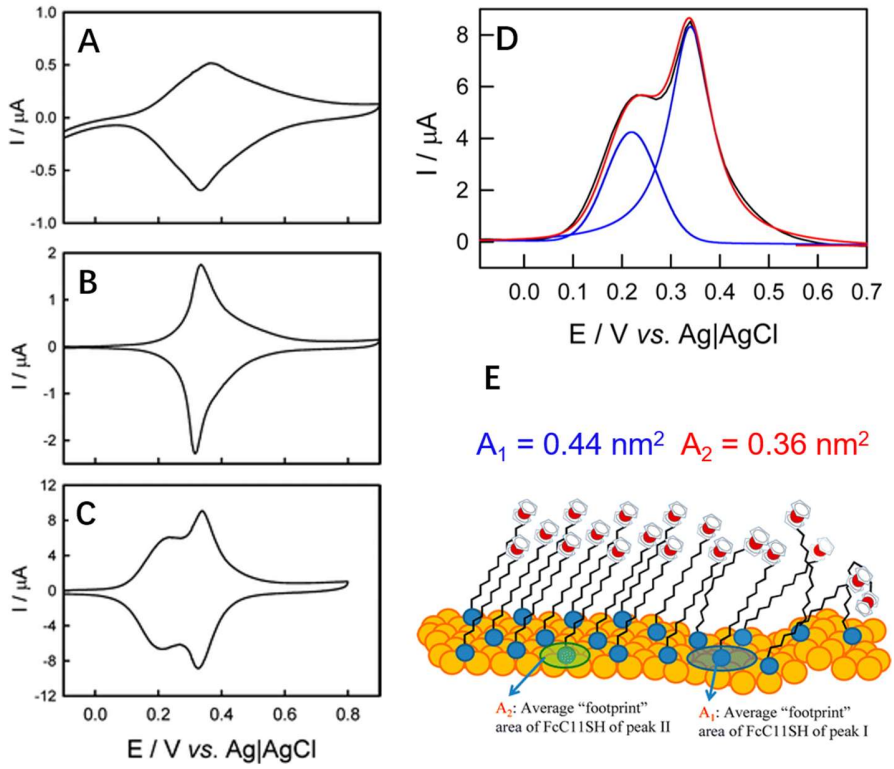

Figure 1.12. CVs of single-component FcC11SH SAMs on (A) mechanically polished gold disk electrode, (B) annealed Au bead electrode, and (C) evaporated gold film on glass; the supporting electrolyte is 1.0 M $HClO_4$, and the scan rate is 50 mV/s. (D) The anodic trace of CV and its respective two deconvolution peaks for the FcC11S-Au SAM formed on evaporated gold film. (E) Schematic view of the proposed orientations and footprint areas in the two different structural domains of FcC11S-Au SAM.

Note: Reprinted with permission from Ref. 239. Copyright (2013), *American Chemical Society.*

We have also conducted an in-depth investigation on the single-component FcC11S- SAM formed on thermally deposited polycrystalline gold film of a planar surface with large fractions of Au (111) lattice. As displayed in Figure 1.12 (C), its CV shows obvious splitting with two peaks observed at lower and higher potentials, which is consistent with others' studies.[213, 214, 296] By integrating the total amount of Faradic charges transported across the electrode-solution interface, the Fc surface densities (Γ_{Fc}) of this FcC11S-Au SAM and other previously reported single-component ferrocenylalkanethiolate SAMs were determined based on the Faraday Law.[213, 214, 239, 296] These results are all similar to the theoretical value (4.6×10^{-10} mol/cm^2) calculated for

closely-packed Fc (treated as sphere with a diameter of 6.6 Å) on a planar surface.[214] The findings above reveal the heterogeneous structural domains even for the densely-packed alkanethiolate SAMs on gold; and the origin of the split CV responses of the Fc terminal groups have been investigated for more than two decades; it is generally accepted that the two peaks located at different potentials are originated from the closely-packed domain with more ordered structure (standing up orientations) and relatively loosely-packed domain with less ordered structure, respectively.[213, 214, 296] For the first time, we have provided the experimental evidence based on conventional CV studies:[239] By deconvoluting the split CV response (as shown in Figure 1.12 D) and quantifying the area contribution from individual CV redox peaks (based on the Gaussian-Lorentzian deconvolution method[213]), it was found that for the single-component FcC11S-Au SAM, the areas occupied by each alkanethiol in the two structural domains are differed by ~20% (0.36 vs. 0.44 nm^2, as indicated in Figure 1.12E). More importantly, as shown in Figure 1.13, upon treating the FcC11S-Au SAM with increasing amount of small organic molecules (nitrobenzene or 1-octanol) in the electrolyte solution, the CV peak at lower potential becomes narrower and sharper while the peak at more positive potential is barely influenced; the theoretical simulation of the peak shape (based on the Frumkin isotherm to determine the intermolecular interaction parameter, $vg\theta_T$[204,219]) also revealed a transition of the intermolecular interaction associated with Fc terminal groups from repulsive to attractive. These results strongly confirmed the relatively loosely packed structural domain corresponding to the CV peak at lower potential, since it can be easily "disturbed". According to a recent study conducted by Nijhuis and co-workers,[297] the distinct CV redox peaks of different structural domains of ferrocenylalkanethiolate SAMs on gold are affected by various environmental factors (e.g., different dielectric media and distributions of ions around Fc^+/Fc terminal groups in loosely and closely packed structural domains) and multiplex intermolecular interactions associated with Fc terminal groups (Fc-Fc, Fc-alkyl chain, Fc-gold interactions).

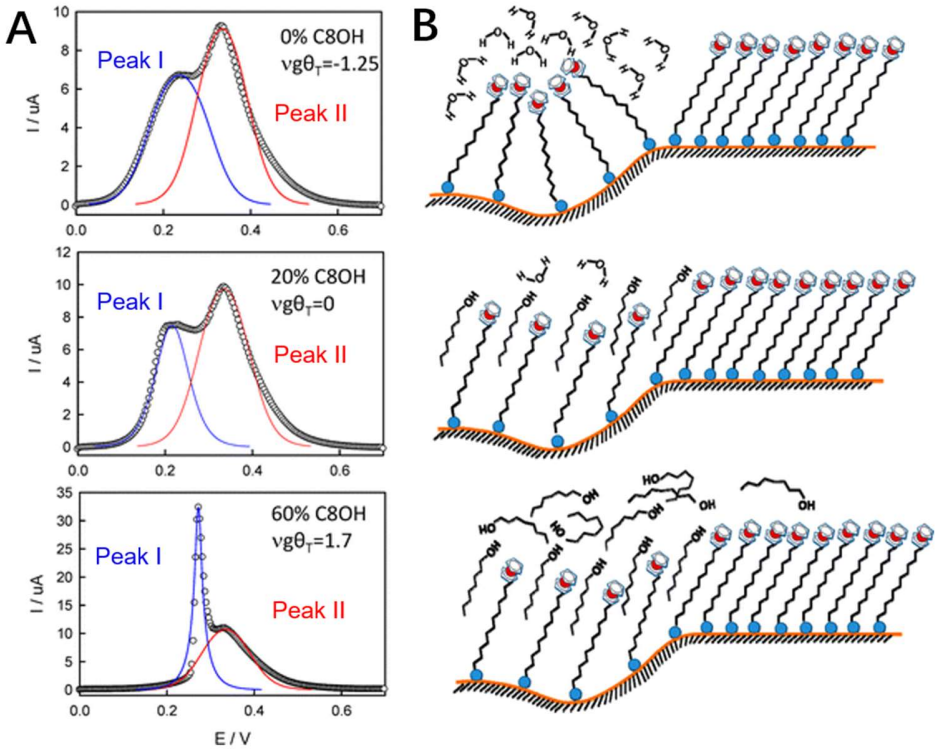

Figure 1.13. (A) Experimental CV anodic wave (open circles) and its simulated (solid lines) *i-E* curves of FcC11S-Au SAMs in 1.0 M $HClO_4$ aqueous solution with various saturation percentages of 1-octanol (C8OH); the saturation percentages of C8OH and the fitted interaction parameters ($vg\theta_T$) for peak I are indicated. (B) Hypothetic structures of FcC11S-Au SAM in electrolyte solution containing different saturation percentages of C8OH.

Note: Reprinted with permission from Ref. 239. Copyright (2013), *American Chemical Society.*

In order to minimize the influence of structural heterogeneity on the redox response of Fc terminal groups, the mixed ferrocenylalkanethiolate / alkanethiolate SAMs have been widely adopted in many studies and applications. Based on the readily determined Γ_{Fc}, the influences of many factors on the thermodynamics and kinetics of mixed alkanethiolate SAMs prepared by co-adsorption or post-assembly exchange methods (described in section 1.2.1) have been investigated. For example, by comparing the mole fraction of FcC6SH in mixed FcC6S-/CnS-Au SAMs (n = 4 to 10) on surface and in the binary assembly solutions, Rowe and Creager discovered the preferential adsorption of relatively longer alkanethiols in the co-assembly process, which manifest primarily during the initial competitive adsorption stage. This can be attributed to the incremental change of

adsorption free energy per methylene group unit, which is also influenced by the type of solvent used in the assembly solution (-1.9 kJ/mol in ethanol and -0.8 kJ/mol in 1-hexanol solution).[240] By monitoring Γ_{Fc} as a function of assembly time, the formation kinetics of mixed alkanethiolate SAMs prepared by post-assembly exchange method can be readily studied;[238, 298] moreover, the level and type of defects in alkanethiolate SAMs can be evaluated by examining the rate of exchange of ferrocenylalkanethiols (more and larger scaled SAM defects lead to faster exchange rates) and their distributions in the mixed SAMs (characterized by CV or STM).[213]

Our group previously explored the distinct structures of mixed alkanethiolate SAMs prepared by two different methods.[188] As shown in Figure 1.13, by examining the CVs of Fc terminal groups in mixed FcC11S-/C11S-Au SAMs prepared by either co-adsorption or post-assembly exchange, it was found that they eventually end up with mixed SAMs of similarly low Fc surface densities (5.5×10^{-11} mol/cm^2 and 5.7×10^{-11} mol/cm^2). However, the mixed SAM produced by the latter method has a pair of broadened CV redox peaks (with more negative fitted $vg\theta_T$ from -0.40 to -0.98) located at a more positive potential (from 179 mV to 251 mV). These CV findings indicate that the co-adsorption method may result in mixed SAMs with more isolated and less interacting Fc terminal groups;[214] whereas, the post-assembly exchange method may lead to mixed SAMs with clustered and buried Fc terminal groups, and therefore the stronger intermolecular interactions among them.

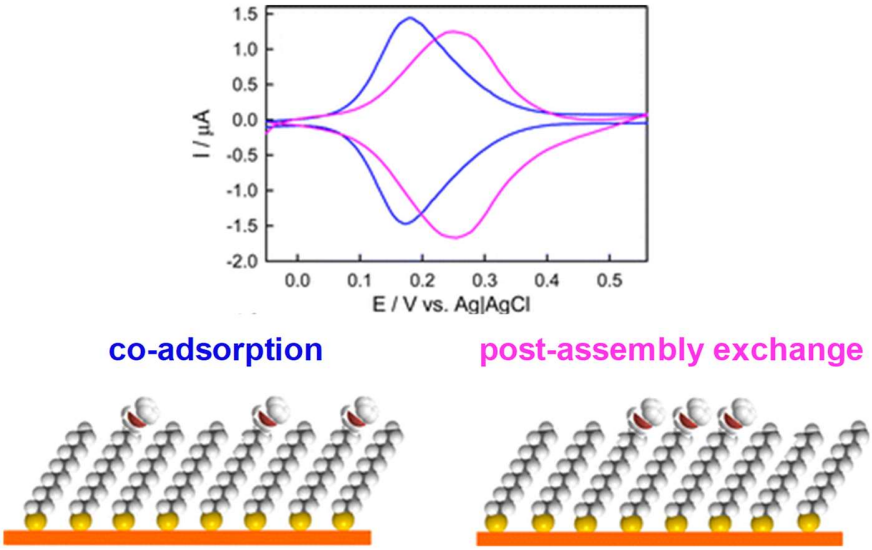

Figure 1.14. Top: CVs of FcC11S-/C11S-Au SAMs prepared by coadsorption (immersion of gold thin film in 1.0 mM mixed FcC11SH/C11SH assembly solution containing 10% mole fraction of FcC11SH) (blue curve) and postassembly exchange (immersing the pre-assembled single FcC11S-Au SAM in a 1.0 mM C11SH solution for 20 h) (pink cruve). Bottom: Schematic view of the proposed structure of mixed FcC11S-/C8S-Au SAM prepared by the two methods.

Note: Reprinted with permission from Ref.188. Copyright (2014), *American Chemical Society.*

Owing to its significantly different charge states at reduced (0) and oxidized form (+1), the redox equilibrium of Fc terminal group on alkanethiolate SAMs is very sensitive to their local environmental conditions. By measuring the CV formal potentials of mixed ferrocenylalkanethiolate SAMs prepared with different lengths of diluent alkanethiols,[215] or in electrolyte solutions with different solvents and ions,[215-218, 268, 299] it was found that the oxidation of Fc terminal group to ferrocenium (Fc^+) is thermodynamically more favored (as indicated by the negative formal potential shifts) in high dielectric aqueous medium with high concentration of hydrophobic anion, such as ClO_4^-. This has been interpreted with various interfacial thermodynamic models (e.g., solvation model,[215] interfacial double layer model,[215] ion pairing model[217]) derived from the fundamental Nernst equation.[149, 203] It should be noted that in real situation various influencing factors are strongly coupled to each other (e.g., the anion pairing behavior of Fc^+ terminal group is strongly affected by the dielectric property of solvent medium),[216, 268] thus the reason behind the changes in CV formal potential could be far more complicated and it requires future efforts to quantify

each influential factor and to develop combined theoretical models.[215] Based on the CV formal potential of Fc^+/Fc terminal groups, the mixed ferrocenylalkanethiolate SAMs can be employed for electrochemical sensing, such as determining the amount of anionic surfactants in electrolyte solution.[300, 301]

In addition to redox thermodynamic study, the mixed ferrocenylalkanethiolate SAMs as the most organized and easily controllable molecular interfaces have been extensively used for investigating long-range ET kinetics. Particularly, the heterogeneous distribution of ET kinetics can be minimized with highly diluted Fc^+/Fc redox centers on surface (more specifically described in chapter 4).

1.3. Thesis scope and structure

As mentioned in section 1.1.4., gaining further fundamental understanding on the binding behavior of the exceptional supramolecular Fc@CB[7] host-guest recognition pair formed at interface will certainly help guide and promote its future applications. Unfortunately, due to the previously described limitations, the two common interfacial Fc@CB[7] host-guest binding systems based on the directly deposited CB[7] monolayer and the covalently immobilized CB[7] (as shown in Figure 1.6) are not ideal for conducting extensive fundamental binding studies. Instead, it requires an easily-accessible, highly-stable, and well-organized “Langmuir-type” molecular interface. As introduced in section 1.2, the mixed-component and redox-active ferrocenylalkanethiolate SAM on gold should be the most ideal interfacial system for this purpose. This includes the strong gold-thiol interaction, the highly-organized alkane chains, the well dispersed and exposed Fc terminal groups (as the CB[7] binding site), as well as the easy and convenient preparation of ferrocenylalkanethiolate SAMs on gold (no synthetic work is needed with commercially available ferrocenyl and diluent alkanethiols). Moreover, for fundamental binding studies the functionalization of CB[7][117] is no longer needed with Fc guests immobilized on surface.

In chapter 2, surface characterization techniques used in this thesis research including electrochemistry, Frontier transform infrared spectroscopy, and contact angle measurements are introduced. In chapter 3, fundamental studies regarding the thermodynamics and kinetics of Fc@CB[7] host-guest binding on mixed ferrocenylundecanethiolate/octanethiolate SAM on gold were conducted by examining its CV responses before and after incubation with CB[7], which forms the basis of understanding host-guest binding at organized molecular interfaces. From chapter 4 to

chapter 6, different applications of interfacial Fc@CB[7] host-guest binding were explored, including its use as a molecular probe for the structural heterogeneity of redox-active alkanethiolate SAMs, as an environmental regulator of interfacial long-range ET process, and as a competitive binding platform for developing the general electrochemical assay for host-guest complexations between CB[7] and drug molecules of interest in pharmaceutical science. Major findings and highlights, as well as future work and prospective (including the idea of adapting this new Fc@CB[7] host-guest binding system for fabricating well-controlled electrochemical biosensors) are presented in chapter 7.

Chapter 2. Methods and techniques

2.1. Electrochemical methods

2.1.1. Cyclic voltammetry (CV)

As described in section 1.1 and 1.2, owing to the operational simplicity and the ability to offer multiple quantitative information, CV is the most popular and powerful electrochemical technique for studying Fc@CB[7] host-guest binding in solution[113-115] and on electrode surface,[123] as well as the redox-active ferrocenylalkanethiolate SAMs formed on electrode surface. Typically, CV measures the current generated by an electrochemical system in response to a cycle of linearly scanned potential as shown in Figure 2.1 (A). For electroactive couples (O and R) in solution, their CV oxidation and reduction peaks usually have a "duck" shape as shown in Figure 2.1 (B), which is governed by both of their redox reaction (e.g., electron transfer) near the electrode-solution interface (origin of the initial rapid current spike) and their diffusion process across a linear concentration gradient from bulk solution to interface (the gradually decreased current response after peak is caused by the enlarged diffusion region). The formal potential ($E^{o\prime}$) of a redox couple can be determined from the average of CV oxidation (E_{pa}) and reduction peak potentials (E_{pc}), as expressed by equation 2.1:[199, 204]

$$E^{o\prime} = \frac{(E_{pa} + E_{pc})}{2} \qquad (2.1)$$

For completely reversible redox processes their redox equilibrium can be described by the Nernst equation, as expressed by equation 2.2,[199, 204]

$$E = E^{o\prime} + \frac{RT}{nF} ln\left(\frac{[O]}{[R]}\right) \qquad (2.2)$$

where F is Faraday's constant (96485.33 C/mol), E^o is the standard reduction potential; R is the universal gas constant (8.314 J mol^{-1} K^{-1}), n is the number of electrons involved in the redox process, T is the temperature, [O] and [R] are the concentrations of the oxidized and reduced form of an electroactive couple. For highly reversible redox process in solution, its CV anodic and cathodic peaks have a separation (ΔE_p) close to $57/n$ mV at room temperature; such a "delay" is caused by the diffusion of redox couple to and from

the electrode surface. For quasi-reversible and non-reversible redox process (slower ET kinetics) their CVs have even larger peak separations.

The scan rate (v) of CV controls how fast the applied voltage is changed. For diffusion-controlled redox process at solution-electrode interface, the faster scan rates result in narrower diffusion layer and stronger current response. A linear relationship is usually observed between the CV peak current (I_{pa} or I_{pc}) and the square root of scan rate ($v^{1/2}$), which can be described by the well-known Randle-Sevcik equation, as expressed by equation 2.3:[199, 204]

$$I_p = 0.446nFAc\left(\frac{nFvD}{RT}\right)^{1/2} \qquad (2.3)$$

where c and D are the concentration and diffusion coefficient of the redox couple; A is the electrode area. By fitting the experimentally measured relationship between I_p and $v^{1/2}$ with Randle-Sevcik equation, it is able to tell whether an electroactive couple is freely diffusing in solution; besides, the diffusion coefficient (D) of the electroactive couple can be determined from the slope of the best linear fitting, the known concentration of redox couple, and the real electrode area.

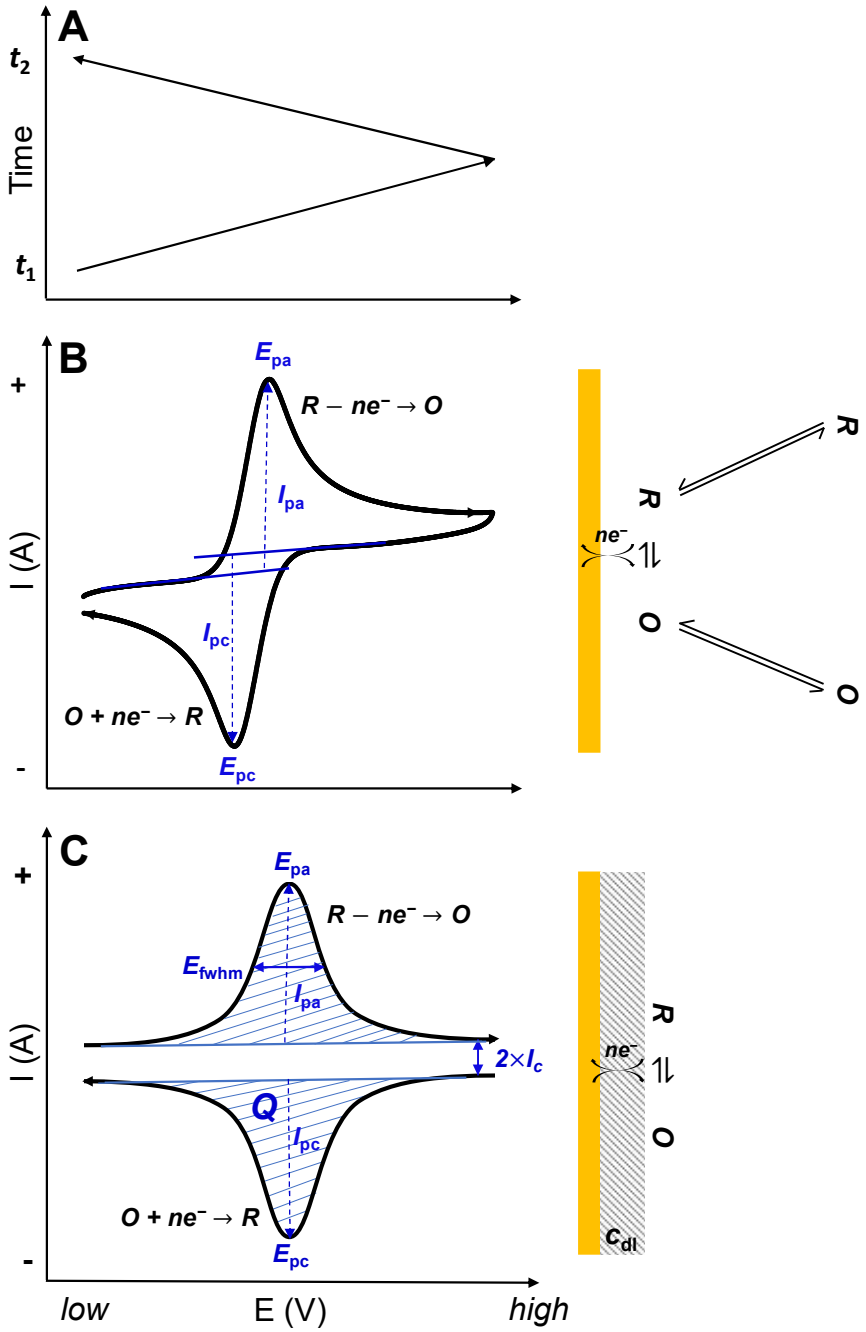

Figure 2.1. **(A) Potential profile as a function of time for a typical CV measurement. (B) A typical CV of solution-diffused redox process. (C) A typical CV of adsorbed redox process; the shaded region in CV represent the integrated redox peak area. The arrows on these CVs indicate the direction of potential scan.**

For electroactive couples adsorbed on an electrode surface, such as the Fc^+/Fc terminal groups of alkanethiolate SAMs (discussed in section 1.2.3), their CV responses are only governed by the interfacial redox process, and thus have significantly different CV characteristics compared to the "duck" shaped CV of solution-diffused redox process. More importantly, without the interference from mass transport process, the CV of adsorbed electroactive couples is much easier for theoretical modeling, which provide substantial quantitative information about the electrochemical system studied.

Figure 2.1 (C) shows a typical CV response of an adsorbed redox process, which has a symmetric pair of oxidation and reduction peaks with no separation between them ($\Delta E_p = 0$). The symmetry is owing to the high reversibility of the adsorbed redox process; that is, at any scanned potential the redox process is fast enough to reach Nernst equilibrium state (as described by equation 2.2); in other words, the net rate of the redox reaction is zero (same oxidation and reduction rates, $I_{pa} = I_{pc}$). The reversibility of redox process can be affected by using faster potential scan rates (v), which result in enlarged CV peak separations and thus the asymmetric CV responses. By plotting experimentally determined ΔE_p as a function of log v, the kinetics of an adsorbed redox process can be analyzed by fitting this relationship with Laviron model (derived from Bulter-Volmer ET kinetics)[220] or Marcus-type model.[221]

Without the influence of mass transport, the CV peak currents (I_{pa} and I_{pc}) shown in Figure 2.1 (C) can not be described by Randle-Sevcik equation; instead, they are directly proportional to scan rate (v). The total amount of Faradic charges (Q) transported from the adsorbed redox couples to electrode during the entire ET process can be determined by integrating the area under CV oxidation or reduction peak (blue shaded region), which can be further used to calculate the surface density (Γ) of adsorbed redox couples, as expressed in equation 2.4:[199, 204]

$$Q = nFA\Gamma \qquad (2.4)$$

The potential (E) of an electrochemical cell directly indicates the free energy change (ΔG) of its redox reaction, which is described as:[149]

$$\Delta G = -nFE \qquad (2.5)$$

In CV, the redox thermodynamics of adsorbed electroactive couples is usually studied from its CV formal potential (or peak potentials if the redox process is highly reversible); the positive and negative formal/peak potential shifts indicate whether a redox process is

thermodynamically more or less favored, which is strongly related to various environmental factors. In some cases, the split CV redox responses were observed,[213-214, 239] which indicate the co-existence of adsorbed redox couples in different thermodynamic states/environments.

Besides the driving force information obtained from the redox potential, the intermolecular interactions among the adsorbed redox couples can be indicated from the width of their CV redox peaks.[204, 219] These are usually studied by fitting the experimental CV peaks with simulated *i-E* curve derived from the Frumkin adsorption isotherm, as expressed by equation 2.6 and 2.7: [204, 219]

$$i = \frac{n^2F^2Av\Gamma_T}{RT}\left[\frac{f(1-f)}{1-2vg\theta_T f(1-f)}\right] \quad (2.6)$$

$$n(E-E_P) = \frac{RT}{F}\left[\ln\left(\frac{f}{1-f}\right) + vg\theta_T(1-2f)\right] \quad (2.7)$$

where Γ_T is the total surface density of adsorbed redox couples; E_p is the CV peak potential; θ_T is the total surface coverage of the redox centers; f is defined as the mole fraction of the oxidized redox centers (θ_O/θ_T) under a certain potential; g describes the intermolecular interaction among their oxidized (O) and reduced forms (R), which has a more specific definition as described by equation 2.8:[204, 219]

$$g = a_O + a_R - 2a_{OR} \quad (2.8)$$

where a_O, a_R and a_{OR} are the interactions among oxidized forms, reduced forms, and between the two of them, respectively. The positive and negative values of a_i indicate the attraction and repulsion forces, respectively. The overall term $vg\theta_T$ in equation 2.6 and 2.7 is defined as the intermolecular interaction parameter. In the theoretical *i-E* curve, the full width at the half of maximum current (E_{fwhm}) is strongly correlated with $vg\theta_T$, which is described by equation 2.9 and 2.10:[204, 219]

$$E_{fwhm} = \frac{2RT}{nF}\left|ln\frac{1+\beta}{1-\beta} - vg\theta_T\beta\right| \quad (2.9)$$

$$\beta = \frac{\sqrt{2-vg\theta_T}}{\sqrt{4-vg\theta_T}} \quad (2.10)$$

According to equation 2.9 and 2.10, an ideal Langmuir type adsorbed redox couples (i.e., no intermolecular interaction) have a E_{fwhm} of 90.6/n mV ($vg\theta_T = 0$); the narrower or wider

peak width than this value indicate the overall attraction ($vg\theta_T > 0$) and repulsion forces ($vg\theta_T < 0$) among the adsorbed redox couples.

The non-Faradic charging current (I_c) between the CV redox peaks (I_c can also be measured from the CV of redox-free electrolyte solution) can be used to determine the interfacial double layer capacitance (C_{dl}), as expressed in equation 2.11:[204]

$$C_{\mathrm{dl}} = \frac{I_{\mathrm{c}}}{Av} \qquad (2.11)$$

C_{dl} strongly depends on the dielectric medium of the interfacial double capacitor, which can be simply described by Helmholtz model, as expressed in equation 2.12:[204]

$$C_{\mathrm{dl}} = \frac{\varepsilon\varepsilon_0}{d} \qquad (2.12)$$

where d is the thickness of the dielectric medium that separates the two charged plates of the capacitor, ε and ε_0 are the dielectric constants of the separation medium and vacuum space (In terms of ferrocenylalkanethiolate SAMs, d and ε are strongly related to the composition, structure, and defects of alkane chains[203]).

2.1.2. Chronoamperometry (CA)

Different from the linear or pulse voltammetric techniques where currents are measured under varied potentials, CA is a potential step technique which measures the current output of an electrochemical system in response to a constant potential applied ($E_{applied}$) as a function of time (t). Figure 2.2 (A) and (B) show a typical Faradic CA current (I_f) response of an adsorbed redox couple, which can be described by equation 2.13:[203, 204]

$$I_f = k_{app} Q \exp\left(-k_{app} t\right) \qquad (2.13)$$

According to equation 2.13, a linear decay (as shown in Figure 2.2C) can be expected with the natural logarithm form of faradic current, as expressed by equation 2.14:

$$ln\ (I_f) = ln\left(k_{\mathrm{app}} Q\right) - k_{\mathrm{app}} t \qquad (2.14)$$

where k_{app} is the apparent ET rate constant under certain $E_{applied}$, which can be determined from either the slope or the y-intercept of equation 2.14.

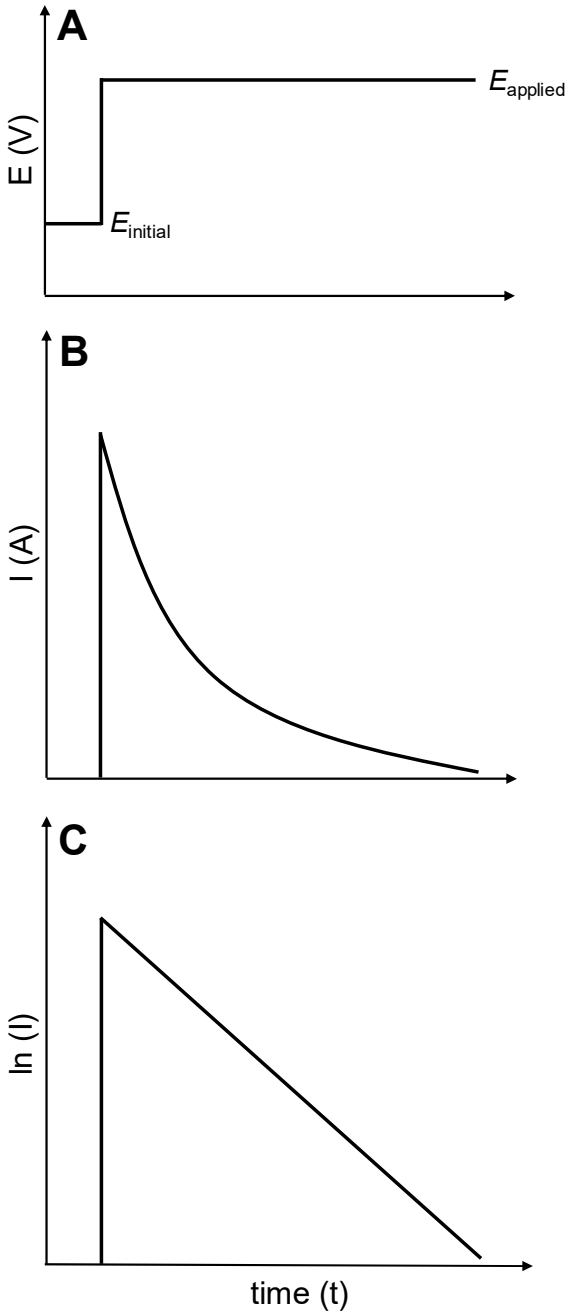

Figure 2.2. (A) Step potential applied in CA. (B) a typical CA Faradic current (I) drop of an adsorbed redox couple. (C) Natural logarithm form of faradic current drop.

By fitting the experimentally measured relationship (Tafel plot) between k_{app} and overpotential (η, as defined by equation 2.15, controls the thermodynamic driving force or

the free energy change of a redox process) with Bulter-Volmer or Marcus-type kinetic models,[203] the important ET kinetic parameters of adsorbed redox couples (standard ET rate constant (k_{et}), reorganization (λ), and electronic coupling factor (H)) can be determined.[203]

$$\eta = E_{applied} - E^{o\prime} \tag{2.15}$$

When applying CA with high $E_{applied}$, two interfering factors need to be considered. One is the stronger charging current (I_c) drop occurring at the initial stage, which could lead to significant deviation from the linear relationship between $\ln(I_f)$ and t as predicted by equation 2.14 (the real current is the sum of I_f and I_c). The other is the large ohmic drop caused by strong current intensity (I), as a result the real potential applied to working electrode could be dramatically smaller than the potential imposed to the electrochemical cell (E_{cell}), as expressed by equation 2.16:[204]

$$E_{applied} = E_{cell} - IR_{sol} \tag{2.16}$$

where R_{sol} is the uncompensated solution resistance that can be determined based on Pouillet's law:[204]

$$R = \frac{1}{\sigma} \times \frac{l}{A} \tag{2.17}$$

where σ is the conductivity of an electrolyte solution, A is the electrode area, and l is the distance between the working and reference electrode (strongly related to the dimension scale of electrochemical cell used).

2.1.3. Electrochemical experimental setup

The electrochemical analysis is usually carried out with a three-electrode cell system consisting of a working electrode (WE), a reference electrode (RE), and a counter electrode (CE),[204] which is illustrated in Figure 2.3. The working electrode is the place where the redox reactions of interest takes place; the reference electrode is a half cell with a known and constant redox potential, which only acts as a reference (no current pass through) to control and measure the potential applied to the working electrode; the counter electrode is used to pass the current needed to balance all currents generated at the working electrode. The three-electrode cell system is connected to a potentiostat, which provides electric power to the system and runs a variety of electroanalytical techniques

(with different ways of voltage output). Figure 2.3 (B) shows a conventional set up of the three-electrode cell system for electrochemical experiments.[199] The electrochemical cell can be a simple glass vial filled with supporting electrolyte solution, and all three electrodes are immersed in electrolyte solution so that a complete electrical circuit can be achieved, as shown in Figure 2.3 (A). A high concentration (≥ 0.1 M) of supporting electrolyte is necessary to ensure a certain level of solution conductivity (i.e., minimize the ohmic drop effect), and neutralize the bias charges formed at the working and the counter electrode. The cap of the glass vial also contains two small holes for deoxygenating the electrolyte solution (by inert gas, such as N_2 or Ar). Moreover, the electrochemical cell is always placed inside a Faraday cage during electrochemical measurements in order to avoid the influences from the environmental electromagnetic fields.

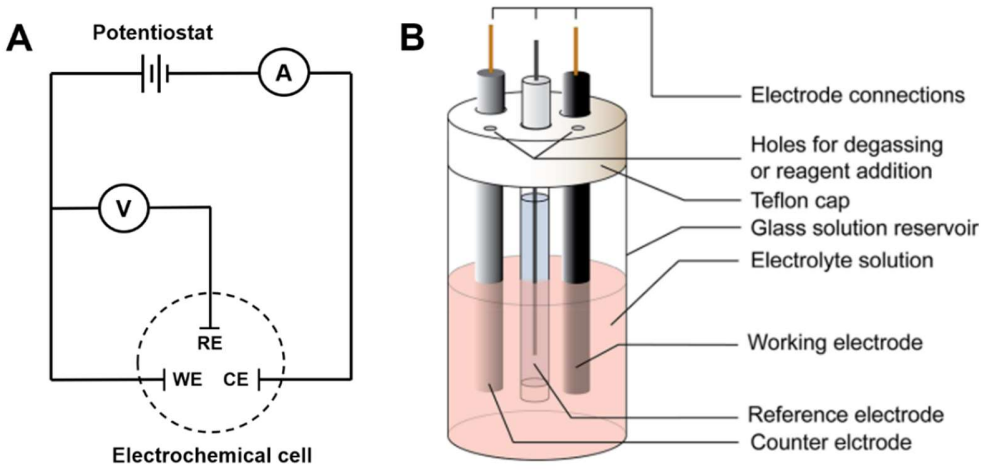

Figure 2.3. Schematic view of (A) the three-electrode electrochemcial detection system and (B) the conventional set-up of electrochemical cell.
Note: (B) is reprinted with permission from Ref. 199. Copyright (2018) *American Chemical Society.*

In this thesis study, all electrochemical measurements were carried out with the three-electrode system and a uniquely designed single-chamber electrochemical cell (fabricated by SFU mechanical shop), for which the details are shown in Figure 2.4. There are two main advantages of this electrochemical cell: First, it allows the use of gold film (physically deposited on glass slide) as a “disposable” working electrode, which is much cheaper than the conventional gold disk working electrode (embedded in a solvent-

resistant and insulating plastic tube, as shown in Figure 2.3B) and does not require the tedious mechanical polish treatment before use. Second, it uses a much smaller volume of electrolyte solution (less than 1 mL) to connect all the three electrodes than the conventional electrochemical cell shown in Figure 2.3 (B), which needs a few milliliters of electrolyte solution.

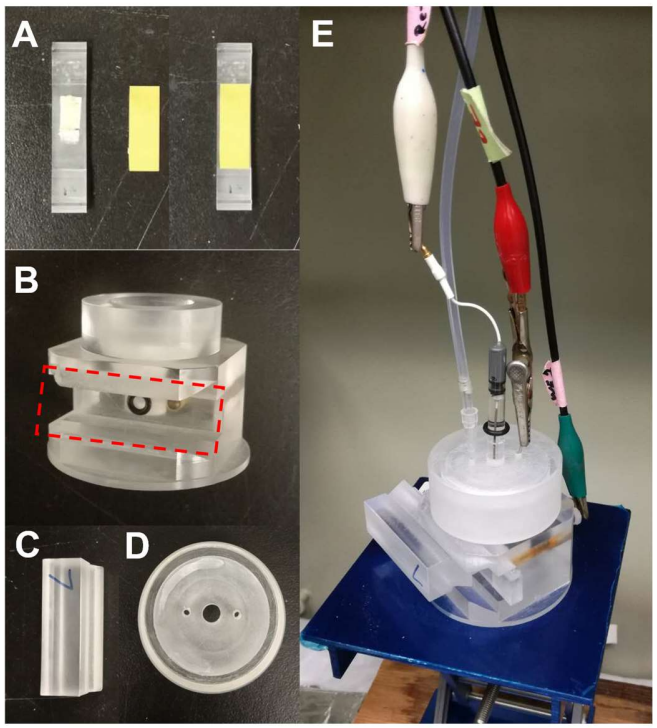

Figure 2.4. Schematic view of the electrochemical cell. It is a single chamber cell made of Plexiglas V-grade acrylic resin consisting of: (A): a holder plate for mounting the working electrode (i.e., a gold slide that has been cut into the proper size). (B): the main body of the cell with an opening on top for adding electrolyte solution, and a side slot (indicated by the red dashed rectangle) for attaching the working electrode. There is a small opening sealed by an O-ring located in the middle of the slot, which defines the geometric area (~ 0.13 cm^2) of gold slide exposed to the electrolyte solution in the cell. (C): a holder to fix the working electrode-mounting plate inside the slot. (D): the cap with three holes of different sizes for inserting Ag/AgCl reference electrode, the Pt counter electrode, and the gas tube line. E shows a photo of the assembled cell that is ready for measurements.

Note: Reprinted with permission from *Anal. Chem.* 2018, 90, 9174-9181. Copyright (2018) *American Chemical Society.* The fabrication of this cell has been patented: Ge, B.; H. Z. Yu. An electrochemical cell designed for sheet-shaped working electrode. CN210720234U, 2020.

In prior to use, the gold film coated glass slide needs to be cut into a small piece (~ 1 × 2 cm^2) so that it fits into the holder plate region shown in Figure 2.4 (B); moreover, it needs to be cleaned by immersing in Piranha solution (3:1 v/v mixture of 96% H_2SO_4 and 30% H_2O_2) for ~10 min at 90 °C (CAUTION: *Piranha solution reacts violently with organics, thus it must be handled with extreme caution*), followed by thorough rinsing with copious amounts of deionized water prior to use. The real area of gold film electrode exposed to electrolyte solution was determined to be (0.15 ± 0.01 cm^2) by measuring and fitting the linear relationship between the CV peak current of 1.0 mM $K_3Fe(CN)_6$ in 1.0 M KCl solution and the potential scan rate with Randles-Sevcik equation (equation 2.3).[204] A platinum wire and a Ag/AgCl wire (immersed in saturated KCl solution) were used as counter and reference electrode throughout this thesis study.

2.2. Fourier-transform infrared spectroscopy (FTIR)

Infrared (IR) spectroscopy is a commonly used technique for identifying the composition and structure of chemicals. It deals with the IR region of the electromagnetic spectrum, which is usually divided into three sub-regions: the near- (wavelength: 0.8-2.5 μm, wavenumber: 14000-4000 cm^{-1}), mid- (wavelength: 2.5-25 μm, wavenumber: 4000-400 cm^{-1}) and far-IR (wavelength: 25-1000 μm, wavenumber: 400-10 cm^{-1}).[149] The principle of IR spectroscopy is that each molecule absorbs specific frequencies of radiations that match the energy required for their transition from electronic ground state to different rotational (far-IR) or vibrational states (near-IR and mid-IR); as the rotational/vibrational states depend on particular mode of molecular motions (e.g., symmetric and antisymmetric stretching, scissoring, rocking, wagging, and twisting) as well as the particular type of chemical bond (bond strength and atom mass), each molecule has its distinctive IR spectrum (absorbance/transmittance vs. wavenumber). More complex molecules have more types of chemical bond and higher degrees of motion freedom/modes (3N–5 vibrational modes for linear molecules and 3N–6 vibrational modes for nonlinear molecules, N is number of atom in each molecule); thus their IR spectra become correspondingly more complex, with multiple peaks forming a characteristic pattern to indicate their identities.[314] In general, IR spectroscopy is more sensitive to those vibrational modes that cause significant changes to the dipole moment of a molecule, such as the asymmetric stretching mode; as a complementary vibrational spectroscopy to

IR, the Raman spectroscopy examines the change on the frequency of light scattered by a molecule, and is more sensitive to the type of vibrations (e.g., symmetric stretching) that change the molecular polarizability (i.e., the distribution of electron clouds).[314]

Unlike conventional spectroscopy which only measures single or narrow-band wavelength of light passing through a monochromator at one time, FTIR spectroscopy allows the simultaneous detection/analysis of a light beam containing a wide range of wavelengths. Because of this, FTIR takes the great advantage of using their sum of energy rather than analyzing the light of single-wavelength or small wavebands, and thus has dramatically improved sensitivity.[314] This intriguing property of FTIR spectroscopy is attributed to a particular component in its spectrometer configuration, i.e., the interferometer as shown in Figure 2.5 (B). Briefly, the interferometer contains a beamsplitter, a stationary mirror (S), and a movable mirror (M); the two mirrors are perpendicular to each other. The beamsplitter is designed to transmit half of the light and reflect half of the light transported from the light source; the transmitted light and the reflected light strike the stationary mirror and the movable mirror, respectively. When reflected back by the mirrors, the two beams of light recombine with each other at the beamsplitter. Based on their difference in the pathlength (δ = 2(MO−SO), O is the central position of beamsplitter), the lights of different wavelengths in the recombined beam could be constructively interfered (δ = nλ; n is an integral number, λ is wavelength), destructively interfered (δ = nλ/2), or at their intermediate states, which result in an overall output intensity (I). If the mirror M moves away from the beamsplitter with a constant interval (d) (start from the position where MO equals to SO), an interferogram curve (I vs. δ) is obtained, which can be decomposed into to the intensities of its component lights of different wavelengths via Fourier analysis/transformation. The resolution of FTIR spectroscopy is approximately equal to ($1/\delta_{max}$); e.g., if the maximum mirror movement (MO−SO) is 2 cm, the resolution is 0.25 cm^{-1}. The wavenumber range of FTIR spectrum is determined by $1/(4d)$; for the most widely used mid-infrared region (~ 4000 cm^{-1} range), d is 0.625 μm.[314]

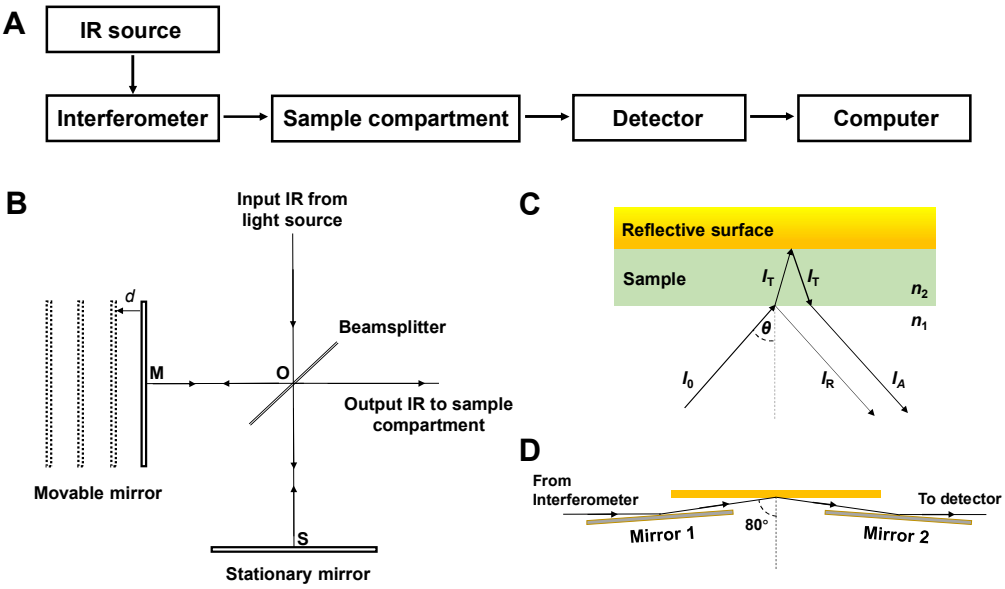

Figure 2.5 (A) Major elements in FTTR spectroscopy. (B) Schemetic view of interferometer. (C) IR beam path for reflection-absorption measurement of thin film sample. (D) Optical arrangement for grazing angle reflectance (θ = 80°).

The different accessories/techniques installed in the sample compartment of FTIR spectroscopy enable its broad application for gas, liquid, and solid samples. In our study, the specular reflection-adsorption accessory/technique was used, which is most appropriate for studying organic thin films coated on a reflective substrate, such as metals.[314,315] As shown in Figure 2.5 (C), for a typical specular reflection, part of the incident IR radiation (I_0) is directly reflected off the sample surface (I_R). The remaining part of I_0 is transmitted into the sample layer, and is reflected back to the sample layer at the substrate surface (I_T). When I_T exits from the surface of the sample layer (I_A), it has passed through the sample layer twice and been adsorbed at characteristic wavelengths. For studying an ultra-thin layer of sample (e.g., SAMs), the "grazing angle" of incidence needs to be applied in order to ensure a high sensitivity. This is because at large incident angles (60°~85°), the *p*-polarized component of electromagnetic radiation undergoes a phase shit of approximately 90°; as a result, the vector sum of the incident and reflected *p*-polarized component gives an intensified vibration oriented perpendicular to the reflective surface.[315] Additionally, the larger incident angle results in longer effective pathway of the transmitted IR radiation (I_T), which also enhances its adsorption according to Beer's Law. As shown in Figure 2.5 (D), the reflection accessory used in our FTIR spectroscopy allows

an incident angle of 80°, which is simply achieved by two tilt mirrors.

The grazing angle based reflection-adsorption FTIR spectroscopy has been widely used for the study and characterization of alkanethiol SAMs on gold.[148,188,189,222] Figure 2.6 shows the FTIR spectra of a single and mixed ferrocenylalkanethiolate SAMs measured in our previous study,[188] where the characteristic absorption peaks corresponding to various vibration modes of C-H bonds in methylene group (-CH_2-), methyl terminal group (-CH_3), and Fc terminal group are clearly observed. More importantly, the degree of structural organization of SAMs were usually evaluated from the peak positions corresponding to the symmetric (ν_s) and antisymmetric stretching (ν_a) modes of -CH_2- groups.[148,189] Besides SAMs, FTIR spectroscopy has been confirmed effective for the characterization of CB[7] molecules deposited on gold surface from its two characteristic absorption peaks corresponding to the stretching vibration of C=O and C–N bonds at 1751 cm^{-1} and 1474 cm^{-1}, respectively.[123]

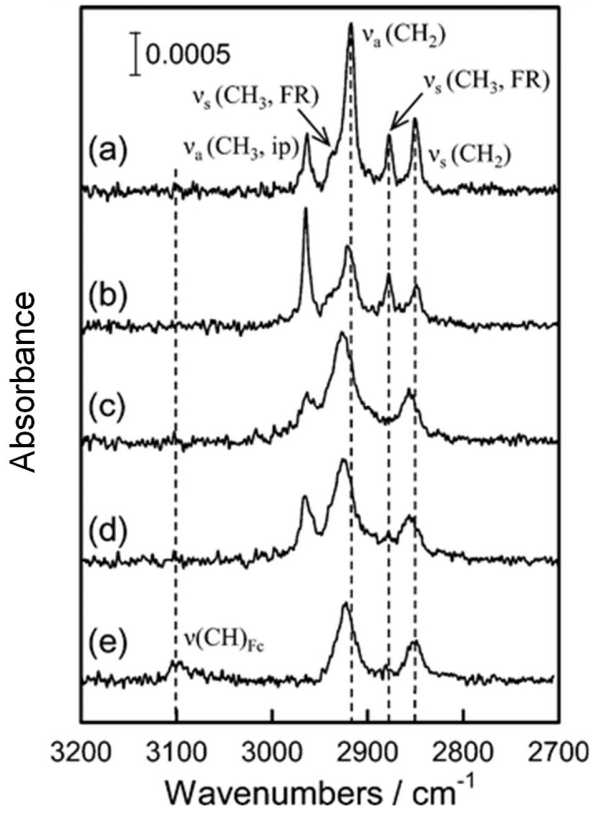

Figure 2.6. FTIR spectra of alkanethiolate SAMs: (a) C18S-Au; (b) C11S-Au; (c) FcC11S-/C11S-Au SAM prepared by the postassembly exchange method; (d) FcC11S-/C11S-Au SAM prepared by the coadsorption method; (e) single-component FcC11S-Au SAM.

Note: Reprinted with permission from Ref.188. Copyright (2014), *American Chemical Society*.

2.3. Contact angle measurement

Wetting measurement is a simple and convenient surface characterization technique by measuring the contact angle of a liquid drop on a solid surface. The contact angle (θ) is determined by the thermodynamic equilibrium of the three interfacial tensions, i.e., the solid−vapor tension (γ_{SG}), the solid−liquid tension (γ_{SL}), and the liquid−vapor tension (γ_{LG}), at the line where the three phases meet, as shown in Figure 2.7. This can be described by Young's equation as expressed in equation 2.18:[302]

$$cos\theta = \frac{(\gamma_{SG} - \gamma_{SL})}{\gamma_{LG}} \qquad (2.18)$$

The contact angle predicted by Young's equation usually deviates from the experimental value (e.g., contact angle hysteresis), this is due to its assumption of an ideal homogeneous and total smooth surface, which cannot be really achieved. Until now, Young's equation has been consistently modified by incorporating more real factors of solid surface (e.g., roughness), and outside factors (e.g., gravity).[302]

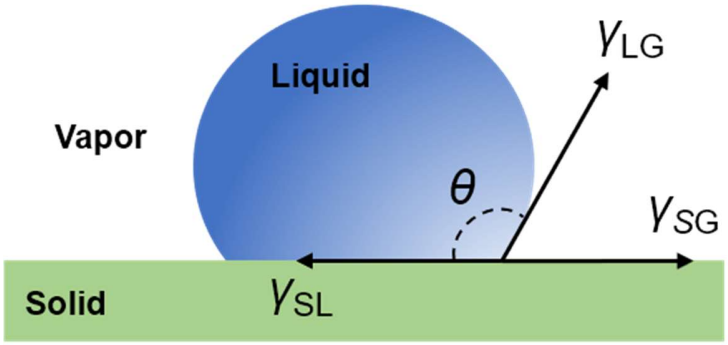

Figure 2.7. Schematic view of a liquid drop on a solid surface showing the quantities in the Young equations. γ_{SG}, γ_{SL} and γ_{LG} represent the solid-gas, solid-liquid, and liquid-gas interfacial energy, respectively; Θ is the contact angle.

Usually, a high contact angle (> 90°) indicates a low solid-liquid interfacial energy, while a low contact angle (< 90°) indicates a high solid-liquid interfacial energy; if the liquid is water, the corresponding surfaces are recognized as hydrophobic and hydrophilic, respectively. The water contact angle measurement has been widely used for the study and characterization of alkanethiolate SAMs on gold, as the surface hydrophobicity is strongly related to their chemical composition (e.g., polarity of terminal groups) and structural property (e.g., degree of organization, packing density).[137,160]

In this thesis, all water contact angles were measured with the goniometer technique, which allows the simple and direct measurement of tangent angle at the three-phase contact point on a sessile drop profile. As illustrated in Figure 2.8, the modern contact angle goniometers usually consist of following parts: A horizontal stage to mount the solid sample; a microliter syringe/pipette to deliver the liquid drop; a light/luminescent source to gain the visibility of the drop profile; and a high-resolution camera to take the amplified

image of the drop profile. In order to establish an advancing contact angle, 1~2 μL of liquid water was slowly added onto the solid sample. The individual contact angle was measured on both sides of the sessile drop profile as it might be unsymmetrical, and for each sample its reported contact angle result is the average value of three measurements at different sites.

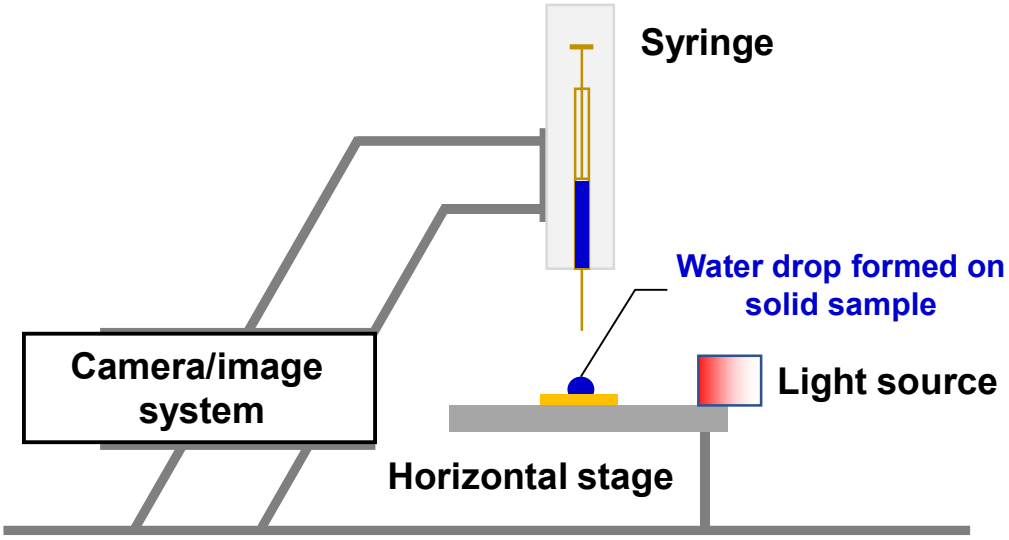

Figure 2.8. Schemetic view of a typical contact angle goniometer.

Chapter 3. Ferrocene@cucurbit[7]uril host-guest binding at organized molecular interface: thermodynamics and kinetic studies

In this chapter, the binding of CB[7] on binary ferrocenylundecanethiolate/octanethiolate SAM gold (FcC11S-/C8S-Au SAM), has been investigated as a trial system to improve our understanding of host-guest chemistry at molecular interfaces. Upon incubation with CB[7] solution, the redox behavior of FcC11S-/C8S-Au changes remarkably, i.e., a new pair of peaks appeared at more positive potential. The ease of quantitation of surface bound-redox species (Fc^+/Fc and Fc^+@CB[7]/Fc@CB[7]) enabled us to determine the thermodynamic formation constants of Fc@CB[7] at FcC11S-/C8S-Au SAM. With time-dependent redox responses, we were able to, for the first time, deduce both the binding and dissociation rate constants. These results showed substantial differences both thermodynamically and kinetically for the formation of host-guest inclusion complex at molecular interfaces with respect to solution-diffused, homogenous environments.

Note: this chapter is adapted with permission from

***Qi, L.**; Tian H.; Shao, H.; Yu H.-Z. Host-Guest Interaction at Molecular Interfaces: Binding of Cucurbit[7]uril on Ferrocenyl Self-Assembled Monolayers on Gold J. Phys. Chem. C, 2017, 121, 7985-7992.* Copyright (2017) American Society of Chemistry.

I have performed most of the experimental work and drafted the paper; Huihui Tian (a visiting student from 2012 to 2015) explored the preparation of mixed FcC11S-/C8S-Au SAMs and performed preliminary CV and FTIR studies. Professor Huibo Shao, the supervisor Huihui Tian at Beijing Institute of Technology, together with Dr. Hogan Yu supervised the entire project and helped with writing the paper.

3.1. Introduction

The ultra-strong and redox-active Fc@CB[7] supramolecular host-guest binding pair has shown great application potentials as an alternative of traditional natural binding pairs (e.g., biotin-avidin, antigen-antibody) for fabricating bio-functional interfaces. So far there have been two general strategies for applying this host-guest binding pair on electrode surfaces, one is the direct deposition of CB[7] monolayer via noncovalent interactions,[123,126] the other one is the covalent immobilization of derivatized CB[7] to functionalized electrode surfaces.[120,122] However, previous electrochemical and microscopic characterizations have confirmed the imperfect structure of directly deposited CB[7] monolayer (complex orientations and multiple layers) with poor Fc packing efficiency (less than 50% of the theoretical value);[126,129] moreover, the stability of noncovalently formed CB[7] monolayer is another concern, where the dissociation of CB[7] from electrode surfaces could happen upon binding with strong guests in solution. The covalent immobilization of CB[7] requires laborious and time-consuming work on molecular synthesis and surface modifications; besides, the functionalization of CB[7] still faces the challenge of low yields (5 ~ 30%).[117] Compared to the tremendous studies in homogeneous solution phase,[46] there is still lack of fundamental understanding about the thermodynamic and kinetic binding behavior of this particular, inclusion type host-guest pair formed at interfaces (with much more complexity and spatial restrictions), which would certainly help guide and promote its wide applications. Due to the above mentioned limitations of the two widely used interfacial Fc@CB[7] host-guest binding systems, they are not ideal for carrying out the fundamental binding studies.

In order to strengthen our understanding about the interfacial Fc@CB[7] host-guest binding, in this chapter we have explored the binding of CB[7] onto a mixed ferrocenylundecanethiolate/octanethiolate SAM on gold (FcC11S-/C8S-Au SAM), which is shown in Figure 3.1. The FcC11S-/C8S-Au SAM can be viewed as a “near-ideal” molecular interface due its high stability, well-organized crystalline structure, dispersed Fc terminal groups (as CB[7] binding sites), easy preparation, and the commercially available raw materials (FcC11SH and C8SH).

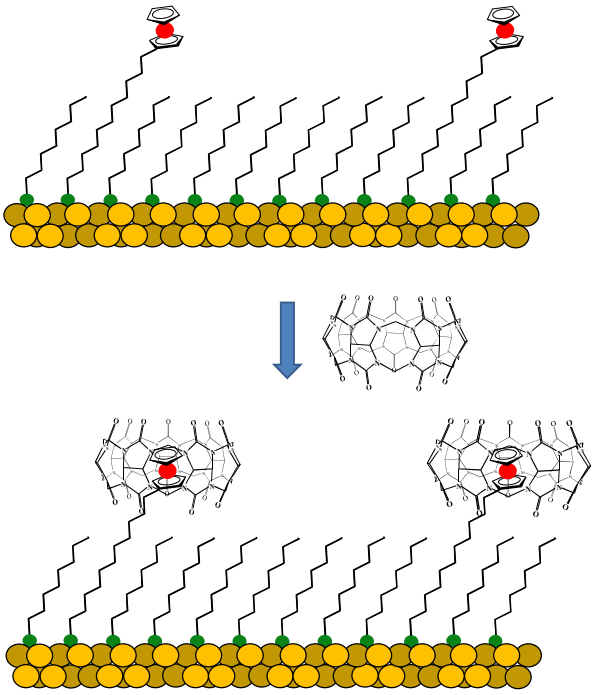

Figure 3.1. Binding of CB[7] onto the "ideal-structured" FcC11S-/C8S-Au SAM.

The formation of Fc@CB[7] host-guest complex on mixed FcC11S-/C8S-Au SAM was characterized by FTIR, water contact angle measurement, and CV. Particularly, based on the remarkably changed CV response of Fc terminal groups upon encapsulation by CB[7], it is easy to quantify the amount of free and bound Fc terminal groups, which enable both thermodynamic and kinetic studies of this widely interested host-guest binding at organized molecular interface. The results of these studies clearly reveal the substantial differences both thermodynamically and kinetically for the formation of Fc@CB[7] host-guest pair on solid surface with respect to in solution environment.

3.2. Experimental details

3.2.1. Reagents and materials

11-Ferrocenyl-1-undecanethiol (98%) was purchased from Dojindo Laboratories Inc. (Tokyo, Japan); 1-ocanethiol (C8SH), cucurbit[7]uril hydrate (CB[7]), sodium perchlorate ($NaClO_4$), sulfuric acid (96%), and hydrogen peroxide (30%) were purchased from Sigma Aldrich (St. Louis, United States). Ethanol (95%) was obtained from Commercial Alcohols

(Toronto, Canada). All chemicals were of ACS reagent-grade and used as received. All solutions were prepared with 95% Ethanol solution or deionized water (> 18.2 MΩ·cm, produced with a Barnstead EasyPure UV/UF compact water system (Dubuque, IA)), and deoxygenated with Ar before use. The gold slide (regular glass slide coated with 5 nm Cr and 100 nm Au film) used as working electrode was purchased from Evaporated Metal Films (EMF) Inc. (New York, United States); the platinum counter electrode and the Ag|AgCl reference electrode were purchased from CH Instrument (Austin, United States).

3.2.2. Preparation of mixed FcC11S-/C8S-Au SAMs and CB[7] binding

The mixed FcC11S-/C8S-Au SAM was prepared according to previously proposed co-adsorption method.[188,214] Briefly, the pretreated gold slides (see section 2.1.3 for details) were immersed in a mixed FcC11SH/C8SH ethanol solution (95%) at room temperature for overnight (> 12 h). The total concentration of the thiols is 1.0 mM with 5% (mole fraction) of FcC11SH. After incubation, the gold slides were thoroughly washed with copious amounts of ethanol solution (95%) and deionized water. For CB[7] host binding, the above prepared mixed FcC11S-/C8S-Au SAM was immersed with different concentrations of CB[7] solution for 180 min, or immersed with 1.0 mM CB[7] solution for different periods of time.

3.2.3. Surface characterizations by various techniques

FTIR and water contact angle were measured for mixed FcC11S-/C8S-Au SAM before and after incubation with 1.0 mM CB[7] for 180 min. CVs were measured for mixed FcC11S-/C8S-Au SAMs before and after incubation with CB[7] of various concentrations and for different times; CVs were also measured for CB[7] pre-saturated FcC11S-/C8S-Au SAM upon incubation with CB[7]-free electrolyte solution for different periods of time.

The reflection-absorption FTIR spectrum was obtained by using a Nicolet Magna 560 Fourier transform infrared spectrometer (Thermo Nicolet Co. Madison, WI) equipped with KBr beam splitter in interferometer, an automated VeeMAX II variable angle accessory (Pike Technologies, Madison, WI) in the sample compartment, and a mercury cadmium telluride (MCT) detector. The *p*-polarized IR laser beam was incident at 80°; the MCT detector was cooled by liquid nitrogen prior to use. The FTIR spectrum was reported as absorbance vs. wavenumber, and the background spectrum was obtained from the

piranha solution-cleaned gold slide. The water contact angles were measured immediately after adding 1~2 μL water droplet onto the solid samples by using AST VCA goniometer system (Billerica, MA).

The CV measurements were carried out in a Faradic cage at room temperature under the protection of Ar; all electrolyte solutions in electrochemical cell were deoxygenated for at least 10 min before use. The CHI 1040A Electrochemical Analyzer was used as potentiostat (Austin, United States). More detailed information of our electrochemical detection system is described in section 2.1.3.

3.3. Results and discussion

3.3.1. Characterization of Fc@CB[7] host-guest complex formed on FcC11S-/C8S-Au SAM

In order to achieve the ideal structure for studying interfacial Fc@CB[7] host-guest binding, the binary FcC11S-/C8S-Au SAM was prepared by co-adsorption method with a low mole fraction of FcC11SH (5%) used in the mixed assembly solution;[188,214] the relatively shorter C8SH was used as diluent alkanethiol in order to ensure the dispersed and exposed Fc terminal groups on SAM, as illustrated in Figure 3.1.

The blue curve in Figure 3.2 (A) shows the CV response of thus prepared binary FcC11S-/C8S-Au SAM. A single pair of symmetric redox peaks was observed, with a formal potential of 262 ± 5 mV, nearly no peak separation (< 5 mV), and a half-height peak width (97 ± 6 mV) close to the theoretical value (90.6 mV at 25 °C) predicted from Langmuir adsorption isotherm.[204] Those CV features have been considered as the characteristic properties of an ideal-structured mixed SAM with well-dispersed and non-interacting redox-active terminal groups.[68] Besides CV characterization, the binary FcC11S-/C8S-Au SAM was also examined by FTIR spectroscopy, with its spectrum shown in Figure 3.2 (B). It can be seen that the adsorption peaks corresponding to various C-H stretching regions (i.e., -CH_2- group of alkane bridge, -CH_3 terminal group, and CH bond of Fc terminal group) are clearly observed for this binary FcC11S-/C8S-Au SAM. According to previous studies, the peak position of ν_a(-CH_2-) found in this study (2924 cm^{-1}) indicate that the shorter and mixed alkanethiolate SAM may have less crystalline

structure with respect to the single C18S-Au SAM, whose ν_a(-CH_2-) was observed at 2918 cm^{-1}.[175,222]

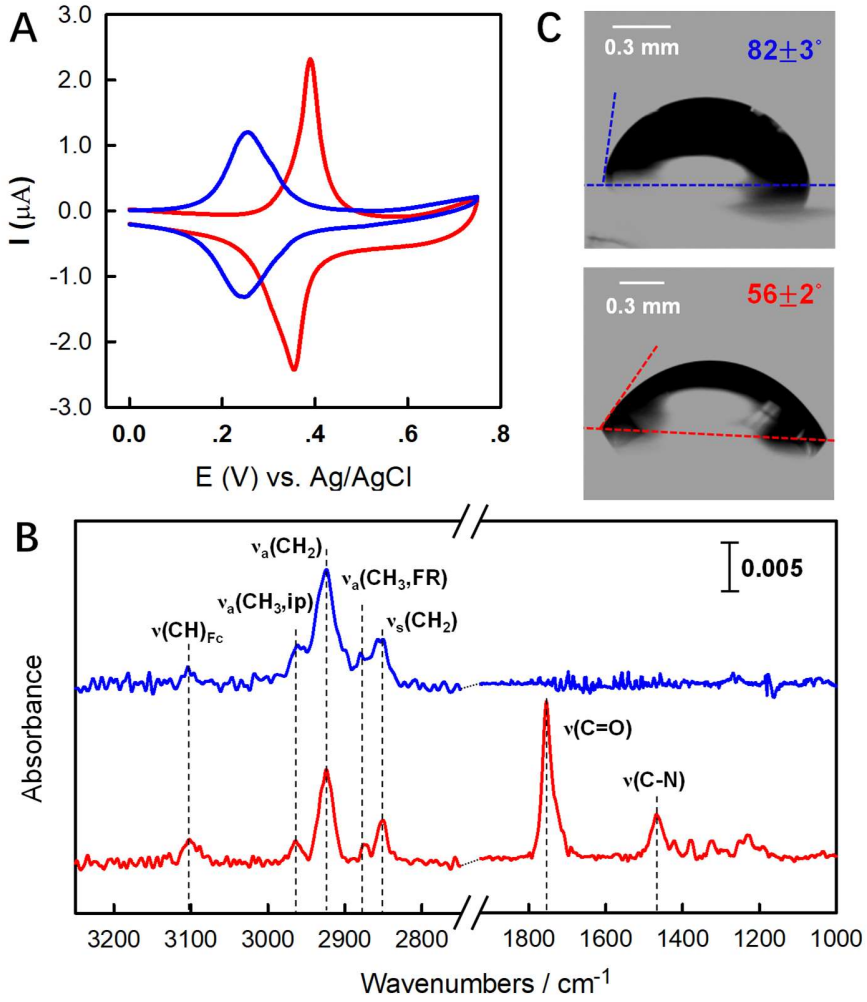

Figure 3.2. (A) CVs of FcC11S-/C8S-Au SAM before (blue curve) and after incubation with 1.0 mM CB[7] for 3 h (red curve). The supporting electrolyte was 0.1 M $NaClO_4$, and the scan rate was 50 mV/s. (B) Reflection-adsorption FTIR spectra of FcC11S-/C8S-Au SAM before (blue curve) and after incubation with 1.0 mM CB[7] for 3 h (red curve). (C) The water contact angles of FcC11S-/C8S-Au SAM before (top) and after incubation with 1.0 mM CB[7] for 3 h (bottom).

Note: Reprinted with permission from *J. Phys. Chem. C* 2017, 121, 7985-7992. Copyright (2017), *American Chemical Society.*

The binding of CB[7] host on this mixed FcC11S-/C8S-Au SAM was also confirmed by FTIR and CV techniques, as well as wetting study. In FTIR spectra, it can be seen that

after incubating FcC11S-/C8S-Au SAM with a high concentration of CB[7] (1.0 mM), two new adsorption peaks appeared at 1751 cm^{-1} and 1474 cm^{-1} (red curve in Figure 3.2B), redpectively, which correspond to the stretching vibrations of C=O and C-N bonds of CB[7]; in the mean time, the adsorption peaks of above mentioned C-H stretching regions remained nearly unchanged in their position and intensity.[123] The wetting study displayed in Figure 3.2 (C) shows a decreased water contact angle (from 82° to 56°) on FcC11S-/C8S-Au SAM after CB[7] incubation, indicating a more hydrophilic surface caused by the electronegative carbonyl portals of CB[7]. As shown in Figure 3.2 (A), the CV response of FcC11S-/C8S-Au SAM also changed dramatically after CB[7] incubation, with its formal potential shifting to much more positive value (375 ± 6 mV). According to the basic thermodynamics of redox process (equation 2.5 in section 2.1.1),[204] the positively shifted formal potential indicates more difficult oxidation of Fc terminal groups upon binding with CB[7]. Interestingly, the similar phenomena were also observed for those cationic Fc derivatives in solution, but not for the neutral Fc derivatives (less than +30 mV formal potential shift upon CB[7] binding).[114-116] A more detailed discussion about their different degrees of formal potential shifts is given in chapter 5 (section 5.3.1).

3.3.2. Thermodynamic study based on CV

Based on earlier described advantages (see section 2.1.1), the thermodynamic stability of Fc@CB[7] host-guest binding on mixed FcC11S-/C8S-Au SAM was investigated by measuring its CV responses after incubation with different concentrations of CB[7]; a long incubation time (180 min) was used in order to ensure the binding can reach equilibrium state. From the results displayed in Figure 3.2 (A), it can be seen that with a low concentration of CB[7] (5 μM), a shoulder peak starts to appear on the right side of the original pair of CV redox peaks; this new pair of redox peaks grows with increased concentrations of CB[7], which should result from more Fc@CB[7] host-guest complexes formed on FcC11S-/C8S-Au SAM. Simultaneously, the original CV redox peaks at lower potential becomes smaller and closer to the new pair of redox peaks, indicating less amount of free Fc terminal groups remained on SAM. The saturation state is reached when CB[7] concentration is higher than 80 μM, where the original CV redox peaks eventually diminishes and the new pair of redox peaks is dominant, indicating that nearly all Fc terminal groups on FcC11S-/C8S-Au SAM are bound to CB[7].

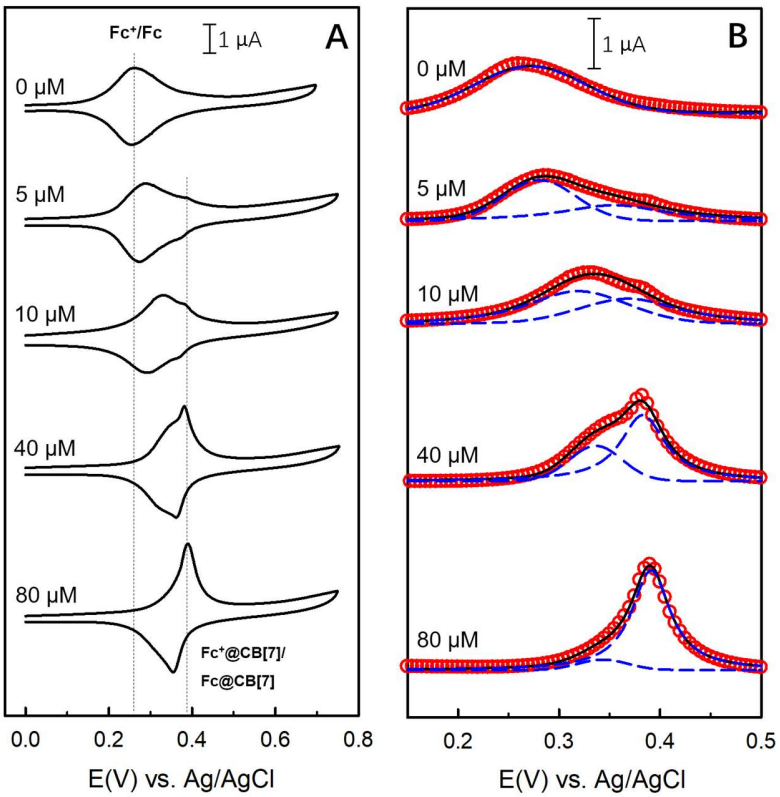

Figure 3.3. (A) CVs of FcC11S-/C8S-Au SAM before and after incubation with different concentrations of CB[7] for 3 h. The supporting electrolyte was 0.1 M $NaClO_4$, and the scan rate was 50 mV/s. (B) Gaussian-Lorentzian deconvolution of the CV anodic wave of FcC11S-/C8S-Au SAM before and after immersing with different concentrations of CB[7] for 3 h. The open circles (red) are the original CV anodic peak with the correction of the capacitive (baseline) current; the dashed lines in blue are the deconvoluted peaks of Fc^+/Fc and Fc^+@CB[7]Fc@CB[7], respectively; the solid line in black is the sum of two deconvoluted peaks.

Note: Reprinted with permission from *J. Phys. Chem. C* 2017, 121, 7985-7992. Copyright (2017), *American Chemical Society*.

As a generally strategy, the Langmuir-type adsorption models are widely used for analyzing the experimentally obtained isotherm data for molecular binding events on surface, from which their thermodynamic equilibrium constants (i.e., formation and dissociation constants) can be determined from the best fitting results.[223] However, the ideal condition assumed by Langmuir adsorption cannot be truly achieved due to the intrinsic complexity of surface (e.g., roughness, defects, nonspecific adsorptions, various

intermolecular interactions among adsorbates), which may strongly affect the accuracy of the fitting results.

The CV results shown in Figure 3.3 (A) indicate that the free Fc terminal group and Fc@CB[7] host-guest complex formed on FcC11S-/C8S-Au SAM have distinct redox peaks located at lower and more positive potentials. Accordingly, it would be possible to quantify their amounts at equilibrium state, which can be further used to directly calculate the formation constant (*K*) of Fc@CB[7] host-guest complex formed on FcC11S-/C8S-Au SAM based on equation 3.1 and 3.2:

$$\mathrm{FcC11S\text{-}/C8S\text{-}Au} + \mathrm{CB[7]} \rightleftharpoons \mathrm{CB[7]@Fc@C11S\text{-}/C8S\text{-}Au} \qquad (3.1)$$

$$K = \frac{\Gamma_{\mathrm{Fc@CB[7]}}}{\Gamma_{\mathrm{Fc}}\, c_{\mathrm{CB[7]}}} \qquad (3.2)$$

Without the interferences from mass transport processes in solution, the amount of adsorbed redox species can be determined by integrating their CV redox peaks.[203] From the CVs shown in Figure 3.3 (A), the total surface density of Fc terminal groups on FcC11S-/C8S-Au SAM was determined to be (5.9 ± 0.4) × 10^{-11} mol/cm^2, based on equation 3.3:

$$\Gamma_{\mathrm{Fc\ (total)}} = \frac{Q_{\mathrm{Fc\ (total)}}}{nFA} \qquad (3.3)$$

where $Q_{\mathrm{Fc\ (total)}}$ is the total faradic charge transported between Fc^+/Fc terminal groups and gold electrode;[203] n = 1 for Fc^+/Fc. One difficulty for quantifying the individual amount of free Fc terminal group and Fc@CB[7] complex is that their CV redox peaks, although located at different potentials, are largely overlapped. The solution to this problem is by deconvoluting the split CV redox peaks with combined distribution functions; and the combination of Gaussian and Lorentzian distributions has been confirmed the most effective CV deconvolution protocol,[213] as shown by equation 3.4:

$$y = a_1 \exp\left[-0.5\left(\frac{x - E_1}{b_1}\right)^2\right] + a_2\left[1 + \left(\frac{x - E_2}{b_2}\right)^2\right]^{-1} + y_0 \qquad (3.4)$$

where a_1 and a_2 represent the peak intensity, E_1 and E_2 represent the peak potentials, b_1 and b_2 represent the peak width, y_0 is a constant. The Gaussian (a_1, E_1 and b_1) and Lorentzian parts (a_2, E_2 and b_2) of equation 3.4 represent the two overlapped CV redox peaks located at lower (peak I) and higher potentials (peak II), respectively. Briefly, the

CV deconvolution was conducted by fitting the baseline (capacitive current) corrected CV anodic waves with equation 3.4; the parameters obtained from the best fit were then used to generate peak I and peak II via Gaussian and Lorentzian functions, respectively. Figure 3.3 (B) shows the Gaussian-Lorentzian deconvolution results (blue dashed lines) for the CVs displayed in Figure 3.3 (A). Based on the area fraction of deconvoluted redox peaks to original CV anodic wave (A_{peak}/A_{total}), the surface density of free Fc terminal groups (Γ_{Fc}) and Fc@CB[7] host-guest complex ($\Gamma_{Fc@CB[7]}$) formed on FcC11S-/C8S-Au SAM were then calculated from equations 3.5 and 3.6:

$$\Gamma_{Fc} = \Gamma_{Fc\ (total)} \frac{A_{peak\ I}}{A_{total}} \tag{3.5}$$

$$\Gamma_{Fc@CB[7]} = \Gamma_{Fc\ (total)} \frac{A_{peak\ II}}{A_{total}} \tag{3.6}$$

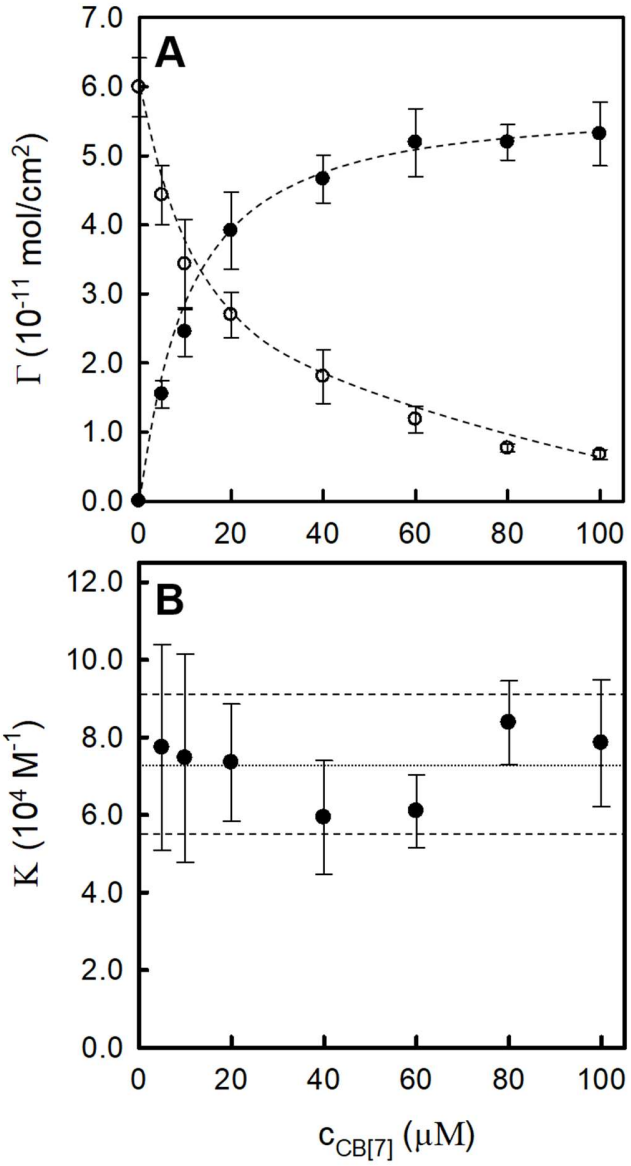

Figure 3.4. Surface densities of free Fc terminal group (open circles) and Fc@CB[7] complex (solid circles) formed on FcC11S-/C8S-Au SAM upon reaching binding equilibrium with different concentrations of CB[7]. The dashed lines are to guide eyes only. (B) Formation constant (*K*) of interfacial Fc@CB[7] host-guest binding determined at different incubation concentrations of CB[7]. The dotted and dashed lines show the average and standard deviations of all *K* values.

Note: Reprinted with permission from *J. Phys. Chem. C* 2017, 121, 7985-7992. Copyright (2017), *American Chemical Society.*

Figure 3.4 (A) summarize the Γ_{Fc} and $\Gamma_{Fc@CB[7]}$ determined at different equilibrium states of Fc@CB[7] host-guest binding on FcC11S-/C8S-Au SAM. It clearly shows that with increased concentration of CB[7] ($c_{CB[7]}$), the value of Γ_{Fc} decreases while that of $\Gamma_{Fc@CB[7]}$ increases monotonically; at high $c_{CB[7]}$ (≥ 80 μM), over 90 % of Fc terminal groups are converted to Fc@CB[7] complex. With the above determined $\Gamma_{Fc@CB[7]}$ and Γ_{Fc}, the *K* value of Fc@CB[7] complex formed on FcC11S-/C8S-Au SAM was calculated at different $c_{CB[7]}$ ($c_{CB[7]}$ remains nearly constant before and after incubation since the amount of CB[7] is in large excess with respect to that of Fc terminal groups on SAM (vide infra)). As displayed in Figure 3.4 (B), these *K* values show no significant variations with an average of $(7.3 \pm 1.8) \times 10^4$ M^{-1}, which further confirm the validity of the CV deconvolution method based on Gaussian-Lorentzian fitting protocol.

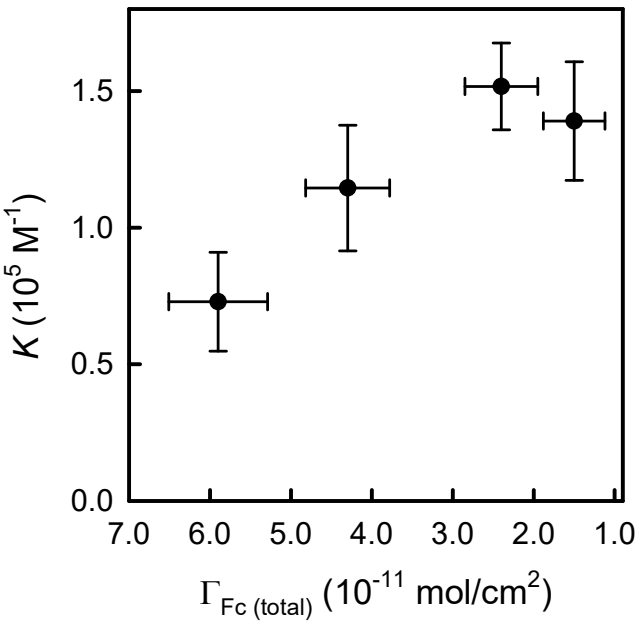

Figure 3.5. The formation constants (*K*) of Fc@CB[7] host-guest binding on FcC11S-/C8S-Au SAMs with different total surface densities of Fc.
Note: Reprinted with permission from *J. Phys. Chem. C* 2019, 123, 26315-26323. Copyright (2019), *American Chemical Society*.

In order to further minimize the influence of surface crowdedness on interfacial Fc@CB[7] host-guest binding, the *K* values were also determined on FcC11S-/C8S-Au SAM with lower total surface density of Fc ($\Gamma_{Fc\ (total)}$). As shown in Figure 3.5, with reduced

mole fraction of FcC11SH used for co-adsorption (from 5% to 1%), the $\Gamma_{Fc\ (total)}$ also decreases accordingly (from 5.9±0.6 × 10^{-11} mol/cm^2 to 1.5±0.4 × 10^{-11} mol/cm^2), which becomes much lower than the surface density of "closely-packed" CB[7] monolayer (7.5 × 10^{-11} mol/cm^2).[123] Based on above described method, it was found that the *K* value can be improved to (1.5 ± 0.3) × 10^5 M^{-1} when $\Gamma_{Fc\ (total)}$ decreases to 2.4 × 10^{-11} mol/cm^2; the even lower $\Gamma_{Fc\ (total)}$ (1.5 × 10^{-11} mol/cm^2) does not result in further improved *K* value.

With above results, it is believed that the thermodynamic stability of ultra-strong Fc@CB[7] host-guest binding pair ($K > 10^9$ M^{-1})[114] is significantly affected even forming at such a highly-organized molecular interface; the possible reasons are given and discussed below. First, as previously revealed by X-ray crystallographic technique, in solution phase Fc has two co-existed orientations inside the inner cavity of CB[7] (with 22° and 78° angles formed between their main molecular axises, as shown in Figure 1.4 of chapter 1); such a geometric feature may indicate a certain degree of rotational freedom of Fc inside CB[7] inner cavity, which enables it to reach the thermodynamically most favorable orientation.[114] In contract, the intrinsic complexity of molecular interfaces (e.g., heterogeneous structural domains, defects, spatial restrictions) could prevent the motion of Fc terminal group to reach its most favored orientations inside CB[7], and thus lead to smaller enthalpy change for Fc@CB[7] host-guest binding on FcC11S-/C8S-Au SAM. Besides, several studies based on reflectometry techniques (X-ray, neutron, electron),[224, 225] and theoretical simulations (MD)[226] have found that for densely-packed alkanethiolate SAMs, their interfacial water solvent molecules evolve into 2~4 nm condensed layer with ice-like crystalline structure; as a result, the entropy gain caused by the release of high energy water molecules trapped inside CB[7][47,108] upon guest binding could also become smaller for Fc@CB[7] binding on FcC11S-/C8S-Au SAM than it in bulk aqueous solution. In addition, the use of electrolyte solution for CV measurement may bring "salt effect" towards CB[7]-guest binding affinity.[269]

3.3.3. Kinetic study based on CV

It is well known that the thermodynamic equilibrium constant of a reversible chemical process can be deduced from its forward (k_1) and backward rate constants (k_{-1}), which is expressed by equation 3.7:[149]

$$K = \frac{k_1}{k_{-1}} \tag{3.7}$$

Therefore, in order to further understand the decreased thermodynamic stability of Fc@CB[7] host-guest complex formed at organized molecular interface, the investigation was proceeded to the binding and dissociation kinetics of CB[7] on FcC11S-/C8S-Au SAM.

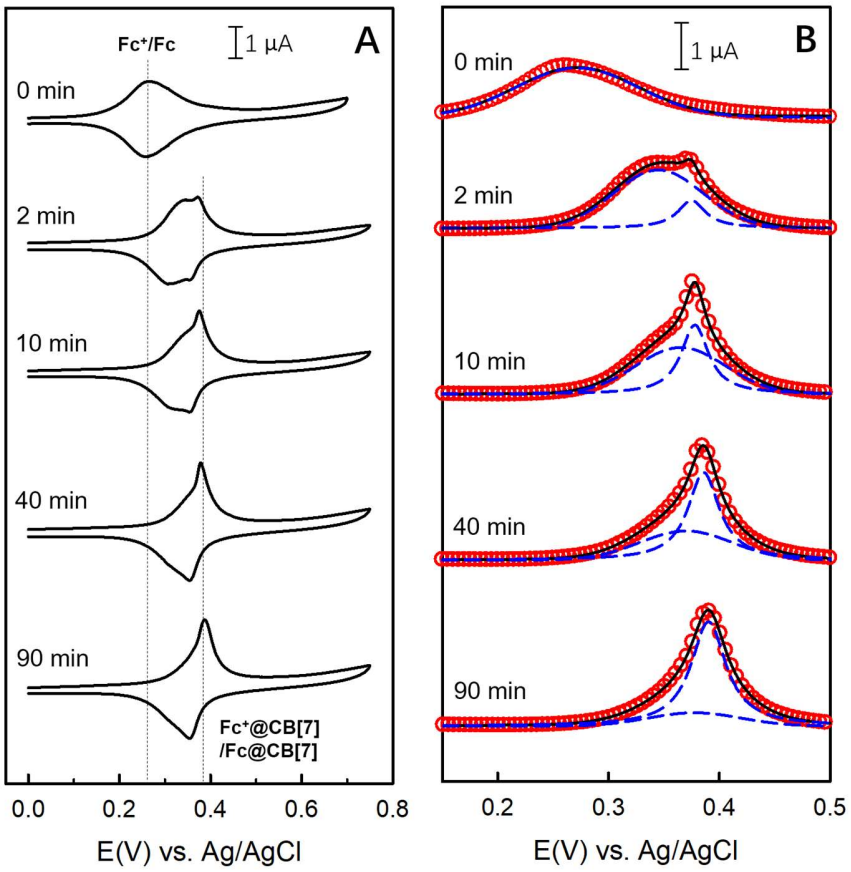

Figure 3.6. **(A) CVs of FcC11S-/C8S-Au SAM before and after incubation with 1.0 mM CB[7] for different periods of time. The supporting electrolyte was 0.1 M $NaClO_4$, and the scan rate was 50 mV/s. (B) Gaussian-Lorentzian deconvolution of the CV anodic waves of FcC11S-/C8S-Au SAM before and after incubation with 1.0 mM CB[7] for different periods of time. The open circles (red) are the original CV anodic peak with the correction of the capacitive (baseline) current; the dashed lines in blue are the deconvoluted peaks of Fc^+/Fc and Fc^+@CB[7]Fc@CB[7], respectively; the solid line in black is the sum of two deconvoluted peaks.**

Note: Reprinted with permission from *J. Phys. Chem. C* 2017, 121, 7985-7992. Copyright (2017), *American Chemical Society.*

The binding process was first studied by measuring the CVs of FcC11S-/C8S-Au SAM (prepared by co-adsorption with 5% mole fraction of FcC11SH) upon incubation with 1.0 mM CB[7] for different periods of time. Figure 3.6 (A) shows that the redox peak corresponding to free Fc terminal groups (located at lower potential) diminishes rapidly with longer incubation time; after 10 min, the new redox peaks (located at more positive potential) corresponding to Fc@CB[7] complex becomes dominant; no further change was observed on CV when the incubation time is over 90 min.

Following the thermodynamic study described above, the CVs in Figure 3.6 (A) were quantitatively analyzed by Gaussian-Lorentzian deconvolution protocol, whose results are displayed in Figure 3.6 (B). Based on these CV deconvolution results, the mole ratio of free Fc terminal groups at different CB[7] incubation times ($(\Gamma_t/\Gamma_0)_{Fc}$) were calculated and plotted in Figure 3.7 (A). It can be seen that $(\Gamma_t/\Gamma_0)_{Fc}$ decreases exponentially with elongated incubation time (t). By treating the CB[7] based host-guest binding reaction as an elementary process,[229,230] the rate law of Fc@CB[7] host-guest binding on FcC11S-/C8S-Au SAM can be expressed as equation 3.8:

$$Rate = -\frac{d(\Gamma_{\mathrm{Fc}})}{dt} = k_1 c_{\mathrm{CB[7]}} \Gamma_{\mathrm{Fc}} \qquad (3.8)$$

In this study, since the amount of CB[7] in incubation solution ($c_{CB[7]} \times$ volume > 10^{-8} mol) is in large excess with respect to the total amount of Fc terminal groups on FcC11S-/C8S-Au SAM ($\Gamma_{Fc\ (total)} \times$ area < 10^{-11} mol), the rate law can be simplified to equation 3.9:

$$Rate = -\frac{d(\Gamma_{\mathrm{Fc}})}{dt} = k' \Gamma_{\mathrm{Fc}} \text{ with } k' = k_1 c_{\mathrm{CB[7]}} \qquad (3.9)$$

where k' is the apparent pseudo-first-order binding rate constant at a given $c_{CB[7]}$.

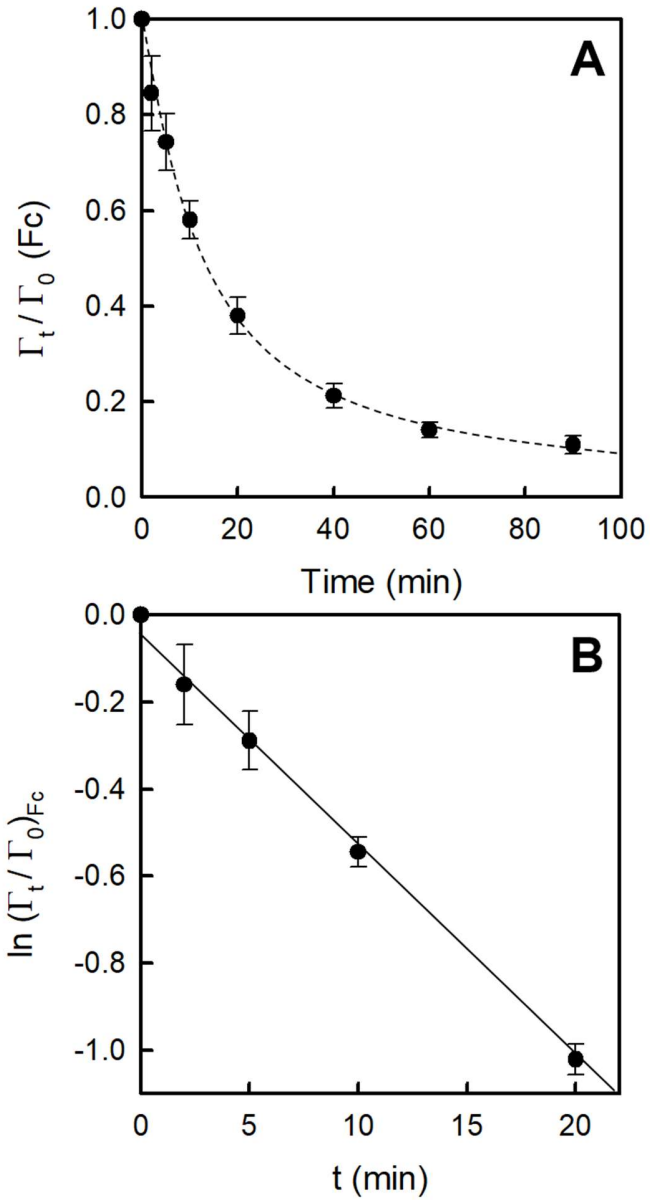

Figure 3.7. **(A) The ratio of free Fc terminal groups on FcC11S-/C8S-Au SAM ($(\Gamma_t/\Gamma_0)_{Fc}$) as the function of CB[7] incubation time (t); Γ_t and Γ_0 are the surface density of free Fc terminal groups at certain incubation time and at initial state. The dashed line is to guide eyes only. (B) The relationship between $\ln(\Gamma_t/\Gamma_0)_{Fc}$ and t; the solid line shows the best linear fit based on pseudo-first-order kinetic model (see the text for details), from which the binding rate constant (k_1) of CB[7] on FcC11S-/C8S-Au SAM was determined.**

Note: Reprinted with permission from *J. Phys. Chem. C* 2017, 121, 7985-7992. Copyright (2017), *American Chemical Society.*

The integration of equation 3.9 provides the natural logarithm correlation between the surface density of free Fc terminal group $(\Gamma_{Fc})_t$ and CB[7] incubation time (t), as expressed by equation 3.10, which can be further converted to the linear relationship as shown in equation 3.11.

$$\ln(\Gamma_{\mathrm{Fc}})_t = \ln(\Gamma_{\mathrm{Fc}})_0 - k'\mathrm{t} \tag{3.10}$$

$$\ln(\frac{\Gamma_{\mathrm{t}}}{\Gamma_0})_{\mathrm{Fc}} = -k'\mathrm{t} \tag{3.11}$$

The experimental data (solid circles) in Figure 3.7 (B) shows the expected linear relationship as predicted by equation 3.11, which validates the pseudo-first-order binding kinetics as deduced above. By fitting this experimental relationship with equation 3.11, we were able to determine *k*' (2.8 ± 0.3 min^{-1}) from the slope of the best linear fit (solid line in Figure 3.7B); then based on equation 3.9 and the known $c_{CB[7]}$ (1.0 mM), k_1 was obtained to be $2.8 \pm 0.3 \times 10^3$ $M^{-1}min^{-1}$.

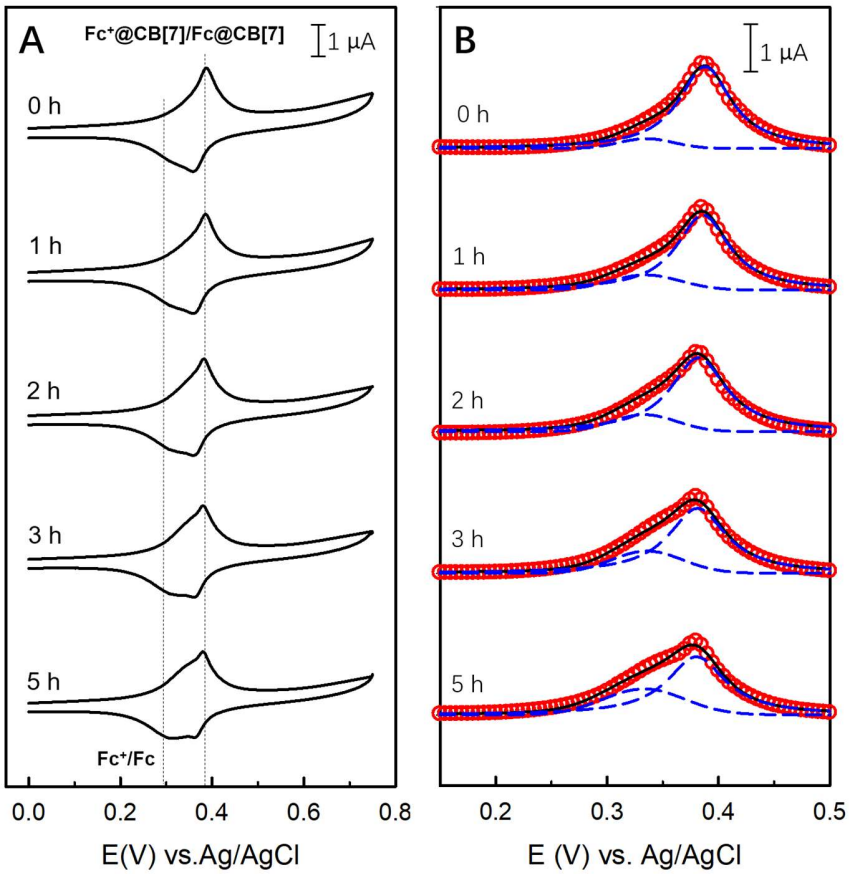

Figure 3.8. **(A) CVs of the CB[7] pre-saturated FcC11S-/C8S-Au SAM (incubating FcC11S-/C8S-Au SAM with 1.0 mM CB[7] for 3 h) upon immersing in a CB[7]-free solution for different periods of time. The scan rate was 50 mV/s, and the electrolyte was 0.1 M $NaClO_4$. (B) Gaussian-Lorentzian deconvolution of the CV anodic wave of CB[7]@FcC11S-/C8S-Au SAM after incubation with 1.0 mM CB[7] for different periods of time. The open circles (red) are the original CV anodic peak with the correction of the capacitive current (baseline); the dashed lines in blue are the deconvoluted redox peaks of Fc^+/Fc and Fc^+@CB[7]Fc@CB[7], respectively; the solid line in black is the sum of two deconvoluted peaks.**

Note: Reprinted with permission from *J. Phys. Chem. C* 2017, 121, 7985-7992. Copyright (2017), *American Chemical Society*.

Besides binding process, the dissociation of Fc@CB[7] host-guest complex formed on FcC11S-/C8S-Au SAM was investigated by first incubating the FcC11S-/C8S-Au SAM (co-adsorption with 5% mole fraction of FcC11SH) in 1.0 mM CB[7] solution for 3 h, then transferring it into a CB[7]-free electrolyte solution and

measuring its CVs at different incubation times. As shown in Figure 3.8 (A), the CV redox peaks at higher potential corresponding to Fc@CB[7] complex gradually decreases; in the meantime, a pair of shoulder redox peaks corresponding to free Fc terminal groups gradually appears at lower potential. It should be noted that even after 5 h incubation, the redox peaks of Fc@CB[7] complex is still predominate, indicative of a rather slow dissociation kinetics. Even simpler than the binding process, the dissociation of Fc@CB[7] complex formed on FcC11S-/C8S-Au SAM can be directly treated as the first-order reaction, for which the rate laws are described from equations 3.12 to 3.14:

$$Rate = -\frac{d\left(\Gamma_{\mathrm{Fc@CB[7]}}\right)}{dt} = k_{-1}\Gamma_{\mathrm{Fc@CB[7]}} \tag{3.12}$$

$$\ln(\Gamma_{\mathrm{Fc@CB[7]}}) = \ln(\Gamma_{\mathrm{Fc@CB[7]}})_0 - k_{-1}\mathrm{t} \tag{3.13}$$

$$\ln(\frac{\Gamma_\mathrm{t}}{\Gamma_0})_{\mathrm{Fc@CB[7]}} = -k_{-1}\mathrm{t} \tag{3.14}$$

where k_{-1} is the dissociation rate constant.

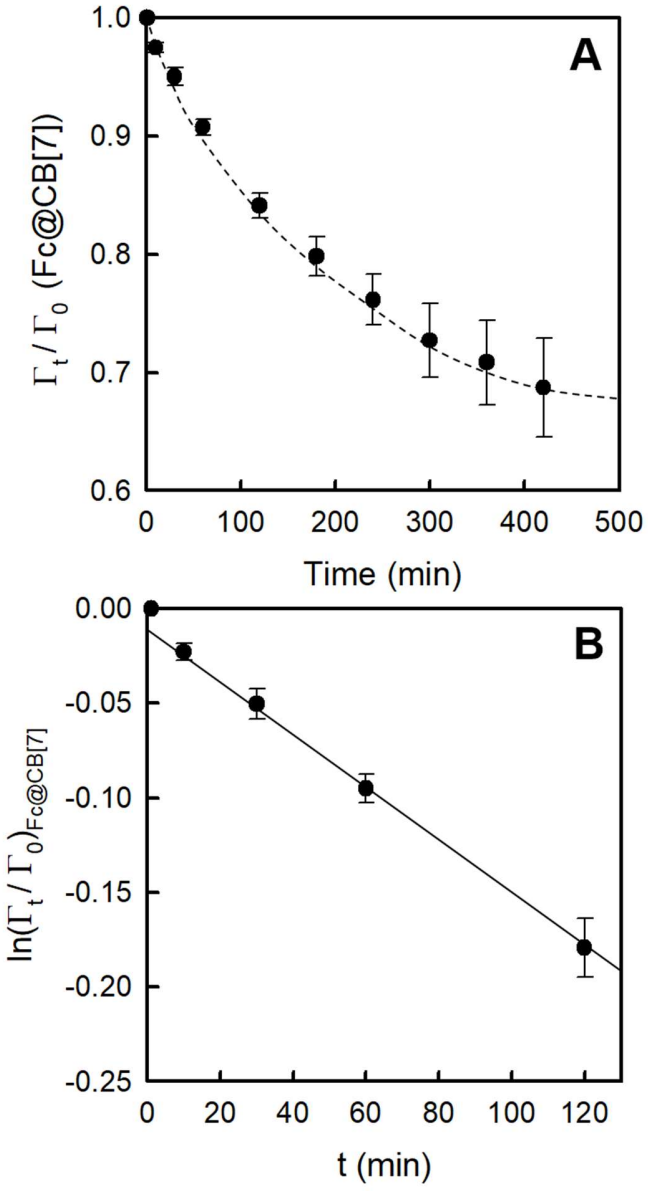

Figure 3.9. (A) The mole fraction of Fc@CB[7] complex remained on FcC11S-/C8S-Au SAM (CB[7] pre-saturtaed) as the function of incubation time (t) in CB[7]-free electrolyte solution. Γ_t and Γ_0 are the surface density of Fc@CB[7] complex at certain incubation time and at initial state. The dashed line is to guide eyes only. (B) The relationship between $\ln(\Gamma_t/\Gamma_0)_{Fc@CB[7]}$ and *t*. The solid line shows the best linear fit based on first-order kinetic model (see text for details), from which the dissociation rate constant (k_{-1}) of Fc@CB[7] complex formed on FcC11S-/C8S-Au SAM was determined.

Note: Reprinted with permission from *J. Phys. Chem. C* 2017, 121, 7985-7992. Copyright (2017), *American Chemical Society.*

Based on the CV deconvolution results shown in Figure 3.8 (B), the mole fraction of Fc@CB[7] complex $(\Gamma_t/\Gamma_0)_{Fc@CB[7]}$ remained on CB[7] pre-saturated FcC11S-/C8S-Au SAM was determined and plotted as the function of its incubation time (t) in a CB[7]-free electrolyte solution, which is shown in Figure 3.9 (A); and its natural logarithm form $(\ln(\Gamma_t/\Gamma_0)_{Fc@CB[7]})$ shows the linear decreasing trend (Figure 3.9B) as predicted from the first-order kinetics. The fitting of this result with equation 3.14 yields a k_{-1} of (0.08 ± 0.01) min^{-1} for the dissociation of Fc@CB[7] host-guest complex formed on FcC11S-/C8S-Au SAM.

The impacts of these kinetic data are substantial. First is their correlation with the experimentally determined formation constant (*K*) of Fc@CB[7] host-guest complex, the other is the comparison with the host-guest reaction kinetics in homogenous solution. For the former, the deduced *K* value (3.5±0.8 × 10^4 M^{-1}) from above determined binding (k_1) and dissociation rate constant (k_{-1}) based on equation 3.7 is similar to the value determined from thermodynamic studies (7.3±1.8 × 10^4 M^{-1} for Fc@CB[7] complex formed on FcC11S-/C8S-Au SAM prepared by co-adsorption with 5% mole fraction of FcC11SH). Their consistency confirms our CV deconvolution based electrochemical quantitative approach as a convenient and reliable tool for studying supramolecular host-guest binding chemistry at electroactive molecular interfaces.

The comparison between above determined kinetic parameters for Fc@CB[7] host-guest binding at organized molecular interfaces with those in solution phase is more intriguing. The high binding affinities of CB[7] with small guest molecules (e.g., naphthylethylammonium cation, berberine, and adamantly guests) in aqueous solution have been attributed to their very large binding rate constant (10^7 to 10^9 $M^{-1}s^{-1}$), as well as their very small dissociation rate constants (10^{-2} to 10^1 s^{-1}). [229-231] Compared with CB[7], CB[6] with a smaller sized inner cavity has many orders of magnitude lower binding rate constants (< 10^4 $M^{-1}s^{-1}$) with guests (e.g., cycloalkylmethylamines, alkylammonium ions);[56,233] and *β*-CD with similar sized inner cavity but significantly different composition and structure has much higher dissociation rate constant (> 10^4 s^{-1}) for its host-guest complexes (e.g. naphthylethanols).[234]

As our experimentally determined dissociation constant (0.0013 s^{-1}) of Fc@CB[7] complex formed on FcC11S-/C8S-Au SAM is similar to the dissociation constants of ultra-stable guest@CB[7] complexes formed in solution, it becomes clear that the major kinetic

difference between the Fc@CB[7] host-guest binding at molecular interface and in homogenous solution is that the former has much lower binding rate constant (< 10^2 $M^{-1}s^{-1}$). According to transition state theory and Arrhenius equation,[149] this could be due to the limited collision frequency and orientation between CB[7] and covalently attached Fc group as the result of strong steric hindrance effect on surface; besides, the electronegative carbonyl portals of immobilized CB[7] on FcC11S-/C8S-Au SAM may cause enhanced activation energy for subsequent CB[7] binding; The exact reasons behind the restricted host-guest binding kinetics at organized molecular interfaces certainly deserve further investigation from both experimental and theoretical aspects.

3.4. Conclusion

For the first time, the formation of Fc@CB[7] host-guest complex at "near-ideal" electroactive self-assembled monolayer on gold was quantitatively evaluated by systematic CV investigations. It was found that compared with free Fc terminal groups, the Fc@CB[7] complex formed on FcC11S-/C8S-Au SAM has a distinct pair of CV redox peaks located at more positive potential. By deconvoluting their overlapped CV redox peaks with Gaussian-Lorentzian fitting protocol, the mole fraction of Fc terminal groups on SAM bound to CB[7] can be easily quantified. Based on this, the thermodynamic study shows that the Fc@CB[7] host-guest binding on FcC11S-/C8S-Au SAM has a moderate thermodynamic stability (sub-μM level formation constant) with respect to its ultra-strong binding in solution phase (above nM level formation constants). The subsequent kinetic study further reveals its much lower binding rate constant, but similar dissociation rate constant compared with those CB[7]-guest pairs formed in solution phase. Although not that impressive, the Fc-terminated alkanethiolate SAMs still provide a reliable and convenient platform for forming stable Fc@CB[7] host-guest complex at molecular interface, as well as for its surface characterizations based on electrochemical and other techniques (e.g., FTIR spectroscopy, contact angle measurement). Following this fundamental study, we subsequently explored the broad application potentials of this new interfacial Fc@CB[7] host-guest binding system, which are described in the chapters 4-6.

Chapter 4.

Host-guest binding as a structural probe for self-assembled monolayers

In this chapter, we combined host-guest recognition chemistry and electrochemical analysis (CV) to demonstrate that the nanometer-sized supramolecular host can be adapted as sensitive probes for the structural heterogeneity in organized molecular assemblies on surface. Based on the distinct CV responses of Fc@CB[7] complex and free Fc terminal group on SAMs, we were able to estimate the conversion rate of Fc to Fc@CB[7], a direct indication of the overall Fc density and uniformity. It was found that the FcC11S-/C8S-Au SAM prepared by co-adsorption in a binary solution with low mole fraction of FcC11SH and by exchanging the pre-assembled C8S-Au SAM with FcC11SH for short time have more uniformly isolated Fc groups. In contrast, the FcC11S-/C8S-Au SAM prepared by exchanging FcC11S-Au SAM with C8SH for prolonged time has non-uniformly clustered Fc groups. These results are consistent with previous studies based on conventional electrochemical or microscopic studies.

Note: this chapter is adapted with permission from:

***Qi, L.**; Tian H.; Shao, H.; Yu H.-Z. Host-Guest Interaction at Molecular Interfaces: Cucurbit[7]uril as a Probe of Structural Heterogeneity in Ferrocenyl Self-Assembled Monolayers on Gold J. Phys. Chem. C, 2018, 122, 15986-15995 (featured as the front cover).* Copyright (2018) American Society of Chemistry

I have performed most of the experimental work and drafted the paper; Huihui Tian (a visiting student from 2012 to 2015) explored the preparation of mixed FcC11S-/C8S-Au SAMs and performed preliminary CV studies. Professor Huibo Shao, the supervisor Huihui Tian at Beijing Institute of Technology, together with Dr. Hogan Yu supervised the entire project and helped with writing the paper.

4.1. Introduction

As one important type of molecular assemblies, the self-assembled monolayers (SAMs) formed on solid substrates have been explored for applications in many fields, such as surface wetting/lubrication,[175,235] photolithography,[143,236] and nanofabrication.[134] With specific terminal groups, additional intriguing functions can be introduced to SAMs, which enable their use for fabricating biosensors[141] and other types of molecular devices.[142,237] Moreover, the properties and functions of SAMs have been found strongly related to their distribution of terminal groups; as a typical example, the Fc-terminated alkanethiolate SAMs on gold have been widely used for studying the long-range ET kinetics.[208-210] For this purpose, an "ideal structured" SAM with uniformly dispersed Fc terminal groups is preferential in order to ensure their noninteracting, independent, and homogeneous ET behavior.[203]

The general strategy for achieving such "ideal structured" SAM is by preparing mixed component ferrocenylalkanethiolate/alkanethiolate SAMs on gold, where the ferrocenylalkanethiols are diluted by another alkanethiols on surface[134] The conventional microscopic (1-2 nm sized "bright spots" observed in STM image)[238] and electrochemical evidences (a single pair of symmetric CV redox peaks with peak width at half-height close to 90.6 mV)[203] have indicated that the mixed Fc-SAMs with ideal structural features could be made by either co-adsorption (with low mole fraction of ferrocenylalkanethiol in the mixed assembly solution)[188, 214] or exchange method (immersing the pre-assembled alkanethiolate SAM with ferrocenylalkanethiol for a short period of time).[238] In addition, our recent CV study indicates that another way of exchange method (i.e., immersing the pre-assembled ferrocenylalkanethiolate SAM with diluent alkanethiol for long period of time) may result in clustered Fc terminal groups (a broad pair of CV redox peaks located at higher potential).[188] However, the distribution of Fc terminal groups probed by above two conventional techniques are not so convinced: First, it is still controversial that whether the tiny regions (nm^2 to μm^2) imaged by microscopic techniques are capable of representing the real scenario at macro-scale ranges; secondly, although CV as a macro-scale technique can provide multiple information about the structure of ferrocenylalkanethiolate SAMs on gold,[46] these information are indirect and inadequate for knowing the exact distribution of Fc terminal groups at molecular level.

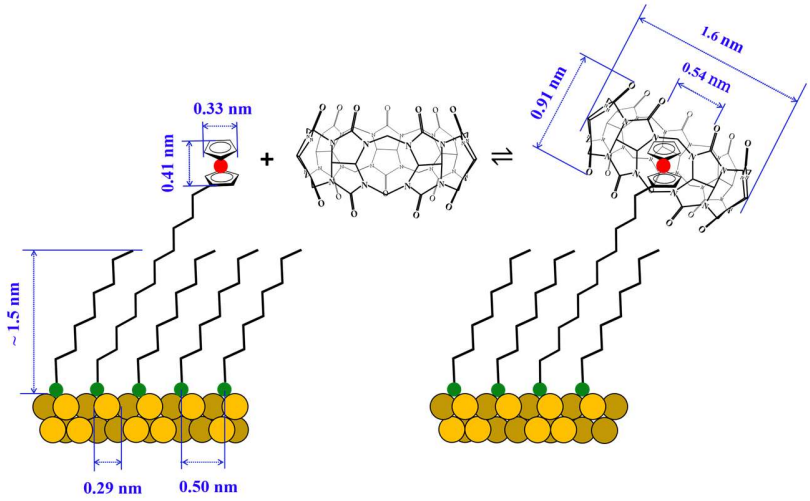

Figure 4.1. Schematic view of the dimensions of Fc@CB[7] host-guest binding on mixed FcC11S-/C8S-Au SAM.

Note: Reprinted with permission from *J. Phys. Chem. C* 2018, 122, 15986-15995. Copyright (2018), *American Chemical Society*.

In chapter 3, it has been confirmed that CB[7] can bind with the Fc terminal group of the mixed FcC11S-/C8S-Au SAM; their strong binding either in solution or at molecular interface can be attributed to the "perfect" geometric match between Fc and the inner cavity of CB[7]. Moreover, according to the dimension of Fc[203] and CB[7][31] shown in Figure 4.1, a CB[7] molecule would occupy much larger area than that of a Fc terminal group on surface; this corresponds well to the previous estimation that the theoretical maximum surface densities of a closely-packed ferrocenylalkanethiolate SAM and a CB[7] monolayer are 4.6×10^{-10} mol/cm^2,[213] and 7.5×10^{-11} mol/cm^2,[126] respectively. Accordingly, the Fc@CB[7] host-guest binding on SAMs should strongly depend on the free space around Fc terminal groups, which directly correlates to their distributions on surface. Therefore, it is possible to probe the distribution of Fc terminal groups on SAMs based on the interfacial Fc@CB[7] host-guest binding, which could provide more reliable and straightforward information compared to the conventional microscopic and electrochemical characterizations.

In this chapter, the degrees of Fc@CB[7] host-guest binding on mixed ferrocenylundecanethiolate/n-alkanethiolate SAMs on gold (FcC11S-/CnS-Au SAM) prepared with different routes and using various lengths of n-alkanethiols were investigated by CV. These binding results as well as their comparison with previous

microscopic and electrochemical studies strongly confirm the great ability of this interfacial Fc@CB[7] host-guest binding pair as a molecular probe for the distribution of Fc terminal groups on SAMs, which further strengthened and extended our understanding about the structural heterogeneity of alkanethiolate SAMs on gold.

4.2. Experimental details

4.2.1. Reagents and materials

1-hexanethiol (C6SH), 1-undecanethiol (C11SH), and 1-tetradecanethiol (C14SH) were purchased from Sigma Aldrich (St. Louis, MO). Other chemicals and materials are same with those described in section 3.2.1 (chapter 3).

4.2.2. Preparation of ferrocenylundecanethiolate/n-alkanethiolate SAMs on Gold (FcC11S-/CnS-Au SAMs) and their incubation with CB[7]

Co-adsorption method for preparing binary FcC11S-/CnS-Au SAMs (n = 6, 8, 11, and 14): the piranha-cleaned gold slides (see section 2.1.3) were immersed in a mixed FcC11SH/CnSH ethanol solution (95%) at room temperature for more than 20 h. The total concentration of thiols was 1.0 mM with different mole factions of FcC11SH ($\chi_{FcC11SH}$). After incubation, the gold slides were thoroughly washed with copious amounts of ethanol solution (95%) and deionized water.

Post-assembly exchange method for preparing mixed FcC11S-/C8S-Au SAMs: the piranha-cleaned gold slides were first immersed in 1.0 mM FcC11SH ethanol solution (95%) at room temperature for more than 20 h (a pre-assembled single FcC11S-Au SAM). Then the gold slides were taken out and immersed into 1.0 mM C8SH ethanol solution (95%) for different periods of time. For direct comparison, the exchange was also carried out in the reversed manner, i.e., a single C8S-Au SAM was first prepared by immersing the piranha-cleaned gold slides in 1.0 mM C8SH ethanol solution (95%) at room temperature for more than 20 h, then the gold slides were taken out and immersed into 1.0 mM FcC11SH ethanol solution (95%) for different periods of time.

To examine the degree of interfacial Fc@CB[7] host-guest binding, the freshly prepared FcC11S-/CnS-Au SAMs were immersed in the aqueous solution containing 1.0 mM CB[7] for 2 h in prior to the CV detections.

4.2.3. Surface characterizations by CV and contact angle measurements

CVs and water contact angles were measured for mixed FcC11S-/CnS-Au SAMs before and after incubation with 1.0 mM CB[7] for 2 h. The detailed information of CV and water contact angle measurements are described in chapter 2 and section 3.2.3 (chapter 3).

4.3. Results and discussion

4.3.1. Fc@CB[7] host-guest binding on FcC11S-/C8S-Au SAM prepared by different routes

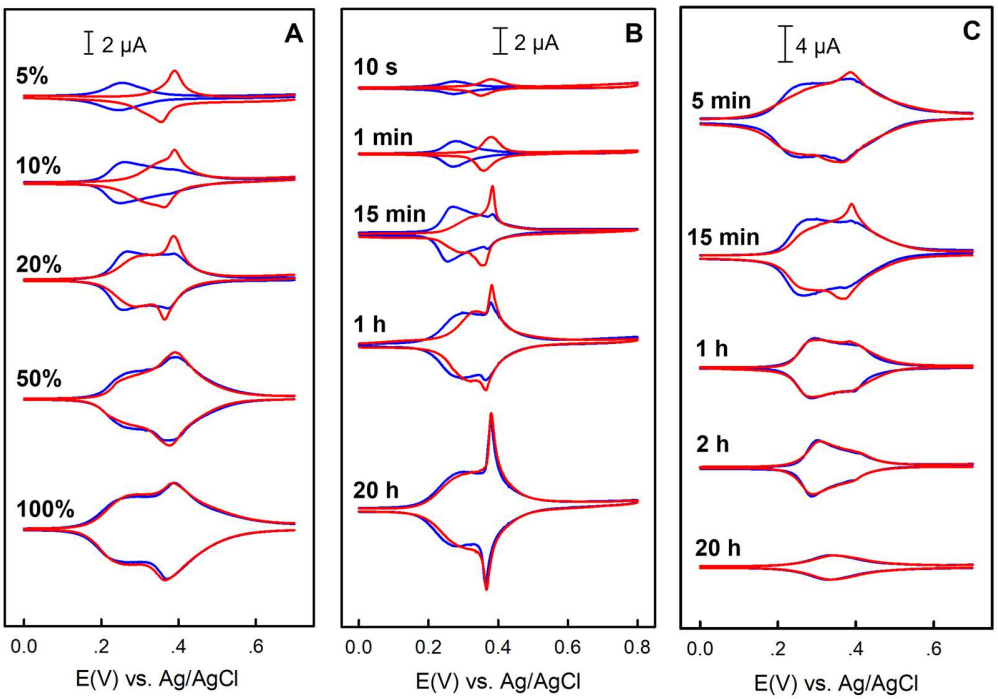

Figure 4.2. CVs of FcC11S-/C8S-Au SAMs prepared by (A) co-adsorption method with different $\chi_{FcC11SH}$, (B) exchange the pre-assembled C8S-Au SAM with 1.0 mM FcC11SH for different periods of time, and (C) exchange the pre-assembled FcC11S-Au SAM with 1.0 mM C8SH for different periods of time. The blue and red curves are the CVs before and after incubation with 1.0 mM CB[7] for 2 h. The supporting electrolyte was 0.1 M $NaClO_4$, and the scan rate was kept as 50 mV/s.

Note: Reprinted with permission from *J. Phys. Chem. C* 2018, 122, 15986-15995. Copyright (2018), *American Chemical Society*.

We first investigated the distribution of Fc terminal groups on mixed FcC11S-/C8S-Au SAMs prepared with various methods. The blue curves in Figure 4.2 (A) show the CVs of FcC11S-/C8S-Au SAMs prepared by co-adsorption method with different mole fractions of FcC11SH ($\chi_{FcC11SH}$). It can be seen that the both size and shape of CVs are highly dependent on $\chi_{FcC11SH}$: For low $\chi_{FcC11SH}$ (5%), only a single pair of symmetric redox peaks is clearly observed; with higher $\chi_{FcC11SH}$, the CVs not only become stronger but also show the appearance of a shoulder pair of redox peaks at more positive potential, which gradually becomes significant. The blue curves in Figure 4.2 (B) and (C) are the CVs of FcC11S-/C8S-Au SAMs prepared by the two exchange methods. As expected, the CV peaks become stronger when exchanging the pre-assembled single C8S-Au SAM with FcC11SH for longer period of time, which is also accompanied with an enhancing shoulder pairs of redox peaks located at higher potential (Figure 4.2B); in contrast, the other way of exchange, i.e., exchanging the pre-assembled single FcC11S-Au SAM with C8SH, results in “opposite” variations on CVs (i.e., shrinking and less splitting CVs with longer exchange time). By integrating the anodic waves of all blue CVs shown in Figure 4.2, the total Fc surface densities (Γ_{Fc}) of FcC11S-/C8S-Au SAMs prepared by various methods were determined based on equation 3.3 (see section 3.3.1) and summarized in Figure 4.3, which are consistent with the visually observed variations on the size of their CVs (i.e., Γ_{Fc} increases with higher $\chi_{FcC11SH}$ or longer exchange time by FcC11SH, but decreases with longer exchange time by C8SH).

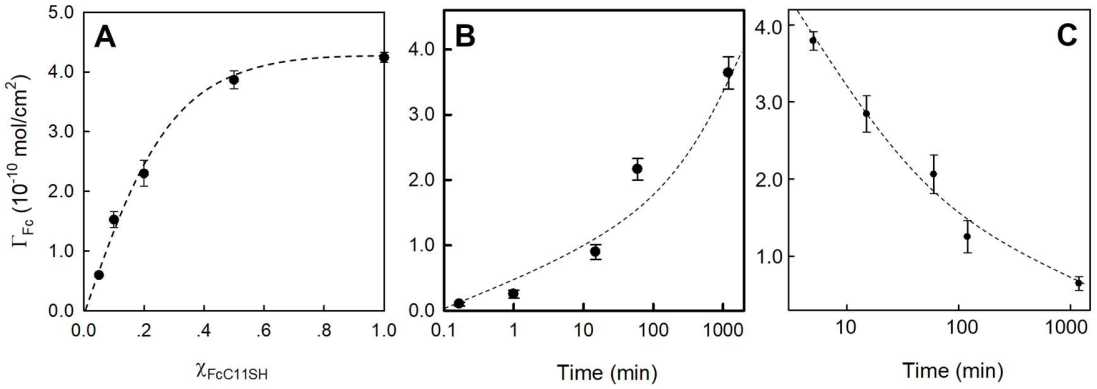

Figure 4.3. Total surface densities of Fc terminal groups (Γ_{Fc}) on FcC11S-/C8S-Au SAMs prepared by (A) co-adsorption with different $\chi_{FcC11SH}$; (B) exchange C8S-Au SAM with FcC11SH for different times; and (C) exchange FcC11S-Au SAM with C8SH for different times. The dashed lines are for eney guide only.

Note: Reprinted with permission from *J. Phys. Chem. C* 2018, 122, 15986-15995. Copyright (2018), *American Chemical Society*.

The red curves in Figure 4.2 are the CVs of these FcC11S-/C8S-Au SAMs after incubation with CB[7], where interesting phenomenon were observed: First, for FcC11S-/C8S-Au SAMs prepared by co-adsorption and by exchanging the pre-assembled single C8S-Au SAM with FcC11SH (Figure 4.2, A and B), remarkable changes were observed at the cases of low Γ_{Fc} (e.g., co-adsorption with $\chi_{FcC11SH}$ of 5%; exchange C8S-Au SAM by FcC11SH for 10 s and 1 min), where the original pair of CV redox peaks vanished and a new pair of redox peaks appeared at more positive potential; this indicates a high conversion rate of Fc terminal group to Fc@CB[7] host-guest complex on SAM. With higher Γ_{Fc} prepared by these two methods (e.g., co-adsorption with $\chi_{FcC11SH}$ of 10% and 20%; exchange C8S-Au SAM by FcC11SH for 15 min and 1 h), the CB[7] incubation induced changes on CVs become rather complicated due to their originally "split" CV responses as caused by more heterogeneously distributed Fc terminal groups on SAMs[213, 239, 297]); specifically, the redox peaks at lower potential (peak I) diminish and shift positively, while the redox peaks at higher potential (peak II) become stronger but show no obvious peak shift; these observations indicate the "preferential" binding of CB[7] to more dispersed Fc terminal groups on SAMs (corresponding to peak I at lower potential),[213, 239] and the resulted Fc@CB[7] host-guest complex may have a strongly overlapped CV redox peak and similar formal potential with the aggregated Fc terminal groups on SAMs (corresponding to peak II at more positive potential);[213, 239] this might be the reason for the

“enhanced” peak II after CB[7] incubation. When Γ_{Fc} is close to its maximum value (e.g., co-adsorption with $\chi_{FcC11SH}$ of 50% and 100%; exchange C8S-Au SAM by FcC11SH for 20 h), there are much less or even negligible changes on the CVs of FcC11S-/C8S-Au SAMs after CB[7] incubation, which is easily understandable as the Fc terminal groups become too crowded to bind with CB[7] (lack of surrounding space). More interestingly, for FcC11S-/C8S-Au SAMs prepared by exchanging the pre-assembled single FcC11S-Au SAM with C8SH (Figure 4.2C), only those at earlier stage of exchange process (5 min and 15 min) show obviously changed CV after CB[7] incubation; while those after long time of exchange ($\geq$ 1h), although has much decreased Γ_{Fc}, show negligible changes after CB[7] incubation. These interesting phenomena indicate that the two different ways of exchange method may eventually result in distinct distributions of Fc terminal groups on FcC11S-/C8S-Au SAM.

In order to quantify the Fc@CB[7] host-guest complex formed on FcC11S-/C8S-Au SAMs prepared by different methods, especially for those with split CV responses before and after CB[7] incubation, the Gaussian-Lorentzian fitting protocol (as described in section 3.3.2) was used to determine the surface densities of Fc contributed from individual redox peaks. In Figure 4.4, an example is provided with the CVs of FcC11S-/C8S-Au SAM prepared by co-adsorption method with $\chi_{FcC11SH}$ of 20%. As clearly depicted, with similar formal potentials the relative size between the two deconvoluted redox peaks (I and II) at lower and higher potentials changes significantly after CB[7] incubation (I’ and II’); the Fc surface densities corresponding to each deconvoluted redox peak ($\Gamma_{I/I'}$ and $\Gamma_{II/II'}$) were then calculated (based on equations 3.5 and 3.6, see section 3.3.2) and summarized in Table 4.1 together with the total Fc surface density (Γ_{Fc}) derived from the original CV anodic waves.

Table 4.1. Quantitative analysis of the CVs of FcC11S-/C8S-Au SAM prepared with a $\chi_{FcC11SH}$ of 20% before and after CB[7] incubation.

	Γ_{Fc} (10^{-10} mol/cm^2)	$\Gamma_{I/I'}$ (10^{-10} mol/cm^2)	$\Gamma_{II/II'}$ (10^{-10} mol/cm^2)
FcC11S-/C8S-Au	2.23 ± 0.22	1.14 ± 0.14	1.16 ± 0.11
CB[7]@FcC11S-/C8S-Au	2.28 ± 0.18	0.82 ± 0.09	1.45 ± 0.12
$\Delta\Gamma$	0.05 ± 0.28	–0.32 ± 0.17	0.29 ± 0.16

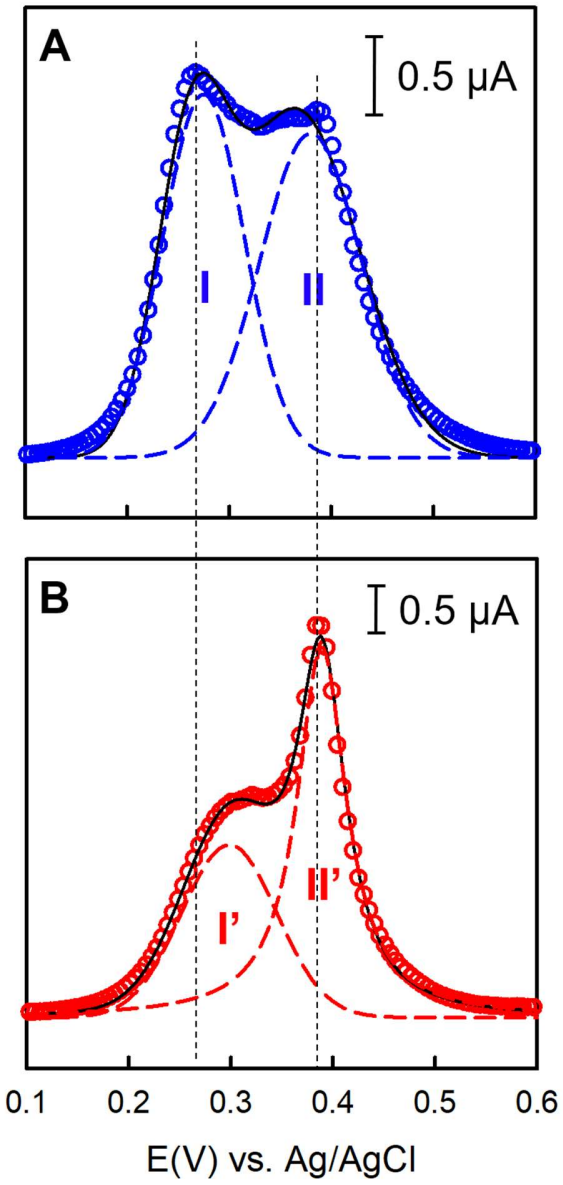

Figure 4.4. Gaussian-Lorentzian deconvolution of the CV anodic waves of (A) FcC11S-/C8S-Au SAM prepared by co-adsorption with $\chi_{FcC11SH}$ of 20% and (B) after incubation with 1.0 mM CB[7] for 2 h. The blue and red circles show the experimental data (i.e., the original CVs); the dashed lines are the deconvoluted redox peaks, and the black solid lines show their sum (i.e., the overall fit).

Note: Reprinted with permission from *J. Phys. Chem. C* 2018, 122, 15986-15995. Copyright (2018), *American Chemical Society*.

It can be seen that within experimental uncertainties, Γ_{Fc} remains unchanged before and after CB[7] incubation ($\Delta\Gamma_{Fc}$ = 0.05±0.28 × 10^{-10} mol/cm^2), which confirms that the CB[7] host binding does not affect the redox activity of Fc terminal groups on SAMs. More importantly, upon CB[7] incubation the decreased Fc surface density corresponding to peak I at lower potential ($\Gamma_{I'} - \Gamma_I$ = –0.32±0.17 ×10^{-10} mol/cm^2) equals to the increased Fc surface density corresponding to peak II at higher potential ($\Gamma_{II'} - \Gamma_{II}$ = 0.29±0.16 ×10^{-10} mol/cm^2). This further confirms that the enhanced peak II to peak II' after CB[7] incubation could be the sum of the redox responses from Fc@CB[7] host-guest complex and the aggregated Fc terminal groups on FcC11S-/C8S-Au SAM. Accordingly, the conversion rate of Fc terminal group to Fc@CB[7] complex ($\chi_{Fc@CB[7]}$) for each SAM can be estimated by equation 4.1:

$$\chi_{\mathrm{Fc@CB[7]}} = \frac{\Gamma_{\mathrm{II}'} - \Gamma_{\mathrm{II}}}{\Gamma_{\mathrm{Fc}}} \qquad (4.1)$$

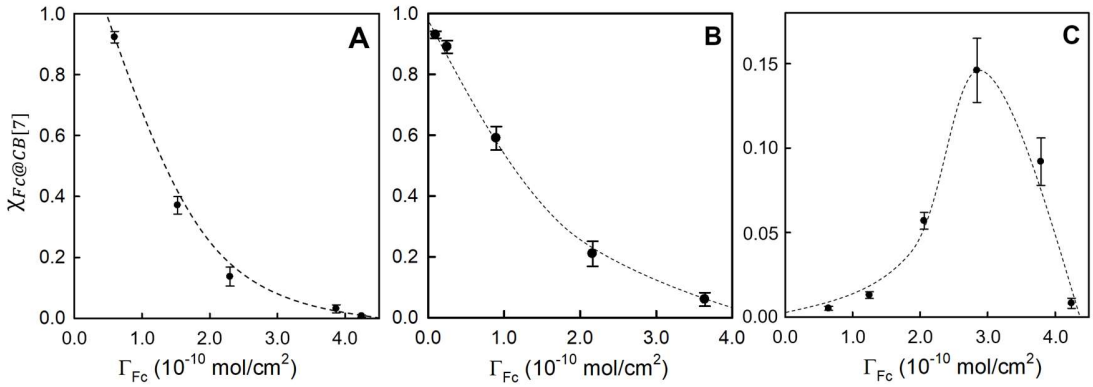

Figure 4.5. Conversion rate of Fc terminal group to Fc@CB[7] host-guest complex ($\chi_{Fc@CB[7]}$) as the function of total Fc surface density (Γ_{Fc}) of FcC11S-/C8S-Au SAMs prepared by (A) co-adsorption method, (B) exchange the pre-assembled C8S-Au SAM with FcC11SH, and (C) exchange the pre-assembled FcC11S-Au SAM with C8SH.

Note: Reprinted with permission from *J. Phys. Chem. C* 2018, 122, 15986-15995. Copyright (2018), *American Chemical Society*.

Based on equation 4.1, $\chi_{Fc@CB[7]}$ was determined as the function of Γ_{Fc} for FcC11S-/C8S-Au SAMs prepared by different methods, which are displayed in Figure 4.5. It can be seen that regardless of the preparation methods, the FcC11S-/C8S-Au SAMs with high Γ_{Fc} (> 3.0×10^{-10} mol/cm^2) all have very low $\chi_{Fc@CB[7]}$ (< 10%); this is because of the too

crowded Fc terminal groups (lack of surrounding space). However, the circumstances become significantly different with decreased Γ_{Fc}: For FcC11S-/C8S-Au SAMs prepared by co-adsorption method and by exchanging the pre-assembled C8S-Au SAM with FcC11SH, their $\chi_{Fc@CB[7]}$ increase with decreased Γ_{Fc}, which reach above 90% when Γ_{Fc} decrease to extremely low level (< 0.5×10^{-10} mol/cm^2). However, for FcC11S-/C8S-Au SAMs prepared by exchanging the pre-assembled FcC11S-Au SAM with C8SH, only a moderate $\chi_{Fc@CB[7]}$ (15%) was found at an intermediate level of Γ_{Fc} (2.8×10^{-10} mol/cm^2); and the further decreased Γ_{Fc} leads to unnoticeable $\chi_{Fc@CB[7]}$ (< 5%).

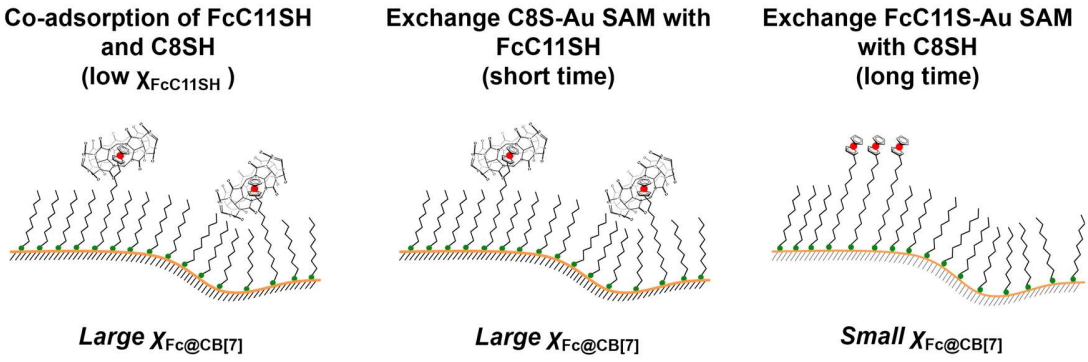

Figure 4.6. Schematic view of the distribution of Fc terminal groups on mixed FcC11S-/C8S-Au SAMs (low Γ_{Fc}) prepared by different methods as probed by Fc@CB[7] host-guest binding.

Note: Reprinted with permission from *J. Phys. Chem. C* 2018, 122, 15986-15995. Copyright (2018), *American Chemical Society.*

By taking into account the CVs before and after CB[7] incubation, as well as the estimated $\chi_{Fc@CB[7]}$, the structural information learned for the mixed FcC11S-/C8S-Au SAMs with low Γ_{Fc} prepared by different methods are illustrated in Figure 4.6 (The drawing of curved gold surfaces represents the atomic level of roughness and crystal defects). Briefly, the ideal-structured mixed SAM with well-dispersed Fc terminal groups (enough surrounding space for CB[7] host binding) could be achieved by co-adsorption with low $\chi_{FcC11SH}$, and by exchanging the pre-assembled C8S-Au SAM with FcC11SH for a short period of time. In contrast, the other way of exchange method may finally result in "clustered" Fc terminal groups on mixed SAM, which are not able to bind with CB[7] due to the lack of surrounding space. Above findings are generally consistent with the previous

studies based on microscopic (STM)[238] and electrochemical characterizations;[214] nevertheless, the interfacial Fc@CB[7] host-guest binding results derived from CV provide much more straightforward and unequivocal evidence for the distribution of Fc terminal groups on SAMs in either macroscale or molecular level.

4.3.2. Fc@CB[7] host-guest binding on mixed FcC11S-/CnS-Au SAMs prepared with different lengths of diluent alkanethiol

Besides different preparation methods, another important modification to mixed ferrocenyllalkanethiolate/alkanethiolate SAMs is to adopt different lengths of diluent alkanethiols, by which one can tune the dielectric properties in the microenvironment of Fc terminal groups.[215, 217, 240] For evaluating the ability of Fc@CB[7] host-guest binding for probing the exposure degree of Fc terminal groups surrounded by different lengths of diluent alkanethiols, three other mixed FcC11S-/CnS-Au SAMs (n = 6, 11, 14) were prepared by co-adsorption method with low $\chi_{FcC11SH}$, and their CVs are shown in Figure 4.7. The original CVs (blue curves) of these binary SAMs are all dominated by single pair of redox peaks without obvious “splitting” shapes; and their redox peaks shift positively with longer diluent alkanethiols (thermodynamically more difficult oxidation of Fc to Fc^+ in less polar microenvironment). Upon CB[7] incubation (red curves), the CV of FcC11S-/C6S-Au SAM shows essentially the same change as that of FcC11S-/C8S-Au SAM; for FcC11S-/C11S-Au SAM, its CV shows a pair of small but discernible shoulder peaks at more positive potential; most strikingly, the CV of FcC11S-/C14S-Au SAM shows almost no changes.

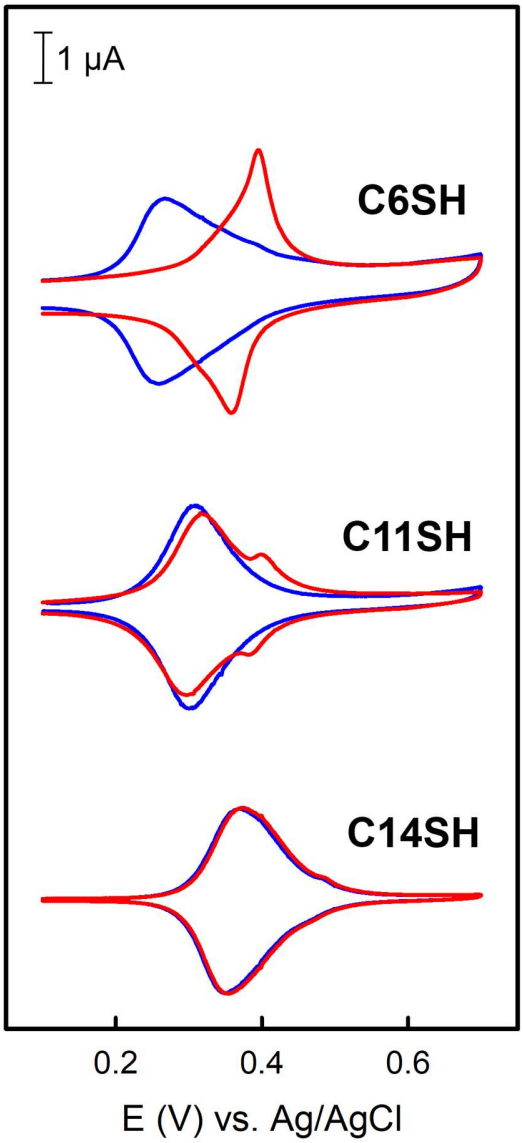

Figure 4.7. CVs of mixed FcC11S-/CnS-Au SAMs prepared by co-adsorption of FcC11SH with different n-alkanethiols: (A) C6SH ($\chi_{FcC11SH}$ = 3%), (B) C11SH ($\chi_{FcC11SH}$ = 10%), and (C) C14SH ($\chi_{FcC11SH}$ = 20%). The blue and red curves are the CVs before and after incubation with 1.0 mM CB[7] for 2 h. The supporting electrolyte was 0.1 M $NaClO_4$, and the scan rate was kept as 50 mV/s.

Note: Reprinted with permission from *J. Phys. Chem. C* 2018, 122, 15986-15995. Copyright (2018), *American Chemical Society.*

By deconvoluting the anodic waves of CVs (shown in Figure 4.7) before and after CB[7] incubation with Gaussian-Lorentzian fitting protocol, the $\chi_{Fc@CB[7]}$ of these mixed

FcC11S-/CnS-Au SAMs were estimated based on equation 4.1 and compared with the $\chi_{Fc@CB[7]}$ of the mixed FcC11S-/C8S-Au SAM prepared by co-adsorption method ($\chi_{FcC11SH}$ = 5%).

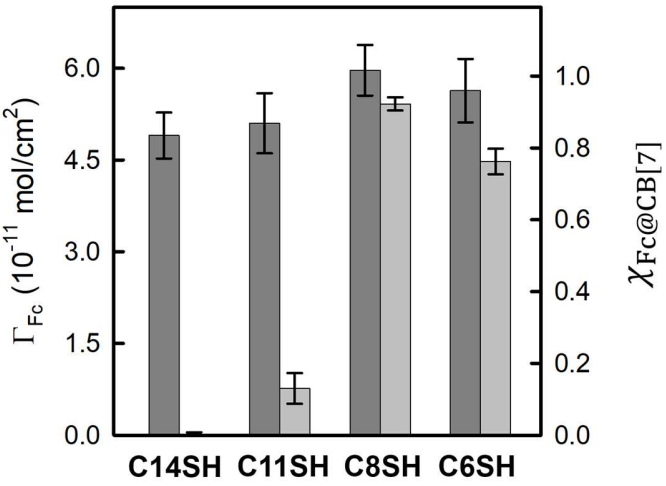

Figure 4.8. Γ_{Fc} (dark gray bars) and $\chi_{Fc@CB[7]}$ (light gray bars) of mixed FcC11S-/CnS-Au SAMs (n = 14, 11, 8, 6) prepared by co-adsorption method (with different $\chi_{FcC11SH}$).

Note: Reprinted with permission from *J. Phys. Chem. C* 2018, 122, 15986-15995. Copyright (2018), *American Chemical Society.*

As shown in Figure 4.8, all these mixed FcC11S-/CnS-Au SAMs have with similar and low Γ_{Fc} (4.5×10^{-11} mol/cm^2 to 6.4×10^{-11} mol/cm^2). Their $\chi_{Fc@CB[7]}$ are highly dependent on the length of diluent alkanethiols: The $\chi_{Fc@CB[7]}$ of FcC11S-/C14S-Au SAM is negligible (< 1%), and it is also small for FcC11S-/C11S-Au SAM (9±3%). In contrast, for FcC11S-/CnS-Au SAMs with short diluent alkanethiols (C8SH and C6SH), their $\chi_{Fc@CB[7]}$ become much higher; moreover, it is also interesting to find a relatively lower $\chi_{Fc@CB[7]}$ for FcC11S-/C6S-Au SAM (76±4%) than that of FcC11S-/C8S-Au SAM (92±3%).

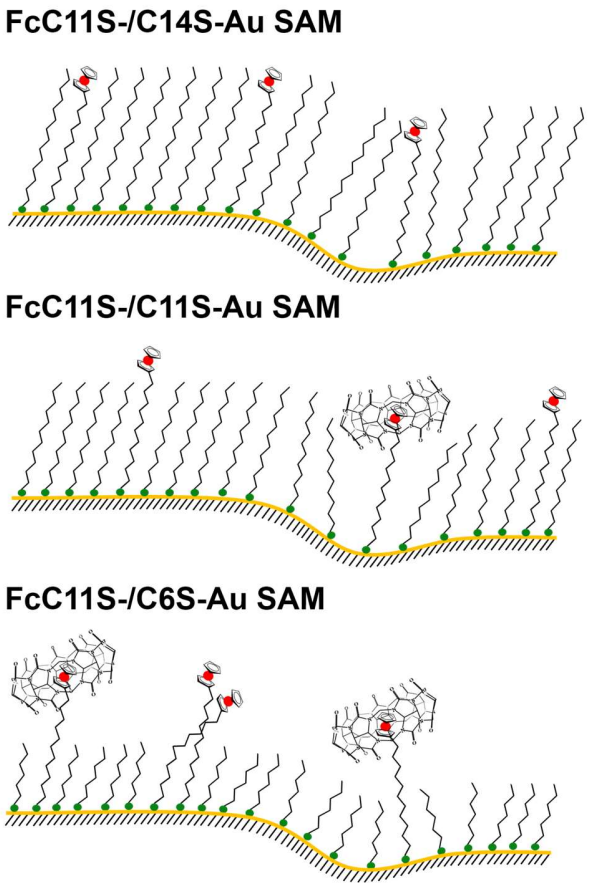

Figure 4.9. Schematic view of the distribution of Fc terminal groups on mixed FcC11S-/CnS-Au SAMs (n = 6, 11, 14) as probed by interfacial Fc@CB[7] host-guest binding.

Note: Reprinted with permission from *J. Phys. Chem. C* 2018, 122, 15986-15995. Copyright (2018), *American Chemical Society*.

Above results clearly reflect that the interfacial host-guest binding between CB[7] and Fc terminal groups on mixed FcC11S-/CnS-Au SAMs is strongly inhibited by using longer diluent alkanethiols (n = 11 and 14), which is indicated by their less changed CVs after CB[7] incubation and the lower value of $\chi_{Fc@CB[7]}$. This could be due to the buried or shielded Fc terminal groups (lack of surrounding space for CB[7] binding) by surrounding longer alkanethiols, as illustrated in the top and middle of Figure 4.9. In contrast, the significantly changed CVs and much higher $\chi_{Fc@CB[7]}$ found for mixed FcC11S-/CnS-Au SAMs prepared with shorter diluent alkanethiols (n = 8 and 6) indicate their more exposed Fc terminal groups (enough surrounding space for CB[7] binding). It is also noticed that

compared with FcC11S-/C8S-Au SAM, the relatively smaller $\chi_{Fc@CB[7]}$ of FcC11S-/C6S-Au SAM may indicate its more complicated distribution and orientation of Fc terminal groups (e.g., small portions of clustered or bent ferrocenylalkanethiols may exist when the diluent alkanethiol is too short, as illustrated in the bottom of Figure 4.9).

4.3.3. Water contact angle measurements of mixed FcC11S-/CnS-Au SAMs prepared under different conditions

As the electronegative carbonyl portals of CB[7] should be less hydrophobic than Fc-terminated alkanethiolate SAMs, in support of above interfacial Fc@CB[7] host-guest binding results obtained by CV, several wetting studies were also carried out with their results shown in Figure 4.10. It is clearly seen that upon CB[7] incubation, only FcC11S-/C8S-Au SAMs prepared by co-adsorption method with low $\chi_{FcC11SH}$ (5%), and by exchanging the pre-assembled C8S-Au SAM with FcC11SH for very short time (1 min) show significantly decreased water contact angles; in contrast, the water contact angles kept nearly constant for mixed FcC11S-/C8S-Au SAMs prepared by exchanging the pre-assembled FcC11S-Au SAM with C8SH for prolonged hours (20 h), the mixed FcC11S-/C14S-Au SAM prepared by co-adsorption, as well as the single-component FcC11S-Au SAM. These results are consistent with the Fc@CB[7] host-guest binding results learned by CV.

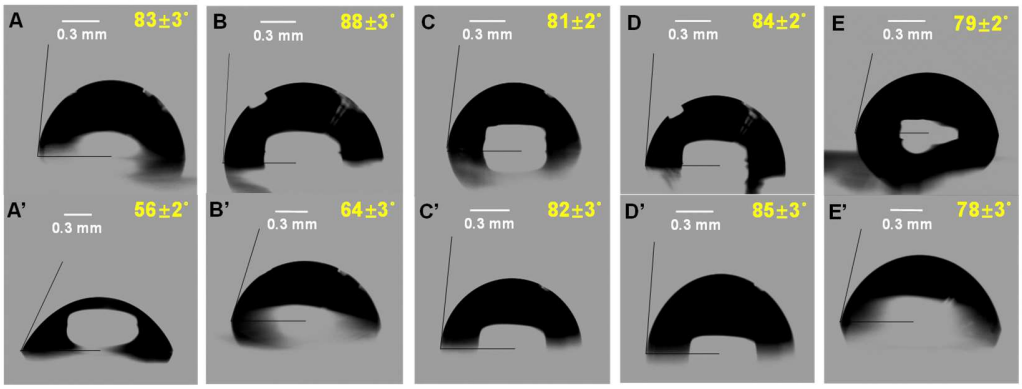

Figure 4.10. Water contact angles before (top) and after (bottom) incubation with 1.0 mM CB[7] for 2 h for (A/A') FcC11S-/C8S-Au SAM prepared by co-adsorption method ($\chi_{FcC11SH}$ = 5%); (B/B') FcC11S-/C8S-Au SAM prepared by exchanging the pre-assembled C8S-Au SAM with 1.0 mM FcC11SH for 1 min; (C/C') FcC11S-/C8S-Au SAM prepared by exchanging the pre-assembled FcC11S-Au SAM with 1.0 mM C8SH for 20 h; (D/D') FcC11S-/C14S-Au SAM prepared by co-adsorption method ($\chi_{FcC11SH}$ = 20%); and (E/E') single-component FcC11S-Au SAM prepared by immersing the gold slide in 1.0 mM FcC11SH solution for 20 h.

Note: Reprinted with permission from *J. Phys. Chem. C* 2018, 122, 15986-15995. Copyright (2018), *American Chemical Society.*

4.4. Conclusion

Based on the CVs before and after CB[7] incubation, as well as the estimated conversion rates of Fc terminal group to Fc@CB[7] host-guest complex, the distribution of Fc terminal groups of various ferrocenyalkanethiolate SAMs were examined. Specifically, the well-dispersed Fc terminal groups as the ideal structural feature for many applications could be achieved by either co-adsorption with low mole fraction of ferrocenylalkanethiol in the mixed assembly solution, or by exchanging the pre-assembled single-component alkanethiolate SAM with ferrocenylalkanethiol for a short period of time. In contrast, the other way of exchange method, and the use of longer diluent alkanethiols may result in clustered or buried Fc terminal groups on mixed SAMs. These results are consistent with and provide stronger complementary evidences to the conventional electrochemical and microscopic characterizations. More importantly, it strongly indicates that by adapting a supramolecular approach, the structural heterogeneity in organized molecular assemblies can be effectively identified.

Chapter 5.

Host-guest binding to regulate long-range electron transfer process in self-assembled monolayers

In this chapter, the long-range electron transfer (ET) of Fc terminal groups on mixed FcC11S-/C8S-Au SAM is investigated upon host-guest encapsulation by CB[7], whose inner cavity provides both a structurally defined and spatially confined nonpolar micro-environment. It was discovered that the CB[7] host binding results in thermodynamically inhibited oxidation of Fc to Fc^+, and retarded ET kinetics between Fc terminal group and gold electrode. By fitting the experimentally obtained Tafel plot with Marcus-Hush-Chidsey model, it was also found that both reorganization energy and electronic coupling for the ET kinetics between Fc terminal group and gold electrode show noticeable decrease upon CB[7] encapsulation. These results not only augment the potential of this supramolecular host-guest pair as an effective and convenient regulator of long-range ET at organized molecular interfaces, but also provide insights for understanding the microenvironmental nature of biological ET processes.

Note: this chapter is adapted with permission from:

***Qi, L.**; Yu H.-Z. Supramolecular Host–Guest Inclusion to Regulate Long-Range Electron Transfer at Highly Oriented Molecular Interfaces J. Phys. Chem. C, 2019, 123,26315-26323.* Copyright (2019) American Society of Chemistry.

5.1. Introduction

Long-range electron transfer (ET) across various molecular bridges have been investigated for decades as they play critical roles in both life science processes (e.g., photosynthesis, respiration, cellular signal transduction, and metabolic cycles)[241,242] and engineering applications (e.g., electrochemical biosensing and energy

conversion/storage).[243,244] Up to date, there have been tremendous amount of efforts on exploring the factors affecting long-range ET processes, such as the length, structure, and composition of the "molecular bridges" between the ET donor and acceptor, as well as their surrounding medium, which provided unequivocal insights for understanding the ET mechanism via tunneling, hopping, or flickering resonance mechanism.[242,245-248]

It is also well known that the ET processes involved in biological systems usually occur in lower dielectric medium (e.g., proteins) with respect to aqueous solution (ε = 78), which would lead to the smaller reorganization energy for ET kinetics according to the prediction of Marcus theory.[248-252] However, the actual impacts of biological medium on the ET kinetics is rather complicated as both faster (e.g., 10^8 ~ 10^{15} folds enhanced ET rates by enzymatic catalysis[250]) and slower ET processes have been found with different structural origins of the low-dielectric medium (i.e., nonpolar structures or fixed polar structures/dipoles).[249-251,253] Therefore, an in-depth understanding about the role of low-dielectric medium with a well-defined structural origin will help to better understand and modulate biological ET processes, as well as guide the design of more efficient molecular electronic devices.

The mixed ferrocenylalkanethiolate/alkanethiolate SAMs on gold with highly-organized structure have been intensively used for long-range ET studies[208,210,254-265] due to the following reasons: First, the covalently immobilized redox-active Fc terminal groups allow the nonadiabatic ET tunneling process across the alkyl bridge (a thickness less than 20 Å) without the interference from the mass transport processes in solution (e.g., diffusion);[208,210,263] besides, by using diluent alkanethiols the Fc terminal groups can be well-separated on mixed SAMs with minimized heterogeneous distribution of ET kinetics.[210,214] With this ideal platform, the influence of many factors (e.g., temperature,[210,263] type of solvent medium[262] and supporting electrolyte,[260,261] chemical nature of bridge and diluent alkanethiols)[256-259] on long-range ET process have been investigated. The thermodynamics of ET can be evaluated from its redox potential, while the kinetics of ET is always evaluated by those important parameters (e.g., standard rate constant k_0, reorganization energy λ, and electronic coupling H) determined from *Bulter-Volmer* or *Marcus*-type kinetic models.[210,220,252] Moreover, the tunneling constant (β), a parameter associated with the ET mechanism, can be obtained by measuring k_0 at different ET distances (controlled by the length of alkyl bridge).[208,254-257]

Based on mixed ferrocenlyalkanethiolate SAMs, previous investigations on low-dielectric ET medium were conducted with different organic solvents.[261,262] Unfortunately, these nonaqueous solvents always bring “global-scale” influences on the structure of alkanethiolate SAMs besides changing the dielectric properties of their surroundings, which impose much difficulty for either accurately measuring or interpreting the results of ET kinetic study.[261] An alternative approach is to use diluent alkanethiols of varied lengths to modulate the dielectric medium around Fc terminal groups on SAMs;[265] however, such approach require massive preparation work on molecular synthesis and modification; moreover, no systematic changes were found on the reorganization energy of Fc terminal surrounded by different lengths of diluting alkanethiols, which indicates that a low-dielectric ET medium might not be well-created by this approach.[265]

Fortunately, the simple and conveniently adapted supramolecular host-guest binding chemistry may provide a promising alternative way for studying the ET behavior of redox-active terminal groups in nonaqueous environment since the inner cavities of macrocyclic host molecules are less polar and polarizable than bulk aqueous medium, which provide lower dielectric ET media upon binding with guests. More importantly, such a host-guest binding based environmental modulation only takes effect at very confined space (molecular range), which would not cause “global” influences on the structure of SAMs. Among all macrocyclic hosts, CB[7] could be most suitable for this purpose due to the extremely low polarity and polarizability of its inner cavity,[37,38] as well as its confirmed strong binding with Fc terminal group on mixed alkanethiolate SAMs (sub-μM level binding affinity as determined in chapter 3). In addition, unlike other host molecules whose binding affinity towards oxidized Fc guests (Fc^+) could be dramatically weak (e.g., K_f of *β*-cyclodextrin@Fc^+ host-guest complex is less than 10^3 M^{-1}),[266,267] CB[7] was confirmed having similar binding affinities towards both reduced and oxidized forms of neutral Fc derivatives, and moderately decreased binding affinity towards oxidized cationic Fc derivatives (1 to 2 orders of magnitude).[113-115]

Inspired by above descriptions, in this chapter, with mixed FcC11S-/C8S-Au SAM as an “ideal” system for both interfacial CB[7] host-guest binding and long-range ET study, the influences of CB[7] binding on the ET behavior (especially the kinetic aspect) of Fc terminal groups were systematically investigated. The results of this study clearly confirm the ability of this supramolecular host-guest binding pair for modulating the local dielectric medium of long-range ET process; moreover, they further reveal the role of a nonpolar-

structure based low-dielectric medium on ET kinetics, which help better understand the rather complicated environmental requirement of the much faster enzymatic ET reactions.

5.2. Experimental details

5.2.1. Reagents and materials

Perchlorate acid (70%) were ordered from Sigma Aldrich (St. Louis, MO), and was diluted to 0.1 M with deionized water. Other chemicals and materials are same with those described in section 3.2.1 (chapter 3).

5.2.2. Preparation of FcC11S-/C8S-Au SAM and CB[7] binding

Briefly, the piranha-cleaned gold slides (see section 2.1.3 for details) were immersed in a mixed FcC11SH/C8SH ethanol solution (95%) at room temperature for more than 20 h. The total concentration of thiols was 1.0 mM with 2% mole faction of FcC11SH. After immersion, the gold slides were thoroughly washed with copious amounts of ethanol solution (95%) and deionized water. For CB[7] binding, the mixed FcC11S-/C8S-Au SAM was incubated with 1.0 mM CB[7] aqueous solution for 2 h.

5.2.3. Electrochemical measurements

CVs and chronoamperometric responses (CAs) were measured for mixed FcC11S-/C8S-Au SAMs before and after CB[7] incubation. The pulse width and the sample interval of CA measurement were set as 100 ms and 0.02 ms, respectively. Other detailed information of our electrochemical detections is described in section 2.1.3 (chapter 2) and section 3.2.3 (chapter 3).

5.3. Results and discussion

5.3.1. Investigate the influence of interfacial Fc@CB[7] host-guest binding on ET thermodynamics

In this study, the mixed FcC11S-/C8S-Au SAM prepared by co-adsorption method with low $\chi_{FcC11SH}$ (2%) was employed due to its ideal structural features and strong host-guest binding ability with CB[7] as confirmed in chapter 3 and 4. Upon well-dispersed and exposed on surface, the microenvironment of Fc terminal groups should be remarkably changed upon binding with CB[7]. The CVs of mixed FcC11S-/C8S-Au SAM before and after CB[7] incubation (1.0 mM, 2 h) were displayed in Figure 5.1.

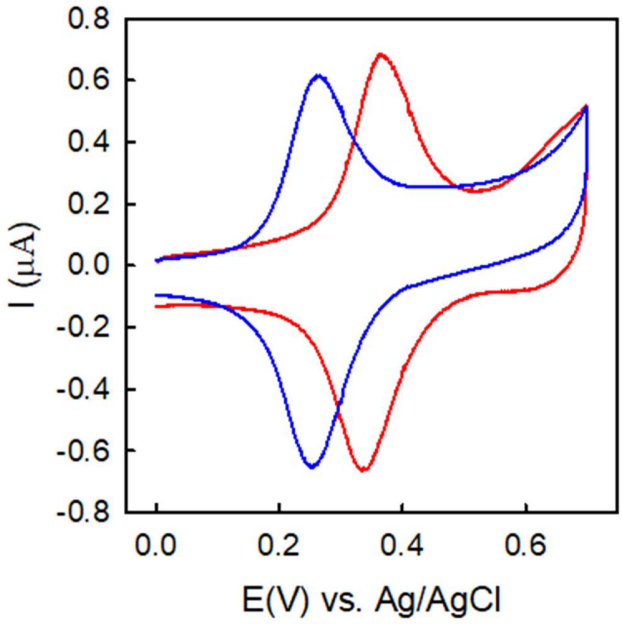

Figure 5.1. CVs of mixed FcC11S-/C8S-Au SAMs prepared by co-adsorption method ($\chi_{FcC11SH}$ = 2%) before (blue curve) and after incubation with 1.0 mM CB[7] for 2 h (red curve). The supporting electrolyte was 0.1 M $HClO_4$, and the potential scan rate (v) was kept at 0.05 V/s.

Note: Reprinted with permission from *J. Phys. Chem. C* 2019, 123, 26315-26323. Copyright (2019), *American Chemical Society*.

Similar to the observations in previous chapters, the CV of FcC11S-/C8S-Au SAM (blue curve) shows a single pair of symmetric redox peaks with half-height peak width (E_{fwhm}) of 97 ± 4 mV, and peak separation (ΔE_p) less than 10 mV. These CV properties indicate the nearly noninteracting and highly-reversible redox behavior of Fc terminal groups.[68,204] By integrating the CV anodic wave and based on equation 3.3 (see section 3.3.2), the surface density of Fc terminal groups (Γ_{Fc}) was determined to be (2.3 ± 0.3) × 10^{-11} mol/cm^2; in terms of the geometric dimension of CB[7] (as illustrated in Figure 4.1 in chapter 4), such a low Γ_{Fc} should ensure enough surrounding space for interfacial Fc@CB[7] host-guest binding. Upon incubation with CB[7], a new pair of redox peaks appeared at more positive potential (red curve), and the integration of its anodic wave gives a similar value of Γ_{Fc} (2.2±0.3 × 10^{-11} mol/cm^2). Based on Gaussian-Lorentzian deconvolution and equation 4.1 (see section 4.3.1), a high conversion rate ($\chi_{Fc@CB[7]}$ > 95%) was estimated from the CVs before and after CB[7] incubation. The unchanged Γ_{Fc} and high $\chi_{Fc@CB[7]}$ confirm that nearly all Fc terminal groups on mixed FcC11S-/C8S-Au SAM were bound to CB7] without losing their redox activity.

The rather remarkable, positive formal potential shift (89 ± 6 mV) observed in Figure 5.1 clearly reflects the influence of CB[7] host binding on the ET thermodynamics of Fc^+/Fc terminal groups, i.e., the oxidation of Fc@CB[7] to Fc^+@CB[7] is more difficult compared with the free Fc^+/Fc. This phenomenon is not exactly the same with previous CV studies of Fc@CB[7] host-guest complexations in solution phase, where the large degree of positive formal potential shifts (80~110 mV) were only observed for cationic Fc derivatives, but not for neutral Fc derivatives (< 30 mV).[114-116] As described by equations 5.1 to 5.5, the formal potential shift ($\Delta E^{o\prime}$) of a redox couple (*R* and *O*) upon ligand (*L*) binding is strongly correlated to their relative binding affinity towards ligand (i.e., K_{RL}/K_{OL}, where K_{RL} and K_{OL} are the formation constants of *R*·*L* and *O*·*L* complex):

$$R - ne^- \rightleftharpoons O \tag{5.1}$$

$$E_1^{o\prime} = E - \frac{RT}{nF} ln\left(\frac{[O]}{[R]}\right) \tag{5.2}$$

$$R \cdot L - ne^- \rightleftharpoons O \cdot L \quad \left(K_{RL} = \frac{[R \cdot L]}{[R][L]}, K_{OL} = \frac{[O \cdot L]}{[O][L]}\right) \tag{5.3}$$

$$E_2^{o\prime} = E - \frac{RT}{nF} ln\left(\frac{[O \cdot L]}{[R \cdot L]}\right) = E^0 - \frac{RT}{nF} ln\left(\frac{K_{OL}}{K_{RL}}\frac{[O]}{[R]}\right) \tag{5.4}$$

$$\Delta E^{o\prime} = E_2^{o\prime} - E_1^{o\prime} = \frac{RT}{nF} ln\left(\frac{K_{RL}}{K_{OL}}\right) \quad (5.5)$$

Based on those earlier CV studies in solution phase and equation 5.5, it has been proposed that CB[7] may have similar binding affinities towards both reduced and oxidized forms of neutral Fc guest (i.e., $K_{OL} \approx K_{RL}$, $\Delta E^{o\prime} \approx 0$).[113] Nevertheless, due to their distinct charge states they could have different thermodynamically most favored orientations inside the inner cavity of CB[7]; therefore, there might be a certain degree of spatial adjustment of neutral Fc guest upon oxidation/reduction in order to achieve their individual most favorable orientation inside CB[7]. In contrast, for cationic Fc guests their positively charged side groups could form additional ion-dipole interactions with the electronegative carbonyl portals of CB[7],[114,115] which may lead to a "locking effect" that restricts the spatial adjustment of Fc^+ residue inside CB[7] through the electrostatic repulsion force; as a result, their thermodynamic binding stability with CB[7] could be affected upon oxidation (i.e., $K_{OL} < K_{RL}$, $\Delta E' > 0$).

For neutral Fc terminal groups on SAMs, it is no doubt that they have much limited motion (particularly rotational) freedom compared with the neutral Fc guests in solution. As a result, it is very likely that neither its reduced nor oxidized form is able to reach their thermodynamic most favorable orientations inside CB[7], and this is, in fact, a possible reason for the relatively moderate binding stability of Fc@CB[7] host-guest complex formed on SAMs (see chapter 3 for detailed thermodynamic study); such an effect could be somehow even stronger for oxidized Fc terminal group with its orientation inside CB[7] "further away" from its thermodynamically most favored state.

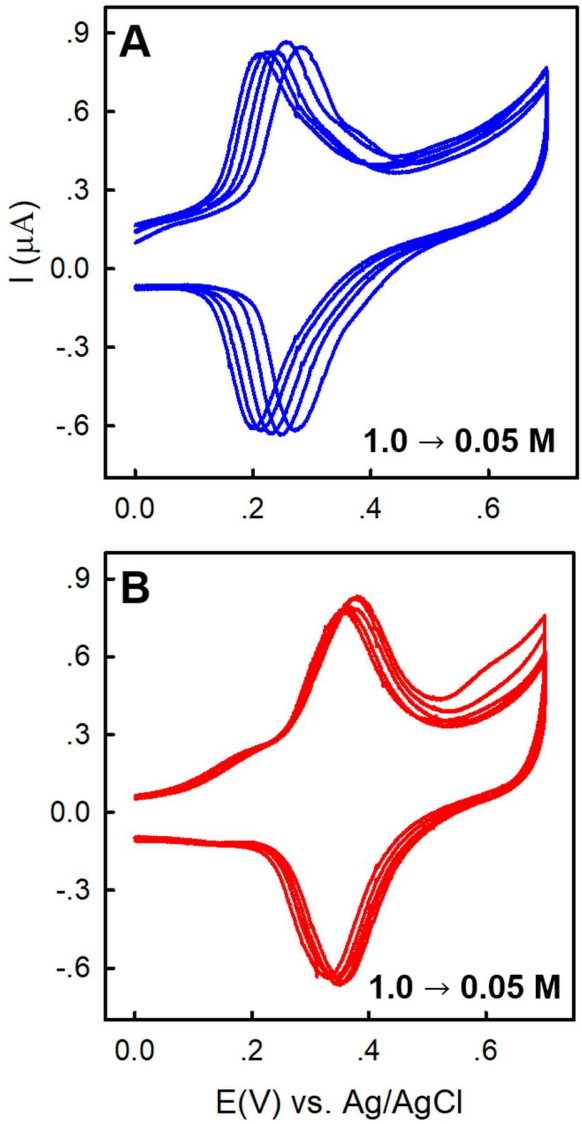

Figure 5.2. CVs of mixed FcC11S-/C8S-Au SAM (prepared by co-adsorption method with $\chi_{FcC11SH}$ of 2%) at different concentrations of $HClO_4$ (0.05 to 1.0 M) before (A) and after (B) incubation with 1.0 mM CB[7] for 2 h. The potential scan rate was kept at 0.05 V/s.

Note: Reprinted with permission from *J. Phys. Chem. C* 2019, 123, 26315-26323. Copyright (2019), *American Chemical Society*.

Besides ligand binding, it has been confirmed that the redox thermodynamics of Fc terminal groups on SAMs is strongly influenced by the ion pairing between the oxidized Fc terminal group (Fc^+) and the anion in solution (ClO_4^- in this study). From thermodynamic aspect, ClO_4^- can neutralize the positive charge of Fc^+ terminal group

upon forming an ion pair, and thus improve its thermodynamic stability within the nonpolar environment of alkane chains. This was evidenced by the negative formal potential shifts of Fc-terminated alkanethiolate SAMs in the electrolyte solution with increasing concentrations of ClO_4^-.[216,217] Due to its nonpolar inner cavity and electronegative carbonyl portals, it is very likely that the CB[7] host binding would inhibit the anion pairing of Fc^+ by limiting the accessibility of ClO_4^- to encapsulated Fc terminal groups on SAMs (i.e., the concentration of ClO_4^- in the local environment of Fc terminal groups could be lower than its concentration in bulk solution). To verify this, CVs of mixed FcC11S-/C8S-Au SAM were measured at different concentrations of electrolyte ($HClO_4$) before and after CB[7] incubation, which are shown in Figure 5.2 (A) and (B). It can be clearly seen that with increased concentration of ClO_4^-, the CV redox peaks of FcC11S-/C8S-Au SAM (Figure 5.2A) show much more obvious negative potential shifts compared with its CVs after CB[7] incubation (Figure 5.2B).

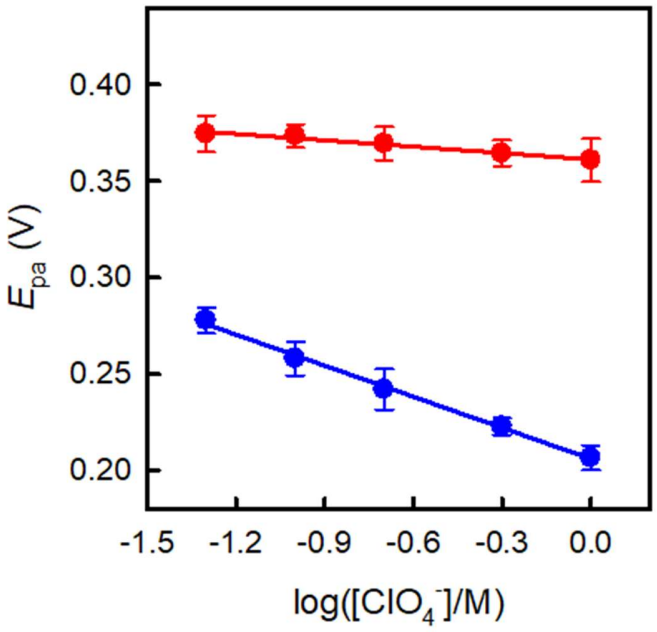

Figure 5.3. The relationship between the CV anodic peak potential (E_{pa}) and the logarithm concentration of ClO_4^- (log([ClO_4^-]) before (blue solid circles) and after CB[7] incubation (red solid circles). The solid lines are the best linear fits to experimental data.

Note: Reprinted with permission from *J. Phys. Chem. C* 2019, 123, 26315-26323. Copyright (2019), *American Chemical Society*.

The relationship between the CV anodic peak potential (E_{pa}) and the logarithm concentration of ClO_4^- (log[ClO_4^-]) were plotted in Figure 5.3. It was found that without CB[7] incubation (blue circles/line), E_{pa} decreases linearly with higher value of log[ClO_4^-], which has a slope of –(54 ± 2) mV (R^2 = 0.9959). This indicates a "near-ideal" ion pairing thermodynamics of Fc^+ terminal groups since our determined slope is close to the theoretical value (–59 mV) predicted from the ion paring model, as expressed by equation 5.6:[216]

$$E_{\mathrm{pa}} = E^{\circ\prime} - \left(\frac{2.303RT}{nF}\right) log\, K - \left(\frac{2.303RT}{nF}\right) log[\mathrm{ClO_4^-}] \;\; (K[\mathrm{ClO_4^-}] \gg 1) \quad (5.6)$$

where $E^{\circ\prime}$ is the formal potential adsorbed Fc^+/Fc redox couples; K is the formation constant of $Fc^+ \cdot ClO_4^-$ ion pair. After CB[7] incubation, the linear fit ends up with a poor slope (−11 ± 1 mV) and a unsatisfactory R^2 value (0.9710), which indicate a significantly affected ion pairing thermodynamics. With inhibited ion paring, the oxidation of Fc@CB[7] to Fc^+@CB[7] could also become less favored on alkanethiolate SAMs. Besides above mentioned two factors, the CB[7] host binding may bring other influence factors to the ET thermodynamics of Fc^+/Fc terminal groups on SAM, such as the varied local electrical field and interfacial double layer capacitance. It is believed that the positive formal potential shifts observed in Figure 5.1 should be an overall effect of various environmental factors brought by interfacial Fc@CB[7] host-guest binding. Further efforts are needed to identify the contribution from different influence factors.

5.3.2. Investigate the influence of interfacial Fc@CB[7] host-guest binding on ET kinetics

In addition to the ET thermodynamics of Fc^+/Fc redox couple, which is strongly related to its distinctive charge states (+1 and 0), it is more interesting to explore the more universal influence caused by CB[7] host binding on the ET kinetics of Fc^+/Fc at such a highly organized molecular interface. This was first investigated by measuring the CVs of FcC11S-/C8S-Au SAM at different potential scan rates (v) before and after CB[7] incubation, which are displayed in Figure 5.3.

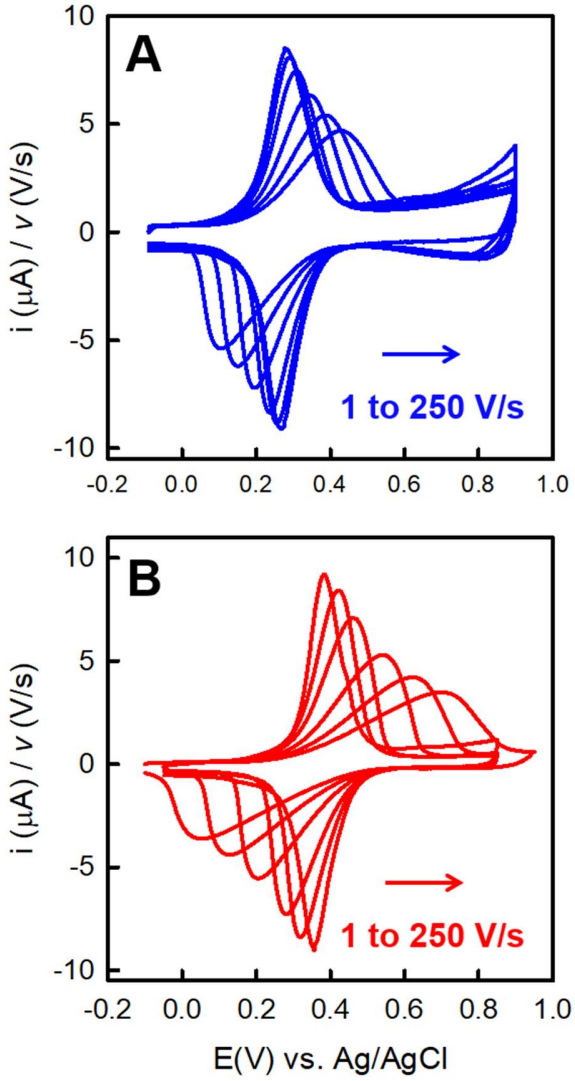

Figure 5.4. CVs of mixed FcC11S-/C8S-Au SAM (prepared by co-adsorption method with $\chi_{FcC11SH}$ of 2%) at different scan rates (*v*) (A) before and (B) after incubation with 1.0 mM CB[7] for 2 h. The current signals are normalized with scan rates (i/*v*). The supporting electrolyte was 0.1 M $HClO_4$.

Note: Reprinted with permission from *J. Phys. Chem. C* 2019, 123, 26315-26323. Copyright (2019), *American Chemical Society.*

It can be seen that with faster potential scan rates (*v*), the CVs of FcC11S-/C8S-Au SAM before and after CB[7] incubation both show increased peak separations. Such a trend is much more significant after CB[7] incubation, which indicates the less reversible and slower ET kinetics of Fc@CB[7] host-guest complex formed on SAMs. For

quantitative analysis, the CV peak separations ($E_{pa} - E_{pc}$) were subsequently plotted with the natural logarithm of potential scan rate (ln *v*), i.e., the Laviron plot, as shown in Figure 5.5 (A).

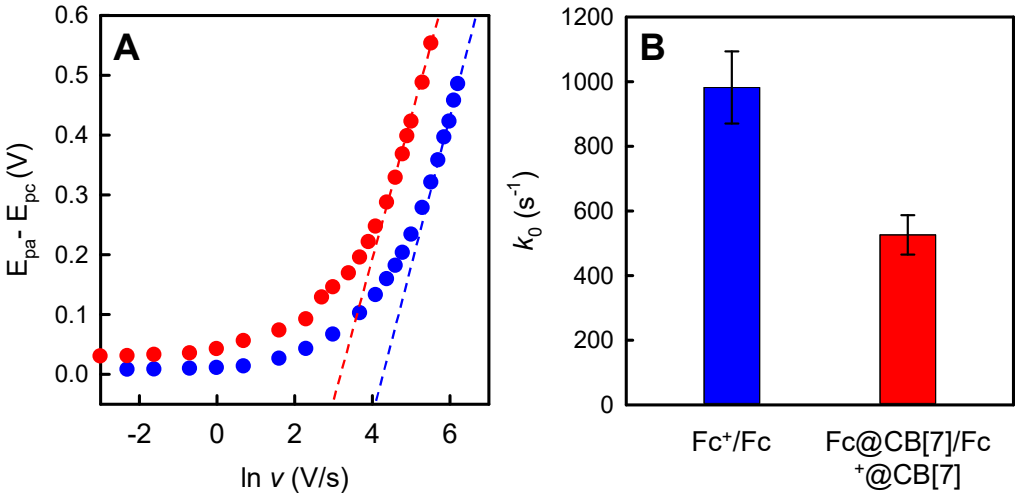

Figure 5.5. (A) Laviron plots (E_{pa}–E_{pc} vs. ln *v*) of FcC11S-/C8S-Au SAMs (prepared by co-adsorption method with $\chi_{FcC11SH}$ of 2%) before (blue solid circles) and after incubation with 1.0 mM CB[7] for 2 h (red solid circles). The dashed lines show the best linear fits to the experimental data at higher scan rates. (B) The k_o of Fc⁺/Fc terminal group and Fc⁺@CB[7]/Fc@CB[7] complex determined from the best linear fits.

Note: Reprinted with permission from *J. Phys. Chem. C* 2019, 123, 26315-26323. Copyright (2019), *American Chemical Society*.

In general, the peak separations are small at low scan rates (ln *v* < 0), indicating the highly reversible ET process; with higher scan rate (ln *v* > 0), the peak separations start to increase, indicating the less reversible ET process. With even higher scan rate, the good linear relationship (R^2 > 0.99) can be observed in both cases before and after CB[7] incubation; however, the linear relationship appears earlier for Fc⁺@CB[7]/Fc@CB[7] complex (when *v* > 80 V/s) than free Fc⁺/Fc terminal groups (when *v* > 250 V/s). Based on the data shown in Figure 5.5 (A), the standard ET rate constant (k_0) was determined by fitting the linear parts with Laviron model (derived from conventional Butler-Volmer kinetic equation), as expressed by equation 5.7:[220]

$$E_{\mathrm{pa}} - E_{\mathrm{pc}} = \frac{RT}{nF}\left(\frac{1}{1-\alpha} + \frac{1}{\alpha}\right) lnv + \frac{RT}{nF(1-\alpha)} ln\frac{(1-\alpha)nF}{RT\boldsymbol{k_o}} + \frac{RT}{nF\alpha} ln\frac{\alpha nF}{RT\boldsymbol{k_0}} \qquad (5.7)$$

where R is the gas constant, T is the temperature, F is the Faradic constant, n is the number of electrons involved in the ET process (n = 1 for Fc^+/Fc), α is the ET coefficient (a symmetric factor of activation energy barrier). For mixed FcC11S-/C8S-Au SAM, the best fit shown in Figure 5.5 (A) (blue dashed line) yields an α of 0.46 ± 0.02 and k_0 of (9.8 ± 1.1) × 10^2 s^{-1}, respectively. The k_0 determined here is a bit lower than those (10^3 to 10^4 s^{-1}) reported for other Fc-terminated alkanethiolate SAMs with similar length of alkyl bridge,[208,257,259] which could be due to the relatively lower concentration of electrolyte (0.1 M $HClO_4$) used in this study in order to minimize the "salt effect" on host-guest binding stability.[269] As shown in Figure 5.6, the k_0 of FcC11S-/C8S-Au SAM can be improved to over 2.0 × 10^3 s^{-1} in 1.0 M $HClO_4$.

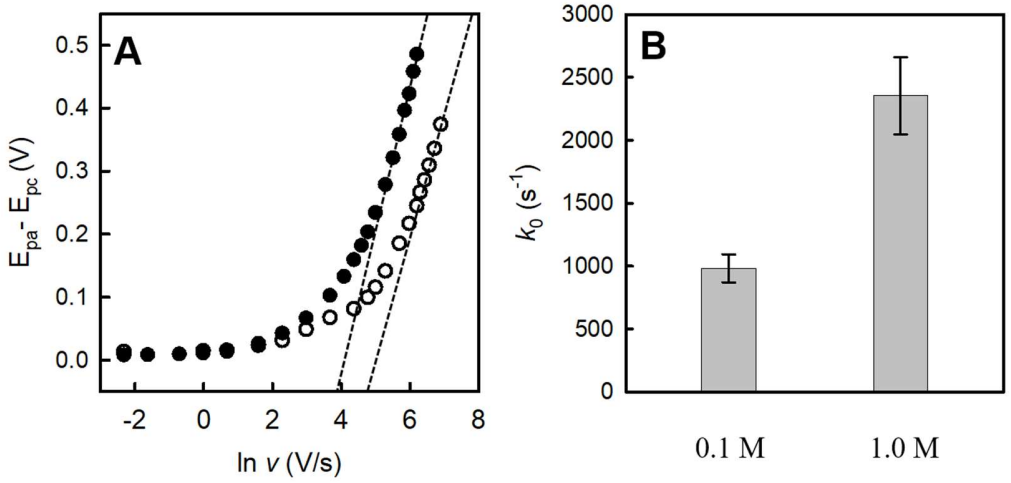

Figure 5.6. **(A) Laviron plots of FcC11S-/C8S-Au SAMs (prepared by co-adsorption method with $\chi_{FcC11SH}$ of 2%) in 0.1 M $HClO_4$ (solid circles) and 1.0 M $HClO_4$ (open circles). The dashed lines show the best linear fits to the experimental data at higher scan rates. (B) The values of k_o determined from the best linear fits: (9.8 ± 1.1) × 10^2 s^{-1} for 0.1 M $HClO_4$ and (2.4 ± 0.3) × 10^3 s^{-1} for 1.0 M $HClO_4$.**

Note: Reprinted with permission from *J. Phys. Chem. C* 2019, 123, 26315-26323. Copyright (2019), *American Chemical Society.*

For FcC11S-/C8S-Au SAM after CB[7] incubation, the best linear fit (red dash line in Figure 5.5 A) yields a similar value of α (0.44 ± 0.02), but a much smaller k_0 (5.3±0.6 × 10^2 s^{-1}). It has been confirmed that the ET process of redox-active terminal groups across alkanethiolate SAMs (thickness less than 20 Å) is dominated by through-bond tunneling

mechanism, for which k_0 decays exponentially with increasing ET distance (r), as described by equation 5.8:[208,245,254-257]

$$k_{0\,(r)} = k_{0\,(r=0)}\mathrm{e}^{-\beta r} \qquad (5.8)$$

where r is controlled by the number of methylene groups (-CH_2-) in alkyl bridges; β is the tunneling constant that depends on the chemical position and physical properties of alkyl bridges. According to previously reported tunneling constant ($\beta \approx 1.1$ per -CH_2-),[208,255] the degree of change on k_0 found in this study (less than 50 %) is smaller than that caused by adding or removing one methylene group to/from alkyl bridge (3-folds smaller or higher k_0 would be expected based on equation 5.8), indicating the minute structural variations of FcC11S-/C8S-Au SAM upon CB[7] binding to its Fc terminal group. Moreover, the change on k_0 found in this study is much less compared to previous studies in solution phase, where 20~50 folds decreased k_0 were observed for various Fc derivatives upon encapsulation by CB[7];[115] however, in solution phase the dramatically decreased k_0 could be mainly attributed to the larger-sized Fc@CB[7] complex, which lead to smaller diffusion coefficient and the longer ET distance (to electrode surface).[115] More interestingly, an increased k_0 was also reported for the self-exchange ET between (trimethylammonio)methylferrocene ($FcTMA^+$) and (trimethylammonio)methylferrocenium ($FcTMA^{2+}$) upon encapsulation by CB[7]; and the possible reason behind this is that CB[7] might bring closer distance between $FcTMA^+$ and $FcTMA^{2+}$ as their intermolecular electrostatic repulsion force could be compensated by the electronegative carbonyl portals of CB[7] (via ion-dipole interactions).[87] In addition to CB[7], the ET studies of redox-active SAMs associated with host-guest binding were also reported with β-cyclodextrin (β-CD);[266,267,270,271] however, the much less stable complexes formed between β-CD and redox-active terminal groups may lead to their dissociations occurred during the ET process,[266, 267] which bring much difficulty on accurately measuring and interpreting the ET kinetic results (both slightly enhanced and reduced k_0 were reported[270,271]). Considering all above, the moderately reduced k_0 found with Fc@CB[7] host-guest complex formed on mixed FcC11S-/C8S-Au SAM may most precisely reflect the kinetic influence of the low-dielectric medium brought by supramolecular host-guest binding.

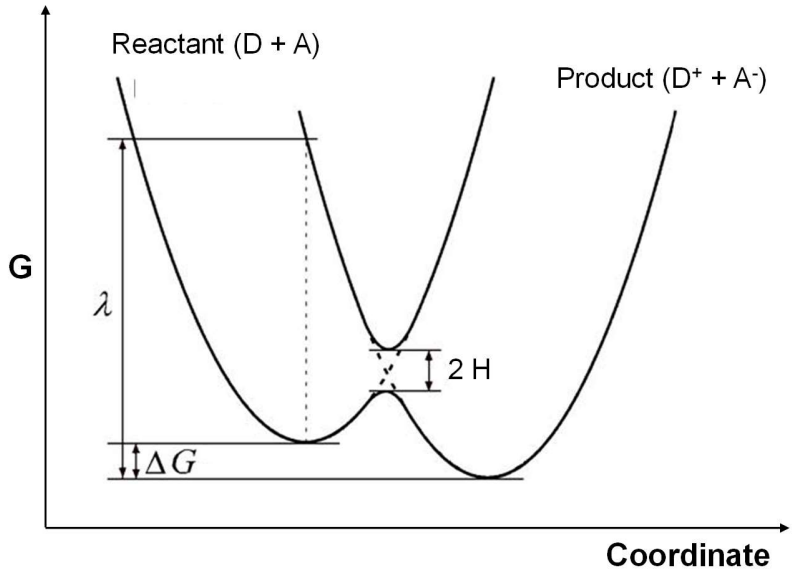

Figure 5.7. The parabola potential energy profile of a ET system as proposed by Marcus theory.

To further confirm that the retarded ET kinetics of Fc@CB[7] host-guest complex formed on SAMs is or partially originated from the nonpolar and low-dielectric inner cavity of CB[7], we subsequently conducted the ET kinetic study with the help of Marcus-type theory.[252] Unlike the conventional ET kinetic models derived from transition state theory (i.e., a chemical reaction must proceed through a specific energic and coordinate pathway with intermediate compound formed, whose free energy determines the reaction rate),[149] Marcus theory considers the fact that for a simple "outer sphere" ET process without chemical bonds formed or broken (e.g., the self-exchange ET between metal ions complexes of different charge states), there is no structurally defined intermediate compound formed; and the electron jump between the donor and acceptor is much faster than other processes occurred in the ET system (e.g., changes on the nuclear coordinate of reactant; rearrangements of solvent orientation in the surrounding). Moreover, such an electron jump was also confirmed an energy conserved process since it can happen in dark.[252] These mean that there should be neither horizontal transition in reaction coordinates (Franck-Condon principle) nor vertical transition in energy for a simple electron jump process. Accordingly, Marcus proposed that the electron jump process happens when the thermo fluctuation states of ET reactant and product (including their molecular vibrational states and surrounding solvation states) match well in both energy level and coordinate (i.e., at the crossing point of their energy profiles);[252] by further

assuming the parabola-shaped energy profiles of ET reactant and product (harmonic oscillators), as shown in Figure 5.7, and by taking into account the electronic coupling (essentially the interaction between the two molecular orbitals involved in ET), the modern Marcus ET model was developed, as expressed in equation 5.9:[203]

$$k_{app} = \frac{4\pi^2 H^2}{h\sqrt{4\pi\lambda k_B T}} exp\left[\frac{-(\Delta G + \lambda)^2}{4\lambda k_B T}\right] \quad (5.9)$$

where k_{app} is the apparent ET rate constant, k_B is the Boltzmann constant (1.38×10^{-23} m^2 kg s^{-2} K^{-1}), h is the Plank's constant (6.63×10^{-34} J · s), and H represents the electronic coupling. The term in the square bracket of equation 5.9 represents the activation energy solved at the crossing point of the two parabola-shaped potential energy profiles (displayed in Figure 5.7), which involves the contribution from the free energy difference (ΔG) between the most stable states of ET reactant and product (i.e., the bottoms of their energy curves), as well as the reorganization energy (λ) needed to rearrange the coordinates of the ET system (so that the ET product with a different charge state can reach its most stable state). According to the prediction of Marcus model, there should be an "inverted" region between k_{app} and ΔG (i.e., k_{app} reaches maximum when $\Delta G = -\lambda$) instead of the monotonical relationship predicted by traditional Bulter-Volmer kinetic model; and the "inverted" region has been experimentally confirmed.[252]

Marcus model was later confirmed also valid for "inner-sphere" ET process (covalently bridged donor and acceptor), and was further derivatized to study the ET kinetics between the redox-active terminal group on SAMs and the metal electrode with continuously distributed electronic states (partially filled band).[210,272] The resulted Marcus-Hush-Chidsey (MHC) model is given as equation 5.10 and 5.11:[272]

$$k_{\mathrm{app}}(\eta) = A\int_{-\infty}^{\infty} \exp\left[-\frac{(x - \lambda \pm e\eta)^2}{4\lambda k_B T}\right] \frac{dx}{1 + \exp\left(\frac{x}{k_B T}\right)} \quad (5.10)$$

$$A = \rho H^2 \left(\frac{k_B \mathrm{T}}{\hbar}\right)\left(\frac{\pi}{\lambda k_B T}\right)^{\frac{1}{2}} \quad (5.11)$$

where A is the pre-factor consisting of the electronic coupling factor (H) and the presumed constant density (ρ) of the electronic states near the Fermi level of metal electrode (0.3 eV^{-1} estimated for gold);[257] η is the overpotential that controls the free energy change (ΔG) of the ET process. The MHC model considers the probability of all electrons in the

electronic states (x) near the Fermi level of metal electrode participating into the ET process, which is achieved by numerically integrating the Marcus model over the Fermi-Dirac distribution, as shown by the integral part of equation 5.10. Based on MHC model, the λ and H of an interfacial ET process can be obtained by fitting the experimentally obtained relationship between k_{app} and η (i.e., Tafel plot) with equation 5.10 and 5.11.

Chronoamperometry (CA) has been confirmed a convenient electrochemical technique for obtaining the experimental Tafel plot. In CA, the overpotential (η) is controlled by the step potential applied to working electrode against the formal potential of adsorbed redox couples ($\eta = E_{\text{applied}} - E^{\circ\prime}$; $\eta > 0$: oxidation, $\eta < 0$: reduction). At a given η, the faradic current (i) of a homogeneously distributed redox couple on surface decays exponentially with time (t), as described by equation 5.12:[203,204]

$$i = k_{app} Q \exp\left(-k_{app} t\right) \tag{5.12}$$

where Q is the total faradic charge transferred between the redox couple and electrode surface. According to equation 5.12, a linear decay can be expected with the natural logarithm of faradic current ($\ln(i)$), as shown by equation 5.13, from which k_{app} can be determined from either slope or intercept.

$$\ln(i) = \ln\left(k_{\text{app}} Q\right) - k_{\text{app}} t \tag{5.13}$$

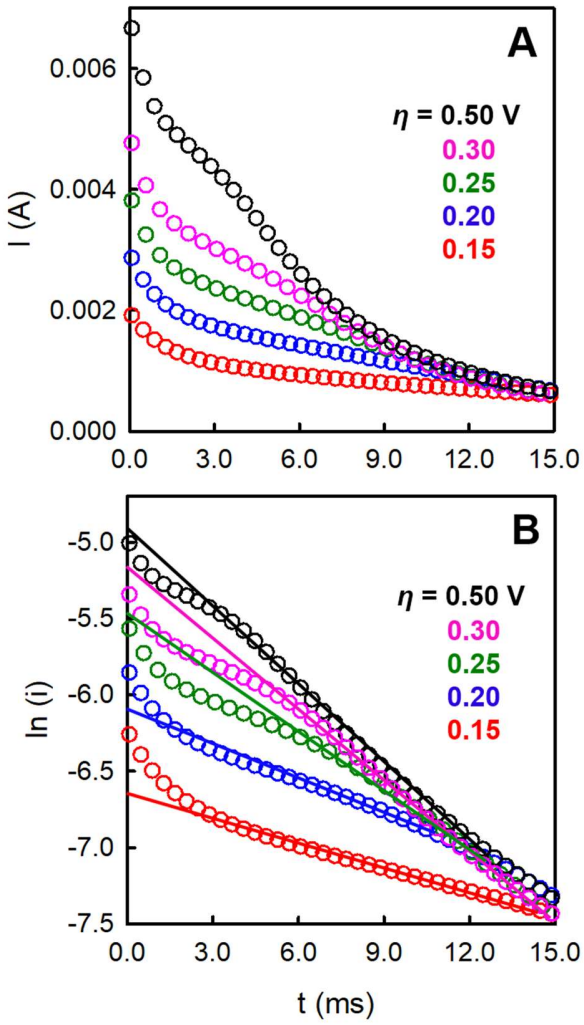

Figure 5.8. **(A) Representative CA current decays and (B) their natural logarithm form at different overpotentials (η) for mixed FcC11S-/C8S-Au SAMs prepared by co-adsorption method with $\chi_{FcC11SH}$ of 2%. The solid lines in (B) indicate the linear part of the faradic current decays in natural logarithm form. The pulse width and sample interval of CA are 100 ms and 0.02 ms respectively.**

Note: Reprinted with permission from *J. Phys. Chem. C* 2019, 123, 26315-26323. Copyright (2019), *American Chemical Society.*

Figure 5.8 (A) shows the representatives of experimentally measured CA current decays of FcC11S-/C8S-Au SAM at different η. The current spikes observed at very earlier stage (< 2 ms) should be caused by the non-Faradic charging current of the interfacial double layer capacitance.[264] Afterwards, the CA currents decrease exponentially with time, which also show the expected linear decays in their natural logarithm form, as shown in

Figure 5.8 (B). The initial data points (0~3 ms) deviated from the linear relationship could be the overall effects of non-Faradic charging response and the uncompensated resistance (*R*);[264] the latter was estimated to be less than 11 Ω based on Pouillet's law ($R = \frac{1}{\sigma} \times \frac{l}{A}$),[204] the conductivity of 0.1 M $HClO_4$ electrolyte solution (σ = 0.32 S/cm), and the dimensions ($l \approx$ 0.5 cm, A = 0.15 cm^2) of the electrochemical cell system used in this study (see Figure 2.4 of chapter 2). According to equation 2.16 (see section 2.1.2), the above determined *R* value does not cause significant ohmic drop (< 0.05 V) with the faradic current intensity shown in Figure 5.8. Based on equation 5.13, the k_{app} corresponding to different η were determined from the linear Faradic current decays; and the experimental Tafel plots ($\ln k_{app}$ vs. η) of mixed FcC11S-/C8S-Au SAM before and after CB[7] incubation are displayed in Figure 5.9.

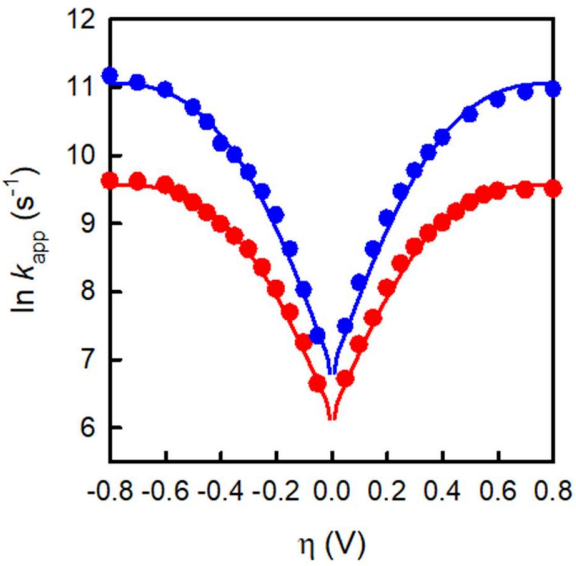

Figure 5.9. Experimental Tafel plots ($\ln k_{app}$ vs. η) of FcC11S-/C8S-Au SAMs (prepared by co-adsorption method with $\chi_{FcC11SH}$ = 2%) before (blue solid circles) and after incubation with 1.0 mM CB[7] for 2 h (red solid circles). The solid lines are the best fitted theoretical Tafel plots generated by the simplified MHC model (equation 5.14).

Note: Reprinted with permission from *J. Phys. Chem. C* 2019, 123, 26315-26323. Copyright (2019), *American Chemical Society*.

It can be seen that for both oxidation (η > 0 V) and reduction (η < 0 V) branches, $\ln k_{app}$ increases sharply with $|\eta|$ at earlier stages (0~0.2 V), and gradually levels off when

$|\eta|$ is larger than 0.5 V. This observation is in good agreement with the prediction of MHC model, i.e., when $|\eta| > \lambda$, further increasing the driving force ($|\eta|$) no longer creates more electronic states to gain the probability of ET.[272] For FcC11S-/C8S-Au SAM after CB[7] incubation, its Tafel plot (red circles) appears at lower position and levels off at relatively smaller η.

Due to its high complexity and difficulty for direct use, the MHC model was usually applied with mathematically approximated versions, such as the one proposed by Zeng et al.,[273] in which the integral part in equation 5.10 was simplified to known functions, as expressed by equation 5.14:

$$i = k_{app}(\eta)Q = A\sqrt{\pi\lambda}\tanh\left(\frac{\eta}{2}\right)\mathrm{erfc}\left(\frac{\lambda - \sqrt{1 + \sqrt{\lambda} + \eta^2}}{2\sqrt{\lambda}}\right) \qquad (5.14)$$

where A is the pre-exponential factor as defined in equation 5.11; Q is the total faradic charge; λ and η are scaled to k_BT and k_BT/e, respectively. A and λ were used to generate the best fitted theoretical Tafel plots as shown by the solid curves in Figure 5.9. The electronic coupling factor H was then calculated from equation 5.11; and k_0 was calculated from equation 5.14 at η = 0 V. These kinetic parameters before and after CB[7] incubation were summarized in Table 5.1. It can be seen that the k_0 determined from CA and simplified MHC model (9.2×10^2 s^{-1}) is close to its value determined from the Laviron's method (9.8×10^2 s^{-1}); the λ (0.80 eV) and H (0.90 cm^{-1}) of FcC11S-/C8S-Au SAM determined here are close to their previously reported values for Fc-terminated alkanethiolate SAMs with similar length of alky bridges.[208,257] Remarkably, both λ and H for the ET between Fc^+/Fc terminal group and gold electrode decrease upon binding with CB[7].

Table 5.1 ET kinetic parameters determined for FcC11S-/C8S-Au SAM before and after CB[7] incubation.

	λ (eV)	H (cm^{-1})	k_o (s^{-1}) by CA	k_o (s^{-1}) by CV
FcC11S-/C8S-Au	0.80	0.90	916	983
CB[7]@FcC11S-/C8S-Au	0.60	0.70	509	528

Note: the relative uncertainties of these values are within 15%

According to Marcus theory, the reorganization energy is defined as the energy needed to rearrange the coordinates of entire ET system in order to reach the most stable state for ET product, which has a different charge state with respect to ET reactant. The total reorganization energy (λ) can be viewed as the sum of two parts, as shown in equation 5.15:[252]

$$\lambda = \lambda_i + \lambda_o \qquad (5.15)$$

where λ_i is the "inner" part of reorganization energy needed to adjust the nuclear coordinates (e.g., bond length and bond angle) of ET reactant and product, while λ_o is the "outer" part of reorganization energy associated with the reorientation of solvent dipoles/molecules. It has been confirmed that the reorganization energy for the nonadiabatic ET process of redox-active SAMs is dominated by the outer part λ_o (λ_i is less than 0.1 eV);[208,261,265] by assuming the solvent medium as a dielectric continuum and the redox couple as simple sphere model, the λ_o of an interfacial ET process can be expressed by equation 5.16:[252]

$$\lambda_o = (e^2 \frac{N_A}{2}) \left(\frac{1}{a} - \frac{1}{2d}\right) \left(\frac{1}{\varepsilon_h} - \frac{1}{\varepsilon_s}\right) \qquad (5.16)$$

where e is the charge of electron; a is the average radius of redox couple; d is the distance between the redox couple and electrode surface; N_A is Avogadro's number (6.02×10^{23}/mol); ε_h and ε_s are the high frequency and static dielectric constants of solvent medium. By assuming the constant geometric factors (a and d) for FcC11S-/C8S-Au SAM before and after CB[7] incubation, the reduced λ indicates a smaller "Pekar factor"

$\left(c_0 = \frac{1}{\varepsilon_h} - \frac{1}{\varepsilon_s}\right)$,[249] which corresponds well to the low dielectric/polarizable medium of CB[7] inner cavity; thus, the reduced λ found in this study validates the ability of CB[7] host-guest binding as an effective environmental modulator of ET kinetics. In addition, the moderately decreased k_0 found in this study more truly reflects the role of a nonpolar structure based low-dielectric medium on ET kinetics compared with the earlier studies of using organic solvents, where their increased k_0 could be mainly attributed to the disordered SAM structure that leads to reduced ET distances.[261]

By and large, the kinetic results described above provide unprecedented insights for unveiling the medium nature of biological enzymatic ET process. So far the studies on enzymatic reactions have revealed that an active domain of protein with pre-organized dipoles/polar structures is necessary for accelerating the ET process.[249-251, 253] Compared to the aqueous medium, such a protein based active domain has a lower dielectric medium as created by the "fixed" arrangement of polar dipoles/polar structures, which are electrostatically "complementary" to the molecular structure of substrate, and thus result in a reduced activation energy. In contrast, the nonpolar structure based lower dielectric medium without such an electrostatic complementarity towards ET reactants/products is believed to cause a higher activation energy.[250,251,253] In this study, since CB[7] host provides a structurally well-defined nonpolar low-dielectric medium, the retarded ET kinetics of Fc@CB[7] host-guest complex formed on SAMs can be viewed as an additional supporting evidence to the important role of electrostatic complementarity in rapid enzymatic ET reactions.

It should be noted that when studying ET kinetics, it is impossible to isolate the medium effect from its complicated structural origins, where different types of covalent bonds and noncovalent interactions may form specific electronic coupling pathways with either constructive or destructive contributions to the overall electronic coupling between the molecular orbitals/electronic states of ET donor and acceptor.[248,256,259,265] Previous ET studies on redox-active SAMs have revealed that the electron coupling factor H and tunneling constant β is very sensitive to the structure and composition of both bridging and diluent alkane chains.[256,265] This may explain why in those earlier studies, the buried redox-active terminal groups by surrounding longer diluent alkanethiols show significantly retarded ET kinetics even without obviously changed reorganization energy (more destructive coupling pathways could be formed).[265] In this study, besides the reduced reorganization energy, we also observed a smaller electronic coupling factor (from 0.90

cm^{-1} to 0.70 cm^{-1}) between the Fc^+/Fc groups and gold electrode after CB[7] incubation, which indicates that the CB[7] host binding may also affect the electronic coupling pathways by introducing more types of noncovalent interactions. To further investigate the influence of host-guest binding on ET coupling or tunneling mechanism, the tunneling constant β can be determined and compared.

5.4. Conclusion

In this chapter, the influences of CB[7] host binding as a showcase of well-confined nonpolar low-dielectric medium on ET behavior were studied with Fc-terminated alkanethiolate SAMs on gold (i.e., FcC11S-/C8S-Au SAM prepared by co-adsorption method 2% mole fraction of FcC11SH), which serves as an ideal system for both ET study and interfacial Fc@CB[7] host-guest binding. It was discovered by CV that the oxidation of Fc terminal groups become thermodynamically more difficult upon CB[7] binding, which might be the overall effect of multiple factors, such as the reduced stability of Fc^+ inside CB[7] and its inhibited ion pairing (with ClO_4^-). In terms of ET kinetics, the analysis of experimental Tafel plots (obtained by CA) with MHC model yields reduced ET rate constant (k_0), reorganization energy (λ), and electronic coupling (H) for the ET between Fc^+/Fc terminal groups and gold electrode upon CB[7] binding. The smaller reorganization energy confirms a low dielectric medium brought by CB[7] binding; the weaker electronic coupling indicates that the reduced k_0 could be the overall result of CB[7] host binding on ET medium and coupling pathways. These results provide indirect insights for understanding the environmental nature of the enzyme active domains (i.e., low dielectric media with “fixed” arrangement of polar components and dipoles, which is electrostatically complementary to the substrate), and augment the application potential of supramolecular host-guest binding as a convenient and efficient way to regulate long-range ET at highly-organized molecular interfaces.

Chapter 6.

Host-guest binding as a convenient method for electrochemical study and quantitation of drug@CB[7] complexations

In this chapter, we developed a general electrochemical assay for drug@CB[7] (as excipient) complexations based on their competitive host-guest binding with Fc@CB[7] complex formed at highly organized molecular interface. Particularly, by incubating a mixture of CB[7] and drug molecule with FcC11S-/C8S-Au SAM, the competitive host-guest binding equilibrium can be quantitatively analyzed from the CV measurements. Based on the known concentrations of CB[7] and drug, as well as the electrochemically determined mole ratio between free and bound Fc terminal groups, the formation constant of drug@CB[7] complexation can be determined. With several drug molecules as examples, we have demonstrated the capability of this electrochemical assay for the thermodynamic study of supramolecular drug@CB[7] complexations interested in pharmaceutical and biomedical science. More importantly, this work also promises a general assay that allows the electrochemical quantitation of electro-inactive analytes based on the competitive host-guest binding at redox-tagged molecular interfaces.

Note: this chapter is adapted with permission from:

***Qi, L.**; Wang, R. B.; Yu H.-Z. Electrochemical Quantitation of Supramolecular Excipient@Drug Complexation: A General Assay Strategy based on Competitive Host Binding with Surface-Immobilized Redox Guest Anal. Chem., 2020, 92, 2168-2175.* Copyright (2020) American Society of Chemistry.

I have performed most of the experimental work and drafted the paper; professor Ruibing Wang at university of Macau, together with Dr. Hogan Yu supervised the entire project and helped with writing the paper.

6.1. Introduction

Owing to the exceptional host-guest binding ability of CB[7] towards a wide range of small aromatic or other ring structured organic compounds (1:1 ratio complexes),[46,106] as well as its excellent biocompatibility and low toxicity, tremendous studies have been focusing on the great application potential of CB[7] as an efficient excipient for many drug molecules interested in pharmaceutical and biomedical science.[58,103,276] For example, CB[7] has been confirmed able to change the chemical, physical, and biological properties of guest compounds;[277] in particular, the enhanced biocompatibility,[278] water solubility,[92] therapeutic activity,[279] as well as the reduced toxicity,[280] masked taste,[281] and modulated pharmacokinetics[282,283] were reported for many drug moelcules upon their encapsulation by CB[7]. Besides, more and more novel *in vivo* drug delivery and release systems have been developed based on drug@CB[7] host-guest complexations.[84,102] Recently, the detection method of drug molecules was also developed based on the optical sensing response to drug@CB[7] host-guest binding.[6]

As the strong binding is a prerequisite for above mentioned applications of drug@CB[7] host-guest complexations, their thermodynamic stability have been widely investigated by isothermal calorimetry and various spectroscopic techniques (e.g., UV-vis and NMR).[58,103,284] Typically, an experimental binding isotherm curve is obtained by recording the signal responses upon titrating a fixed concentration of drug molecule with increasing concentrations of CB[7] (as ligand); by fitting the experimental binding isotherm curve with proper binding models (1:1 binding model for drug@CB[7] complexation), those important thermodynamic parameters (i.e., enthalpy and entropy changes, dissociation/formation constants) can be determined.[281,285] The ability of various analytical techniques for studying the thermodynamic stability of host-guest complexes highly depends on their sensitivity (i.e., the lower concentration can be accurately detected, the stronger molecular binding can be effectively evaluated). Moreover, for ultra-strong host-guest complexes (nM or even higher levels of binding affinity), the multi-steps competitive binding experiment and much more complicated competitive binding models are required for accurately determining their formation/dissociation constants.

Considering the high sensitivity, easy quantitation, and convenient operation, electrochemical techniques could be promising for evaluating the thermodynamics of supramolecular host-guest complexations. However, there are two main factors that

limiting the application of electroanalysis in host-guest binding study. First, most host and guest molecules (including CB[7] and most drug molecules) are redox-inactive; thus no direct redox signals can be obtained for evaluating their binding behavior. Secondly, for electroactive guest species (e.g., Fc and its derivatives) in solution, usually a high concentration (sub mM level) is needed to generate a distinguishable diffusion-controlled redox current signal against the background charging current signal.[114,115] In comparison, without the influences from mass transport process, only small amount of adsorbed electroactive species on surface is able to generate strong faradic current signal, which makes it possible to investigate the strong molecular binding events occurred at interfaces.[286,287] As described from chapter 3 to chapter 5, the study of Fc@CB[7] host-guest binding on highly-organized FcC11S-/C8S-Au SAM can be viewed as a good example, where the highly reversible CV redox peaks can be clearly seen with the Fc surface density as low as 10^{-11} to 10^{-10} mol/cm^2. More remarkably, its thermodynamic binding stability can be quantitively evaluated by integrating and deconvoluting the CVs of FcC11S-/C8S-Au SAM after CB[7] incubation (the split CVs were deconvoluted into two redox peaks corresponding to free Fc terminal group and Fc@CB[7] complex formed on SAM), which allowed the direct calculation of its formation constant.

Inspired by this new interfacial Fc@CB[7] host-guest binding system, herein we proposed a general electrochemical assay for the thermodynamic study of redox-inactive drug@CB[7] complexations based on their competitive host-guest binding with Fc@CB[7] complex formed at organized molecular interface.

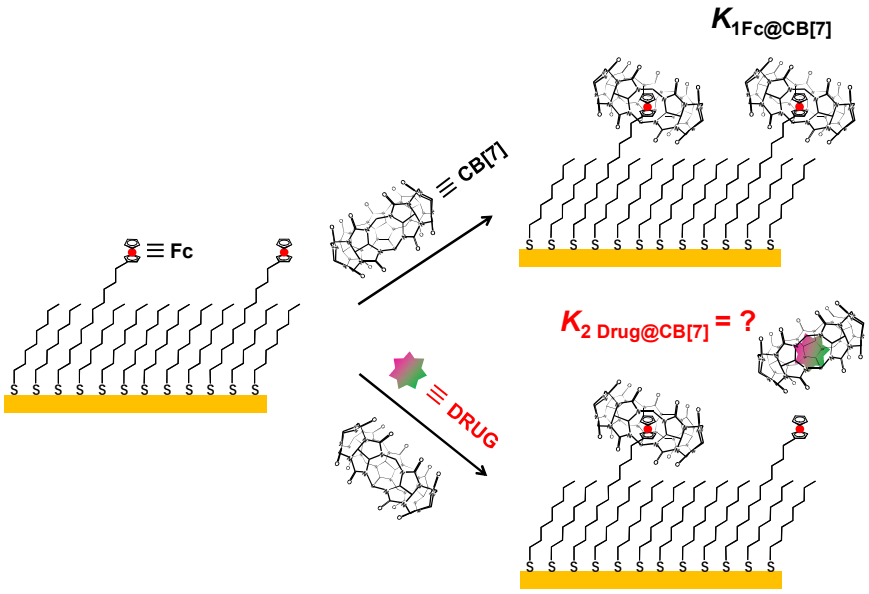

Figure 6.1. Schematic view of a general electrochemical strategy for studying the thermodynamic stability of drug@CB[7] complexation (K_2) based on its competitive host-guest binding with Fc@CB[7] complex (known binding affinity K_1) formed on FcC11S-/C8S-Au SAM.

Note: Reprinted with permission from *Anal. Chem.* 2020, 92, 2168-2175. Copyright (2020), *American Chemical Society.*

As shown in Figure 6.1, compared to only incubation with CB[7] (top), the incubation of FcC11S-/C8S-Au SAM with the mixture of CB[7] and drug molecule (bottom) is expected to reach a competitive host-guest binding equilibrium between the drug@CB[7] complex formed in solution and Fc@CB[7] complex formed on SAM. Therefore, it is possible to quantitatively analyze the thermodynamic stability (K_2) of drug@CB[7] complexation based on the CV of FcC11S-/C8S-Au SAM at competitive host-guest binding equilibrium, as well as the earlier determined binding affinity (K_1) of Fc@CB[7] complex formed on FcC11S-/C8S-Au SAM.

In this chapter, the feasibility of this idea was tested with several drug molecules as example; all of them can form 1:1 ratio host-guest complexes with CB[7], and their formation constants have been previously determined based on conventional spectroscopic and calorimetric titration studies. Besides thermodynamic study, the application potential of this redox-active alkanethiolate SAM based competitive host-guest binding strategy as a convenient electrochemical assay for drug quantitation was also evaluated.

6.2. Experimental details

6.2.1. Reagents and materials

Denatonium benzoate (DB) and alagebrium (ALA) were obtained from Dr. Ruibing Wang's lab (Institute of Chinese Medical Sciences, University of Macau). Adamantanol (AdOH) and Ferrocenylmethanol (97%) were purchased from Sigma Aldrich (St. Louis, MO). Other chemicals and materials are same with those described in section 3.2.1 (chapter 3).

6.2.2. Preparation of FcC11S-/C8S-Au SAM by co-adsorption method

It is same with the procedure described in section 5.2.2 of chapter 5.

6.2.3. Competitive host-guest binding study on FcC11S-/C8S-Au SAM

For carrying out the competitive host-guest binding studies at organized molecular interface, the above prepared FcC11S-/C8S-Au SAMs were incubated in aqueous solution containing 20 μM CB[7] and different concentrations of drug compound (DB, ALA, or AdOH) for 2 h.

6.2.4. Electrochemical measurements

CVs were measured for FcC11S-/C8S-Au SAMs before and after incubation with the mixed solution containing 20 μM CB[7] and different concentrations of drug (DB, ALA, or AdOH) for 2 h. Other detailed information of our electrochemical detection system is described in section 2.1.3 and section 3.2.3.

6.3. Results and discussion

6.3.1. Drug candidates used in this study

In order to evaluate the feasibility of the competitive host-guest binding idea shown in Figure 6.1, three drug candidates were tested in this study, as shown in Figure 6.2, which all have previously confirmed strong 1:1 binding with CB[7] in aqueous solution.[281,284,285]

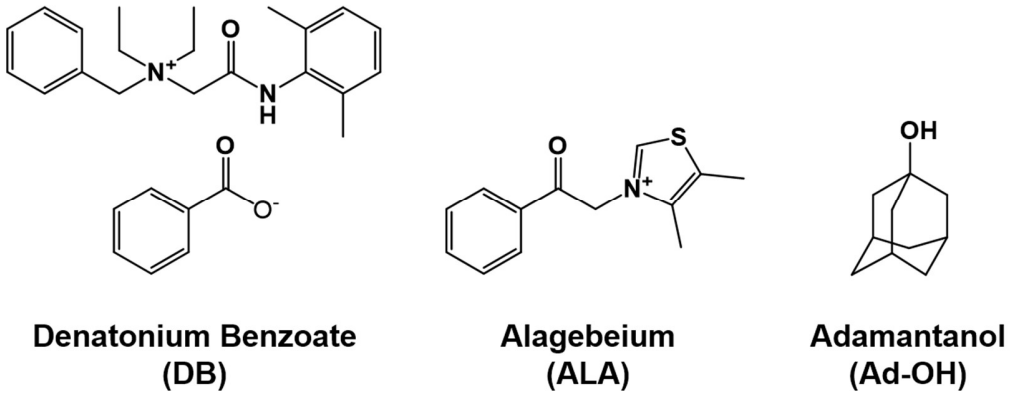

Figure 6.2. Drug candidates tested in this study

Note: Reprinted with permission from *Anal. Chem.* 2020, 92, 2168-2175. Copyright (2020) *American Chemical Society*

The first candidate is denatonium benzoate (DB), the bitterest compound recorded in the world,[288] which is popularly used in placebo medications and to discourage the consumption of harmful alcohols. The earlier study based on H-NMR titration study have revealed that the denatonium cation of this drug compound can form strong host-guest complex with CB[7] (K_f = 4.6±0.1 × 10^5 M^{-1}), by which its bitter taste can be largely concealed.[281] The second candidate is alagebrium (ALA), which is widely used in the treatment of diabetic and cardiovascular diseases. It was found that the therapeutic efficacy of ALA can be significantly improved upon forming host-guest complex with CB[7] (K_f = 7.3±0.6 × 10^5 M^{-1} as determined by isothermal titration calorimetry).[285] The third candidate is adamantanol (AdOH), which is an important raw material for drug synthesis;[289,290] compared with above two drug compounds, AdOH has much stronger

host-guest binding towards CB[7] (K_f = 4.3±1.5 × 10^9 M^{-1} as determined by competitive NMR titration).[284]

The redox activity of these drug candidates was first examined by comparing their CVs with a known redox molecule, ferrocenemethanol ($FcCH_2OH$). In Figure 6.3, It can be seen that only 2.0 mM $FcCH_2OH$ causes strong diffusion-controlled CV redox peaks (red curve), while no redox peaks were observed for all the three drag candidates (their CVs are similar to the background charging current of 1.0 M KCl (black curve)). These results clearly indicate that the drug candidates selected in this study have no redox activity, which is hard to be directly studied by electrochemical techniques.

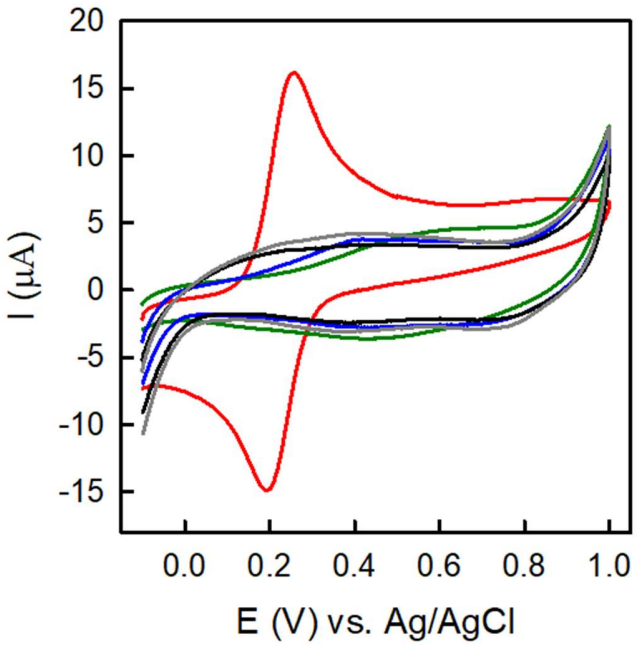

Figure 6.3. CVs of 2.0 mM $FcCH_2OH$ in 1.0 M KCl (red curve), 2.0 mM DB in 1.0 M KCl (green curve), 2.0 mM ALA in 1.0 M KCl (blue curve), 2.0 mM AdOH in 1.0 M KCl (gray curve), and 1.0 M KCl only (black curve); the scan rate was kept at 0.05 V/s.

Note: Reprinted with permission from *Anal. Chem.* 2020, 92, 2168-2175. Copyright (2020), *American Chemical Society.*

A key factor for the competitive host-guest binding idea shown in Figure 6.1 is that there should be no strong interactions between the drug molecules and the Fc terminal groups on SAM, so that the changes observed on CVs of FcC11S-/C8S-Au SAM are only

caused by Fc@CB[7] host-guest binding; in other words, the competitive host-guest binding equilibrium should be only formed between drug@CB[7] complexation in solution and Fc@CB[7] binding on SAM. In order to verify this, the CVs of FcC11S-/C8S-Au SAM were examined before and after incubation with the three drug candidates, which are displayed in Figure 6.4:

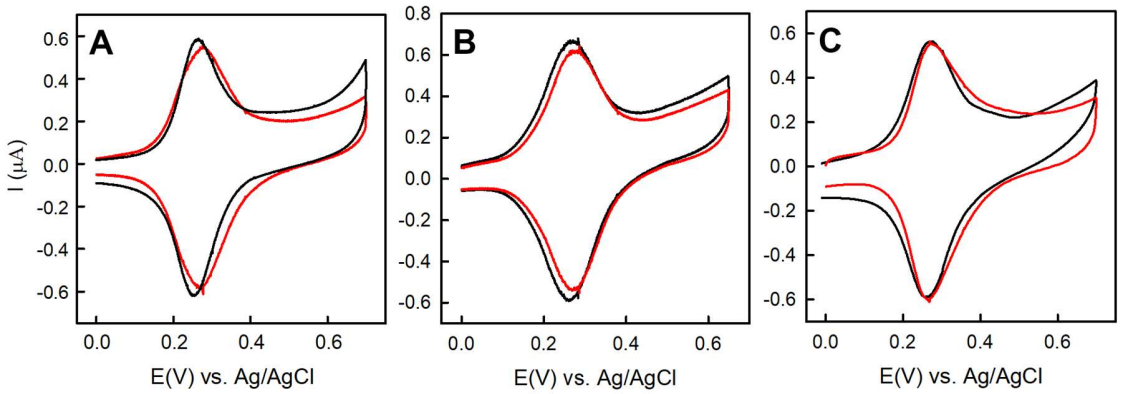

Figure 6.4. CVs of FcC11S-/C8S-Au SAMs prepared by co-adsorption (χ_{Fc}^{soln} = 2%) before (black curves) and after (red curves) incubation with (A) 100 μM DB, (B) 100 μM ALA, and (C) 100 μM AdOH. The supporting electrolyte was 0.1 M $NaClO_4$, and the potential scan rate (*v*) was kept at 0.05 V/s.

Note: Reprinted with permission from *Anal. Chem.* 2020, 92, 2168-2175. Copyright (2020), *American Chemical Society.*

It can be seen that all three drug candidates with a high concentration (0.1 mM) bring no significant changes on the original CV of FcC11S-/C8S-Au SAM (the slight deviations are possibly due to their nonspecific adsorptions on SAMs, which cause small variations on the background charging current), indicating that there is no strong interactions between these drug compounds and Fc terminal groups on SAM.

6.3.2. Thermodynamic study of Drug@CB[7] complexations based on competitive host-guest binding

The feasibility of this competitive host-guest binding based electrochemical assay was first evaluated with DB by comparing the CVs of FcC11S-/C8S-Au SAM after incubation with CB[7] only, and after incubation with the mixture of CB[7] and DB. Figure

6.5 (A) shows that after incubation with 20 μM CB[7], the original single pair CV redox peaks of FcC11S-/C8S-Au SAM almost shifts to another single pair of redox peaks located at more positive potential. According to the studies in chapter 3 and chapter 4, this indicates that a large fraction of Fc terminal groups are converted to Fc@CB[7] complexes on SAM. In contrast, when using the mixed solution of CB[7] and DB (each of 20 μM), an obvious splitting can be observed on the CV of FcC11S-/C8S-Au SAM after incubation (red curve in Figure 6.5B); this can be viewed as a strong evidence for the competitive host-guest binding occurred at interface since the split CV indicates a decreased fraction of Fc terminal groups converted to Fc@CB[7] complexes on SAM. The competitive two host-guest binding equilibriums are expressed as equation 6.1 and 6.2:

CB[7] + FcC11S-/C8S-Au ⇌ CB[7]@FcC11S-/C8S-Au

$$K_1 = \frac{\Gamma_{\mathrm{Fc@CB[7]}}}{[\mathrm{CB[7]}]\,\Gamma_{\mathrm{Fc}}} \qquad (6.1)$$

CB[7] + DB ⇌ CB[7]@DB

$$K_2 = \frac{[\mathrm{DB@CB[7]}]}{[\mathrm{CB[7]}]\,[\mathrm{DB}]} \qquad (6.2)$$

Based on the Gaussian-Lorentzian fitting protocol described in section 3.3.2 (chapter 3), the anodic wave of the split CV response (red curve in Figure 6.5B) was deconvoluted, whose result is shown as the blue dashed lines in Figure 6.6. From the two deconvoluted CV redox peaks, the mole ratio between free Fc terminal groups and Fc@CB[7] complexes formed on FcC11S-/C8S-Au SAM ($\Gamma_{Fc@CB[7]}/\Gamma_{Fc}$) was determined to be 1.52 ± 0.28 at competitive host-guest binding equilibrium.

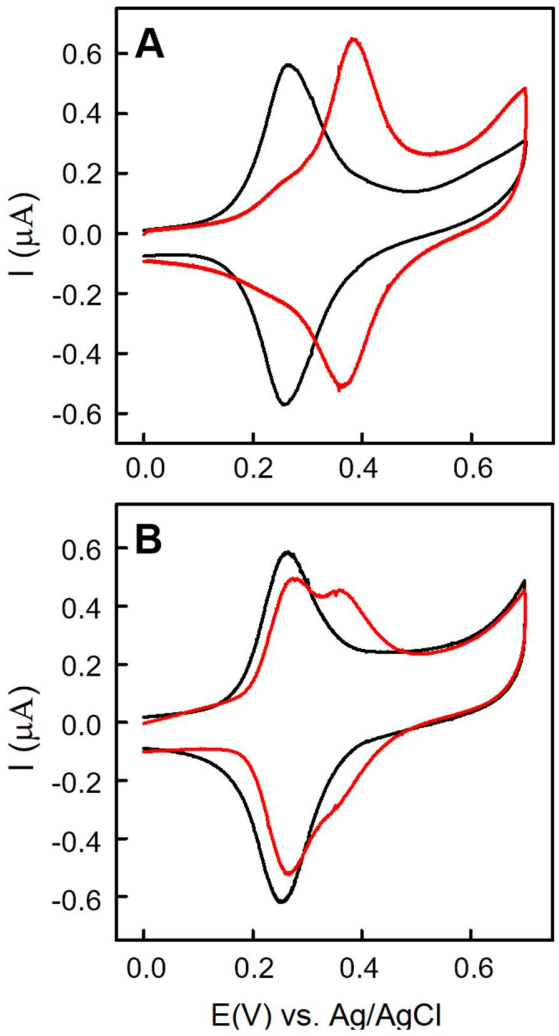

Figure 6.5. **CVs of FcC11S-/C8S-Au SAMs prepared by co-adsorption ($\chi_{FcC11SH}$ = 2%) before (black curve) and after (red curves) incubation with (A) 20 μM CB[7] solution or (B) the mixed solution containing 20 μM CB[7] and 20 μM DB for 2 h. The supporting electrolyte was 0.1 M $NaClO_4$, and the potential scan rate (v) was kept at 0.05 V/s.**

Note: Reprinted with permission from *Anal. Chem.* 2020, 92, 2168-2175. Copyright (2020), *American Chemical Society.*

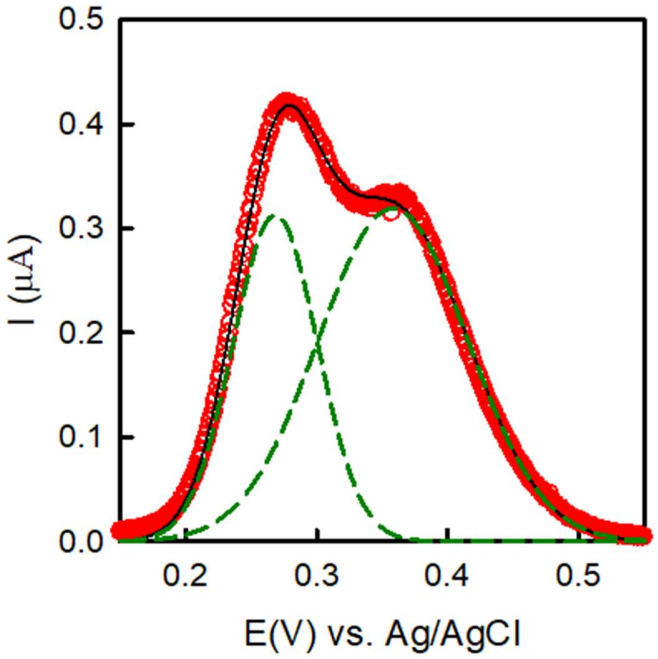

Figure 6.6. Gaussian-Lorentzian deconvolution of the CV anodic wave of FcC11S-/C8S-Au SAM prepared by co-adsorption ($\chi_{FcC11SH}$ = 2%) after incubation with the mixed solution containing 20 μM CB[7] and 20 μM DB for 2 h. The red circles show the experimental data (original CV); the green dashed lines represent the two deconvoluted redox peaks corresponding to Fc^+/Fc (lower potential) and Fc^+@CB[7]/Fc@CB[7] (higher potential), respectively; the black solid line shows the overall fit.

Note: Reprinted with permission from *Anal. Chem.* 2020, 92, 2168-2175. Copyright (2020), *American Chemical Society*.

In chapter 3, it has been determined that K_1 of Fc@CB[7] host-guest complex formed on FcC11S-/C8S-Au SAM prepared by co-adsorption with $\chi_{FcC11SH}$ of 2% is (1.5 ± 0.3) × 10^5 M^{-1}. Based on K_1 and $\Gamma_{Fc@CB[7]}/\Gamma_{Fc}$, the equilibrated concentration of CB[7] in solution ([CB[7]]) can be determined based on equation 6.3:

$$[\mathrm{CB[7]}] = \frac{\Gamma_{\mathrm{CB[7]@Fc}}}{K_1\,\Gamma_{\mathrm{Fc}}} \qquad (6.3)$$

Subsequently, the equilibrated concentration of DB@CB[7] host-guest complex formed in solution ([DB@CB[7]]) can be obtained by subtracting [CB[7]] and the "effect concentration" of Fc@CB[7] host-guest complex formed on SAM (i.e., the concentration

as if they were all released from surface and dispersed throughout the sample solution[286]) from the total concentration of CB[7] ($c_{CB[7]}$), as shown by equation 6.4:

$$[\mathrm{DB@CB[7]}] = c_{\mathrm{CB[7]}} - [\mathrm{CB[7]}] - \Gamma_{\mathrm{CB[7]@Fc}} \frac{A}{V} \qquad (6.4)$$

where A is the real electrode area (0.15 cm^2), V is the solution volume (1.0 mL). Since the maximum "effective concentration" of Fc@CB[7] host-guest complexby assuming 100% conversion rate of Fc terminal group to Fc@CB[7] complex on SAM (~ 3.0 nM) is still much smaller than $c_{CB[7]}$ and [CB[7]] (μM level), the equation 6.4 can be simplified to equation 6.5:

$$[\mathrm{DB@CB[7]}] = c_{\mathrm{CB[7]}} - [\mathrm{CB[7]}] \qquad (6.5)$$

Afterwards, the equilibrated concentration of DB ([DB]) can be obtained based on equation 6.6 (i.e., subtract [DB@CB[7]] from the total concentration of DB (c_{DB})):

$$[\mathrm{DB}] = c_{\mathrm{DB}} - [\mathrm{CB[7]@DB}] \qquad (6.6)$$

Once the equilibrated concentrations of CB[7], DB@CB[7] host-guest complex and DB are all known, the formation constant (K_2) of DB@CB[7] host-guest complex can be calculated by equation 6.2. Based on the above described procedure and the Gaussian-Lorentzian deconvolution result shown in Figure 6.6, the K_2 of DB@CB[7] host-guest complexation was determined to be (1.0±0.4) × 10^5 M^{-1}. The uncertainty of K_2 is propagated from the experimental uncertainties of $\Gamma_{Fc@CB[7]}/\Gamma_{Fc}$ (originated from the intrinsic surface heterogeneity and the limited accuracy of Gaussian-Lorentzian fitting protocol) and the uncertainty of K_1.

Similar to the observations with DB, Figure 6.7(A) shows that the incubation of FcC11S-/C8S-Au SAM with the mixed solution of CB[7] and ALA (each of 20 μM) result in the change from its original single pair of CV redox peak (black curve) to split CV response (red curve); the Gaussian-Lorentzian deconvolution result of its CV anodic wave after incubation is shown in Figure 6.7 (B), from which the $\Gamma_{Fc@CB[7]}/\Gamma_{Fc}$ and K_2 of ALA@CB[7] host-guest complexation were determined to be 0.94 ± 0.13 and (3.3±1.2) ×10^5 M^{-1}, respectively (based on equations 6.2 to 6.6).

Besides DB and ALA, whose previously determined formation constant[281,285] are similar to K_1 of Fc@CB[7] host-guest complex formed on FcC11S-/C8S-Au SAM (sub-μM level), this competitive host-guest binding based novel electrochemical strategy was then

tested with AdOH, which has over nM level binding affinity towards CB[7].[284] Interestingly, such an ultra-strong drug@CB[7] host-guest binding resulted in “distinct” CV phenomenon. As shown in Figure 6.8 (A), the incubation of FcC11S-/C8S-Au SAM with the mixed solution containing 20 μM CB[7] and 20 μM AdOH, brought no obvious changes to its original CV redox peaks (the black and blue curves); this result indicates that very little Fc terminal groups are converted to Fc@CB[7] complex on SAM after incubation, which should be attributed to the much stronger AdOH@CB[7] host-guest binding in solution. In comparison, as shown by the red curve in Figure 6.8 (A), the split CV appeared upon reducing the total concentration of AdOH (15 μM) in the mixed incubation solution (CB[7] was still 20 μM), where there was excess amount of CB[7] (> 5 μM) to bind with Fc terminal groups on SAM. Similarly, based on the deconvolution result ($\Gamma_{Fc@CB[7]}/\Gamma_{Fc}$ = 0.78 ± 0.13) shown in Figure 6.8 (B) and the equations 6.2 to 6.6, the K_2 of AdOH@CB[7] host-guest complexation in solution was determined to be (14.2 ± 42.8) ×10^5 M^{-1}; clearly, the rather huge propagated uncertainty (over 300%, its origin is discussed below) indicates the limitation of the current system in evaluating the thermodynamic stability of ultra-strong drug@CB[7] host-guest complexations.

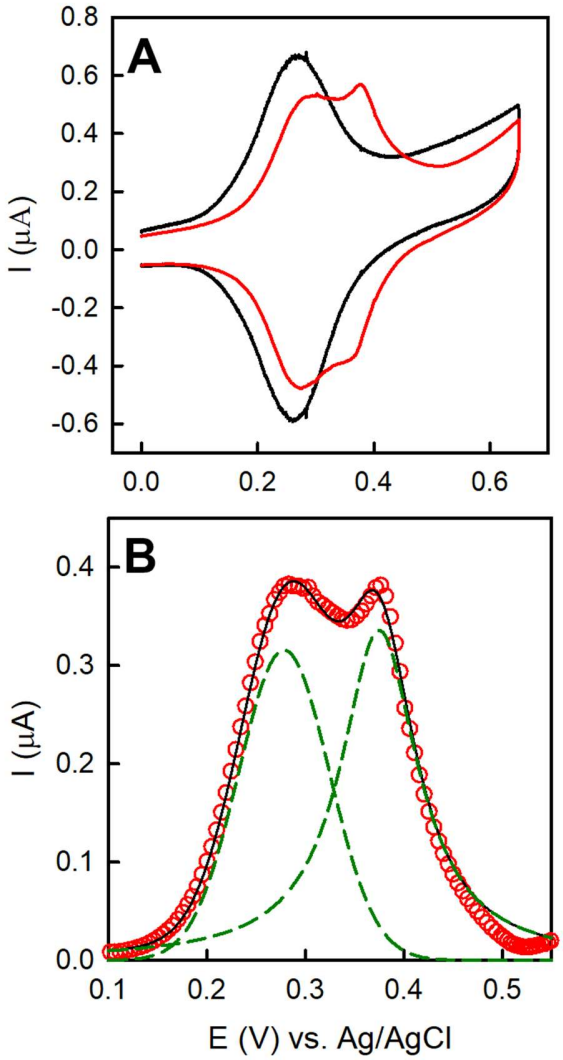

Figure 6.7. **(A) CVs of FcC11S-/C8S-Au SAM prepared by co-adsorption ($\chi_{FcC11SH}$ = 2%) before (black curve) and after (red curve) incubation with the mixed solution containing 20 μM CB[7] and 20 μM ALA for 2 h. The supporting electrolyte was 0.1 M $NaClO_4$, and the scan rate was kept at 0.05 V/s. (B) Gaussian-Lorentzian deconvolution for the anodic wave of the red CV curve shown in (A); the red circles show the experimental data (original CV); the green dashed lines represent the two deconvoluted redox peaks corresponding to Fc^+/Fc (lower potential) and Fc^+@CB[7]/Fc@CB[7] (higher potential), respectively; the black solid line shows the overall fit.**

Note: Reprinted with permission from *Anal. Chem.* 2020, 92, 2168-2175. Copyright (2020), *American Chemical Society.*

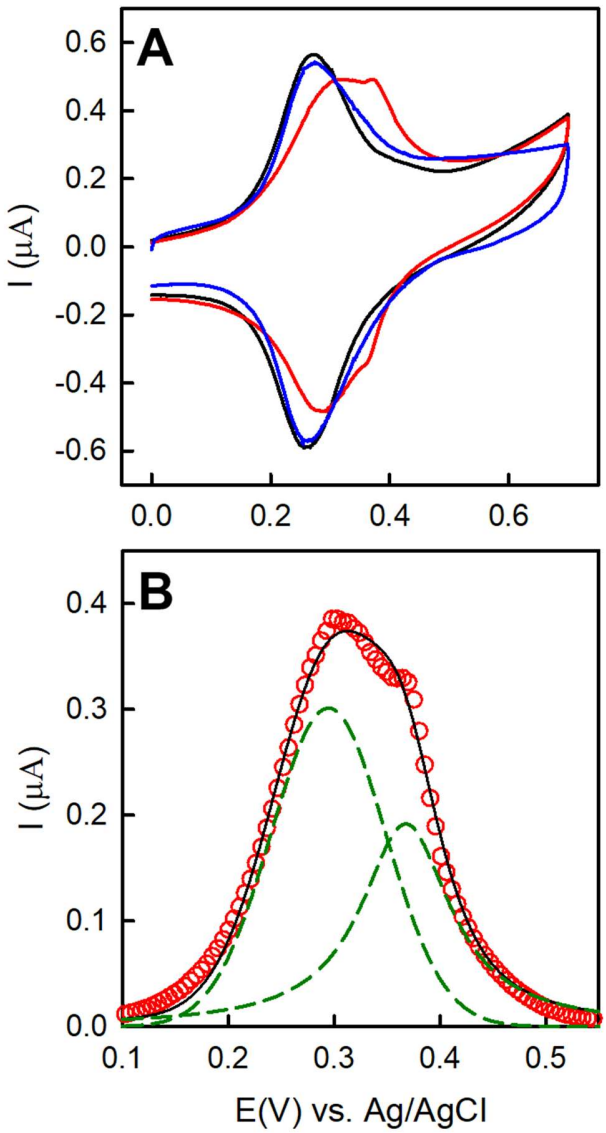

Figure 6.8. **(A) CVs of FcC11S-/C8S-Au SAMs prepared by co-adsorption ($\chi_{FcC11SH}$ = 2%) before (black curve) and after incubation with the mixed solution containing 20 μM CB[7] and 20 μM AdOH (blue curve), or the mixed solution containing 20 μM CB[7] and 15 μM AdOH (red curve) for 2 h. The supporting electrolyte was 0.1 M $NaClO_4$, and the potential scan rate was kept at 0.05 V/s. (B) Gaussian-Lorentzian deconvolution result of the red CV anodic wave shown in (A); the red circles show the experimental data (original CV); the green dashed lines represent the two deconvoluted redox peaks corresponding to Fc^+/Fc (lower potential) and Fc^+@CB[7]/Fc@CB[7] (higher potential), respectively; the black solid line shows the overall fit.**

Note: Reprinted with permission from *Anal. Chem.* 2020, 92, 2168-2175. Copyright (2020), *American Chemical Society.*

Table 6.1. Total and equilibrated concentrations of CB[7], drug molecules, and drug@CB[7] complexes associated with this competitive host-guest binding system, as well as the electrochemically determined formation constants of drug@CB[7] complexes.

	DB	ALA	AdOH
c_{drug} (μM)	20.0	20.0	15.0
$c_{CB[7]}$ (μM)	20.0	20.0	20.0
$K_{1\ (Fc@CB[7])}$ (M^{-1})	$(1.5\pm0.3)\times10^5$	$(1.5\pm0.3)\times10^5$	$(1.5\pm0.3)\times10^5$
$\Gamma_{Fc@CB[7]}/\Gamma_{Fc}$	1.52±0.28	0.94±0.13	0.78±0.13
[CB[7]] (μM)	10.1±2.4	6.4±1.5	5.2±1.4
[drug@CB[7]] (μM)	9.9±2.4	13.6±1.5	14.8±1.4
[Drug] (μM)	10.1±2.4	6.4±1.5	0.2±1.4
$K_{2\ (drug@CB[7])}$ (M^{-1}) in this study	$(1.0\pm0.4)\times10^5$	$(3.3\pm1.2)\times10^5$	$(14.2\pm42.8)\times10^5$
$K_{2\ (drug@CB[7])}$ (M^{-1}) from literature	$(4.6\pm0.1)\times10^5$ [281]	$(7.3\pm0.6)\times10^5$ [285]	$(4.3\pm1.5)\times10^9$ [284]

Note: Reprinted with permission from *Anal. Chem.* 2020, 92, 2168-2175. Copyright (2020), *American Chemical Society.*

In Table 6.1, the related total and equilibrated concentrations, surface densities, as well as the K_2 values of the three drug@CB[7] host-guest complexes determined in this work and reported in previous studies are summarized. For DB@CB[7] and ALA@CB[7] host-guest complexations, their K_2 values determined here are in same order of magnitude compared with their previously reported values based on conventional NMR or ITC titration methods; their relatively smaller K_2 found in this study might be attributed to the "salt effect" on the stability of host-guest binding (especially for cationic guests),[269] since a certain concentration of electrolyte (0.1 M $NaClO_4$ used in this study) is needed for CV measurements.[203] As the binding affinities of most drug@CB[7] complexations reported so far are μM or sub-μM level,[58,103,277] the results obtained with DB and ALA confirm the great application potential of this competitive host-guest binding based electrochemical assay as a general strategy for evaluating the thermodynamic stability of nonredox-active drug@CB[7] host-guest complexations.

As for AdOH@CB[7] host-guest binding, it is not meaningful to compare the K_2 determined in this study with its value determined by conventional titration method, since the former has “unacceptable” level of accuracy with its propagated relative uncertainty (R_{sd}) over 100%. This is not surprising when the binding affinity of drug@CB[7] host-guest complex formed in solution is much higher than the Fc@CB[7] host-guest complex formed on SAMs; as a result, there would be very tiny amount of free drug molecules remained in solution at competitive binding equilibrium (i.e., [drug] is very small) since nearly all drug molecules are complexed by CB[7]. Such a small [drug] cannot be effectively determined due to the limited accuracy of Gaussian-Lorentzian deconvolution method (e.g., there might be more than two overlapped redox peaks under the split CVs;[297]) and the intrinsic heterogeneity of substrate surface (the R_{sd} of $\Gamma_{Fc@CB[7]}/\Gamma_{Fc}$ obtained from several repeating experiments is ~ 15%, which could lead to over 100% propagated uncertainty to [drug] if its value is very small).

Although it is difficult to accurately quantify the thermodynamic stability of ultra-strong drug@CB[7] host-guest complexations with the current system, the qualitative voltammetric evaluation is still feasible as indicated by the CVs (blue and black curves) shown in Figure 6.8 (A). That is, if the drug@CB[7] host-guest complexation is much stronger than the Fc@CB[7] host-guest binding at molecular interface, the incubation of FcC11S-/C8S-Au SAM with the mixed solution containing same concentrated CB[7] and drug would bring no obvious change to its CV response (i.e., nearly no Fc@CB[7] complex formed on SAM).

6.3.3. Electrochemical quantitation of drug based on competitive host-guest binding

Besides the thermodynamic study described above, this redox-active SAM based competitive host-guest binding strategy may be capable of electrochemically detecting the nonredox-active drug compounds in solution (the more drugs competitively binding with CB[7] in their mixed solution, the less amount of CB[7] bound to Fc terminal groups on SAM, which, according to above study, can be quantitatively reflected by CV). Such a detection principle reassembles the idea of conventional, indirect competitive immunoassays but has its particular merits: First, unlike the conventional immunoassays that require customized, animal-based processes to obtain specific antibodies for

individual drug compound (as target antigen),[291] the artificially synthesized CB[7] macrocyclic host can accommodate many drug compounds with satisfied affinity, specificity, and simplificity.[58,277] Secondly, with the strong and distinct CV redox peaks of Fc terminal group (serves as the role of surface-bound competitive antigen) and Fc@CB[7] host-guest complex formed on SAM, no additional signal modification is needed for generating the sensing response; in contrast, the time consuming and complicated covalent signal labeling is usually required for conventional immunoassay.

With DB as an example, the feasibility of this electrochemical drug assay has been proved with the CV results shown in Figure 6.9, which exhibits the CVs of FcC11S-/C8S-Au SAMs after incubation with the mixed solution containing 20 μM CB[7] and different concentrations of DB. It can be seen from Figure 6.9 (A) that when there is no DB in the solution (c_{DB} = 0), the CV of FcC11S-/C8S-Au SAM shows a single pair of redox peaks located at a higher potential, which results from the Fc@CB[7] host-guest complexes formed on SAM; with increased c_{DB} (5 to 60 μM), the CVs gradually shift negatively to the single pair of redox peaks located at lower potential, which corresponds to the free Fc terminal groups on SAM; no further change on CV is observed when c_{DB} is higher than 60 μM. In order to quantify the "sensing" responses, all CVs shown in Figure 6.9 (A) were deconvoluted by Gaussian-Lorentzian fitting protocol. Based on the deconvolution results displayed in Figure 6.9 (B), the mole fraction of free Fc terminal groups on SAM ($\Gamma_{Fc}/\Gamma_{Fc\ total}$) was plotted as the function of c_{DB} in the mixed incubation solution, which is shown in Figure 6.10. It is clear that $\Gamma_{Fc}/\Gamma_{Fc\ total}$ increases proportionally with c_{DB} at early stage, and reaches plateau at c_{DB} of ~30 μM. In fact, the concentration level of DB used for poisoning prevention is usually 22 μM (10 mg/L) or higher,[292] for which the present assay can certainly accommodate such tests. The proof-of-concept results shown in Figure 6.9 and 6.10 clearly demonstrate the great potential of such a redox-active SAM based competitive host-guest binding system as an electrochemical assay for drug detection, which is simpler and more convenient than those conventional methods relying on titrimetric, chromatographic, spectroscopic, or immune techniques.[293]

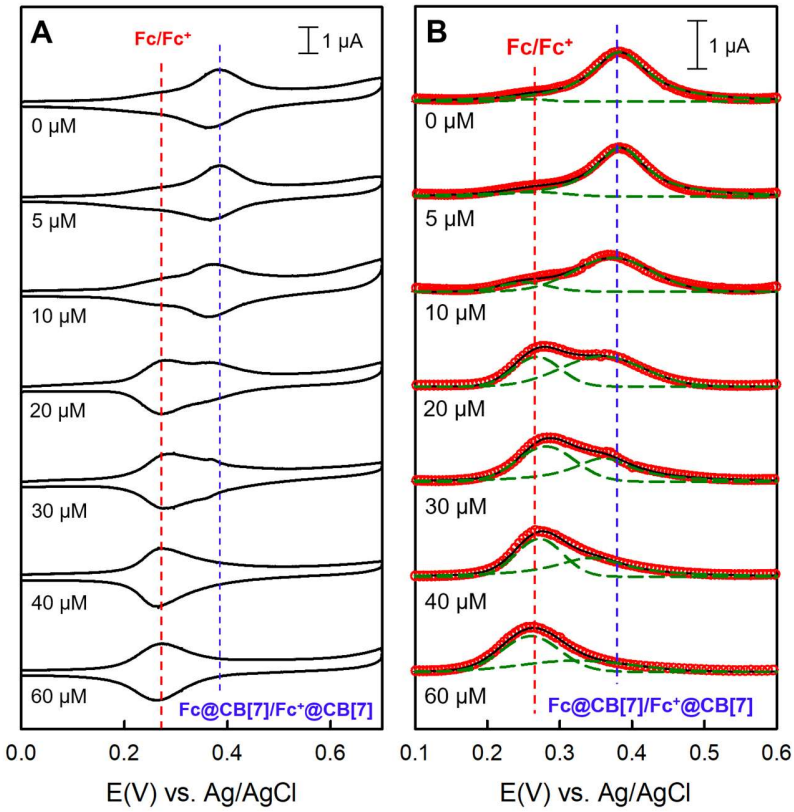

Figure 6.9. **(A) CVs of FcC11S-/C8S-Au SAMs prepared by co-adsorption method ($\chi_{FcC11SH}$ = 2%) after incubation with a mixed solution containing 20 μM CB[7] and different concentrations of DB for 2 h. The supporting electrolyte was 0.1 M $NaClO_4$, and the potential scan rate (v) was kept at 0.05 V/s. (B) Gaussian-Lorentzian deconvolution results of the CV anodic waves shown in (A); the red circles show the experimental data (original CV); the green dashed lines represent the two deconvoluted redox peaks corresponding to Fc^+/Fc (lower potential) and Fc^+@CB[7]/Fc@CB[7] (higher potential), respectively; the balck solid line shows the overall fit.**

Note: Reprinted with permission from *Anal. Chem.* 2020, 92, 2168-2175. Copyright (2020), *American Chemical Society.*

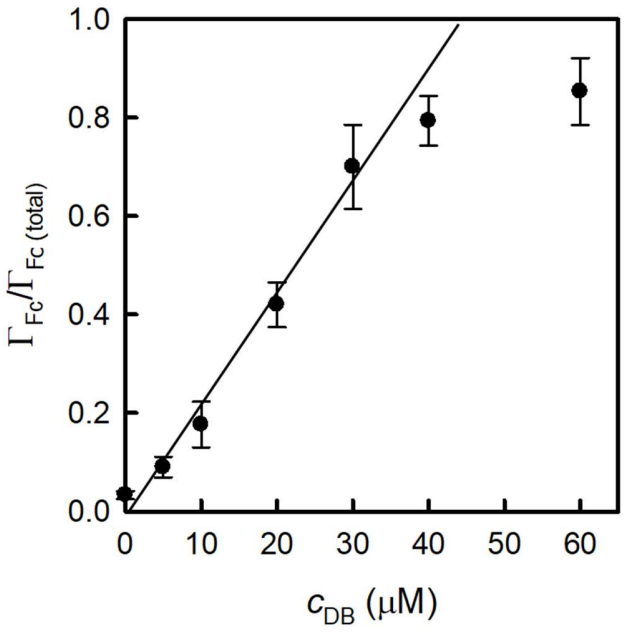

Figure 6.10. The mole fraction of free Fc terminal groups ($\Gamma_{Fc}/\Gamma_{Fc\ total}$) on FcC11S-/C8S-Au SAM prepared by co-adsorption method ($\chi_{FcC11SH}$ = 2%) as a function of total DB concentration (c_{DB}) in the mixed incubation solution with 20 μM CB[7]. The black solid line is the best linear fit to the data points between 0 and 30 μM DB (R^2 = 0.9862).

Note: Reprinted with permission from *Anal. Chem.* 2020, 92, 2168-2175. Copyright (2020), *American Chemical Society.*

It should be noted that in terms of practical application, there are still limitations for this competitive host-guest binding based electrochemical assay, such as the prerequisite of preparing high-quality SAMs, the narrow-range binding affinities of drug@CB[7] complexations can be quantitatively studied, and the nonspecific adsorption problem. Nevertheless, with additional efforts some of these limitations could be mitigated. For example, the quantitative ability of this method can be extended to ultra-strong drug@CB[7] host-guest complexations by further improving the binding affinity of Fc@CB[7] host-guest complex formed on SAM; the nonspecific adsorption problem can be mitigated by using diluent alkanethiols with more hydrophilic or hydrophobic terminal groups (based on the composition of drug compound). Despite of these, this novel method exhibits great potential of broader applications. Firstly, it should be capable of investigating the kinetics of drug@CB[7] complexations, which will help to guide the design of more efficient CB[7]-based drug delivery system. Not limiting to drug molecules, this competitive

host-guest binding based electrochemical assay could be also applied for other biomedically/pharmaceutically interested guest@CB[7] complexations with intriguing properties and functions.[58, 294] With more advanced nanoelectrode techniques, the ultra-small sample volume analysis, which is of great significance in terms of studying trace amount of biomolecules, could be achieved with this method as well. In addition to CB[7], it is also expected that this method could be extended to broad macrocyclic host-guest complexations. All these new directions to expand the spectrum of this novel electrochemical assay is the long-term goal of this thesis study.

6.4. Conclusion

In this study, a redox-active Fc-SAM based competitive host-guest binding strategy has been proposed as convenient and sensitive electrochemical assay for the thermodynamic stability of nonredox-active drug@CB[7] host-guest complexations interested in pharmaceutical and biomedical science. With three representative drug molecules as examples, it has been confirmed by CV that when drug@CB[7] host-guest complexations (e.g., DB@CB[7] and ALA@CB[7]) are as strong as the Fc@CB[7] host-guest binding on FcC11S-/C8S-Au SAM (sub-μM level binding affinity), their binding affinities can be quantitatively evaluated; when drug@CB[7] host-guest complexation is much stronger than Fc@CB[7] host-guest binding on FcC11S-/C8S-Au SAM (e.g., AdOH@CB[7], nM level binding affinity), its ultra-strong binding can still be qualitatively assessed. Moreover, the prospect of using this redox-active SAM based competitive host-guest binding strategy as a quantitative electrochemical assay for drug detection was also demonstrated by the varied CVs of FcC11S-/C8S-Au SAM in response to different concentrations of drug (DB) in the mixed incubation solution (with a fixed concentration of CB[7]). In addition to drug@CB[7] complexations, this proposed strategy shed lights on how “ordinary” supramolecular host-guest complexes without redox activity can be electrochemically studied, which would certainly promote the adaptation of electrochemical analysis in either fundamental studies of supramolecular host-guest chemistry or its practical applications.

Chapter 7.

Summary and outlook

7.1. Summary

In this thesis study, we explored the surface binding stability of the ultra-strong host-guest recognition pairs formed between macrocyclic CB[7] (host) and redox-active Fc (guest). The system chosen for this study was the redox-active binary FcC11S-/C8S-Au SAM as it offers the advantages of high stability, highly-organized structure, and well-dispersed Fc terminal groups (as CB[7] host binding sites). The CV studies confirm that compared with the free Fc terminal group, the Fc@CB[7] host-guest complex formed on FcC11S-/C8S-Au SAM has a pair of distinct redox peaks located at a more positive potential; by deconvoluting and integrating the splited CV redox peaks, free and CB[7]-bound Fc terminal groups were quantified, which allowed for the direct thermodynamic and kinetic investigations. Compared with previous studies in solution phase, it was found that the stability of this host-guest recognition pair, even formed at such an "ideal" molecular interface, is largely reduced as indicated by its dramatically decreased binding affinity (from over nM level to sub-μM level) and association rate constant (from close to diffusion-controlled process to less than 10^4 M^{-1} s^{-1}). Nevertheless, its binding affinity is still acceptable for practical use and could be further improved (vide infra).

By evaluating the changes on CV responses, which reflect the fraction of Fc terminal groups bound to CB[7], this interfacial host-guest recognition pair can be employed as a robust and convenient molecular probe for the distribution of Fc terminal groups (isolated or clustered, buried or exposed) on SAMs. Compared with the conventional electrochemical and microscopic characterizations, this novel method provides more direct and reliable information to reveal the structural heterogeneity of the mixed ferrocenylalkanethiolate/alkanethiolate SAMs prepared via different routes or conditions. The extremely low polarizability of CB[7] inner cavity also enables CB[7] to be used as a local environmental regulator for the ET behavior of guest species; this was confirmed by the decreased ET rate constant (from 10^3 s^{-1} to 5×10^2 s^{-1}), the smaller reorganization energy (from 0.8 eV to 0.6 eV), and the weakened electronic coupling (from 0.9 cm^{-1} to 0.7 cm^{-1}) of Fc terminal group upon encapsulation by CB[7]. These kinetic studies provide

further insights into the environmental requirement (i.e., a fixed arrangement of dipoles that is electrostatically complementary to substrate) of biological enzymatic ET processes. In addition, based on the competitive host-guest binding associated with the Fc@CB[7] host-guest complex formed on FcC11S-/C8S-Au SAM, an universal electrochemical quantitative assay was developed for evaluating the thermodynamic stability of non-electroactive drug@CB[7] host-guest complexations, which allows for drug quantitation in pharmaceutical/biomedical applications.

7.2. Future studies from fundamental aspects

In order to further promote the broad application of this new interfacial Fc@CB[7] host-guest system, more in depth fundamental studies are essential for answering the key question: why the ultra-strong binding affinity of Fc@CB[7] host-guest complex formed in solution phase is significantly decreased upon transferring onto molecular interface? Although CV as a convenient and quantitative characterization technique is suitable for investigating the binding behavior of CB[7] to Fc terminated electroactive SAMs, it lacks the ability to provide molecular/atomic level of information, which need to be studied by other characterization techniques. For example, by examining this interfacial host-guest binding with microscopic techniques, the detailed morphology and distribution of Fc@CB[7] host-guest complexes formed on FcC11S-/C8S-Au SAM could be obtained; with the help of X-ray based crystallographic techniques, it is possible to see how different is the orientation of Fc terminal group inside the inner cavity of CB[7] compared with the orientations of free Fc guest inside CB[7] (displayed in Figure 1.4 of chapter 1). This may reveal the different spatial arrangement of their intermolecular interactions in solution and on surface; X-ray or neutron reflectometry techniques can also be used to explore the structure and density of the water layer near the CB[7]-bound FcC11S-/C8S-Au SAM,[224-226] which could strongly affect the entropy gain associated with the release of high energy water molecules from the inner cavity of CB[7]; By taking the advantage of structurally well-defined and organized FcC11S-/C8S-Au SAM, the application of computing/theoretical chemistry, such as DFT and MD, may allow for the simulation of thermodynamic and structural parameters associated with this interfacial host-guest binding. It is believed that the information obtained from these methods and techniques will certainly help to answer the above-mentioned questions. Meanwhile, the influence of other factors on the interfacial Fc@CB[7] host-guest binding can also be investigated,

such as the hydrophilic terminal group of diluent alkanethiols, the odd-even effect of ferrocenylalkanethiol, and the cationic derivatizations on Fc terminal group (form additional ion-dipole interactions with CB[7]); these studies will help explore possible approaches to improve its stability. The binding kinetics of this particular host-guest pair formed at organized molecular interface can be further studied by measuring its rate constants at different temperatures, from which the activation energy and pre-exponential factor (related to collision frequency and orientation) can be determined (based on Arrhenius equation) and compared.[149] The influence of CB[7] host binding on the ET mechanism can be further investigated by measuring the tunneling constant across Fc-SAMs (obtained from the slope of $\ln k_{et}$ vs. n, where n is the number of methylene groups in alkane bridge).[245]

7.3. Future studies of application perspectives

An important future goal of this thesis is to explore the potential application of this intriguing interfacial Fc@CB[7] host-guest binding system for developing better-controlled, more versatile, and reusable bio-functional devices.

The multiple-charged DNA strands with highly flexible and programmable structure, and the sequence-dependent ligand binding (Aptamer) and catalytic functions (DNAzyme) have been widely applied as a new generation of material for fabricating versatile bio-functional devices.[303,304] Particularly, the successful immobilization of redox-labeled DNA probes on electrode surface (e.g., through thiolated DNA) have greatly promoted the development of convenient electrochemical biosensors for a wide range of analytes.[305-308] Unfortunately, as both a chemically and structurally complex biopolymer, the immobilized DNA monolayers on solid substrates always have high degree of structural heterogeneity (large fraction of aggregated or clustered domains) and strong nonspecific adsorptions,[309] which strongly affect the interfacial DNA-analyte binding behavior, and cause poor sensing sensitivity and reproducibility.[310]

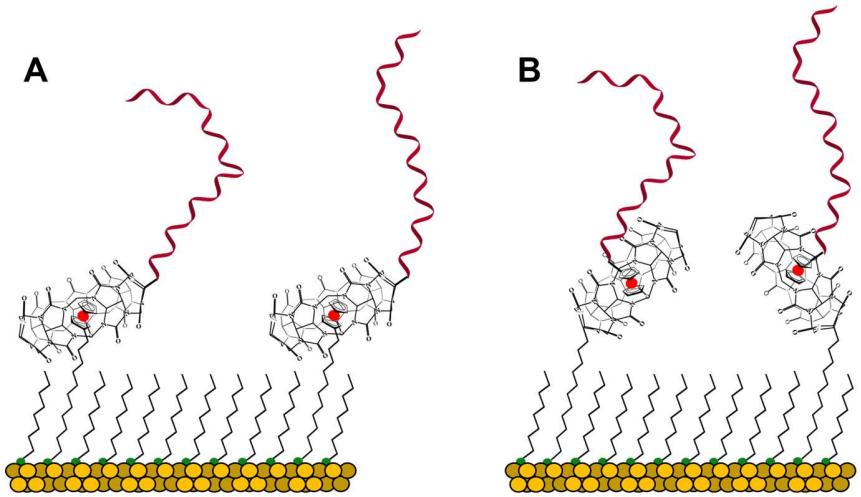

Figure 7.1. Preparation of DNA monolayer on highly organized molecular interface: (A) immobilization of CB[7]-coupled DNA on Fc-terminated mixed alkanethiolate SAM on gold; (B) immobilization of Fc-coupled DNA on CB[7]-terminated mixed alkanethiolate SAM on gold.

Based on the new interfacial Fc@CB[7] host-guest binding system developed in this thesis, a novel strategy for fabricating DNA monolayer based electrochemical biosensors is proposed here, as shown in Figure 7.1. The (A) and (B) in Figure 7.1 are two different options of this novel strategy: In (A), the DNA probe is immobilized on surface via interfacial host-guest binding between the CB[7]-coupled DNA and Fc terminal group on mixed alkanethiolate SAMs on gold. In (B), Fc guest is coupled to DNA while CB[7] is attached to surface as the terminal group of alkanethiolate SAMs. There are several intriguing advantages expected with this novel DNA immobilization strategy. First, the nonspecific adsorption of DNA on gold can be largely inhibited by the pre-assembled alkanethiolate SAMs; second, with the strict 1:1 ratio host-guest binding between CB[7] and Fc as well as the rather large molecular size of CB[7] along with a much limited surface density ($< 7 \times 10^{-11}$ mol/Cm^2),[126] the formation of aggregated or clustered DNA domains could be inhibited. In addition to mitigating the intrinsic limitation of DNA monolayers, this interfacial Fc@CB[7] host-guest binding-based DNA immobilization strategy may provide additional merits towards electrochemical sensing and characterization. For example, the redox response of Fc as well as its changes induced by the CB[7] host binding would allow for the easy and informative electrochemical investigations on thermodynamic and kinetics properties of DNA monolayer. For the design shown in Figure 7.1 (B), the surface density

of DNA monolayer can be easily quantified from the redox response of Fc that is conjugated to the DNA probe via 1:1 stoichiometry. More importantly, the redox response of Fc can serve as an internal reference for developing ratiometric electrochemical biosensors with higher reproducibility in sensing and background signals, and thus a improved detection limit.[310] Last but not the least, the noncovalent nature of Fc@CB[7] host-guest binding pair may allow these electrochemical biosensors to be regenerated or recycled by removing DNA probes from the surface by adding another strong guest molecule (through competitive host-guest binding).

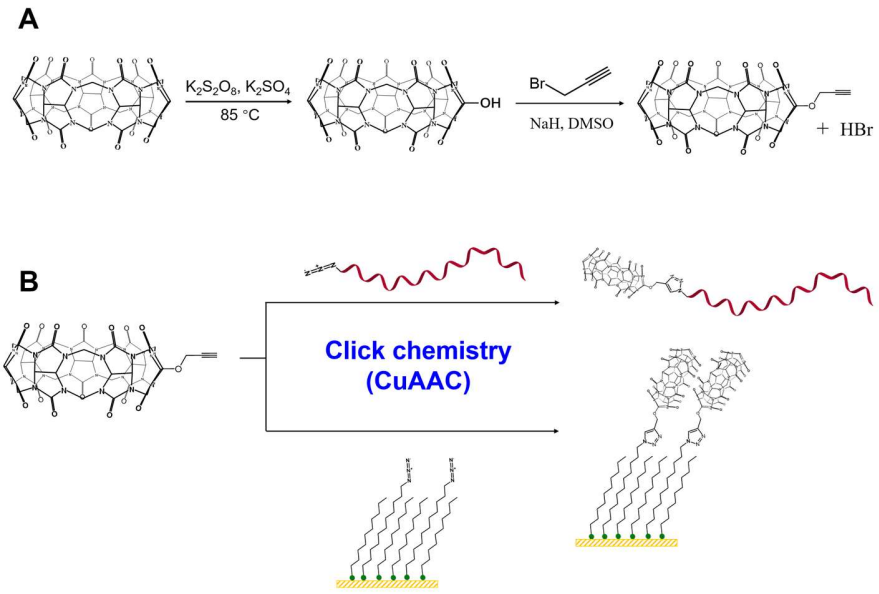

Figure 7.2. (A) A proposed synthetic approach of propargyl CB[7] based on Ref.313. (B) Covalent coupling of propargyl CB[7] to azide-terminated DNA strand or azide-terminated alkanethiolate SAMs on gold via Cu(I)-catalyzed azide–alkyne cycloaddition (CuAAC).

As the Fc-conjugated DNA[311] and various ferrocenylalkanethiol derivatives[312] are all commercially available, the main challenge of this novel DNA immobilization strategy is the covalent coupling of CB[7] to DNA strand or to alkanethiolate SAMs. A possible solution is to introduce an alkyne group to CB[7] via the previously reported synthetic procedure of propargyl CB[6].[313] Briefly, as illustrated in Figure 7.2 (A), CB[7] will be first oxidized by $K_2S_2O_8$ with proper amount of K_2SO_4 in order to generate the monohydroxyl group, then the alkyne group can be introduced to the monohydroxylated CB[7] via its

reaction with propargyl-bromide. Based on the advantageous (simple, fast, and high yields) “click” chemistry of Cu(I)-catalyzed azide–alkyne cycloaddition (CuAAC), the propargyl-CB[7] can be subsequently conjugated to a commercially available azide-DNA, or to the azide-terminated alkanethiolate SAMs on gold, as illustrated in Figure 7.2 (B).

Not limiting to DNA, this new interfacial Fc@CB[7] host-guest binding system could be applied for immobilizing other types of biosensing entities (e.g., proteins and cells) with versatile functions. It is also interesting to investigate this new interfacial Fc@CB[7] host-guest binding system on gold nanoparticles or gold nanoarrays, which have more complex surface structure and morphology, distinctive physical and chemical properties, as well as expanded application fields. In addition to Fc@CB[7] host-guest binding, the use of electroactive alkanethiolate SAMs as a “near ideal” system for electrochemical characterization and applications could be applied to other widely interested supramolecular host-guest recognition pairs, such as the 1:2 ratio host-guest complexes formed with CB[8],[51,52] which might enable more convenient surface immobilization strategies.

References

(1) Lehn, J. M. Supramolecular chemistry—scope and perspectives molecules, supermolecules, and molecular devices (Nobel Lecture). *Angewandte Chemie International Edition in English* **1988**, *27*, 89-112.

(2) Ariga, K.; Kunitake, T. Supramolecular chemistry-fundamentals and applications: advanced textbook; *Springer Science / Business Media*, **2006**.

(3) Klok, H. A.; Lecommandoux, S. Supramolecular materials via block copolymer self‐assembly. *Advanced Materials* **2001**, *13*, 1217-1229.

(4) Kolesnichenko, I. V.; Anslyn, E. V. Practical applications of supramolecular chemistry. *Chemical Society Reviews* **2017**, *46*, 2385-2390.

(5) Jain, A.; George, S. J. New directions in supramolecular electronics. *Materials Today* **2015**, *18*, 206-214.

(6) Bell, T. W.; Hext, N. M. Supramolecular optical chemosensors for organic analytes. *Chemical Society Reviews* **2004**, *33*, 589-598.

(7) Ragazzon, G.; Baroncini, M.; Ceroni, P.; Credi, A.; Venturi, M. Electrochemically Controlled Supramolecular Switches and Machines. **2017**, 343-368.

(8) Amabilino, D. B.; Smith, D. K.; Steed, J. W. Supramolecular materials. *Chemical Society Reviews* **2017**, *46*, 2404-2420.

(9) Ellis, R. J.; Meridiano, Y.; Muller, J.; Berthon, L.; Guilbaud, P.; Zorz, N.; Antonio, M. R.; Demars, T.; Zemb, T. Complexation‐Induced Supramolecular Assembly Drives Metal‐Ion Extraction. *Chemistry‐A European Journal* **2014**, *20*, 12796-12807.

(10) You, L.; Zha, D.; Anslyn, E. V. Recent advances in supramolecular analytical chemistry using optical sensing. *Chemical Reviews* **2015**, *115*, 7840-7892.

(11) Schneider, H.-J. Supramolecular systems in biomedical fields; *Royal Society of Chemistry*, **2013**.

(12) Scarso, A.; Ballester, P. Supramolecular Aspects in Catalysis. *Frontiers in Chemistry* **2019**, *7*, 174.

(13) Lehn, J.-M. From supramolecular chemistry towards constitutional dynamic chemistry and adaptive chemistry. *Chemical Society Reviews* **2007**, *36*, 151-160.

(14) Lehn, J. M. Perspectives in chemistry—aspects of adaptive chemistry and materials. *Angewandte Chemie International Edition* **2015**, *54*, 3276-3289.

(15) Lichtenthaler, F. W. 100 Years “Schlüssel‐Schloss‐Prinzip”: What Made Emil Fischer Use this Analogy? *Angewandte Chemie International Edition in English* **1995**, *33*, 2364-2374.

(16) Koshland Jr, D. E. The key–lock theory and the induced fit theory. *Angewandte Chemie International Edition in English* **1995**, *33*, 2375-2378.

(17) Pedersen, C. J. Crown Ether Compounds. *Journal of the American Chemical Society* **1967**, *89*, 7077-7091.

(18) Christy, F. A.; Shrivastav, P. S. Conductometric studies on cation-crown ether complexes: a review. *Critical Reviews in Analytical Chemistry* **2011**, *41*, 236-269.

(19) Tsukube, H. Armed crown ether complexes in supramolecular assembly. *Coordination Chemistry Reviews* **1996**, *148*, 1-17.

(20) Kimura, E.; Koike, T. Dynamic anion recognition by macrocyclic polyamines in neutral pH aqueous solution: development from static anion complexes to an enolate complex. *Chemical Communications* **1998**, *15*, 1495-1599.

(21) Kimura, E. Distinctive coordination chemistry and biological relevance of complexes with macrocyclic oxo polyamines. *Journal of Coordination Chemistry* **1986**, *15*, 1-28.

(22) Schneider, H.-J.; Yatsimirsky, A. K. Selectivity in supramolecular host–guest complexes. *Chemical Society Reviews* **2008**, *37*, 263-277.

(23) Del Valle, E. M. Cyclodextrins and their uses: a review. *Process Biochemistry* **2004**, *39*, 1033-1046.

(24) Steed, J. W.; Atwood, J. L. *Supramolecular Chemistry*; John Wiley & Sons, **2013**.

(25) Rekharsky, M. V.; Inoue, Y. Complexation thermodynamics of cyclodextrins. *Chemical Reviews* **1998**, 98, 1875-1918.

(26) Behrend, R.; Meyer, E.; Rusche, F. I. Ueber condensationsproducte aus glycoluril und formaldehyd. *Justus Liebigs Annalen der Chemie* **1905**, *339*, 1-37.

(27) Freeman, W.; Mock, W.; Shih, N. Cucurbituril. *Journal of the American Chemical Society* **1981**, *103*, 7367-7368.

(28) Kim, J.; Jung, I.-S.; Kim, S.-Y.; Lee, E.; Kang, J.-K.; Sakamoto, S.; Yamaguchi, K.; Kim, K. New cucurbituril homologues: syntheses, isolation, characterization, and X-ray crystal structures of cucurbit [n] uril (n= 5, 7, and 8). *Journal of the American Chemical Society* **2000**, *122*, 540-541.

(29) Isaacs, L. The mechanism of cucurbituril formation. *Israel Journal of Chemistry* **2011**, *51*, 578-591.

(30) Day, A. I.; Blanch, R. J.; Coe, A.; Arnold, A. P. The effects of alkali metal cations on product distributions in cucurbit [n] uril synthesis. *Journal of Inclusion Phenomena and Macrocyclic Chemistry* **2002**, *43*, 247-250.

(31) Lee, J. W.; Samal, S.; Selvapalam, N.; Kim, H.-J.; Kim, K. Cucurbituril homologues and derivatives: new opportunities in supramolecular chemistry. *Accounts of Chemical Research* **2003**, *36*, 621-630.

(32) Bardelang, D.; Udachin, K. A.; Leek, D. M.; Margeson, J. C.; Chan, G.; Ratcliffe, C. I.; Ripmeester, J. A. Cucurbit [n] urils (n= 5–8): a comprehensive solid state study. *Crystal Growth & Design* **2011**, *11*, 5598-5614.

(33) Buschmann, H.-J.; Cleve, E.; Schollmeyer, E. Cucurbituril as a ligand for the complexation of cations in aqueous solutions. *Inorganica Chimica Acta* **1992**, *193*, 93-97.

(34) Hwang, I.; Jeon, W. S.; Kim, H. J.; Kim, D.; Kim, H.; Selvapalam, N.; Fujita, N.; Shinkai, S.; Kim, K. Cucurbit [7] uril: A Simple Macrocyclic, pH‐Triggered Hydrogelator Exhibiting Guest‐Induced Stimuli‐Responsive Behavior. *Angewandte Chemie International Edition* **2007**, *46*, 210-213.

(35) Nau, W. M.; Florea, M.; Assaf, K. I. Deep inside cucurbiturils: physical properties and volumes of their inner cavity determine the hydrophobic driving force for host–guest complexation. *Israel Journal of Chemistry* **2011**, *51*, 559-577.

(36) Mecozzi, S.; Rebek, J., Julius. The 55% solution: a formula for molecular recognition in the liquid state. *Chemistry–A European Journal* **1998**, *4*, 1016-1022.

(37) Marquez, C.; Nau, W. M. Polarizabilities inside molecular containers. *Angewandte Chemie International Edition* **2001**, *40*, 4387-4390.

(38) Mohanty, J.; Nau, W. M. Ultrastable rhodamine with cucurbituril. *Angewandte Chemie International Editio*n **2005**, *44*, 3750-3754.

(39) Kim, K.; Selvapalam, N.; Ko, Y. H.; Park, K. M.; Kim, D.; Kim, J. Functionalized cucurbiturils and their applications. *Chemical Society Reviews* **2007**, 36, 267-279.

(40) Gao, R. H.; Chen, L. X.; Chen, K.; Tao, Z.; Xiao, X. Development of hydroxylated cucurbit [n] urils, their derivatives and potential applications. *Coordination Chemistry Reviews* **2017**, *348*, 1-24.

(41) Zhao, J.; Kim, H. J.; Oh, J.; Kim, S. Y.; Lee, J. W.; Sakamoto, S.; Yamaguchi, K.; Kim, K. Cucurbit[n]uril derivatives soluble in water and organic solvents. *Angewandte Chemie International Edition* **2001**, *40*, 4233-4235.

(42) Buschmann, H.-J.; Jansen, K.; Meschke, C.; Schollmeyer, E. Thermodynamic data for complex formation between cucurbituril and alkali and alkaline earth cations in aqueous formic acid solution. *Journal of Solution Chemistry* **1998**, *27*, 135-140.

(43) Blanco, E.; Quintana, C.; Hernández, P.; Hernández, L. A voltammetric study of the interaction between cucurbit[6]uril and divalent metal ions. *Electroanalysis* **2010**, *22*, 2123-2130.

(44) Masson, E.; Ling, X.; Joseph, R.; Kyeremeh-Mensah, L.; Lu, X. Cucurbituril chemistry: a tale of supramolecular success. *Rsc Advances* **2012**, *2*, 1213-1247.

(45) Assaf, K. I.; Nau, W. M. Cucurbiturils: from synthesis to high-affinity binding and catalysis. *Chemical Society Reviews* **2015**, *44*, 394-418.

(46) Shetty, D.; Khedkar, J. K.; Park, K. M.; Kim, K. Can we beat the biotin–avidin pair?: cucurbit [7] uril-based ultrahigh affinity host–guest complexes and their applications. *Chemical Society Reviews* **2015**, *44*, 8747-8761.

(47) Biedermann, F.; Uzunova, V. D.; Scherman, O. A.; Nau, W. M.; De Simone, A. Release of high-energy water as an essential driving force for the high-affinity binding of cucurbit [n] urils. *Journal of the American Chemical Society* **2012**, *134*, 15318-15323.

(48) Rekharsky, M. V.; Mori, T.; Yang, C.; Ko, Y. H.; Selvapalam, N.; Kim, H.; Sobransingh, D.; Kaifer, A. E.; Liu, S.; Isaacs, L. A synthetic host-guest system achieves avidin-biotin affinity by overcoming enthalpy–entropy compensation. *Proceedings of the National Academy of Sciences* **2007**, *104*, 20737-20742.

(49) Buschmann, H.-J.; Cleve, E.; Jansen, K.; Schollmeyer, E. Determination of complex stabilities with nearly insoluble host molecules: cucurbit [5] uril, decamethylcucurbit [5] uril and cucurbit [6] uril as ligands for the complexation of some multicharged cations in aqueous solution. *Analytica Chimica Acta* **2001**, *437*, 157-163.

(50) Rekharsky, M. V.; Ko, Y. H.; Selvapalam, N.; Kim, K.; Inoue, Y. Complexation thermodynamics of cucurbit [6] uril with aliphatic alcohols, amines, and diamines. *Supramolecular Chemistry* **2007**, *19*, 39-46.

(51) Jeon, W. S.; Kim, H.-J.; Lee, C.; Kim, K. Control of the stoichiometry in host–guest complexation by redox chemistry of guests: inclusion of methylviologen in cucurbit[8]uril. *Chemical Communications* **2002**, *17*, 1828-1829.

(52) Gao, Z.-Z.; Lin, R.-L.; Bai, D.; Tao, Z.; Liu, J.-X.; Xiao, X. Host-guest complexation of cucurbit [8] uril with two enantiomers. *Scientific Reports* **2017**, *7*, 44717.

(53) Cheng, X. J.; Liang, L. L.; Chen, K.; Ji, N. N.; Xiao, X.; Zhang, J. X.; Zhang, Y. Q.; Xue, S. F.; Zhu, Q. J.; Ni, X. L. Twisted cucurbit [14] uril. *Angewandte Chemie International Edition* **2013**, *52*, 7252-7255.

(54) Liu, S.; Zavalij, P. Y.; Isaacs, L. Cucurbit [10] uril. *Journal of the American Chemical Society* **2005**, *127*, 16798-16799.

(55) Márquez, C.; Hudgins, R. R.; Nau, W. M. Mechanism of host− guest complexation by cucurbituril. *Journal of the American Chemical Society* **2004**, *126*, 5806-5816.

(56) Marquez, C.; Nau, W. M. Two Mechanisms of Slow Host–Guest Complexation between Cucurbit [6] uril and Cyclohexylmethylamine: pH ‐ Responsive Supramolecular Kinetics. *Angewandte Chemie International Edition* **2001**, *40*, 3155-3160.

(57) Ling, X.; Samuel, E. L.; Patchell, D. L.; Masson, E. Cucurbituril slippage: Translation is a complex motion. *Organic Letters* **2010**, *12*, 2730-2733.

(58) Nau, W. M.; Assaf, K.; Das, D. Applications of Cucurbiturils in Medicinal Chemistry and Chemical Biology. *Frontiers in Chemistry* **2019**, *7*, 619.

(59) Ding, Z.-J.; Zhang, H.-Y.; Wang, L.-H.; Ding, F.; Liu, Y. A heterowheel [3] pseudorotaxane by integrating β-cyclodextrin and cucurbit[8]uril inclusion complexes. *Organic Letters* **2011**, *13*, 856-859.

(60) Mukhopadhyay, P.; Zavalij, P. Y.; Isaacs, L. High fidelity kinetic self-sorting in multi-component systems based on guests with multiple binding epitopes. *Journal of the American Chemical Society* **2006**, *128*, 14093-14102.

(61) Wyman, I. W.; Macartney, D. H. Host− guest complexes and pseudorotaxanes of cucurbit [7] uril with acetylcholinesterase inhibitors. *The Journal of Organic Chemistry* **2009**, *74*, 8031-8038.

(62) Masson, E.; Lu, X.; Ling, X.; Patchell, D. L. Kinetic vs thermodynamic self-sorting of cucurbit [6] uril, cucurbit [7] uril, and a spermine derivative. *Organic Letters* **2009**, *11*, 3798-3801.

(63) Kolman, V.; Kulhanek, P.; Sindelar, V. Inclusion of carboxyl function inside of cucurbiturils and its use in molecular switches. *Chemistry–An Asian Journal* **2010**, *5*, 2386-2392.

(64) Zhang, H.; Wang, Q.; Liu, M.; Ma, X.; Tian, H. Switchable V-type [2] pseudorotaxanes. *Organic Letters* **2009**, *11*, 3234-3237.

(65) Zhang, Z.-J.; Zhang, Y.-M.; Liu, Y. Controlled molecular self-assembly behaviors between cucurbituril and bispyridinium derivatives. *The Journal of Organic Chemistry* **2011**, *76*, 4682-4685.

(66) Chakrabarti, S.; Mukhopadhyay, P.; Lin, S.; Isaacs, L. Reconfigurable four-component molecular switch based on pH-controlled guest swapping. *Organic Letters* **2007**, *9*, 2349-2352.

(67) Sobransingh, D.; Kaifer, A. E. Electrochemically switchable cucurbit [7] uril-based pseudorotaxanes. *Organic Letters* **2006**, *8*, 3247-3250.

(68) Gadde, S.; Batchelor, E. K.; Kaifer, A. E. Electrochemistry of redox active centres encapsulated by non-covalent methods. *Australian Journal of Chemistry* **2010**, *63*, 184-194.

(69) Gadde, S.; E Kaifer, A. Cucurbituril complexes of redox active guests. *Current Organic Chemistry* **2011**, *15*, 27-38.

(70) Hwang, I.; Ziganshina, A. Y.; Ko, Y. H.; Yun, G.; Kim, K. A new three-way supramolecular switch based on redox-controlled interconversion of hetero-and homo-guest-pair inclusion inside a host molecule. *Chemical Communications* **2009**, *4*, 416-418.

(71) Hennig, A.; Bakirci, H.; Nau, W. M. Label-free continuous enzyme assays with macrocycle-fluorescent dye complexes. *Nature Methods* **2007**, *4*, 629.

(72) Appel, E. A.; Biedermann, F.; Rauwald, U.; Jones, S. T.; Zayed, J. M.; Scherman, O. A. Supramolecular cross-linked networks via host− guest complexation with cucurbit [8] uril. *Journal of the American Chemical Society* **2010**, *132*, 14251-14260.

(73) Liu, Y.; Yu, Y.; Gao, J.; Wang, Z.; Zhang, X. Water‐soluble supramolecular polymerization driven by multiple host‐stabilized charge‐transfer interactions. *Angewandte Chemie International Edition* **2010**, *49*, 6576-6579.

(74) Lee, J. W.; Ko, Y. H.; Park, S. H.; Yamaguchi, K.; Kim, K. Novel pseudorotaxane‐terminated dendrimers: supramolecular modification of dendrimer periphery. *Angewandte Chemie International Edition* **2001**, *40*, 746-749.

(75) Ong, W.; Kaifer, A. E. Molecular Encapsulation by Cucurbit [7] uril of the Apical 4, 4′‐Bipyridinium Residue in Newkome‐Type Dendrimers. *Angewandte Chemie International Edition* **2003**, *42*, 2164-2167.

(76) Wang, W.; Kaifer, A. E.: Cucurbituril and cyclodextrin complexes of dendrimers. In Inclusion Polymers; *Springer*, **2009**, 1-54.

(77) Coulston, R. J.; Jones, S. T.; Lee, T.-C.; Appel, E. A.; Scherman, O. A. Supramolecular gold nanoparticle–polymer composites formed in water with cucurbit [8] uril. *Chemical Communications* **2011**, *47*, 164-166.

(78) Liu, J.; Lan, Y.; Yu, Z.; Tan, C. S.; Parker, R. M.; Abell, C.; Scherman, O. A. Cucurbit [n] uril-based microcapsules self-assembled within microfluidic droplets: A versatile approach for supramolecular architectures and materials. *Accounts of Chemical Research* **2017**, *50*, 208-217.

(79) An, Q.; Chen, Q.; Zhu, W.; Li, Y.; Tao, C.-a.; Yang, H.; Li, Z.; Wan, L.; Tian, H.; Li, G. A facile method for preparing one-molecule-thick free-standing organic nanosheets with a regular square shape. *Chemical Communications* **2010**, *46*, 725-727.

(80) Young, J. F.; Nguyen, H. D.; Yang, L.; Huskens, J.; Jonkheijm, P.; Brunsveld, L. Strong and reversible monovalent supramolecular protein immobilization. *ChemBioChem* **2010**, *11*, 180-183.

(81) Freitag, M.; Galoppini, E. Cucurbituril complexes of viologens bound to TiO2 films. *Langmuir* **2010**, *26*, 8262-8269.

(82) da Silva, L. F. S.; Demets, G. J.-F.; Taviot-Guého, C.; Leroux, F.; Valim, J. B. Unusual incorporation of neutral and low water-soluble guest molecules into layered double hydroxides: the case of cucurbit [6 and 7] uril inclusion hosts. *Chemistry of Materials* **2011**, *23*, 1350-1352.

(83) Yang, H.; Tan, Y.; Wang, Y. Fabrication and properties of cucurbit [6] uril induced thermo-responsive supramolecular hydrogels. *Soft Matter* **2009**, *5*, 3511-3516.

(84) Saleh, N. i.; Koner, A. L.; Nau, W. M. Activation and Stabilization of Drugs by Supramolecular pKa Shifts: Drug‐Delivery Applications Tailored for Cucurbiturils. *Angewandte Chemie International Edition* **2008**, *47*, 5398-5401.

(85) Saleh, N. i.; Al-Soud, Y. A.; Al-Kaabi, L.; Ghosh, I.; Nau, W. M. A coumarin-based fluorescent PET sensor utilizing supramolecular pKa shifts. *Tetrahedron letters* **2011**, *52*, 5249-5254.

(86) Shaikh, M.; Mohanty, J.; Singh, P. K.; Nau, W. M.; Pal, H. Complexation of acridine orange by cucurbit [7] uril and β-cyclodextrin: photophysical effects and p K a shifts. *Photochemical & Photobiological Sciences* **2008**, *7*, 408-414.

(87) Yuan, L.; Macartney, D. H. Kinetics of the Electron Self-Exchange and Electron-Transfer Reactions of the (Trimethylammonio) methylferrocene Host− Guest Complex with Cucurbit [7] uril in Aqueous Solution. *The Journal of Physical Chemistry B* **2007**, *111*, 6949-6954.

(88) Zhang, W.; Gan, S.; Vezzoli, A.; Davidson, R. J.; Milan, D. C.; Luzyanin, K. V.; Higgins, S. J.; Nichols, R. J.; Beeby, A.; Low, P. J. Single-Molecule Conductance of Viologen–Cucurbit [8] uril Host–Guest Complexes. *ACS nano* **2016**, *10*, 5212-5220.

(89) Koner, A. L.; Nau, W. M. Cucurbituril encapsulation of fluorescent dyes. *Supramolecular Chemistry* **2007**, *19*, 55-66.

(90) Dsouza, R. N.; Pischel, U.; Nau, W. M. Fluorescent dyes and their supramolecular host/guest complexes with macrocycles in aqueous solution. *Chemical reviews* **2011**, *111*, 7941-7980.

(91) Dong, N.; Xue, S.-F.; Zhu, Q.-J.; Tao, Z.; Zhao, Y.; Yang, L.-X. Cucurbit [n] urils (n= 7, 8) binding of camptothecin and the effects on solubility and reactivity of the anticancer drug. *Supramolecular Chemistry* **2008**, *20*, 663-671.

(92) Ma, D.; Hettiarachchi, G.; Nguyen, D.; Zhang, B.; Wittenberg, J. B.; Zavalij, P. Y.; Briken, V.; Isaacs, L. A cyclic cucurbit[n]uril molecular containers enhance the solubility and bioactivity of poorly soluble pharmaceuticals. *Nature chemistry* **2012**, *4*, 503-510.

(93) Tuncel, D.; Artar, M.; Hanay, S. B. The effect of cucurbit [n] uril on the solubility, morphology, and the photophysical properties of nonionic conjugated polymers in an aqueous medium. *Journal of Polymer Science Part A: Polymer Chemistry* **2010**, *48*, 4894-4899.

(94) Mock, W. L.; Irra, T. A.; Wepsiec, J. P.; Adhya, M. Catalysis by cucurbituril. The significance of bound-substrate destabilization for induced triazole formation. *The Journal of Organic Chemistry* **1989**, *54*, 5302-5308.

(95) Wang, Y.-H.; Cong, H.; Zhao, F.-F.; Xue, S.-F.; Tao, Z.; Zhu, Q.-J.; Wei, G. Selective catalysis for the oxidation of alcohols to aldehydes in the presence of cucurbit [8] uril. *Catalysis Communications* **2011**, *12*, 1127-1130.

(96) Rekharsky, M. V.; Yamamura, H.; Mori, T.; Sato, A.; Shiro, M.; Lindeman, S. V.; Rathore, R.; Shiba, K.; Ko, Y. H.; Selvapalam, N. Supramolecular Complexation of *N*-Alkyl- and *N*, *N*'-Dialkylpiperazines with Cucurbit[6]uril in Aqueous Solution and in the Solid State. *Chemistry – A European Journal* **2009**, *15*, 1957-1965.

(97) Wang, R.; Yuan, L.; Macartney, D. H. Cucurbit[7]uril mediates the stereoselective [4+ 4] photodimerization of 2-aminopyridine hydrochloride in aqueous solution. *The Journal of organic chemistry* **2006**, *71*, 1237-1239.

(98) Liu, L.; Yang, B.; Katz, T. J.; Poindexter, M. K. Improved methodology for photocyclization reactions. *The Journal of Organic Chemistry* **1991**, *56*, 3769-3775.

(99) Pemberton, B. C.; Raghunathan, R.; Volla, S.; Sivaguru, J. From containers to catalysts: supramolecular catalysis within cucurbiturils. *Chemistry–A European Journal* **2012**, *18*, 12178-12190.

(100) Yan, X.; Pan, W.; Qu, H.; Duan, X. Supramolecular Interface for Biochemical Sensing Applications. *Handbook of Macrocyclic Supramolecular Assembly* **2019**, 1-40.

(101) Barrow, S. J.; Kasera, S.; Rowland, M. J.; del Barrio, J.; Scherman, O. A. Cucurbituril-based molecular recognition. *Chemical Reviews* **2015,** *115*, 12320-12406.

(102) Walker, S.; Oun, R.; McInnes, F. J.; Wheate, N. J. The potential of cucurbit [n] urils in drug delivery. *Israel Journal of Chemistry* **2011**, *51*, 616-624.

(103) Yin, H.; Wang, R. Applications of Cucurbit [n] urils (n= 7 or 8) in Pharmaceutical Sciences and Complexation of Biomolecules. *Israel Journal of Chemistry* **2018**, *58*, 188-198.

(104) Zhang, P.; Qin, S.; Qi, M.; Fu, R. Cucurbit[n]urils as a new class of stationary phases for gas chromatographic separations. *Journal of Chromatography A* **2014**, *1334*, 139-148.

(105) Ma, L.; Liu, S.; Wang, Q.; Yao, L.; Xu, L. Cucurbit (6) uril immobilized on silica: A novel high‐performance liquid chromatographic stationary phase. *Journal of separation science* **2015**, *38*, 1082-1089.

(106) Cao, L.; Šekutor, M.; Zavalij, P. Y.; Mlinarić‐Majerski, K.; Glaser, R.; Isaacs, L. Cucurbit [7] uril· guest pair with an attomolar dissociation constant. *Angewandte Chemie International Edition* **2014**, *53*, 988-993.

(107) Lee, S. J. C.; Lee, J. W.; Lee, H. H.; Seo, J.; Noh, D. H.; Ko, Y. H.; Kim, K.; Kim, H. I. Host–guest chemistry from solution to the gas phase: an essential role of direct interaction with water for high-affinity binding of cucurbit [n] urils. *The Journal of Physical Chemistry B* **2013**, *117*, 8855-8864.

(108) Biedermann, F.; Nau, W. M.; Schneider, H. J. The Hydrophobic Effect Revisited—Studies with Supramolecular Complexes Imply High‐Energy Water as a Noncovalent Driving Force. *Angewandte Chemie International Edition* **2014**, *53*, 11158-11171.

(109) Kealy, T.; Pauson, P. A new type of organo-iron compound. *Nature* **1951**, *168*, 1039.

(110) Seiwert, B.; Karst, U. Ferrocene-based derivatization in analytical chemistry. *Analytical and bioanalytical chemistry* **2008**, *390*, 181.

(111) Wilkinson, G.; Rosenblum, M.; Whiting, M.; Woodward, R. The structure of iron bis-cyclopentadienyl. *Journal of the American Chemical Society* **1952**, *74*, 2125-2126.

(112) Astruc, D. Why is ferrocene so exceptional? *European Journal of Inorganic Chemistry* **2017**, 2017, 6-29.

(113) Ong, W.; Kaifer, A. E. Unusual electrochemical properties of the inclusion complexes of ferrocenium and cobaltocenium with cucurbit [7] uril. *Organometallics* **2003**, *22*, 4181-4183.

(114) Jeon, W. S.; Moon, K.; Park, S. H.; Chun, H.; Ko, Y. H.; Lee, J. Y.; Lee, E. S.; Samal, S.; Selvapalam, N.; Rekharsky, M. V. Complexation of ferrocene derivatives by the cucurbit [7] uril host: a comparative study of the cucurbituril and cyclodextrin host families. *Journal of the American Chemical Society* **2005**, *127*, 12984-12989.

(115) Cui, L.; Gadde, S.; Li, W.; Kaifer, A. E. Electrochemistry of the inclusion complexes formed between the cucurbit [7] uril host and several cationic and neutral ferrocene derivatives. *Langmuir* **2009**, *25*, 13763-13769.

(116) Kaifer, A. E. Electrochemical properties of cucurbit [7] uril complexes of ferrocenyl derivatives. *Inorganica Chimica Acta* **2017**, *468*, 77-81.

(117) Ayhan, M. M.; Karoui, H.; Hardy, M.; Rockenbauer, A.; Charles, L.; Rosas, R.; Udachin, K.; Tordo, P.; Bardelang, D.; Ouari, O. Comprehensive synthesis of monohydroxy–cucurbit [n] urils (n= 5, 6, 7, 8): high purity and high conversions. *Journal of the American Chemical Society* **2015**, *137*, 10238-10245.

(118) Jon, S. Y.; Selvapalam, N.; Oh, D. H.; Kang, J.-K.; Kim, S.-Y.; Jeon, Y. J.; Lee, J. W.; Kim, K. Facile synthesis of cucurbit [n] uril derivatives via direct functionalization: expanding utilization of cucurbit [n] uril. *Journal of the American Chemical Society* **2003**, *125*, 10186-10187.

(119) Vinciguerra, B.; Cao, L.; Cannon, J. R.; Zavalij, P. Y.; Fenselau, C.; Isaacs, L. Synthesis and self-assembly processes of monofunctionalized cucurbit [7] uril. *Journal of the American Chemical Society* **2012**, *134*, 13133-13140.

(120) Ahn, Y.; Jang, Y.; Selvapalam, N.; Yun, G.; Kim, K. Supramolecular velcro for reversible underwater adhesion. *Angewandte Chemie International Edition* **2013**, *52*, 3140-3144.

(121) Lee, D.-W.; Park, K. M.; Banerjee, M.; Ha, S. H.; Lee, T.; Suh, K.; Paul, S.; Jung, H.; Kim, J.; Selvapalam, N. Supramolecular fishing for plasma membrane proteins using an ultrastable synthetic host–guest binding pair. *Nature Chemistry* **2011**, *3*, 154.

(122) Hwang, I.; Baek, K.; Jung, M.; Kim, Y.; Park, K. M.; Lee, D.-W.; Selvapalam, N.; Kim, K. Noncovalent immobilization of proteins on a solid surface by cucurbit [7] uril-ferrocenemethylammonium pair, a potential replacement of Biotin− Avidin Pair. *Journal of the American Chemical Society* **2007**, *129*, 4170-4171.

(123) An, Q.; Li, G.; Tao, C.; Li, Y.; Wu, Y.; Zhang, W. A general and efficient method to form self-assembled cucurbit [n] uril monolayers on gold surfaces. *Chemical Communications* **2008**, *17*, 1989-1991.

(124) Neirynck, P.; Brinkmann, J.; An, Q.; van der Schaft, D. W.; Milroy, L.-G.; Jonkheijm, P.; Brunsveld, L. Supramolecular control of cell adhesion via ferrocene–cucurbit [7] uril host–guest binding on gold surfaces. *Chemical Communications* **2013**, *49*, 3679-3681.

(125) Brinkmann, J.; Wasserberg, D.; Jonkheijm, P. Redox-active host-guest supramolecular assemblies of peptides and proteins at surfaces. *European Polymer Journal* **2016**, *83*, 380-389.

(126) Lee, D.-W.; Park, K. M.; Gong, B.; Shetty, D.; Khedkar, J. K.; Baek, K.; Kim, J.; Ryu, S. H.; Kim, K. A simple modular aptasensor platform utilizing cucurbit [7] uril and a ferrocene derivative as an ultrastable supramolecular linker. *Chemical Communications* **2015**, *51*, 3098-3101.

(127) Li, H.; Yang, Y.-W. Gold nanoparticles functionalized with supramolecular macrocycles. *Chinese Chemical Letters* **2013**, *24*, 545-552.

(128) Lv, Y.; Tao, C.-A.; Huang, J.; Li, Y.; Wang, F.; Cai, F.; Wang, J. Self-assembly of cucurbit [7] uril on the surface of graphene/gold modified electrode: A novel electrochemical sensing platform. *Nanomaterials and Nanotechnology* **2016**, *6*, 1847980416682443.

(129) Blanco, E.; Quintana, C.; Hernández, L.; Hernández, P. Atomic force microscopy study of new sensing platforms: cucurbit [n] uril (n= 6, 7) on gold. *Electroanalysis* **2013**, *25*, 263-268.

(130) Ertl, G. Reactions at surfaces: From atoms to complexity (Nobel lecture). *Angewandte Chemie International Edition* **2008**, *47*, 3524-3535.

(131) Brinkmann, J. Dynamic bioactive surfaces for cells using cucurbiturils. **2016**.

(132) Somorjai, G. A.; Li, Y. Introduction to surface chemistry and catalysis. *John Wiley & Sons*, **2010**.

(133) You, Y.; Zhou, K.; Guo, B.; Liu, Q.; Cao, Z.; Liu, L.; Wu, H.-C. Measuring binding constants of cucurbituril-based host–guest interactions at the single-molecule level with nanopores. *ACS sensors* **2019**, *4*, 774-779.

(134) Love, J. C.; Estroff, L. A.; Kriebel, J. K.; Nuzzo, R. G.; Whitesides, G. M. Self-assembled monolayers of thiolates on metals as a form of nanotechnology. *Chemical Reviews* **2005**, *105*, 1103-1170.

(135) Vericat, C.; Vela, M. E.; Corthey, G.; Pensa, E.; Cortés, E.; Fonticelli, M. H.; Ibanez, F.; Benitez, G.; Carro, P.; Salvarezza, R. C. Self-assembled monolayers of thiolates on metals: a review article on sulfur-metal chemistry and surface structures. *Rsc Advances* **2014**, *4*, 27730-27754.

(136) He, T.; He, J.; Lu, M.; Chen, B.; Pang, H.; Reus, W. F.; Nolte, W. M.; Nackashi, D. P.; Franzon, P. D.; Tour, J. M. Controlled modulation of conductance in silicon devices by molecular monolayers. *Journal of the American Chemical Society* **2006**, *128*, 14537-14541.

(137) Tsai, P.-S.; Yang, Y.-M.; Lee, Y.-L. Fabrication of Hydrophobic Surfaces by Coupling of Langmuir− Blodgett Deposition and a Self-Assembled Monolayer. *Langmuir* **2006**, *22*, 5660-5665.

(138) Feng, Y.; Teo, W. K.; Siow, K. S.; Gao, Z.; Tan, K. L.; Hsieh, A. K. Corrosion protection of copper by a self‐assembled monolayer of alkanethiol. *Journal of The Electrochemical Society* **1997**, *144*, 55.

(139) Sukenik, C. N.; Balachander, N.; Culp, L. A.; Lewandowska, K.; Merritt, K. Modulation of cell adhesion by modification of titanium surfaces with covalently attached self‐assembled monolayers. *Journal of biomedical materials research* **1990**, *24*, 1307-1323.

(140) Houston, J. E.; Kim, H. I. Adhesion, friction, and mechanical properties of functionalized alkanethiol self-assembled monolayers. *Accounts of chemical research* **2002**, *35*, 547-553.

(141) Chaki, N. K.; Vijayamohanan, K. Self-assembled monolayers as a tunable platform for biosensor applications. *Biosensors and Bioelectronics* **2002**, *17*, 1-12.

(142) Arya, S. K.; Solanki, P. R.; Datta, M.; Malhotra, B. D. Recent advances in self-assembled monolayers based biomolecular electronic devices. *Biosensors and Bioelectronics* **2009**, 24, 2810-2817.

(143) Liu, G.-Y.; Xu, S.; Qian, Y. Nanofabrication of self-assembled monolayers using scanning probe lithography. *Accounts of Chemical Research* **2000**, *33*, 457-466.

(144) Wilbur, J. L.; Kumar, A.; Kim, E.; Whitesides, G. M. Microfabrication by microcontact printing of self‐assembled monolayers. *Advanced Materials* **1994**, *6*, 600-604.

(145) Tarlov, M. J.; Burgess Jr, D. R.; Gillen, G. UV photopatterning of alkanethiolate monolayers self-assembled on gold and silver. *Journal of the American Chemical Society* **1993**, *115*, 5305-5306.

(146) Mino, N.; Ozaki, S.; Ogawa, K.; Hatada, M. Fabrication of self-assembled monolayer patterns by selective electron beam irradiation and a chemical adsorption technique. *Thin Solid Films* **1994**, *243*, 374-377.

(147) Nuzzo, R. G.; Allara, D. L. Adsorption of bifunctional organic disulfides on gold surfaces. *Journal of the American Chemical Society* **1983**, *105*, 4481-4483.

(148) Marc, D. P.; Thomas, B. B.; David, L. A.; Chdisy, C. E. D. Structural Characterization of n-Alkyl Thiol Monolayers on Gold by Optical Ellipsometry, Infrared Spectroscopy. *Journal of the American Chemical Society* **1987**, *109*, 3559-3568.

(149) Pauling, L. General chemistry. *Courier Corporation*, **1988**.

(150) Häkkinen, H. The gold–sulfur interface at the nanoscale. *Nature Chemistry* **2012**, *4*, 443.

(151) Voznyy, O.; Dubowski, J. J.; Yates, J. T.; Maksymovych, P. The role of gold adatoms and stereochemistry in self-assembly of methylthiolate on Au(111). *J. Am. Chem. Soc.* **2009***, 131***,** 12989–12993.

(152) Wetterer, S.; Lavrich, D.; Cummings, T.; Bernasek, S.; Scoles, G. Energetics and kinetics of the physisorption of hydrocarbons on Au (111). *The Journal of Physical Chemistry B* **1998**, *102*, 9266-9275.

(153) Schreiber, F. Structure and growth of self-assembling monolayers. *Progress in Surface Science* **2000**, *65*, 151-257.

(154) Poirier, G. E. Surface stress, kinetics, and structure of alkanethiol self-assembled monolayers. *Langmuir* **2004**, *20*, 7090-7096.

(155) Vericat, C.; Vela, M.; Benitez, G.; Carro, P.; Salvarezza, R. Self-assembled monolayers of thiols and dithiols on gold: new challenges for a well-known system. *Chemical Society Reviews* **2010**, *39*, 1805-1834.

(156) Dubois, L. H.; Zegarski, B. R.; Nuzzo, R. G. Molecular ordering of organosulfur compounds on Au (111) and Au (100): Adsorption from solution and in ultrahigh vacuum. *The Journal of Chemical Physics* **1993**, *98*, 678-688.

(157) Dubois, L. H.; Nuzzo, R. G. Synthesis, structure, and properties of model organic surfaces. *Annual Review of Physical Chemistry* **1992**, *43*, 437-463.

(158) Poirier, G. Mechanism of formation of Au vacancy islands in alkanethiol monolayers on Au (111). *Langmuir* **1997**, *13*, 2019-2026.

(159) Poirier, G.; Tarlov, M. The c(4x2) superlattice of n-alkanethiol monolayers self-assembled on Au (111). *Langmuir* **1994**, *10*, 2853-2856.

(160) Vericat, C.; Vela, M.; Salvarezza, R. Self-assembled monolayers of alkanethiols on Au (111): surface structures, defects and dynamics. *Physical Chemistry Chemical Physics* **2005**, *7*, 3258-3268.

(161) Hammer, B.; Norskov, J. K. Why gold is the noblest of all the metals. *Nature* **1995**, *376*, 238-240.

(162) Xia, Y.; Zhao, X.-M.; Kim, E.; Whitesides, G. M. A selective etching solution for use with patterned self-assembled monolayers of alkanethiolates on gold. *Chemistry of Materials* **1995**, *7*, 2332-2337.

(163) Wittstock, G.; Hesse, R.; Schuhmann, W. Patterned self‐assembled alkanethiolate monolayers on gold. Patterning and imaging by means of scanning electrochemical microscopy. *Electroanalysis* **1997**, *9*, 746-750.

(164) Burke, L.; Nugent, P. The electrochemistry of gold: I the redox behaviour of the metal in aqueous media. *Gold Bulletin* 1**997**, *30*, 43-53.

(165) Huang, X.; Jain, P. K.; El-Sayed, I. H.; El-Sayed, M. A. Gold nanoparticles: interesting optical properties and recent applications in cancer diagnostics and therapy. Future Medicine **2007**, 681-693.

(166) Shukla, R.; Bansal, V.; Chaudhary, M.; Basu, A.; Bhonde, R. R.; Sastry, M. Biocompatibility of gold nanoparticles and their endocytotic fate inside the cellular compartment: a microscopic overview. *Langmuir* **2005**, *21*, 10644-10654.

(167) Dai, Z.; Ju, H. Effect of chain length on the surface properties of ω-carboxy alkanethiol self-assembled monolayers. *Physical Chemistry Chemical Physics* **2001**, *3*, 3769-3773.

(168) Ishida, T.; Nishida, N.; Tsuneda, S.; Hara, M.; Sasabe, H.; Knoll, W. Alkyl chain length effect on growth kinetics of n-alkanethiol self-assembled monolayers on gold studied by X-ray photoelectron spectroscopy. *Japanese Journal of Applied Physics* **1996**, *35*, L1710.

(169) Millone, M. a. A. D.; Hamoudi, H.; Rodríguez, L.; Rubert, A.; Benítez, G. A.; Vela, M. a. E.; Salvarezza, R. C.; Gayone, J. E.; Sánchez, E. A.; Grizzi, O. Self-assembly of alkanedithiols on Au (111) from solution: effect of chain length and self-assembly conditions. *Langmuir* **2009**, *25*, 12945-12953.

(170) Bain, C. D.; Troughton, E. B.; Tao, Y. T.; Evall, J.; Whitesides, G. M.; Nuzzo, R. G. Formation of monolayer films by the spontaneous assembly of organic thiols from solution onto gold. *Journal of the American Chemical Society* **1989**, *111*, 321-335.

(171) Yamada, R.; Sakai, H.; Uosaki, K. Solvent effect on the structure of the self-assembled monolayer of alkanethiol. *Chemistry Letters* **1999**, *28*, 667-668.

(172) Sur, U. K.; Lakshminarayanan, V. A study of the hydrophobic properties of alkanethiol self-assembled monolayers prepared in different solvents. *Journal of Electroanalytical Chemistry* **2004**, *565*, 343-350.

(173) Yamada, R.; Wano, H.; Uosaki, K. Effect of temperature on structure of the self-assembled monolayer of decanethiol on Au (111) surface. *Langmuir* **2000**, *16*, 5523-5525.

(174) Bensebaa, F.; Voicu, R.; Huron, L.; Ellis, T. H.; Kruus, E. Kinetics of formation of long-chain n-alkanethiolate monolayers on polycrystalline gold. *Langmuir* **1997**, *13*, 5335-5340.

(175) Laibinis, P. E.; Whitesides, G. M.; Allara, D. L.; Tao, Y. T.; Parikh, A. N.; Nuzzo, R. G. Comparison of the structures and wetting properties of self-assembled monolayers of n-alkanethiols on the coinage metal surfaces, copper, silver, and gold. *Journal of the American Chemical Society* **1991**, *113*, 7152-7167.

(176) Guo, L.-H.; Facci, J. S.; McLendon, G.; Mosher, R. Effect of gold topography and surface pretreatment on the self-assembly of alkanethiol monolayers. *Langmuir* **1994**, *10*, 4588-4593.

(177) Boeckl, M.; Graham, D. Self-assembled monolayers: Advantages of pure alkanethiols. *Material Matters* **2006**, *1*, 3-5.

(178) Schönenberger, C.; Sondag-Huethorst, J.; Jorritsma, J.; Fokkink, L. What Are the" Holes" in Self-Assembled Monolayers of Alkanethiols on Gold? *Langmuir* **1994**, *10*, 611-614.

(179) O'Dwyer, C.; Gay, G.; Viaris de Lesegno, B.; Weiner, J. The nature of alkanethiol self-assembled monolayer adsorption on sputtered gold substrates. *Langmuir* **2004**, *20*, 8172-8182.

(180) Che, G.; Li, Z.; Zhang, H.; Cabrera, C. R. Voltammetry of defect sites at a self-assembled monolayer on a gold surface. *Journal of Electroanalytical Chemistry* **1998**, *453*, 9-17.

(181) Folkers, J. P.; Laibinis, P. E.; Whitesides, G. M.; Deutch, J. Phase behavior of two-component self-assembled monolayers of alkanethiolates on gold. *The Journal of Physical Chemistry* **1994**, *98*, 563-571.

(182) Tamada, K.; Hara, M.; Sasabe, H.; Knoll, W. Surface phase behavior of n-alkanethiol self-assembled monolayers adsorbed on Au (111): An atomic force microscope study. *Langmuir* **1997**, *13*, 1558-1566.

(183) Bain, C. D.; Whitesides, G. M. Formation of two-component surfaces by the spontaneous assembly of monolayers on gold from solutions containing mixtures of organic thiols. *Journal of the American Chemical Society* **1988**, *110*, 6560-6561.

(184) Kang, J. F.; Liao, S.; Jordan, R.; Ulman, A. Mixed self-assembled monolayers of rigid biphenyl thiols: Impact of solvent and dipole moment. J*ournal of the American Chemical Society* **1998**, *120*, 9662-9667.

(185) Heister, K.; Allara, D.; Bahnck, K.; Frey, S.; Zharnikov, M.; Grunze, M. Deviations from 1: 1 compositions in self-assembled monolayers formed from adsorption of asymmetric dialkyl disulfides on gold. *Langmuir* **1999**, *15*, 5440-5443.

(186) Azehara, H.; Yoshimoto, S.; Hokari, H.; Akiba, U.; Taniguchi, I.; Fujihira, M. Investigation of the structure of self-assembled monolayers of asymmetrical disulfides on Au (111) electrodes by electrochemical desorption. *Journal of Electroanalytical Chemistry* **1999**, *473*, 68-74.

(187) Nishida, N.; Hara, M.; Sasabe, H.; Knoll, W. Formation and exchange processes of alkanethiol self-assembled monolayer on Au (111) studied by thermal desorption spectroscopy and scanning tunneling microscopy. *Japanese Journal of Applied Physics* **1997**, *36*, 2379.

(188) Tian, H.; Xiang, D.; Shao, H.; Yu, H.-Z. Electrochemical identification of molecular heterogeneity in binary redox self-assembled monolayers on gold. *The Journal of Physical Chemistry C* **2014**, *118*, 13733-13742.

(189) Vericat, C.; Vela, M.; Benitez, G.; Gago, J. M.; Torrelles, X.; Salvarezza, R. Surface characterization of sulfur and alkanethiol self-assembled monolayers on Au (111). *Journal of Physics: Condensed Matter* **2006**, *18*, R867.

(190) Whitesides, G. M.; Laibinis, P. E. Wet chemical approaches to the characterization of organic surfaces: self-assembled monolayers, wetting, and the physical-organic chemistry of the solid-liquid interface. *Langmuir* **1990**, *6*, 87-96.

(191) Samant, M. G.; Brown, C. A.; Gordon, J. G. Structure of an ordered self-assembled monolayer of docosyl mercaptan on gold (111) by surface x-ray diffraction. *Langmuir* **1991**, *7*, 437-439.

(192) Strong, L.; Whitesides, G. M. Structures of self-assembled monolayer films of organosulfur compounds adsorbed on gold single crystals: electron diffraction studies. *Langmuir* **1988**, *4*, 546-558.

(193) Camillone III, N.; Chidsey, C. E.; Eisenberger, P.; Fenter, P.; Li, J.; Liang, K.; Liu, G. Y.; Scoles, G. Structural defects in self‐assembled organic monolayers via combined atomic beam and x‐ray diffraction. *The Journal of Chemical Physics* **1993**, *99*, 744-747.

(194) Ohtsuka, T.; Sato, Y.; Uosaki, K. Dynamic ellipsometry of a self-assembled monolayer of a ferrocenylalkanethiol during oxidation-reduction cycles. *Langmuir* **1994**, *10*, 3658-3662.

(195) Azzaroni, O.; Vela, M.; Andreasen, G.; Carro, P.; Salvarezza, R. Electrodesorption potentials of self-assembled alkanethiolate monolayers on Ag (111) and Au (111). An electrochemical, scanning tunneling microscopy and density functional theory study. *The Journal of Physical Chemistry B* **2002**, *106*, 12267-12273.

(196) Vargas, M. C.; Giannozzi, P.; Selloni, A.; Scoles, G. Coverage-dependent adsorption of CH3S and (CH3S) 2 on Au (111): A density functional theory study. *The Journal of Physical Chemistry B* **2001**, *105*, 9509-9513.

(197) Tupper, K. J.; Brenner, D. W. Molecular dynamics simulations of friction in self-assembled monolayers. *Thin Solid Films* **1994**, *253*, 185-189.

(198) Hu, L.; Zhang, L.; Hu, M.; Wang, J.-S.; Li, B.; Keblinski, P. Phonon interference at self-assembled monolayer interfaces: Molecular dynamics simulations. *Physical Review B* **2010**, *81*, 235427.

(199) Elgrishi, N.; Rountree, K. J.; McCarthy, B. D.; Rountree, E. S.; Elisenhart, T. T.; Dempsey, J. L. A Practical Beginner's Guide to Cyclic Voltammetry. *Journal of Chemical Education* **2018**, *95*, 197-206.

(200) García-Raya, D.; Madueño, R.; Sevilla, J. M.; Blázquez, M.; Pineda, T. Electrochemical characterization of a 1, 8-octanedithiol self-assembled monolayer (ODT-SAM) on a Au (1 1 1) single crystal electrode. *Electrochimica Acta* **2008**, *53*, 8026-8033.

(201) Campuzano, S.; Pedrero, M.; Montemayor, C.; Fatás, E.; Pingarrón, J. M. Characterization of alkanethiol-self-assembled monolayers-modified gold electrodes by electrochemical impedance spectroscopy. *Journal of Electroanalytical Chemistry* **2006**, *586*, 112-121.

(202) Finklea, H. O.; Snider, D. A.; Fedyk, J.; Sabatani, E.; Gafni, Y.; Rubinstein, I. Characterization of octadecanethiol-coated gold electrodes as microarray electrodes by cyclic voltammetry and ac impedance spectroscopy. *Langmuir* **1993**, *9*, 3660-3667.

(203) Eckermann, A. L.; Feld, D. J.; Shaw, J. A.; Meade, T. J. Electrochemistry of redox-active self-assembled monolayers. *Coordination Chemistry Review*s **2010**, *254*, 1769-1802.

(204) Bard, A. J.; Faulkner, L. R.; Leddy, J.; Zoski, C. G. Electrochemical methods: fundamentals and applications; John Wiley & Sons. **2001**.

(205) Page, J. A.; Wilkinson, G. The polarographic chemistry of ferrocene, ruthenocene and the metal hydrocarbon ions. *Journal of the American Chemical Society* **1952**, *74*, 6149-6150.

(206) Nesmeyanov, A. N. Chemistry of ferrocene. **1968**.

(207) Balavoine, G.; Daran, J.-C.; Iftime, G.; Manoury, E.; Moreau-Bossuet, C. Selective synthesis of ferrocenes. *Journal of Organometallic Chemistry* **1998**, *567*, 191-198.

(208) Smalley, J. F.; Feldberg, S. W.; Chidsey, C. E.; Linford, M. R.; Newton, M. D.; Liu, Y.-P. The kinetics of electron transfer through ferrocene-terminated alkanethiol monolayers on gold. *The Journal of Physical Chemistry* **1995**, *99*, 13141-13149.

(209) Guo, L.-H.; Facci, J. S.; McLendon, G. Distance dependence of electron transfer rates in bilayers of a ferrocene Langmuir-Blodgett monolayer and a self-assembled monolayer on gold. *The Journal of Physical Chemistry* **1995**, *99*, 8458-8461.

(210) Chidsey, C. E. Free energy and temperature dependence of electron transfer at the metal-electrolyte interface. *Science* **1991**, *251*, 919-922.

(211) Ho, M. Y.; Li, P.; Estrela, P.; Goodchild, S.; Migliorato, P. Detection of molecular interactions with modified ferrocene self-assembled monolayers. *The Journal of Physical Chemistry B* **2010**, *114*, 10661-10665.

(212) Brown, A. P.; Anson, F. C. Cyclic and differential pulse voltammetric behavior of reactants confined to the electrode surface. *Analytical Chemistry* **1977**, *49*, 1589-1595.

(213) Lee, L. Y. S.; Sutherland, T. C.; Rucareanu, S.; Lennox, R. B. Ferrocenylalkylthiolates as a probe of heterogeneity in binary self-assembled monolayers on gold. *Langmuir* **2006**, *22*, 4438-4444.

(214) Chidsey, C. E.; Bertozzi, C. R.; Putvinski, T.; Mujsce, A. Coadsorption of ferrocene-terminated and unsubstituted alkanethiols on gold: electroactive self-assembled monolayers. *Journal of the American Chemical Society* **1990**, *112*, 4301-4306.

(215) Rowe, G. K.; Creager, S. E. Solvent and double-layer effects on redox reactions in self-assembled monolayers of ferrocenyl-alkanethiolates on gold. *Journal of Electroanalytical Chemistry* **1997**, 420, 291-299.

(216) Andreu, R.; Calvente, J. J.; Fawcett, W. R.; Molero, M. Role of ion pairing in double-layer effects at self-assembled monolayers containing a simple redox couple. *The Journal of Physical Chemistry B* **1997**, *101*, 2884-2894.

(217) Rowe, G. K.; Creager, S. E. Redox and ion-pairing thermodynamics in self-assembled monolayers. *Langmuir* **1991**, *7*, 2307-2312.

(218) Valincius, G.; Niaura, G.; Kazakevičienė, B.; Talaikytė, Z.; Kažemėkaitė, M.; Butkus, E.; Razumas, V. Anion effect on mediated electron transfer through ferrocene-terminated self-assembled monolayers. *Langmuir* **2004**, *20*, 6631-6638.

(219) Laviron, E. Surface linear potential sweep voltammetry: Equation of the peaks for a reversible reaction when interactions between the adsorbed molecules are taken into account. *Journal of Electroanalytical Chemistry and Interfacial Electrochemistry* **1974**, *52*, 395-402.

(220) Laviron, E. General expression of the linear potential sweep voltammogram in the case of diffusionless electrochemical systems. *Journal of Electroanalytical Chemistry and Interfacial Electrochemistry* **1979**, *101*, 19-28.

(221) Tender, L.; Carter, M. T.; Murray, R. W. Cyclic voltammetric analysis of ferrocene alkanethiol monolayer electrode kinetics based on Marcus theory. *Analytical Chemistry* **1994**, *66*, 3173-3181.

(222) Popenoe, D. D.; Deinhammer, R. S.; Porter, M. D. Infrared spectroelectrochemical characterization of ferrocene-terminated alkanethiolate monolayers at gold. *Langmuir* **1992**, *8*, 2521-2530.

(223) Shirtcliffe, N. Surface chemistry of solid and liquid interfaces. By HY Erbil. *ChemPhysChem* **2008**, *9*, 646-647.

(224) James, M.; Ciampi, S.; Darwish, T. A.; Hanley, T. L.; Sylvester, S. O.; Gooding, J. J. Nanoscale water condensation on click-functionalized self-assembled monolayers. *Langmuir* **2011**, *27*, 10753-10762.

(225) Ruan, C.-Y.; Lobastov, V. A.; Vigliotti, F.; Chen, S.; Zewail, A. H. Ultrafast electron crystallography of interfacial water. *Science* **2004**, *304*, 80-84.

(226) Li, E.; Du, Z.; Yuan, S. Properties of a water layer on hydrophilic and hydrophobic self-assembled monolayer surfaces: A molecular dynamics study. *Science China Chemistry* **2013**, *56*, 773-781.

(227) Newcomb, L. B.; Tevis, I. D.; Atkinson, M. B.; Gathiaka, S. M.; Luna, R. E.; Thuo, M. Odd–even effect in the hydrophobicity of n-alkanethiolate self-assembled monolayers depends upon the roughness of the substrate and the orientation of the terminal moiety. *Langmuir* **2014**, *30*, 11985-11992.

(228) Ramin, L.; Jabbarzadeh, A. Odd–even effects on the structure, stability, and phase transition of alkanethiol self-assembled monolayers. *Langmuir* **2011**, *27*, 9748-9759.

(229) Tang, H.; Fuentealba, D.; Ko, Y. H.; Selvapalam, N.; Kim, K.; Bohne, C. Guest binding dynamics with cucurbit [7] uril in the presence of cations. *Journal of the American Chemical Society* **2011**, *133*, 20623-20633.

(230) Miskolczy, Z.; Biczók, L. Kinetics and thermodynamics of berberine inclusion in cucurbit [7] uril. *The Journal of Physical Chemistry B* **2014**, *118*, 2499-2505.

(231) Gomez-Casado, A.; Jonkheijm, P.; Huskens, J. Recognition properties of cucurbit [7] uril self-assembled monolayers studied with force spectroscopy. *Langmuir* **2011**, *27*, 11508-11513.

(232) Murov, S. L.; Carmichael, I.; Hug, G. L.: Handbook of photochemistry; CRC Press, **1993**.

(233) Mock, W. L.; Shih, N. Y. Dynamics of molecular recognition involving cucurbituril. *Journal of the American Chemical Society* **1989**, *111*, 2697-2699.

(234) Barros, T.; Stefaniak, K.; Holzwarth, J.; Bohne, C. Complexation of Naphthylethanols with β-Cyclodextrin. *The Journal of Physical Chemistry A* **1998**, *102*, 5639-5651.

(235) Irving, D. L.; Brenner, D. W. Diffusion on a self-assembled monolayer: molecular modeling of a bound+ mobile lubricant. *The Journal of Physical Chemistry B* **2006**, *110*, 15426-15431.

(236) Krämer, S.; Fuierer, R. R.; Gorman, C. B. Scanning probe lithography using self-assembled monolayers. *Chemical Reviews* **2003**, *103*, 4367-4418.

(237) Schön, J. H.; Meng, H.; Bao, Z. Self-assembled monolayer organic field-effect transistors. *Nature* **2001**, *413*, 713-716.

(238) Fujii, S.; Kurokawa, S.; Murase, K.; Lee, K.-H.; Sakai, A.; Sugimura, H. Self-assembled mixed monolayer containing ferrocenylthiol molecules: STM observations and electrochemical investigations. *Electrochimica Acta* **2007**, *52*, 4436-4442.

(239) Tian, H.; Dai, Y.; Shao, H.; Yu, H.-Z. Modulated intermolecular interactions in ferrocenylalkanethiolate self-assembled monolayers on gold. *The Journal of Physical Chemistry C* **2013**, *117*, 1006-1012.

(240) Rowe, G. K.; Creager, S. E. Chain length and solvent effects on competitive self-assembly of ferrocenylhexanethiol and 1-alkanethiols onto gold. *Langmuir* **1994**, *10*, 1186-1192.

(241) Moser, C. C.; Keske, J. M.; Warncke, K.; Farid, R. S.; Dutton, P. L. Nature of biological electron transfer. *Nature* **1992**, *355*, 796-802.

(242) Shah, A.; Adhikari, B.; Martic, S.; Munir, A.; Shahzad, S.; Ahmad, K.; Kraatz, H.-B. Electron transfer in peptides. *Chemical Society Reviews* **2015**, *44*, 1015-1027.

(243) Schröder, U. Anodic electron transfer mechanisms in microbial fuel cells and their energy efficiency. *Physical Chemistry Chemical Physics* **2007**, *9*, 2619-2629.

(244) Freire, R. S.; Pessoa, C. A.; Mello, L. D.; Kubota, L. T. Direct electron transfer: an approach for electrochemical biosensors with higher selectivity and sensitivity. *Journal of the Brazilian Chemical Society* **2003**, *14*, 230-243.

(245) Adams, D. M.; Brus, L.; Chidsey, C. E.; Creager, S.; Creutz, C.; Kagan, C. R.; Kamat, P. V.; Lieberman, M.; Lindsay, S.; Marcus, R. A. Charge transfer on the nanoscale: current status. *The Journal of Physical Chemistry B* **2003**, *107*, 6668-6697.

(246) Zhang, Y.; Liu, C.; Balaeff, A.; Skourtis, S. S.; Beratan, D. N. Biological charge transfer via flickering resonance. *Proceedings of the National Academy of Sciences* **2014**, *111*, 10049-10054.

(247) Newton, M. D. Quantum chemical probes of electron-transfer kinetics: the nature of donor-acceptor interactions. *Chemical Reviews* **1991**, *91*, 767-792.

(248) Newton, M. D. Medium reorganization and electronic coupling in long-range electron transfer. *Journal of Electroanalytical Chemistry* **1997**, *438*, 3-10.

(249) Krishtalik, L. I. The medium reorganization energy for the charge transfer reactions in proteins. *Biochimica et Biophysica Acta (BBA)-Bioenergetics* **2011**, *1807*, 1444-1456.

(250) Yadav, A.; Jackson, R. M.; Holbrook, J. J.; Warshel, A. Role of solvent reorganization energies in the catalytic activity of enzymes. *Journal of the American Chemical Society* **1991**, *113*, 4800-4805.

(251) Cannon, W. R.; Benkovic, S. J. Solvation, reorganization energy, and biological catalysis. *Journal of Biological Chemistry* **1998**, *273*, 26257-26260.

(252) Marcus, R. A. Electron transfer reactions in chemistry. *Theory and experiment. Reviews of Modern Physics* **1993**, *65*, 599.

(253) Fried, S. D.; Boxer, S. G. Electric fields and enzyme catalysis. *Annual Review of Biochemistry* **2017**, *86*, 387-415.

(254) Carter, M. T.; Rowe, G. K.; Richardson, J. N.; Tender, L. M.; Terrill, R. H.; Murray, R. W. Distance dependence of the low-temperature electron transfer kinetics of (ferrocenylcarboxy)-terminated alkanethiol monolayers. *Journal of the American Chemical Society* **1995**, *117*, 2896-2899.

(255) Robinson, D. B.; Chidsey, C. E. Submicrosecond electron transfer to monolayer-bound redox species on gold electrodes at large overpotentials. *The Journal of Physical Chemistry B* **2002**, *106*, 10706-10713.

(256) Napper, A. M.; Liu, H.; Waldeck, D. H. The nature of electronic coupling between ferrocene and gold through alkanethiolate monolayers on electrodes: The importance of chain composition, interchain coupling, and quantum interference. *The Journal of Physical Chemistry B* **2001**, *105*, 7699-7707.

(257) Weber, K.; Hockett, L.; Creager, S. Long-range electronic coupling between ferrocene and gold in alkanethiolate-based monolayers on electrodes. *The Journal of Physical Chemistry B* **1997**, *101*, 8286-8291.

(258) Sek, S.; Misicka, A.; Bilewicz, R. Effect of interchain hydrogen bonding on electron transfer through alkanethiol monolayers containing amide bonds. *The Journal of Physical Chemistry B* **2000**, *104*, 5399-5402.

(259) Sumner, J.; Weber, K.; Hockett, L.; Creager, S. Long-range heterogeneous electron transfer between ferrocene and gold mediated by n-alkane and N-alkyl-carboxamide bridges. *The Journal of Physical Chemistry B* **2000**, *104*, 7449-7454.

(260) Filippini, G.; Goujon, F.; Bonal, C.; Malfreyt, P. Environment effect on the redox properties of Self-Assembled Monolayers: a theoretical investigation of the nature of the supporting electrolyte. *Soft Matter* **2011**, *7*, 8961-8968.

(261) Ravenscroft, M. S.; Finklea, H. O. Kinetics of electron transfer to attached redox centers on gold electrodes in nonaqueous electrolytes. *The Journal of Physical Chemistry* **1994**, *98*, 3843-3850.

(262) Nikitina, V. A.; Rudnev, A. V.; Nazmutdinov, R. R.; Tsirlina, G. A.; Wandlowski, T. Solvent effect on electron transfer through alkanethiols. *Journal of Electroanalytical Chemistry* **2018**, *819*, 58-64.

(263) Smalley, J. F.; Finklea, H. O.; Chidsey, C. E.; Linford, M. R.; Creager, S. E.; Ferraris, J. P.; Chalfant, K.; Zawodzinsk, T.; Feldberg, S. W.; Newton, M. D. Heterogeneous electron-transfer kinetics for ruthenium and ferrocene redox moieties through alkanethiol monolayers on gold. *Journal of the American Chemical Society* **2003**, *125*, 2004-2013.

(264) Finklea, H. O.; Hanshew, D. D. Electron-transfer kinetics in organized thiol monolayers with attached pentaammine (pyridine) ruthenium redox centers. *Journal of the American Chemical Society* **1992**, *114*, 3173-3181.

(265) Finklea, H. O.; Liu, L.; Ravenscroft, M. S.; Punturi, S. Multiple electron tunneling paths across self-assembled monolayers of alkanethiols with attached ruthenium (II/III) redox centers. *The Journal of Physical Chemistry* **1996**, *100*, 18852-18858.

(266) Hod, I.; Farha, O. K.; Hupp, J. T. Modulating the rate of charge transport in a metal–organic framework thin film using host: guest chemistry. *Chemical Communications* **2016**, *52*, 1705-1708.

(267) Matsue, T.; Evans, D. H.; Osa, T.; Kobayashi, N. Electron-transfer reactions associated with host-guest complexation. Oxidation of ferrocenecarboxylic acid in the presence of. beta.-cyclodextrin. *Journal of the American Chemical Society* **1985**, *107*, 3411-3417.

(268) Xiang, D.; Gao, G.; Shao, H.; Li, H.; Zhang, H.-L.; Yu, H.-Z. Redox behavior and ion-pairing thermodynamics of ferrocene and its derivatives in the organic phase. *The Journal of Physical Chemistry C* **2010**, *114*, 617-621.

(269) Ong, W.; Kaifer, A. E. Salt effects on the apparent stability of the cucurbit [7] uril− methyl viologen inclusion complex. *The Journal of Organic Chemistry* **2004**, *69*, 1383-1385.

(270) Swiech, O.; Chmurski, K.; Bilewicz, R. Molecular interactions of β-cyclodextrins with monolayers containing adamantane and anthraquinone guest groups. *Supramolecular Chemistry* **2010**, *22*, 461-466.

(271) Ju, H.; Leech, D. Host− Guest Interaction at a Self-Assembled Monolayer/Solution Interface: An Electrochemical Analysis of the Inclusion of 11-(Ferrocenylcarbonyloxy) undecanethiol by Cyclodextrins. *Langmuir* **1998**, *14*, 300-306.

(272) Henstridge, M. C.; Laborda, E.; Rees, N. V.; Compton, R. G. Marcus–Hush–Chidsey theory of electron transfer applied to voltammetry: A review. *Electrochimica Acta* **2012**, *84*, 12-20.

(273) Zeng, Y.; Smith, R. B.; Bai, P.; Bazant, M. Z. Simple formula for marcus–hush–chidsey kinetics. *Journal of Electroanalytical Chemistry* **2014**, *735*, 77-83.

(274) Savéant, J.-M. Effect of ion pairing on the mechanism and rate of electron transfer. Electrochemical aspects. *The Journal of Physical Chemistry B* **2001**, *105*, 8995-9001.

(275) Marcus, R. Ion pairing and electron transfer. *The Journal of Physical Chemistry B* **1998**, *102*, 10071-10077.

(276) Kuok, K. I.; Li, S.; Wyman, I. W.; Wang, R. Cucurbit [7] uril: an emerging candidate for pharmaceutical excipients. *Annals of the New York Academy of Sciences* **2017**, *1398*, 108-119.

(277) Yin, H.; Wang, Z.; Wang, R. Modulation of Chemical and Biological Properties of Biomedically Relevant Guest Molecules by Cucurbituril-Type Hosts. *Handbook of Macrocyclic Supramolecular Assembly* **2019**, 1-25.

(278) Zhang, X.; Xu, X.; Li, S.; Wang, L.-H.; Zhang, J.; Wang, R. A systematic evaluation of the biocompatibility of cucurbit [7] uril in mice. *Scientific Reports* **2018**, *8*, 1-7.

(279) Yang, X.; Wang, Z.; Niu, Y.; Chen, X.; Lee, S. M.; Wang, R. Influence of supramolecular encapsulation of camptothecin by cucurbit [7] uril: reduced toxicity and preserved anti-cancer activity. *MedChemComm* **2016**, *7*, 1392-1397.

(280) Uzunova, V. D.; Cullinane, C.; Brix, K.; Nau, W. M.; Day, A. I. Toxicity of cucurbit [7] uril and cucurbit [8] uril: an exploratory in vitro and in vivo study. *Organic & Biomolecular Chemistry* **2010**, *8*, 2037-2042.

(281) Yang, X.; Li, S.; Zhang, Q.-W.; Zheng, Y.; Bardelang, D.; Wang, L.-H.; Wang, R. Concealing the taste of the Guinness World's most bitter substance by using a synthetic nanocontainer. *Nanoscale* **2017**, *9*, 10606-10609.

(282) Li, F.; Gorle, A. K.; Ranson, M.; Vine, K. L.; Kinobe, R.; Feterl, M.; Warner, J. M.; Keene, F. R.; Collins, J. G.; Day, A. I. Probing the pharmacokinetics of cucurbit [7, 8 and 10] uril: and a dinuclear ruthenium antimicrobial complex encapsulated in cucurbit [10] uril. *Organic & Biomolecular Chemistry* **2017**, *15*, 4172-4179.

(283) Plumb, J. A.; Venugopal, B.; Oun, R.; Gomez-Roman, N.; Kawazoe, Y.; Venkataramanan, N. S.; Wheate, N. J. Cucurbit [7] uril encapsulated cisplatin overcomes cisplatin resistance via a pharmacokinetic effect. *Metallomics* **2012**, *4*, 561-567.

(284) Moghaddam, S.; Yang, C.; Rekharsky, M.; Ko, Y. H.; Kim, K.; Inoue, Y.; Gilson, M. K. New ultrahigh affinity host− guest complexes of cucurbit [7] uril with bicyclo [2.2. 2] octane and adamantane guests: Thermodynamic analysis and evaluation of m2 affinity calculations. *Journal of the American Chemical Society* **2011**, *133*, 3570-3581.

(285) Li, S.; Ding, Y. F.; Yin, H.; Wang, C.; Bardelang, D.; Wang, L. H.; Wang, R. Encapsulation of AGE‐Breaker Alagebrium by Cucurbit [7] uril Improved the Stability of Both Its Carbonyl α‐Hydrogen and Thiazolium C2‐Hydrogen. Chemistry‐*An Asian Journal* **2016**, *11*, 3126-3133.

(286) Esteban Fernandez de Avila, B.; Watkins, H. M.; Pingarrón, J. M.; Plaxco, K. W.; Palleschi, G.; Ricci, F. Determinants of the detection limit and specificity of surface-based biosensors. *Analytical chemistry* **2013**, *85*, 6593-6597.

(287) Cheng, A. K.; Ge, B.; Yu, H.-Z. Aptamer-based biosensors for label-free voltammetric detection of lysozyme. *Analytical chemistry* **2007**, *79*, 5158-5164.

(288) Glenday, C.: *Guinness World Records* 2013; Bantam, **2013**.

(289) Spasov, A.; Khamidova, T.; Bugaeva, L.; Morozov, I. Adamantane derivatives: Pharmacological and toxicological properties. *Pharmaceutical Chemistry Journal* **2000**, *34*, 1-7.

(290) Lamoureux, G.; Artavia, G. Use of the adamantane structure in medicinal chemistry. *Current Medicinal Chemistry* **2010**, *17*, 2967-2978.

(291) Darwish, I. A. Immunoassay methods and their applications in pharmaceutical analysis: basic methodology and recent advances. *International Journal of Biomedical Science: IJBS* **2006**, *2*, 217.

(292) Kwiatkowski, A.; Czerwicka, M.; Smulko, J.; Stepnowski, P. Detection of denatonium benzoate (Bitrex) remnants in noncommercial alcoholic beverages by raman spectroscopy. *Journal of Forensic Sciences* **2014**, *59*, 1358-1363.

(293) Siddiqui, M. R.; AlOthman, Z. A.; Rahman, N. Analytical techniques in pharmaceutical analysis: A review. *Arabian Journal of chemistry* **2017**, *10*, S1409-S1421.

(294) Li, W.; Bockus, A. T.; Vinciguerra, B.; Isaacs, L.; Urbach, A. R. Predictive recognition of native proteins by cucurbit [7] uril in a complex mixture. *Chemical Communications* **2016**, *52*, 8537-8540.

(295) Oh, S. K.; Baker, L. A.; Crooks, Electrochemical rectification using mixed monolayers of redox-active ferrocenyl dendrimers and n-alkanethiols. *Langmuir*, **2002**, *18*, 6981-6987.

(296) Rudnev, A. V.; Yoshida, K.; Wandlowski, T. Electrochemical characterization of self-assembled ferrocene-terminated alkanethiol monolayers on low-index gold single crystal electrodes. *Electrochemical Acta*, **2013**, *87*, 770-778.

(297) Nerngchamnong, N.; Thompson, D.; Cao, L.; Yuan, L.; Jiang, L.; Roemer, M.; Nujhuis, C. A. Nonideal electrochemical behavior of ferrocenyl–alkanethiolate SAMs maps the microenvironment of the redox unit. *J. Phys. Chem. C* **2015**, *119*, 21978-21991.

(298) Collard, D. M.; Fox, M. A. Use of electroactive thiols to study the formation and exchange of alkanethiol monolayers on gold. *Langmuir* **1991**, *7*, 1192-1197.

(299) Ju, H.; Leech, D. Effect of electrolytes on the electrochemical behaviour of 11-(ferrocenylcarbonyloxy)undecanethiol SAMs on gold disk electrodes. *Phys. Chem. Chem. Phys.* **1999**, *1*, 1549-1554.

(300) Dionne, E. R.; Sultana, T.; Norman, L. L.; Toader, V.; Badia, A. Redox-induced ion pairing of anionic surfactants with ferrocene-terminated self-assembled monolayers: faradaic electrochemistry and surfactant aggregation at the monolayer/liquid interface. *J. Am. Chem. Soc.* **2013**, *135*, 17457-17468.

(301) Dionne, E. R.; Badia, A. Electroactive self-assembled monolayers detect micelle formation. *ACS Appl. Mater. Interfaces* **2017**, *9*, 5607-5621.

(302) Good, R. J. Contact angle, wetting, and adhesion: a critical review. *Journal of Adhesion Science and Technology* **1992**, *6*, 1269-1302.

(303) Ye, D.; Zuo, X.; Fan, C. DNA nanotechnology-enabled interfacial engineering for biosensor development. *Annual Review of Analytical Chemistry* **2018**, *11*, 171-195.

(304) Seeman, N. C.; Sleiman, H. F. DNA nanotechnology. *Nature Reviews Materials* **2017**, *3*, 1-23.

(305) Kogikoski Jr, S.; Paschoalino, W. J.; Cantelli, L.; Silva, W.; Kubota, L. T. Electrochemical sensing based on DNA nanotechnology. *TrAC Trends in Analytical Chemistry* **2019**.

(306) Tang, Y.; Ge, B.; Sen, D.; Yu, H.-Z. Functional DNA switches: rational design and electrochemical signaling. *Chemical Society Reviews* **2014**, *43*, 518-529.

(307) Willner, I.; Zayats, M. Electronic aptamer‐based sensors. *Angewandte Chemie International Edition* **2007**, *46*, 6408-6418.

(308) Schoukroun-Barnes, L. R.; Macazo, F. C.; Gutierrez, B.; Lottermoser, J.; Liu, J.; White, R. J. Reagentless, structure-switching, electrochemical aptamer-based sensors. *Annual Review of Analytical Chemistry* **2016**, *9*, 163-181.

(309) Bizzotto, D.; Burgess, I. J.; Doneux, T.; Sagara, T.; Yu, H.-Z. Beyond simple cartoons: challenges in characterizing electrochemical biosensor interfaces. *ACS sensors* **2018**, *3*, 5-12.

(310) Du, Y.; Lim, B. J.; Li, B.; Jiang, Y. S.; Sessler, J. L.; Ellington, A. D. Reagentless, ratiometric electrochemical DNA sensors with improved robustness and reproducibility. *Analytical Chemistry* **2014**, *86*, 8010-8016.

(311) Ihara, T.; Maruo, Y.; Takenaka, S.; Takagi, M. Ferrocene-oligonucleotide conjugates for electrochemical probing of DNA. *Nucleic Acids Research* **1996**, *24*, 4273-4280.

(312) Uosaki, K.; Sato, Y.; Kita, H. Electrochemical characteristics of a gold electrode modified with a self-assembled monolayer of ferrocenylalkanethiols. *Langmuir* **1991**, *7*, 1510-1514.

(313) Munteanu, M.; Choi, S.; Ritter, H. Cyclodextrin-click-cucurbit [6] uril: Combi-receptor for supramolecular polymer systems in water. *Macromolecules* **2009**, *42*, 3887-3891.

(314) Daniel, C. H. Quantitative chemical analysis. 7th edition. W. H. *Freeman and Company*, **2007**.

(315) Khoshhesab, Z. M. Reflectance IR spectroscopy. *Infrared spectroscopy—materials science, engineering and technology.* **2012***, 11,* 233-244.

Appendix A. Additional experimental results

1. Determination of real electrode area based on Randle-Sevcik equation

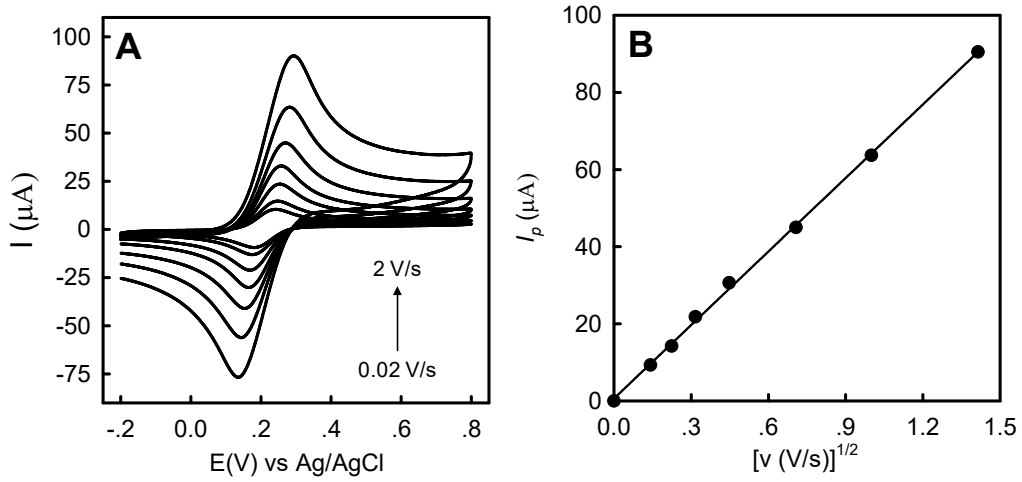

(A) CVs of 1.0 mM $K_4Fe(CN)_6$ in 1.0 M KCl recorded at different scan rates. (B) The relationship between the CV peak current (I_p) of and the square root of scan rate ($v^{1/2}$); the solid line is the best linear fitting based on Randle-Sevcik equation (equation 2.3). The good linear relationship (R^2 > 0.99) confirms the diffusion-controlled redox behavior; and the real electrode area (A = 0.15 ± 0.01 cm^2) was determined from the value of slope.

2. CV and water contact angle characterizations of based gold slide before and after cleaning with piranha solution

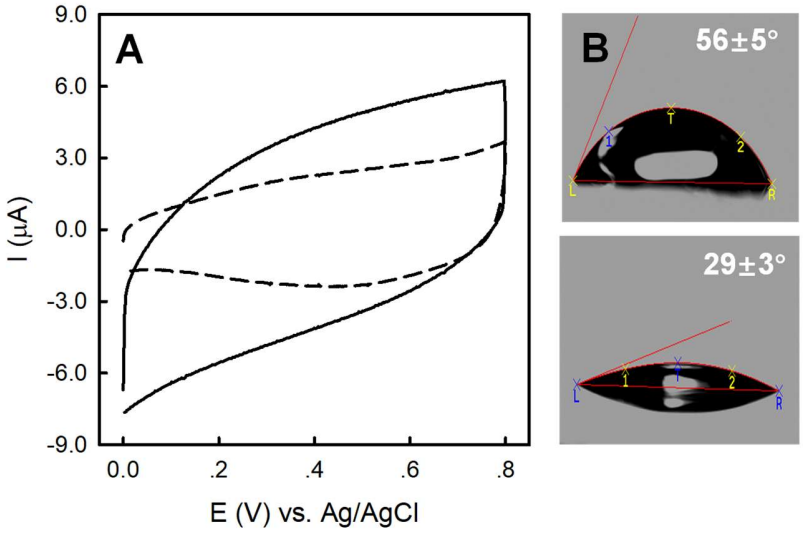

CVs of gold slide before (dashed line) and after (solid line) cleaning with host Piranha solution (following the procedure described in section 2.1.3). The electrolyte solution is 1.0 M KCl; the scan rate is 100 mV/s. (B) Water contact angles of gold slide before (top) and after (bottom) cleaning with host Piranha solution. These results indicate the existence of organic contaminations on uncleaned gold slide (lower charging current and higher water contact angle).

3. CV study of directly deposited CB[7] monolayer on gold

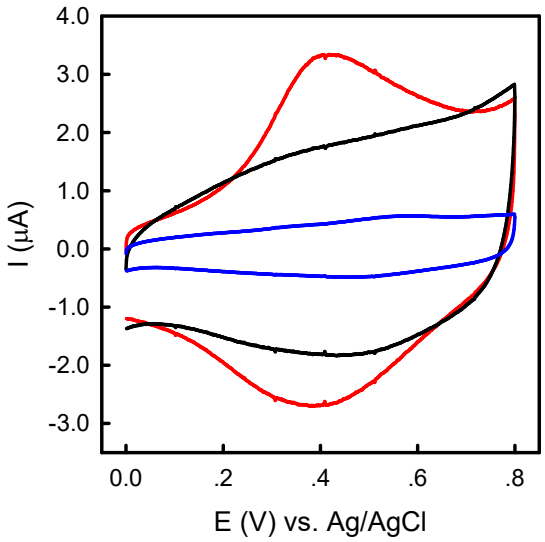

CVs of CB[7] monolayer (formed by immersing the cleaned gold slide in 2.0 mM CB[7] solution for overnight) before (black curve) and after incubation with 1.0 mM $FcCH_2OH$ solution for 2 h (red curve) (the Γ_{Fc} determined by integrating the anodic wave is 6.8±0.9 × 10^{-11} mol/cm^2), and then treating with 1.0 mM C8SH solution (95% ethanol) for only 5 min (black curve). The electrolyte solution is 0.1 M $NaClO_4$; the scan rate is 100 mV/s. These results confirm that the directly deposited CB[7] monolayer on gold can be easily replaced by C8SH.

4. CV study of host-guest binding between ferrocenemethanol ($FcCH_2OH$) and CB[7] in aqueous solution

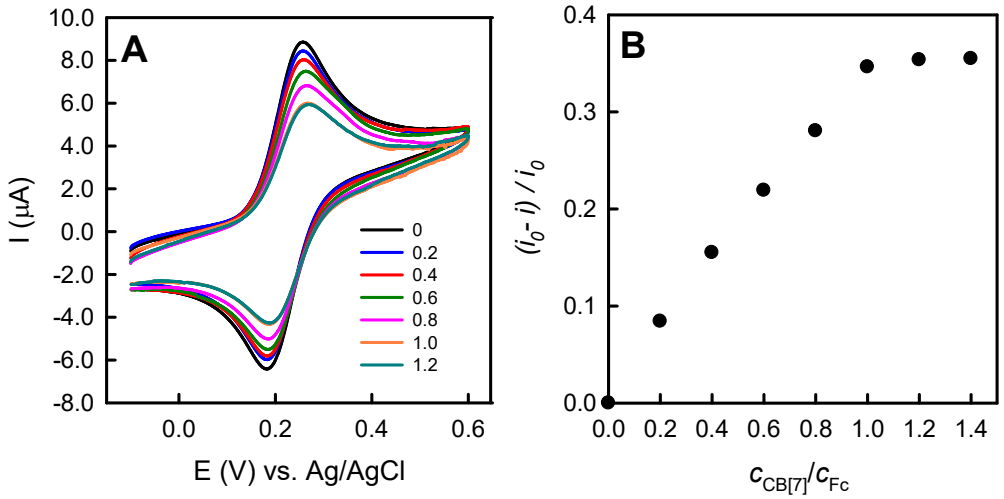

(A) CVs of 1.0 mM $FcCH_2OH$ in the presence of different concentrations of CB[7]. The supporting electrolyte is 1.0 M KCl, and the scan rate is kept at 50 mV/s. (B) The fraction of peak current change ($(i_0 - i)/i_0$, where i_0 and i are the peak current of $FcCH_2OH$ before and after adding CB[7]) as a function of the molar ratio between CB[7] and $FcCH_2OH$ ($c_{CB[7]}/c_{Fc}$). These results confirm their 1:1 mole ratio binding (from the turning point of the binding isotherm curve). The decreased CV peak currents upon CB[7] binding is caused by the smaller diffusion coefficient of $FcCH_2OH$@CB[7] host-guest complex than the free $FcCH_2OH$.

5. The standard ET rate constant of FcC11S-/C8S-Au SAMs with different surface densities of Fc

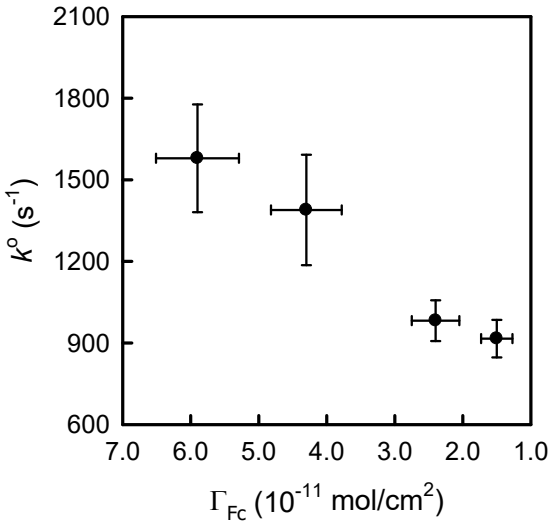

The standard ET rate constant (k_0) was determined by Laviron method for mixed FcC11S-&C8S-Au SAM prepared by co-adsorption with 5%, 3%, 2%, and 1% mole fraction of FcC11SH in the mixed assembly solution. It was found that k_0 decreases with increased surface density of Fc, which might be due to the higher degree of SAM disorders/defects.

6. Compare the CVs of mixed FcC11S-/C10S-Au SAM in the electrolyte solution with different type of cations

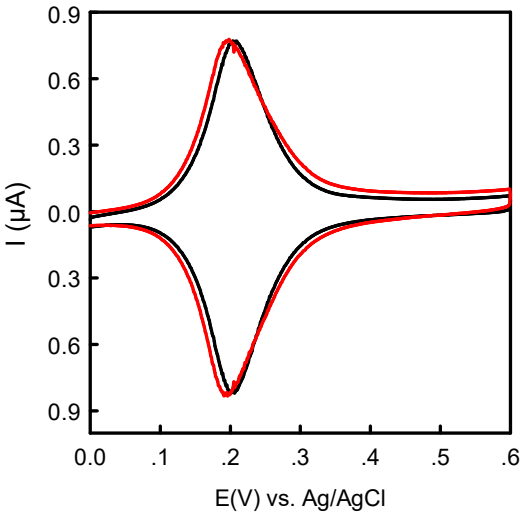

Red curve: CV of FcC11S-/C10S-Au SAM (prepared by co-adsorption method with 10% mole fraction of FcC11SH in the mixed assembly solution) in 1.0 M $HClO_4$; Black curve: CV of FcC11S-/C10S-Au SAM in 1.0 M $NaClO_4$. The CV scan rate was 0.05 V/s. It shows that the different types of cation (Na^+ and H^+) has no significant influences on the CV of mixed Fc-SAMs on gold.

Appendix B. Binary thiolate DNA/ferrocenyl self-assembled monolayer on gold: a versatile platform for probing biosensing interface

This is a study I did for another research project related to the electrochemical characterization and biosensing application of DNA self-assembled monolayers on gold. In this study, a binary component thiolated DNA/ferrocenyl-6-hexathiolate SAM on gold was developed where the surface properties of DNA (density, distribution, and orientation) can be effectively evaluated from the CV response of Fc^{+}/Fc terminal group. This study is published and reprinted below with permission from *Anal. Chem.* 2020, 92, 2168-2175. Copyright (2018) *American Chemical Society.*

Huihui Tian, a visiting student from 2012 to 2014, preliminarily explored the proper conditions for preparing this mixed DNA/ferrocenyl SAM and did some CV characterizations.

analytical chemistry

Article

Cite This: Anal. Chem. 2018, 90, 9174−9181

pubs.acs.org/ac

Binary Thiolate DNA/Ferrocenyl Self-Assembled Monolayers on Gold: A Versatile Platform for Probing Biosensing Interfaces

Lin Qi,[†] Huihui Tian,[†,‡] and Hua-Zhong Yu*[,†]

[†]Department of Chemistry, Simon Fraser University, Burnaby, British Columbia V5A 1S6, Canada

[‡]National Center for Nanoscience and Technology, Beijing 100190, P.R. China

Supporting Information

ABSTRACT: The properties of DNA self-assembled monolayers (SAMs) have strong influences on the interfacial DNA−analyte binding behavior, which further affect the performance of biosensors built upon. In this work, we prepared binary thiolate DNA/6-ferrocenyl-1-hexanethiol (FcC6SH) SAMs on gold (DNA/FcC6S-Au) for convenient electrochemical characterization and subsequent data analysis. Our cyclic voltammetric (CV) studies confirmed that the redox responses of surface-tethered Fc and electrostatically bound $[Ru(NH_3)_6]^{3+}$ are capable of providing quantitative information regarding the DNA film properties, including the surface density, structural heterogeneity, and molecular orientation under different preparation and measurement conditions. With the binary thiolate DNA/FcC6S-Au SAM prepared in the conventional post-assembly exchange protocol as a trial system, we are demonstrating the capability of introducing redox-active thiols as passivating and labeling reagents for preparing many other DNA-based biosensing interfaces via varied assembly steps and under different measurement conditions.

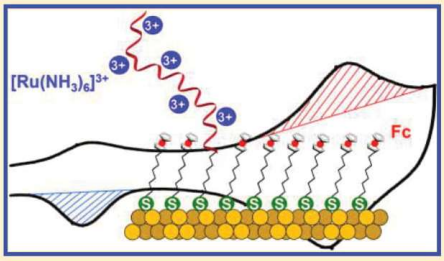

Over the past two decades, self-assembled monolayers (SAMs) of thiolate oligonucleotides with designed sequences have attracted considerable attention for the design and fabrication of DNA-based biosensors targeting a wide range of analytes (from small molecules and ions to protein biomarkers).[1−12] As a versatile platform for biosensing, the binding of analytes to surface tethered DNA strands (probes) can be readily transduced into electrochemical signals for direct measurements or for subsequent amplifications.[6−13] It has been confirmed that the surface density of DNA strands plays a key role in the sensor performance as it affects the accessibility of solution-diffused analytes to the electrode-bound probes (i.e., the interfacial binding efficiency).[14−20] In addition, nonspecific adsorption of DNA probes and the ionic environment of the testing solution have significant influences on the sensor performance as well.[21−27]

In order to achieve the desired sensing performance, binary thiolate DNA/6-mercapto-1-hexanenol (MCH) SAMs on gold have been first explored by Herne and Tarlov,[28] where MCH, a short alkanethiol with a hydroxyl terminus, serves as both diluting and blocking purposes, i.e., to reduce the surface density of DNA strands and to remove nonspecifically adsorbed species. Subsequently, these binary thiolate DNA/MCH SAMs have been widely adapted for the development of biosensors[6−10] and have been extensively characterized.[14,29−41]

The other important task to characterize DNA SAMs and other biosensing interfaces is the search of an appropriate labeling technique and corresponding signal reading method. In the past, many different labeling reagents (e.g., florescent tags,[29−32] redox centers,[33−38,40] and radio-isotopes[28]) in conjunction with spectroscopic[14,22,26,28,39] and microscopic techniques[41−43] have been explored for the structural characterization of DNA SAMs. Among these techniques, electrochemistry remains as one of the most popular methods for studying DNA SAMs on electrode owing to its simplicity, cost-effectiveness, and capability of quantitation.[33,35−38,40] The attachment of redox centers to DNA SAMs has been achieved via covalent bonding,[34] intercalation,[36,37] or electrostatic interaction.[33,35,38,40] For the former, a redox center is typically attached to the 5′- or 3′-terminus of a DNA strand and thus has a straightforward stoichiometry (1:1), for which ferrocene has been one of the most popular choices for this purpose (Scheme 1A).[34] However, the covalent attachment of redox moieties to presynthesized DNA strands is a laborious and time-consuming process; it also suffers from the relatively weak redox signal due to the limited surface density of redox centers.[35]

A more convenient noncovalent labeling strategy involves electrostatic binding of positively charged redox species, e.g., $[Ru(NH_3)_6]^{3+}$, onto negatively charged DNA phosphate backbones (Scheme 1B).[33,35,38,40] The electrostatic interaction allows for the binding of multiple redox centers on the same DNA strand, which ensures an amplified signal for electrochemical measurements. Unfortunately, the equilibrium

Received: April 13, 2018
Accepted: June 25, 2018
Published: June 25, 2018

DOI: 10.1021/acs.analchem.8b01655
Anal. Chem. 2018, 90, 9174−9181

Scheme 1. Pictorial View of a Binary Thiolate DNA/MCH SAM Covalent Labeling with Fc (A) and Electrostatic Labeling with $[Ru(NH_3)_6]^{3+}$ (B) and Binary Thiolate DNA/FcC6SH SAM on Gold (C)

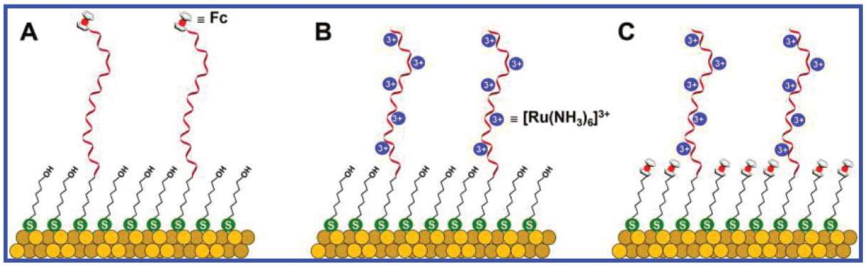

between the solution-diffused and surface-bound redox cations is easily affected by the solution environment (e.g., ionic strength and types of ionic species).[44] More importantly, due to the nonspecific nature of the electrostatic binding, other structural information beyond the surface density (e.g., uniformity, orientation) about DNA SAMs cannot be derived.

With a conceptually different approach, Kertesz et al. have discovered that a thiol-tethered anthraquinone (AQ) molecule can be used to electrochemically "titrate" the gold surface modified with DNA/MCH SAMs, particularly the denaturing process of double-stranded DNA on the surface.[45] Their system takes the advantages of redox species that are bonded to gold electrode through alkanethiolate "bridges", which not only avoids the laborious redox labeling on DNA strands but also ensures strong, reversible, and stable redox responses due to the close proximity to the electrode and high packing density.[46]

Herein, we explore the construction of binary thiolate DNA/6-ferrocenyl-1-hexanethiol SAMs on gold (DNA/FcC6S-Au) by replacing MCH with 6-ferrocenyl-1-hexanethiol (FcC6SH) as the diluting and blocking reagent (Scheme 1C). It is important to note that FcC6SH also serves as a robust electrochemical probe.[47−52] Particularly, we will investigate the cyclic voltammetric (CV) responses of Fc^+/Fc in the binary thiolate DNA/FcC6S-Au SAMs prepared with different deposition concentrations of DNA and in solutions with different types and concentrations of electrolytes. It is expected that the surface density, distribution, and molecular orientation of surface-bound DNA strands can be effectively revealed on the basis of our comprehensive analysis of their distinct CV responses.

EXPERIMENTAL SECTION

Reagents and Materials. The disulfide-modified oligonucleotide with the sequence HO−$(CH_2)_6$−S−S−$(CH_2)_6$−O−5′-ATC TAC GAA TTC ATC AGG GCT AAA GAG TGC AGA GTT ACT TAG-3′ was synthesized by the Integrated DNA Technologies Inc. (Coralville, IA). 6-Ferrocenyl-1-hexanethiol (FcC6SH), 6-mercapto-1-hexanenol (MCH), 1-hexanethiol (C6SH), hexaammineruthenium(III) chloride ($[Ru(NH_3)_6]Cl_3$), sodium perchlorate ($NaClO_4$), and tris (2-carboxyethyl) phosphine hydrochloride (TCEP) were ordered from Sigma-Aldrich (St. Louis, MO). Ethanol (95%) was purchased from Commercial Alcohols (Toronto, ON). All chemicals were of ACS reagent grade and used as received. Deionized water (>18.2 MΩ·cm) was produced with a Barnstead EasyPure UV/UF compact water system (Dubuque, IA). All solutions used throughout the experiment were prepared with the deionized water and deoxygenated with Ar. Gold slides (regular glass slides coated with 5 nm Cr and 100 nm Au) were purchased from Evaporated Metal Films (EMF) Inc. (Ithaca, NY).

Electrode Modification. The disulfide-modified oligonucleotide was reduced with 10 mM TCEP in 100 mM Tris-HCl buffer (pH = 7.4) at room temperature for 2 h. Thus obtained oligonucleotide solution was desalted by gel filtration with a MicroSpin G-50 Column (Amersham Bioscience, Bath, England), where the reduced thiolate oligonucleotide (HS-C6-DNA) was eluted first while the much smaller thiol (e.g., MCH) remained in the column. After purification, the oligonucleotide solution was diluted with the immobilization buffer (10 mM Tris-HCl, 150 mM LiCl, 50 mM $MgCl_2$, pH = 7.4) to the desired concentrations prior to use. The presence of divalent cation Mg^{2+} (50 mM) in the immobilization buffer ensures the assembly of DNA strands on the surface with high packing densities.[39]

The gold slides (100 nm gold film with dominating Au ⟨111⟩ crystalline facets) were cut into small pieces (1 × 2 cm^2) and cleaned in a Piranha solution (3:1 mixture of 96% H_2SO_4 and 30% H_2O_2) for 5−7 min at 90 °C, followed by rinsing with copious amounts of deionized water and drying with N_2 (*Caution: one should be extremely careful when handling Piranha solutions as they are very corrosive and react violently with organics*). Binary thiolate DNA/FcC6S-Au SAMs were prepared according to a widely adopted two-step procedure.[35] Briefly, 20 μL droplets of oligonucleotide solutions (in the immobilization buffer) at different concentrations were added onto the cleaned gold slides, which were then incubated at room temperature in a humidity box overnight (>12 h). After thorough rinsing with the immobilization buffer and deionized water, the DNA modified gold slides were immersed into 1.0 mM FcC6SH ethanol solution for 2 h, followed by thorough rinsing with ethanol and deionized water. Ethanol (95%) is one of the most widely used solvents for preparing alkanethiolate SAMs since it can solvate a variety of alkanethiols with different degrees of polarities and chain lengths.[53]

To prepare binary 6-ferrocenyl-1-hexanethiol/1-hexanethiol SAM on gold (FcC6S-/C6S-Au SAM), the freshly cleaned gold slides were immersed in a binary C6SH/FcC6SH ethanol solution overnight (>12 h). The total concentration of thiols was kept at 1.0 mM, and the mole fraction of FcC6SH was 10%. After immersion, the gold slides were thoroughly rinsed with ethanol and deionized water.

DOI: 10.1021/acs.analchem.8b01655
Anal. Chem. 2018, 90, 9174−9181

Electrochemical Measurements. Electrochemical measurements were carried out in a three-electrode single-chamber cell made of Plexiglas V-grade acrylicresin, with a CHI 1040A Electrochemical Analyzer (Austin, TX). The cell has an opening at one side, where the gold slide (working electrode) is attached. The area of the working electrode exposed to the electrolyte (0.15 cm^2) was defined by an O-ring seal (see Figure S6) and estimated on the basis of the Randles-Sevcik equation by measuring the CVs in 1.0 mM aqueous $K_3Fe(CN)_6$ at varied scan rates.[54]

For evaluating the surface density of DNA in binary thiolate DNA/FcC6S-Au SAMs, 5.0 μM $[Ru(NH_3)_6]Cl_3$ in 10 mM Tris-HCl buffer (pH = 7.4) was used as the electrolyte solution for the CV measurements.[35,38] For examining the CV responses of Fc^+/Fc in binary thiolate DNA/FcC6S-Au SAMs, the electrolyte was a solution containing different concentrations of $NaClO_4$. All CV measurements were performed at a scan rate of 0.1 V/s and in a Faraday cage at room temperature.

■ RESULTS AND DISCUSSION

As shown in Scheme 1, binary thiolate DNA/FcC6S-Au SAMs are different from the two traditional strategies (covalent modification of DNA with redox centers or electrostatic binding of electroactive cations on DNA strands) as the redox active alkanethiols are directly attached to gold electrode (which also serves for the passivation purpose). With this unique system, we can monitor redox signals from both surface-tethered FcC6SH and electrostatically bound $[Ru(NH_3)_6]^{3+}$; its preparation is not complicated either (i.e., replacing MCH with FcC6SH in the conventional two-step procedure for the preparation of binary thiolate DNA/MCH SAMs).[28,33,35,38,40] The first question we are interested in answering is how well we can modulate the surface density of DNA strands, for which we systematically changed the concentration of DNA deposition solutions while maintaining the same concentration of FcC6SH for the passivation/labeling step. For direct determination of the surface concentrations of DNA strands, we have carried out the CV measurements in an electrolyte solution containing 5.0 μM $[Ru(NH_3)_6]^{3+}$.[35,38]

Titration of DNA Surface Density. As shown in Figure 1A, two pairs of clear-cut redox peaks can be observed with formal potentials at −254 ± 6 mV and 368 ± 9 mV (vs Ag/AgCl), respectively. The peaks at more negative potential correspond to the reduction of electrostatically bound $[Ru(NH_3)_6]^{3+}$ to $[Ru(NH_3)_6]^{2+}$ (cathodic) and its reoxidation (anodic); we noted that an increased concentration of $[Ru(NH_3)_6]^{3+}$ results in a gradual growing of this peak before reaching the saturation at 5.0 μM (Supporting Information). The peaks at more positive potential are attributed to the Fc^+/Fc couple, which also appear without adding $[Ru(NH_3)_6]^{3+}$ to the electrolyte. The simultaneous observation of the two sets of peaks confirms the formation of binary thiolate DNA/FcC6S-Au SAMs on gold; more importantly, with higher concentrations of DNA in the deposition solution, the redox peaks of $[Ru(NH_3)_6]^{3+/2+}$ become more pronounced, while those of Fc^+/Fc are getting smaller. This confirms that more DNA strands are immobilized on gold and less FcC6SH molecules are "needed" to passivate the surface. On the basis of the CV responses shown in Figure 1A, the exact surface densities of DNA and FcC6SH in the binary thiolate DNA/FcC6S-Au SAMs can be determined. The surface density of DNA (Γ_{DNA})

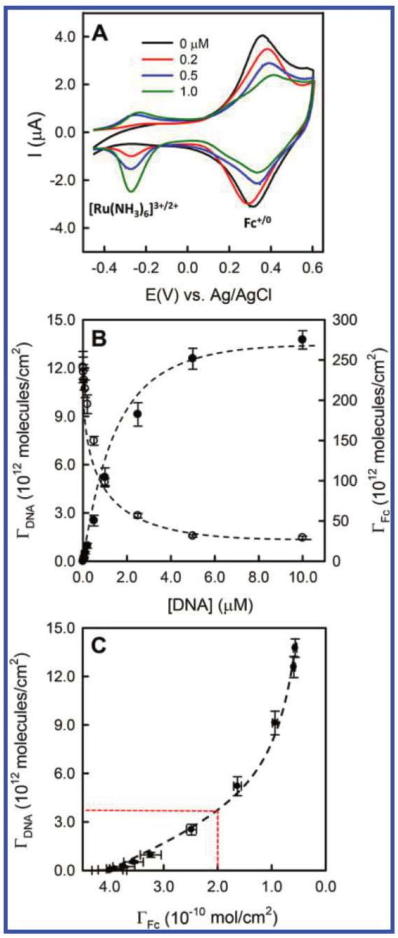

Figure 1. (A) CVs of binary thiolate DNA/FcC6S-Au SAMs prepared via the incubation with different concentrations of thiolated DNA and post-assembly exchange with 1.0 mM FcC6SH. The electrolyte solution is 10 mM Tris-HCl buffer containing 5.0 μM $[Ru(NH_3)_6]Cl_3$ (pH = 7.4), and the scan rate is 50 mV/s. (B) Surface densities of DNA (solid circles) and Fc (open circles) in binary thiolate DNA/FcC6S-Au SAMs prepared with different concentrations of thiolate DNA. (C) The relationship between the surface density of DNA and Fc in binary thiolate DNA/FcC6S-Au SAMs. The black dashed lines are to guide the eyes only.

can be calculated from the reduction peak of $[Ru(NH_3)_6]^{3+}$ by using eqs 1 and 2[35,38,54]

$$\Gamma_{Ru} = \frac{Q_{Ru}N_A}{nFA} \quad (1)$$

$$\Gamma_{DNA} = \Gamma_{Ru} \times \left(\frac{z}{m}\right) \quad (2)$$

DOI: 10.1021/acs.analchem.8b01655
Anal. Chem. 2018, 90, 9174−9181

where Q_{Ru} is the integrated faradic charge of the cathodic peak (reduction of $[Ru(NH_3)_6]^{3+}$ to $[Ru(NH_3)_6]^{2+}$); n is the number of electrons involved in this redox reaction; F is the faradic constant; A is the working electrode area; N_A is the Avogadro's number; z is the charge of $[Ru(NH_3)_6]^{3+}$; m is the number of nucleotides of the DNA strand. Equation 2 is valid on the basis of the assumption that the negative charges on the DNA phosphate backbones are solely compensated by $[Ru(NH_3)_6]^{3+}$.[38] We believe that this assumption is well satisfied under our experimental conditions as low ionic strength Tris buffer (10 mM) was used as the electrolyte and that a 5.0 μM concentration of $[Ru(NH_3)_6]^{3+}$ has been confirmed to be adequate to "saturate" the DNA SAMs.[35]

In comparison, the determination of the surface density of Fc^+/Fc (Γ_{Fc}) in binary thiolate DNA/FcC6S-Au SAMs is rather straightforward, which can be directly calculated from its CV peaks on the basis of eq 3[48−52,54]

$$\Gamma_{Fc} = \frac{Q_{Fc}}{nFA} \tag{3}$$

where Q_{Fc} is the integrated faradic charge of the anodic peak (oxidation of Fc to Fc^+).

As shown in Figure 1B, the surface density of DNA (Γ_{DNA}) initially increases and then reaches a maximum upon increasing the concentration of DNA in the deposition solution (from 0.1 to 10 μM); meanwhile, the Fc surface density (Γ_{Fc}) decreases rapidly despite the concentration of FcC6SH in the passivation step being kept rather high and constant (1.0 mM). The highest Γ_{DNA} achieved via such a two-step assembly procedure ($13.6 \pm 0.8 \times 10^{12}$ molecules/cm^2) is close to that of binary thiolate DNA/MCH SAMs,[35] indicating that FcC6SH is capable of passivating the DNA-modified electrode surface (for which MCH has been typically used).

The analytical aspect of the correlation between Γ_{DNA} and Γ_{Fc} in the binary thiolate DNA/FcC6S-Au SAMs should be emphasized (Figure 1C); it can be reserved as a calibration curve for determining Γ_{DNA} indirectly by measuring Γ_{Fc} (i.e., carrying out CV scans in redox indicator-free electrolytes). For an example, if we had determined the Γ_{Fc} to be 2.0×10^{-10} mol/cm^2, the Γ_{DNA} value should be at 3.6×10^{12} molecules/cm^2 (as pointed out with the red dashed lines in Figure 1C), a near "ideal" surface density for efficient hybridization with complementary strands.[14] This is particularly useful when subsequent applications of such DNA sensing surfaces are prone to interferences from highly charged cationic species.

Evaluation of Structural Heterogeneity. Besides the surface density determination/calibration, the CV responses of the Fc^+/Fc couple may provide more information about the structure of DNA monolayers on the surface. For this purpose, the CV responses of Fc^+/Fc were examined in an electrolyte containing 0.1 M $NaClO_4$, as ClO_4^- has been confirmed to form strong ion pairs with Fc^+ cations in ferrocenyl-alkanethiolate SAMs.[48,49,54] As shown in Figure 2A, the CV peaks of Fc^+/Fc in binary thiolate DNA/FcC6S-Au SAMs are not as symmetric as expected for a reversible one-electron charge transfer process of surface-bound redox centers.[54] Consistent with the CV responses depicted in Figure 1A, with higher concentrations of DNA used for the deposition, the CV responses of Fc^+/Fc became less pronounced (i.e., both reduction and oxidation peaks had lower peak currents). As highlighted in Figure 2A, the capacitive current observed at lower potential enlarges significantly with increased surface density of DNA strands. On the basis of the difference in the charging current between the forward and reverse scans (within a potential range that no faradic process occurs), the potential scan rate (v), and the electrode area (A), one can determine the double layer capacitance (C_{dl}) of the binary thiolate DNA/FcC6S-Au SAMs according to eq 4[54]

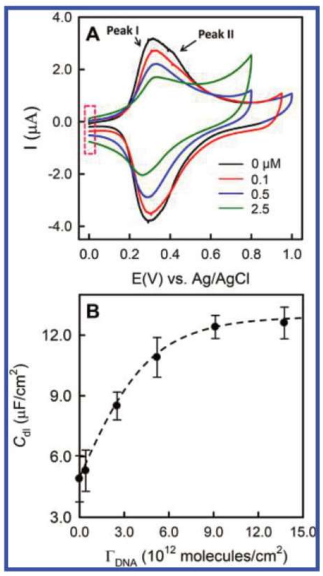

Figure 2. (A) CVs of Fc^+/Fc in binary thiolate DNA/FcC6S-Au SAMs prepared with different deposition concentrations of DNA. The electrolyte was 0.1 M $NaClO_4$, and the scan rate was kept at 50 mV/s for all measurements. (B) Estimated interfacial capacitance (C_{dl}) of binary thiolate DNA/FcC6S-Au SAMs with different DNA surface densities. The dashed line is to guide the eyes only.

$$C_{dl} = \frac{I_c}{2Av} \tag{4}$$

In Figure 2B, we have shown the dependence of thus determined C_{dl} values as the function of the DNA surface densities. It is intriguing to notice that the C_{dl} value increases monotonically when increasing the surface density of DNA strands (i.e., increasing the thiolate DNA concentration in the deposition solution). As has been discussed previously, C_{dl} can be interpreted with the Helmholtz model as shown in eq 5[54]

$$C_{dl} = \frac{\varepsilon\varepsilon_o}{d} \tag{5}$$

where d is the thickness of the dielectric medium that separates the two conducting plates and ε and ε_o are the dielectric constants of separation medium and free space. In the binary thiolate DNA/FcC6S-Au SAMs, the ε and d can be considered to represent the ionic permeability and thickness of the alkane layer. Thus, the increasing C_{dl} indicates that the higher surface density of DNA strands may reduce the thickness or enhance the permeability of the alkane layer, which could be attributed to its less packing density and more defect sites (e.g., pinholes, collapsed alkane chains).[47]

On closer inspection of the CV response of Fc^+/Fc in Figure 2A, we should observe the shoulder peak appearing at a more

DOI: 10.1021/acs.analchem.8b01655
Anal. Chem. 2018, 90, 9174−9181

positive potential (peak II) than the main peak (peak I). For the situation where no DNA strands are assembled on the surface (i.e., single-component FcC6S-Au SAMs), the peak splitting is the most obvious (black curve in Figure 2A). We have previously confirmed for single-component FcC11S-Au SAMs that such a peak-spitting behavior is due to the existence of two different structural domains and relates to the morphology of multicrystalline gold electrode (with different packing densities).[52] As the concentration of thiolate DNA increased from 0.1 to 2.5 μM in the deposition solution, the Fc^+/Fc redox peaks apparently became more symmetric; i.e., the right-side shoulder peak decreases in its amplitude. In order to quantitatively "analyze" such a trend, we have adapted the Gaussian−Lorentzian fitting protocol as a tentative solution to deconvolute the anodic peaks shown in Figure 2A.[48] As depicted in Figure 3A, although all anodic waves (pink circles) of Fc^+/Fc can be deconvoluted into two distinct peaks (blue dashed lines) and both of them became smaller, the shoulder peak at a more positive potential decreases faster. The change in the relative contribution of these two peaks to the overall Fc surface density was further illustrated by plotting the fraction of each peak (A/A_{total}) as the function of the DNA surface density in the binary thiolate DNA/FcC6S-Au SAMs (Figure 3B). With very low Γ_{DNA} values, their fractions are comparable; for higher Γ_{DNA} values, peak I becomes clearly dominate (accounts for more than 80% of the total peak area), which indicates a less heterogeneous structure of the mixed monolayers.

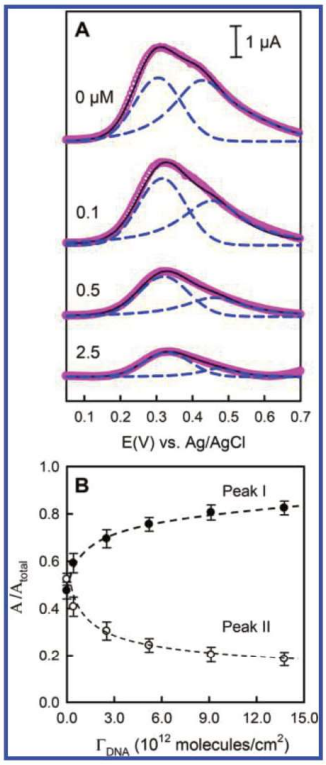

Figure 3. (A) Gaussian−Lorentzian deconvolution of the CV anodic waves of Fc^+/Fc in binary thiolate DNA/FcC6S-Au SAMs prepared with different deposition concentrations of DNA. The pink circles are the experimental data (i.e., the original CV anodic waves); the blue dashed lines and black solid lines are the deconvoluted two peaks and their sum (i.e., the overall fit). (B) The fractions of deconvoluted redox peaks to the overall CV anodic wave of Fc^+/Fc (A/A_{total}) in binary thiolate DNA/FcC6S-Au SAMs with different DNA surface densities. The dashed lines are to guide the eyes only.

The main peak (peak I) of the anodic wave of Fc^+/Fc was further analyzed (fitted) on the basis of the theoretical $i-E$ relationship derived from the Frumkin adsorption isotherm, as described by eqs 6 and 7[54,55]

$$i = \frac{n^2F^2Av\Gamma_T}{RT}\left[\frac{f(1-f)}{1-2\nu g\theta_T f(1-f)}\right] \quad (6)$$

$$n(E-E_p) = \frac{RT}{F}\left[\ln\left(\frac{f}{1-f}\right) + \nu g\theta_T(1-2f)\right] \quad (7)$$

where Γ_T is the surface density of redox centers (Fc^+/Fc); v is the potential scan rate; E_p is the redox peak potential; θ_T is the total surface coverage of the redox centers; f is defined as the fraction of oxidized redox centers ($f = \theta_O/\theta_T$) under a certain potential. The parameter $\nu g\theta_T$ describes the intermolecular interaction force among the adsorbed redox centers. According to the Frumkin adsorption isotherm, the peak width at half peak current (E_{fwhm}) is correlated with the intermolecular interaction factors among the surface tethered redox centers, which can be calculated from eqs 8 and 9[55]

$$E_{fwhm} = \frac{2RT}{nF}\left|\ln\frac{1+\beta}{1-\beta} - \nu g\theta_T\beta\right| \quad (8)$$

with

$$\beta = \frac{\sqrt{2-\nu g\theta_T}}{\sqrt{4-\nu g\theta_T}} \quad (9)$$

According to eqs 8 and 9, if $\nu g\theta_T = 0$, it indicates that there are no interactions among the surface tethered redox centers, whose adsorption behavior obeys the Langmuir isotherm, and E_{fwhm} equals 90.6 mV; when $\nu g\theta_T < 0$, i.e., a repulsion force exists among the surface tethered redox centers and E_{fwhm} is wider than 90.6 mV; when $\nu g\theta_T > 0$, i.e., it is expected that an attraction force exists among the surface tethered redox centers and the peak becomes sharper ($E_{fwhm} < 90.6$ mV).

As described in eqs 6 and 7, the potential (E) and current (i) are both functions of f (0−1.0); therefore, the main oxidation peak of Fc^+/Fc can be simulated using E_p and $\nu g\theta_T$ as two fitting parameters. The best fits were displayed in Figure 4A, while Figure 4B shows the dependence of the peak width (E_{fwhm}) and intermolecular interaction factor ($\nu g\theta_T$) on the surface density of DNA strands. Regardless of the surface density of DNA, we have observed much broader (than ideal) peaks and the simulated $\nu g\theta_T$ values are also negative. More importantly, with increased Γ_{DNA}, this peak becomes even broader, as the repulsion force among the redox centers is getting evidently stronger (Figure 4B).

The above-described CV responses of Fc^+/Fc (Figure 2) and the fitting results (Figures 3 and 4) indicate that, with

DOI: 10.1021/acs.analchem.8b01655
Anal. Chem. 2018, 90, 9174−9181

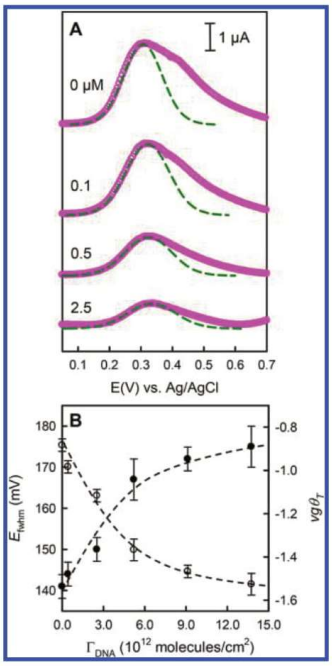

Figure 4. (A) Theoretical i–E curves of the major redox peaks (peak I) of Fc^+/Fc in binary thiolate DNA/FcC6S-Au SAMs prepared with different deposition concentrations of DNA. The pink circles are the experimental data (i.e., the original CV anodic waves); the green dashed lines are the simulated redox peaks generated by the theoretical i–E equations on the basis of the Frumkin adsorption isotherm. (B) The E_{fwhm} and $\nu g\theta_\Gamma$ values of simulated peak I of Fc^+/Fc in binary thiolate DNA/FcC6S-Au SAMs as a function of DNA surface density.

higher DNA surface density in binary thiolate DNA/FcC6S-Au SAMs, the mixed monolayer has increased permeability, less heterogeneous structure, and stronger intermolecular interactions (repulsion). These observations indicate that the backfilling of preassembled DNA monolayer on gold leads to clustered DNA domains, which should have a strong impact on the packing of diluting FcC6SH molecules. Previous studies based on electrochemical and in situ fluorescence microscopy have revealed that the binary thiolate DNA/MCH SAMs prepared via post-assembly exchange with MCH consist of heterogeneously distributed DNA strands with aggregated DNA clusters on gold.[30,31] The present results can be viewed as additional evidence for the inevitable existence of aggregated DNA clusters in binary thiolate DNA SAMs, which promote us to consider alternative preparation methods and optimized conditions for better performance of biosensing interfaces.[31,56]

Exploration of Molecular Orientation. The molecular orientation of surface-tethered DNA strands is another important factor to dictate their biosensing performance, and it is sensitive to the type and concentration of the adjacent electrolyte as well.[57] Zhang et al. previously discovered that the conformation of DNA strands in binary thiolate DNA/MCH SAM has a strong influence on the distribution of ions across the DNA–solution interface, which not only causes the "Donnan potential" but also affects the ion-pairing behavior between solution-diffused ClO_4^- and the Fc^+ terminal group of DNA strands.[58] It is interesting to compare the thiolate DNA/FcC6S-Au system with their intriguing observations, and therefore, we investigated the CV peak potential of Fc^+/Fc in binary thiolate DNA/FcC6S-Au SAMs as a function of the $NaClO_4$ concentration in the electrolyte solution to probe potential conformational changes of the surface-tethered DNA strands.

Prior to the study of thiolate DNA/FcC6S-Au SAMs, we have tested binary thiolate FcC6S-/C6S-Au SAMs ($\Gamma_{Fc} = 7.6 \pm 0.9 \times 10^{-11}$ mol/cm^2) as a trial system. In Figure 5A, we have

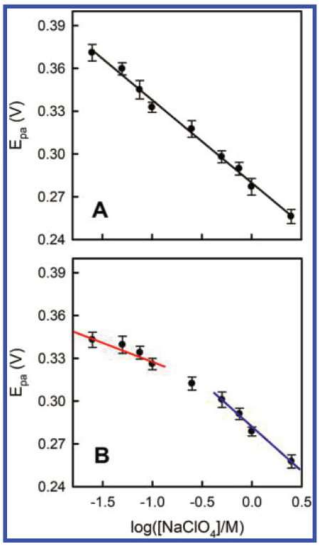

Figure 5. Relationship between the CV anodic peak potential (E_{pa}) of Fc^+/Fc and the logarithm concentration of $NaClO_4$ for (A) binary FcC6S-/C6S-Au and (B) binary thiolate DNA/FcC6S-Au SAMs with similar Fc surface densities. The solid lines are the linear fits over different concentration ranges of $NaClO_4$.

shown the CV anodic peak potential of Fc^+/Fc (E_{pa}) as a function of the logarithm concentration of $NaClO_4$ (log-[$NaClO_4$]). In consideration of the ion-pair formation between Fc^+ and ClO_4, this relationship can be expressed as eq 10[49]

$$E_{pa} = E^{o\prime} - \left(\frac{2.303RT}{nF}\right)\log K - \left(\frac{2.303RT}{nF}\right)\log[ClO_4^-] (K[ClO_4^-] \gg 1) \quad (10)$$

where $E^{o\prime}$ is the formal potential of Fc^+/Fc; K is the formation constant of the $Fc^+ \cdot ClO_4^-$ ion pair. The best linear fit to the experimental data shown in Figure 5A yields a slope of −51.9 ± 1.8 mV, which is close to the theoretical value of −59.2 mV (at 25 °C).[49] This result indicates that there is a "near ideal" ion-pairing behavior between ClO_4^- and Fc^+ on binary thiolate FcC6S-/C6S-Au SAMs within a broad range of electrolyte concentrations.

For binary thiolate DNA/FcC6S-Au SAMs with a similar Fc surface density ($\Gamma_{Fc} = 8.1 \pm 0.7 \times 10^{-11}$ mol/cm^2), we have

DOI: 10.1021/acs.analchem.8b01655
Anal. Chem. 2018, 90, 9174–9181

observed that the E_{pa} of the Fc^+/Fc CV peak also shifts negatively with increasing log[$NaClO_4$] in the electrolyte (Figure 5B). Remarkably, two distinct linear regions were identified over the same concentration range of $NaClO_4$ (Figure 5B) as that in Figure 5A. At higher concentrations of $NaClO_4$ (0.5 to 2.5 M), the fitted slope of −52.4 ± 2.7 mV shows no obvious difference from binary thiolate FcC6S-/C6S-Au SAMs; at lower concentrations (0.025 to 0.075 M), the slope of −21.5 ± 4.8 mV indicates an "unusual" ion-pair formation behavior.

On the basis of eq 10, the formation constant (K) of $Fc^+ \cdot ClO_4^-$ ion pairs was also determined from the intercepts of the linear fittings shown in Figure 5 ($E^{o\prime}$ in eq 10 was obtained from the CVs of Fc^+/Fc in 10 mM Tris buffer where the ion-pairing effect is assumed negligible). The linear fit in Figure 5A gives a K value of 269 M^{-1}, while the two distinct linear regions at lower and higher concentration ranges of $NaClO_4$ in Figure 5B give the K values of 32 and 186 M^{-1}, respectively.

Consistent with previous observations, the two distinct linear regions shown in Figure 5B can be attributed to the conformational change of DNA SAMs in response to varied salt concentrations, particularly the interfacial distribution of electrolyte ions.[57,58] Specifically, at low salt concentrations, the negatively charged DNA strands usually have a "standing up" orientation on the surface due to their intermolecular electrostatic repulsion force (Scheme 2A); in this case, the DNA layer has a preferential permeability to Na^+ so that it is more difficult for ClO_4^- to pass through the DNA layer, which leads to a much lower concentration of ClO_4^- in the local environment of surface tethered Fc^+/Fc than in the bulk solution. Moreover, the negatively charged phosphate groups of the DNA strand may cause a competitive binding effect toward the ion-pairing between Fc^+ and ClO_4^-; as a potential result, their overall binding charge ratio may also be changed. Therefore, the "unusual" ion-pairing behavior observed at low salt concentrations could be the overall effects of these factors induced by the "standing up" conformation of the DNA monolayer. In contrast, the high salt concentrations usually lead to a "collapsed" DNA layer, whose negative charges are fully compensated by cations in solutions (Scheme 2B). As a result, the DNA layer also loses its preferential ionic permeability, which leads to the "normal" ion-pairing behavior between surface-bound Fc^+ groups and ClO_4^- anions in solution. Besides the two distinct linear regions, the significantly reduced formation constant (K) of $Fc^+ \cdot ClO_4^-$ ion pairs at lower concentrations further confirms the inhibited ion-pairing between Fc^+ and ClO_4^- with "standing up" DNA strands in binary thiolate DNA/FcC6S-Au SAMs.

It should be pointed out that the above studied binary thiolate DNA/FcC6S-Au SAMs are merely trial systems for differently prepared or more sophisticated biosensing interfaces, yet we have demonstrated the capability of conventional electrochemical characterization upon introduction of redox-active thiols for passivation and labeling purposes. Beyond the surface density titration, heterogeneous structure evaluation, and molecular orientation exploration, it is entirely possible to investigate many other factors (e.g., type of ions, solvent, temperature, sequence and length of DNA) affecting the thermodynamics and kinetics of the DNA self-assembly process. Further studies of binary thiolate DNA/FcC6S-Au SAMs prepared via different assembly steps and other DNA-modified biosensing interfaces are currently underway in our laboratory but are beyond the scope of this publication.

Scheme 2. Proposed Molecular Orientation of DNA Strands in Binary Thiolate DNA/FcC6S-Au SAMs and the Distribution of Ions at the Interface[a]

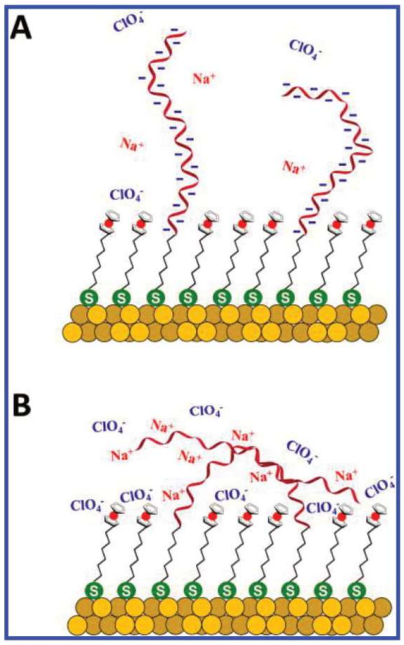

[a](A) Low concentration of $NaClO_4$. (B) High concentration of $NaClO_4$.

CONCLUSION

By replacing the conventional diluting reagent with an electroactive alkanethiol in the formation of binary monolayers, we are able to create a versatile platform to investigate the structural properties of DNA-based biosensing interfaces. In particular for a mixed thiolate DNA/FcC6S-Au monolayer, with standard electrochemical studies (e.g., cyclic voltammetry in the absence or presence of redox cations in solution), not only the surface density of DNA probes can be "titrated", but also the structural heterogeneity and molecular orientation of the binary SAMs can be evaluated. More importantly, the present study reveals the potential of this novel approach of surface passivation and redox labeling as a robust and convenient platform for investigating many other biosensing interfaces, particularly DNA-modified surfaces prepared in different assembly steps.

ASSOCIATED CONTENT

Supporting Information

The Supporting Information is available free of charge on the ACS Publications website at DOI: 10.1021/acs.analchem.8b01655.

Additional CV results of binary thiolate DNA/MCH, thiolate DNA/FcC6S-Au (in the presence of different

DOI: 10.1021/acs.analchem.8b01655
Anal. Chem. 2018, 90, 9174−9181

concentrations of $[Ru(NH_3)_6]^{3+}$ and different concentrations of $NaClO_4$), FcC6S-/C6S-Au (in the presence of different concentrations of $NaClO_4$), and DNA/FcC6S-Au SAMs (in which DNA strands were unmodified); schematic view of the electrochemical cell setup (PDF)

AUTHOR INFORMATION

Corresponding Author

*E-mail: hogan_yu@sfu.ca.

ORCID

Hua-Zhong Yu: 0000-0003-1411-3156

Notes

The authors declare no competing financial interest.

ACKNOWLEDGMENTS

We gratefully acknowledge the financial support from the Natural Sciences and Engineering Research Council (NSERC) of Canada (PI: H.-Z.Y.) and China Scholarship Council (H.T. visiting fellowship).

REFERENCES

(1) Saidur, M. R.; Aziz, A. R. A.; Basirun, W. J. *Biosens. Bioelectron.* **2017**, *90*, 125−139.
(2) Hvastkovs, E. G.; Buttry, D. A. *Analyst* **2010**, *135*, 1817−1829.
(3) Fahlman, R. P.; Sen, D. *J. Am. Chem. Soc.* **2002**, *124*, 4610−4616.
(4) Tang, Y.; Ge, B.; Sen, D.; Yu, H.-Z. *Chem. Soc. Rev.* **2014**, *43*, 518−529.
(5) Drummond, T. G.; Hill, M. G.; Barton, J. K. *Nat. Biotechnol.* **2003**, *21*, 1192−1199.
(6) Cheng, A. K. H.; Ge, B.; Yu, H.-Z. *Anal. Chem.* **2007**, *79*, 5158−5164.
(7) Xiao, Y.; Lubin, A. A.; Heeger, A. J.; Plaxco, K. W. *Angew. Chem.* **2005**, *117*, 5592−5595.
(8) Cai, H.; Lee, T. M.-H.; Hsing, I.-M. *Sens. Actuators, B* **2006**, *114*, 433−437.
(9) Baker, B. R.; Lai, R. Y.; Wood, M. S.; Doctor, E. H.; Heeger, A. J.; Plaxco, K. W. *J. Am. Chem. Soc.* **2006**, *128*, 3138−3139.
(10) Zuo, X.; Song, S.; Zhang, J.; Pan, D.; Wang, L.; Fan, C. *J. Am. Chem. Soc.* **2007**, *129*, 1042−1043.
(11) Ge, Z.; Lin, M.; Wang, P.; Pei, H.; Yan, J.; Shi, J.; Huang, Q.; He, D.; Fan, C.; Zuo, X. *Anal. Chem.* **2014**, *86*, 2124−2130.
(12) Yu, Y.; Chen, Z.; Shi, L.; Yang, F.; Pan, J.; Zhang, B.; Sun, D. *Anal. Chem.* **2014**, *86*, 8200−8205.
(13) Wu, L.; Xiong, E.; Zhang, X.; Zhang, X.; Chen, J. *Nano Today* **2014**, *9*, 197−211.
(14) Peterson, A. W.; Heaton, R. J.; Georgiadis, R. M. *Nucleic Acids Res.* **2001**, *29*, 5163−5168.
(15) Ricci, F.; Lai, R. Y.; Heeger, A. J.; Plaxco, K. W.; Sumner, J. J. *Langmuir* **2007**, *23*, 6827−6834.
(16) Macedo, L. J. A.; Miller, E. N.; Opdahl, A. *Anal. Chem.* **2017**, *89*, 1757−1763.
(17) Mirmomtaz, E.; Castronovo, M.; Grunwald, C.; Bano, F.; Scaini, D.; Ensafi, A. A.; Scoles, G.; Casalis, L. *Nano Lett.* **2008**, *8*, 4134−4139.
(18) Wong, I. Y.; Melosh, N. A. *Biophys. J.* **2010**, *98*, 2954−2963.
(19) Li, Z.; Zhang, L.; Mo, H.; Peng, Y.; Zhang, H.; Xu, Z.; Zheng, C.; Lu, Z. *Analyst* **2014**, *139*, 3137−3145.
(20) Doneux, T.; De Rache, A.; Triffaux, E.; Meunier, A.; Steichen, M.; Buess-Herman, C. *ChemElectroChem* **2014**, *1*, 147−157.
(21) Kimura-Suda, H.; Petrovykh, D. Y.; Tarlov, M. J.; Whitman, L. J. *J. Am. Chem. Soc.* **2003**, *125*, 9014−9015.
(22) Wolf, L. K.; Gao, Y.; Georgiadis, R. M. *Langmuir* **2004**, *20*, 3357−3361.
(23) Domínguez, C. M.; Ramos, D.; Mendieta-Moreno, J. I.; Fierro, J. L. G.; Mendieta, J.; Tamayo, J.; Calleja, M. *Sci. Rep.* **2017**, *7*, 536.
(24) Ray, S. G.; Cohen, H.; Naaman, R.; Rabin, Y. *J. Am. Chem. Soc.* **2005**, *127*, 17138−17139.
(25) Asanuma, H.; Noguchi, H.; Uosaki, K.; Yu, H.-Z. *J. Am. Chem. Soc.* **2008**, *130*, 8016−8022.
(26) Kick, A.; Bönsch, M.; Kummer, K.; Vyalikh, D. V.; Molodtsov, S. L.; Mertig, M. *J. Electron Spectrosc. Relat. Phenom.* **2009**, *172*, 36−41.
(27) Robinson, H.; Gao, Y.-G.; Sanishvili, R.; Joachimiak, A.; Wang, A. H.-J. *Nucleic Acids Res.* **2000**, *28*, 1760−1766.
(28) Herne, T. M.; Tarlov, M. J. *J. Am. Chem. Soc.* **1997**, *119*, 8916−8920.
(29) Kaiser, W.; Rant, U. *J. Am. Chem. Soc.* **2010**, *132*, 7935−7945.
(30) Meunier, A.; Triffaux, E.; Bizzotto, D.; Buess-Herman, C.; Doneux, T. *ChemElectroChem* **2015**, *2*, 434−442.
(31) Murphy, J. N.; Cheng, A. K. H.; Yu, H.-Z.; Bizzotto, D. *J. Am. Chem. Soc.* **2009**, *131*, 4042−4050.
(32) Rant, U.; Arinaga, K.; Fujita, S.; Yokoyama, N.; Abstreiter, G.; Tornow, M. *Langmuir* **2004**, *20*, 10086−10092.
(33) Steel, A. B.; Herne, T. M.; Tarlov, M. *J. Anal. Chem.* **1998**, *70*, 4670−4677.
(34) Mucic, R. C.; Herrlein, M. K.; Mirkin, C. A.; Letsinger, R. L. *Chem. Commun.* **1996**, 555−557.
(35) Ge, B.; Huang, Y.-C.; Sen, D.; Yu, H.-Z. *J. Electroanal. Chem.* **2007**, *602*, 156−162.
(36) Ceres, D. M.; Udit, A. K.; Hill, H. D.; Hill, M. G.; Barton, J. K. *J. Phys. Chem. B* **2007**, *111*, 663−668.
(37) Kelley, S. O.; Barton, J. K.; Jackson, N. M.; Hill, M. *G. Bioconjugate Chem.* **1997**, *8*, 31−37.
(38) Yu, H.-Z.; Luo, C. Y.; Sankar, C. G.; Sen, D. *Anal. Chem.* **2003**, *75*, 3902−3907.
(39) Petrovykh, D. Y.; Kimura-Suda, H.; Whitman, L. J.; Tarlov, M. J. *J. Am. Chem. Soc.* **2003**, *125*, 5219−5226.
(40) Lao, R.; Song, S.; Wu, H.; Wang, L.; Zhang, Z.; He, L.; Fan, C. *Anal. Chem.* **2005**, *77*, 6475−6480.
(41) Li, Z.; Zhang, L.; Zeng, S.; Zhang, M.; Du, E.; Li, B. *J. Electroanal. Chem.* **2014**, *722-723*, 131−140.
(42) Rekesh, D.; Lyubchenko, Y.; Shlyakhtenko, L. S.; Lindsay, S. M. *Biophys. J.* **1996**, *71*, 1079.
(43) Kelley, S. O.; Barton, J. K.; Jackson, N. M.; McPherson, L. D.; Potter, A. B.; Spain, E. M.; Allen, M. J.; Hill, M. G. *Langmuir* **1998**, *14*, 6781−6784.
(44) Su, L.; Sen, D.; Yu, H.-Z. *Analyst* **2006**, *131*, 317−322.
(45) Kertesz, V.; Whittemore, N. A.; Chambers, J. Q.; McKinney, M. S.; Baker, D. C. *J. Electroanal. Chem.* **2000**, *493*, 28−36.
(46) Häkkinen, H. *Nat. Chem.* **2012**, *4*, 443−455.
(47) Eckermann, A. L.; Feld, D. J.; Shaw, J. A.; Meade, T. *J. Coord. Chem. Rev.* **2010**, *254*, 1769−1802.
(48) Lee, L. Y. S.; Sutherland, T. C.; Rucareanu, S.; Lennox, R. B. *Langmuir* **2006**, *22*, 4438−4444.
(49) Rowe, G. K.; Creager, S. E. *Langmuir* **1991**, *7*, 2307−2312.
(50) Chidsey, C. E. D.; Bertozzi, C. R.; Putvinski, T. M.; Mujsce, A. M. *J. Am. Chem. Soc.* **1990**, *112*, 4301−4306.
(51) Tian, H.; Xiang, D.; Shao, H.; Yu, H.-Z. *J. Phys. Chem. C* **2014**, *118*, 13733−13742.
(52) Tian, H.; Dai, Y.; Shao, H.; Yu, H.-Z. *J. Phys. Chem. C* **2013**, *117*, 1006−1012.
(53) Love, J. C.; Estroff, L. A.; Kriebel, J. K.; Nuzzo, R. G.; Whitesides, G. M. *Chem. Rev.* **2005**, *105*, 1103−1169.
(54) Bard, A. J.; Faulkner, L. R. *Electrochemical methods: fundamentals and applications*, 2nd ed.; John Wiley & Sons Inc.: Hoboken, U.S.A., 2001.
(55) Laviron, E. *J. Electroanal. Chem. Interfacial Electrochem.* **1974**, *52*, 395−402.
(56) Bizzotto, D.; Burgess, I. J.; Doneux, T.; Sagara, T.; Yu, H.-Z. *ACS Sensors* **2018**, *3*, 5−12.
(57) Baumann, C. G.; Smith, S. B.; Bloomfield, V. A.; Bustamante, C. *Proc. Natl. Acad. Sci. U. S. A.* **1997**, *94*, 6185−6190.
(58) Zhang, J.; Zhao, Y.; Yuan, C.-G.; Ji, L.-N.; Yu, X.-D.; Wang, F.-B.; Wang, K.; Xia, X.-H. *Langmuir* **2014**, *30*, 10127−10132.

DOI: 10.1021/acs.analchem.8b01655
Anal. Chem. 2018, 90, 9174−9181

Appendix C. List of other publications

1. N. Gan, K. Liu, **L. Qi**, G. Zhang, Y. Guo, D. Sen and H.-Z. Yu, “DNAzyme-Catalyzed Click Chemistry for Facilitated Immobilization of Redox Functionalities on Self-Assembled Monolayers” *J. Phys. Chem. C*, **2020**, accepted.

My contribution: Assistance in writing and revision of this paper.

2. **L. Qi**, Y. Tang, B. Chakraborty, D. Sen and H.-Z. Yu, “An Immobilized DNA Switch Modulated by Intermolecular Interactions” *J. Phys. Chem. C*, **2020**, 124, 13779-13788.

My contribution (co-1st author): Writing and revision of this paper.

3. X. Gao, **L. Qi**, K. Liu, C. Meng, Y. Li and H.-Z. Yu, Exonuclease I-assisted General Strategy to Convert Aptamer-based Electrochemical Biosensors from "Signal-off" to "Signal-On" *Anal. Chem.*, **2020**, 92, 6229-6234.

My contribution: Assistance in writing and revision of this paper; doing additional experiments suggested by the reviewers.

4. F. Ma, **L. Qi**, O. Einarson, D. Sen, and H.-Z. Yu, A Divergent Pair of Ultrasensitive Mechanoelectronic Nanoswitches made out of DNA *Anal. Chem.,* **2019**, 91, 8244-8251.

My contribution: Writing and revision of this paper.

5. H. Tian, **L. Qi**, D. Xiang, H. Shao, H.-Z. Yu, Homogenized redox behavior of electroactive self-assembled monolayers on gold in the organic phase, *Electrochim. Acta* **2015**, 170, 369-375.

My contribution: Assistance in revision of this paper; doing additional experiments suggested by the reviewers.